FRICTION WEAR LUBRICATION

2

Tribology Handbook

FRICTION
WEAR
LUBRICATION

VOI. 2

ТРЕНИЕ, ИЗНАШИВАНИЕ И СМАЗКА

Под редакцией И. В. КРАГЕЛЬСКОГО и В. В. АЛИСИНА

Издательство «Машиностроение», Москва

FRICTION WEAR LUBRICATION

Vol 2

Tribology Handbook

Edited by Prof. I. V. KRAGELSKY
D. Sc. (Eng.)
V. V. ALISIN
Cand. Sc. (Eng.)
Institute for Machine Sciences, Moscow

Translated from
the Russian
by
Felix Palkin
and Valerian Palkin

Mir Publishers
Moscow

First published 1981
Revised from the 1978 *Russian edition*

The Russian Alphabet and Transliteration

Аа	a	Кк	k	Хх	kh
Бб	b	Лл	l	Цц	ts
Вв	v	Мм	m	Чч	ch
Гг	g	Нн	n	Шш	sh
Дд	d	Оо	o	Щщ	shch
Ее	e	Пп	p	ъ	″
Ёё	ë	Рр	r	ы	y
Жж	zh	Сс	s	ь	′
Зз	z	Тт	t	Ээ	e
Ии	i	Уу	u	Юю	yu
Йй	y	Фф	f	Яя	ya

The Greek Alphabet

Αα	Alpha	Ιι	Iota	Ρρ	Rho
Ββ	Beta	Κκ	Kappa	Σσ	Sigma
Γγ	Gamma	Λλ	Lambda	Ττ	Tau
Δδ	Delta	Μμ	Mu	Υυ	Upsilon
Εε	Epsilon	Νν	Nu	Φφ	Phi
Ζζ	Zeta	Ξξ	Xi	Χχ	Chi
Ηη	Eta	Οο	Omicron	Ψψ	Psi
Θϑθ	Theta	Ππ	Pi	Ωω	Omega

На английском языке

CONTENTS

Chapter 21. Transmissions [Prof. Yu. N. Drozdov, D. Sc. (Eng.)]

Chapter 11

FRICTION AND WEAR IN AGGRESSIVE MEDIA

The wear of rubbing parts whose material develops chemical interaction with the ambient medium is defined by the USSR State Standard as *mechano-corrosive wear*. In effect, this is the destruction of the rubbing surfaces caused by the two processes running at once: corrosion and mechanical wear. The latter can be produced both by the sliding friction of the mating surfaces and by the flow of the medium with or without hard particles therein under conditions that may or may not give rise to cavitation. Corrosion can be caused by either chemical or electrochemical interaction between the material and the medium.

The contact of metal with dry gases (particularly at elevated temperatures) and with non-conductive liquids results in chemical corrosion, that is, a direct reaction of the metal with the medium which generates no electric current.

The contact of metal with electrolytes (the aqueous solutions of acids, salts, and alkalis; brines, etc.) gives rise to electrochemical corrosion, in which the interaction between the metal and the medium involves two distinct but interconnected processes—anodic and cathodic ones, that is, *oxidation* (the dissolving of the metal in one region) and *reduction* (the reduction of oxygen and other oxidizers in another region). In this case the dissolving of the metal produces electric current. The anodic process is a direct transfer of metal atoms in the form of ions into the solution. The cathodic process is the assimilation of redundant electrons by atoms, molecules or ions of the solution.

The films that emerge on the rubbing surfaces differ in properties from those formed in static conditions, due to the fact that friction of metals in conducting media is influenced considerably by electrochemical processes. The protective properties and frictional be-

haviour of the films can be partly characterized by changes in their electrode potentials, i.e. an electrode potential φ_{fr} of the surfaces in friction and an electrode potential φ_{rem} of the surfaces with removed films [3]. The convergence of φ_{fr} and φ_{rem} signifies that the film is removed during friction and seizure is possible; the growing difference between φ_{fr} and φ_{rem} indicates the presence of protective films reducing the rate of wear. The value of φ_{rem} is variable depending on the medium and the material of the part.

The following parts of machines and apparatus are subject to mechano-corrosive wear under different operating conditions:

(a) in sliding friction—face seals in reactors, centrifuges, and separators; sliding bearings in reactors and sealed pumps; glands in stuffing boxes; pistons in pumps, etc.;

(b) hydroabrasive wear—diffuser discs in centrifugal driers; mixers and impellers in reactors; centrifugal pump components; screws, blades and screens in centrifuges, etc.;

(c) gas-and-abrasive wear—blast blower components in boiler plants; chimneys; air-pressure mill components, etc.;

(d) wear by cavitation—mixers and impellers in reactors; propellers in marine vessels, etc.;

(e) wear by oxidation—dry friction bearings, vanes and cylinders in centrifugal blast blowers;

(f) in fretting—threaded assemblies, etc.

Investigations into mechano-corrosive wear have indicated that processes running at the sliding interface are complex and interdependent, and they require careful study [3, 11, 15, 26].

11.1. WEAR RESISTANCE OF MATERIALS

Materials for rubbing parts are selected in accordance with the operating conditions and considerations of cost. The principal requirement is a wear resistance that ensures the specified service life. Wear resistance is determined by the mechanical and physical properties of the materials and by the electrochemical (chemical) properties of the metal-electrolyte (metal-medium) system.

The corrosion resistance of materials has to be high enough; according to [14] it must not be worse than the fourth grade specified by the Standard, and the material must not be susceptible to intercrystalline corrosion, to corrosive cracking and to spot corrosion, etc.

It should be borne in mind that the corrosion resistance values specified by the Standard and determined in laboratory or industrial tests may sometimes significantly differ from the values observed in actual operating conditions. In other words, data obtained in testing must be regarded as approximate.

The materials of rubbing parts should have no tendency to seizure and scuffing during operation. The proper choice of material and

working conditions that exclude plastic deformations of rubbing surfaces helps to meet this requirement. The presence of passivating protective layers on the rubbing surfaces often facilitates friction involving elastic or plastic deformation and improves their resistance to wear, hindering the development of microcutting conditions. On the contrary, an active state of the rubbing surfaces is accompanied by the loosening of their surface layers and leads to a higher wear rate. Such surface layers are subject to fatigue wear and microcutting because the subsurface layers undergo elastic or plastic predeformation and even cutting.

The rate of wear of materials rubbing in aggressive media is determined by the rate of formation of surface films and their destruction in friction and also by the rate of mechanical wear.

Therefore, the choice of wear-resistant materials for a given application should be made through a simulation of actual working conditions and the rate of corrosion at the rubbing interface.

Increased wear life can be achieved either by the formation of passivating protective films on the rubbing surfaces through the addition of corrosion inhibitors to the aggressive medium or by selection of materials with maximum wear resistance.

Since temperature considerably accelerates the process of corrosion, measures should be taken to reduce the temperature in the friction zone [5].

Load on the sliding pair tangibly affects its wear life. Stresses at the spots of real contact grow with the load, which may result in the plastic deformation of asperities and even in seizure and microcutting. Increased loading also results in sharply elevated temperatures at the sliding interface. To avoid such effects, the minimum possible loads and hard materials should be used in tribological joints.

Increased sliding speed results in greater wear of rubbing materials, but this increase in wear rate is generally due to rising temperature at the friction zone, a longer path of friction and a longer time of exposure of the materials to the aggressive medium [4, 10].

Abrasive particles on the rubbing surfaces and in the flow of the ambient medium also sharply increase the wear. Under such conditions the protective measures are:

—to remove abrasive particles, especially those of high hardness, from the working medium;

—to reduce the corrosive action of the medium by introducing corrosion inhibitors and by lowering the temperature;

—to use hard corrosion-resistant materials, and, wherever possible, non-metals;

—to reduce loads in the joint and the forces exerted upon the rubbing surfaces by abrasive particles in the flow of the aggressive medium. This can be done by reducing the flow velocity, the angle of incidence of the flow (under 10°) and the size of the abrasive particles.

11.2. MATERIALS FOR TRIBOLOGICAL JOINTS

11.2.1. Steels and Alloys

When selecting metallic materials, priority should be given to those with the maximum possible corrosion resistance. The most commonly used materials and the corresponding aggressive media are given in Table 11.1.

When considering materials for face seals and sliding bearings, it must be taken into account that high-alloy stainless steels have low hardness. Such steels should be paired only with soft antifriction materials, for example, graphitized carbon-based, polymeric, etc.

In high-velocity flows of aggressive liquids carrying abrasive particles, use must be made of high-alloy stainless steels in combination with protective elements made of materials БСГ-60, СГ-Т or С-2.

Rubbing parts in highly aggressive media operating at high temperatures are made of high-alloy corrosion-resistant nickel-molybdenum and nickel-chromium-molybdenum alloys (ХН65МВ, etc.).

Rolling bearings used in aggressive media are made of stainless steel 95Х18 with a high chromium content.

Three grades of standardized low-alloy corrosion-resistant alloys (ЧНХТ, ЧН1ХМД and ЧН1МШ) are used, mainly for service in aggressive gases at elevated temperatures. Their applications are outlined in Table 11.2.

Alloys 15Х28Л and 15Х34Л with a high chromium content exhibit good wear resistance in various aggressive media, especially with abrasives.

All the metals are heat treated for increased hardness and corrosion resistance.

The tendency to seizure in many stainless steel grades can be weakened by nitriding. The wear resistance of machine parts made of low-alloy and some stainless steels (30Х13, etc.) can be substantially increased by borating. In some cases diffusion chromium plating proves to be more effective as it increases hardness, wear resistance, erosion resistance, resistance to seizure, and resistance to corrosion in some media [12]. Carburized steel subjected to diffusion chrome plating has a high resistance to abrasive wear in numerous media.

11.2.2. Carbon-Base Antifriction Materials

Carbon-based antifriction materials are used when other antifriction materials (bronze, babbitts, metal-ceramic, etc.) are unacceptable, because the rubbing parts work in direct contact with an aggressive medium. Carbon antifriction materials exhibit high

Table 11.1

Steels and alloys used in corrosive media

Grade	GOST (State Standard)	Medium
12X13, 40X13, 95X18, 14X17H2, 10X14Г14H4T, 20X13H4Г9		Water, steam, salt solutions at room temperature, food media at room temperature
15X25T, 09X15H8Ю, 07X16H6, 08X22H6T, 12X18H10T	5632-72	Salt solutions varying in concentration and temperature, solutions of nitric acid and some organic acids
08X21H6M2T, 10X17H13M3T, 08X17H15M3T		Solutions of organic acids
06XH28МДТ		Solutions of sulphuric, phosphoric, silicofluoric, and some other acids
XH65MB		Acids at elevated temperatures
ВК3, ВК6, ВК8	3882-74	Water, weak solutions of salts, acids and alkalis
Hard facing with stellite B3K H12	ТИ-60-68 ТП-145-65	Water, weak solutions of salts, acids and alkalis

Table 11.2

Application of corrosion-resistant cast irons [13]

Grade	Application
ЧНХТ	Rubbing components in piston-type internal combustion engines, gas-engine compressors, and paper-making machinery subject to wear in gaseous aggressive media and aqueous solutions
Н1ХМД	Rubbing components in piston-type machines, internal combustion engines, and compressors subject to wear and corrosion in gaseous media (fuel combustion products, industrial-grade oxygen, etc.)
ЧН1МШ	The same as ЧНХТ and ЧН1ХМД, but with improved mechanical properties and thermal stability for operation at up to 500°C

Table 11.3

Physico-mechanical properties of carbon antifriction materials

Grade	Density, g/cm³	Ultimate strength*1, kgf/cm²		Compression modulus E·10⁻⁵, kgf/cm²	Shore hardness	Thermal conductivity coefficient at 20°C kcal/(m·h·°C)	Linear expansion coefficient at 20-100°C α·10⁶, 1/°C
		tensile	bending				
Roasted							
АО-600, ТУ 48-20-4—72	1.60-1.65	1100-1500	500-700	1.4	55-60	20	5
АО-1500, ТУ 48-20-4—72	1.70-1.80	1500-1800	600-800	1.6	60-65		
АО-600-С05, ТУ 48-20-3—72	2.8-3.1	2500-2700	900-1100				6-7
АО-600-Б83, ТУ 48-20-3—72	2.7-3.0	2400-2600	800-900	1.7	70-75	30	6.5
АО-1500-С05, ТУ 48-20-3—72	2.7-3.0	2600-2800	1000-1200				6-7
АО-1500-Б83, ТУ 48-20-3—72	2.6-2.9	2500-2700	900-1000	1.7		30	6.5
2П-1000Ф*2, ТУ 16-538-252-75	1.65	1600-1700	600-750	1.4	70-75	70	6.0
Himanit-T, ТУ 48-0120-17—74	1.85-1.89	1300-1700	320-380	—	80		10
АГ-600, ТУ 48-20-4—72	1.65-1.75	600-800	350-400	1.0	43-45	50	5
АГ-1500, ТУ 48-20-4—72	1.70-1.80	800-1000	400-500	1.3	45-50		
АГ-600-С05, ТУ 48-20-3—72	2.6-3.1	1400-1500	550-700	1.35	65-70		6-8
АГ-600-Б83, ТУ 48-20-3—72	2.5-2.8	1300-1400	450-550	1.35	70-72		6.5
АГ-1500-С05, ТУ 48-20-3—72	2.5-3.1	1500-1600	600-750	1.35	65-70	70	6-8
АГ-1500-Б83, ТУ 48-20-3—72	2.4-2.8	1400-1500	500-600	1.35	70-72		6.5
АПГС, ТУ 48-20-20—72	2.4-2.7	1400-1500	600-700	1.1-1.2	—	85-95	
АПГ-Б83, ТУ 48-20-20—72	2.3-2.6	1450-1650	650-750	1.1-1.2	—	90-100	7-8

*1 The ultimate strength values are statistical, being 1.5-2 times greater than specified by ТУ.
*2 Impregnated with phenol formaldehyde resin by the user.
Note: Mean impact strength is 2 to 4 kgf·cm/cm².

chemical stability and are employed for seal rings, sliding bearings, vanes in rotor-type blast blowers, etc.

High compressive strength allows such materials to be used in high-load applications. Carbon-base materials resist thermocracking at sharp temperature changes (typical of machine start-up and shut-down). The impact strength of these materials is low, which disqualifies them for applications involving impact loading and vibrations. They are capable of elastic deformation only and, when deformed in excess of 1 to 2 percent, they break down; bending loads also cause destruction to these materials.

All carbon-base materials have lower linear expansion coefficients than metals, and this should be allowed for when fastening the components. The carbon materials are porous to 12-20 percent, and their impermeability is improved by impregnating with metals and resins.

Commercially available antifriction carbon materials and their physical and mechanical properties and applications are given in Tables 11.3 and 11.4.

Roasted materials (AO) feature increased hardness and strength but reduced heat conduction against graphitized materials (АГ).

Table 11.4

Suitability of non-metal materials for aggressive media

Medium	Material											
	2П-1000-Ф	АО-1500-С05	АО-1500-Б83	АГ-1500-С05	АГ-1500-Б83	Himanit-T	Ф4Г21М7	Ф4К20	СГ-Т	СГ-П	С-2	ЦМ-332
Sea water	+	+	+	+	+	+	+	+	+	+	+	+
$NaClO_4$ (0.5%, 20°C)	—	—	—	—	—	—	+	+	+	+	+	+
$KMnO_4$ (0.5%, 20°C)	+	+	+	+	+	+	+	+	+	+	+	+
$KMnO_4$ (0.5%, 100°C)	—	—	—	—	—	—	+	+	+	+	+	+
HNO_3 (65%, 50°C)	—	—	—	—	—	—	+	+	+	+	+	+
HNO_3 (70%, 110°C)	—	—	—	—	—	—	—	—	±	±	+	+
H_2SO_4 (< 48%, —120°C)	+	+	—	+	—	+	—	—	+	+	+	+
H_2SO_4 (> 96%, —20°C)	—	—	—	—	—	—	+	+	+	+	+	+
HCl (36%, 20°C)	+	—	—	—	—	+	+	+	+	+	+	+
HCl (34%, 100°C)	+	—	—	—	—	+	+	+	+	+	+	+
HF (40%)	—	—	—	—	—	—	+	+	—	—	—	+
HF (70%)	—	—	—	—	—	—	+	+	—	—	—	—
NaOH (20%, 20°C)	—	—	—	—	—	+	+	+	+	+	+	+
NaOH (30%, 80°C)	—	—	—	—	—	+	+	+	±	±	±	—
CH_3COOH (10%, 80°C)	+	—	—	—	—	+	+	+	+	+	+	+
H_3PO_4	—	—	—	—	—	+	+	+	+	+	+	+

Designations: + suitable; —not suitable; ± limited use.

The АО and АГ type materials are produced either porous or impregnated with babbitt or lead containing 5 percent tin. The Himanit-T material is impregnated with furfuryl alcohol and heat-treated at 300°C, which makes it highly impermeable.

The maximum permissible temperatures are given in Table 11.5, and the maximum safe loads for carbon materials pairing various

Table 11.5

Maximum permissible temperatures for antifriction and hard non-metal materials

Material	Temperature °C	Material	Temperature °C	Material	Temperature °C
2П-1000-Ф	140	АГ-1500-Б83	200	СГ-Т	400
АО-1500-С05	300	Himanit-T	300	СГ-П	400
АО-1500-Б83	200	Ф4Г21М7	120	С-2	400
АГ-1500-С05	300	Ф4-К20	120	ЦМ-332	200

Table 11.6

Maximum permissible specific loads (kgf/cm²) in single and double axial seals without sealed-liquid pressure

Material	Metal hard to		Hard non-metal materials	
	HB 150	Over *HRC* 40	СГ-Т, СГ-П	С-2, ЦМ-332
2П-1000-Ф	—	10	35	20
АО-1500-С05	—	5	20	10
АО-1500-Б83	—	5	15	7
АГ-1500-С05	5	10	15	10
АГ-1500-Б83	5	10	10	7
Himanit-T	10	10	60	60
Ф4Г21М7	5	5	5	5
Ф4К20	5	5	5	5
СГ-Т	—	—	30	—
СГ-П	—	—	30	—
С-2	—	—	—	—
ЦМ-332	—	—	—	—

types of materials, in Table 11.6. The carbon materials are easily machined, and the rubbing surfaces of carbon seal rings used in face seals are lapped to a surface finish of 0.08-0.16 μm R_a and a flatness within 0.0009 mm [8].

The dimensions of blanks of commercially available carbon materials are given in Table 11.7.

Recommendations for design of components made of carbon-base materials are given in [23].

Table 11.7

Dimensions (mm) of blanks of antifriction carbon materials

Grade	Specifications (ТУ)	Outside diameter	Inside diameter	Height
АО-1500-С05 АО-1500-Б83 АГ-1500-С05 АГ-1500-Б83	48-20-3—72	57, 120, 140, 170	—	⩽ 200
2П-1000	16-538-252—75	90	—	55
		100	—	55
		140	—	55
		154	70	100
		230	100	38
		245	100	38
		205×145×38		
Himanit-T	48-0120-17—74	⩽ 290	⩽ 250	⩽ 200

11.2.3. Hard Non-Metal Materials

Superhard non-metal materials, such as siliconized graphites СГ-М, СГ-П, СГ-Т and boron-siliconized graphite БСГ-60, silicon-carbide С-2, ceramic ЦМ-332, find ever-growing application in tribological joints of equipment used in the chemical industry.

The properties of such materials are given in Table 11.8.

The principal advantage of graphite-silicon-carbide compositions is high wear resistance as compared with that of other metals or non-metals. Siliconized graphite in face seals or sliding bearings can be paired with any polymers or carbon-base materials, providing a wear life 10 to 100 times that of other materials.

In movable joints with adequate lubrication, even by an aggressive medium, use is made of sliding pairs СГ-П against СГ-П. An instance is the sliding bearings of sealed pumps and submersible high-pressure pumps [20]. Siliconized graphite can be employed in movable joints operating in contact with any aggressive media except fluorine, bromine, and iodine compounds, concentrated alkaline solutions, and strong oxidizers.

Machine components of siliconized graphite are obtained by machining from graphites (grades ПГ-50, ПРОГ-2400, or pressed blanks) and subsequently impregnating with liquid silicon. The interaction between the silicon and the graphite results in silicon carbide.

Table 11.8

Physico-mechanical properties of hard non-metal materials

Material	Density, g/cm³, no less	Ultimate strength, kgf/mm²			Impact strength, kgf·cm/cm²	Elasticity modulus E·10⁻⁵, kgf/cm²	Hardness	Thermal conductivity at 20°C, kcal/(m·h·°C)	Linear expansion coefficient at 20-100°C, α·10⁻⁶ 1/°C
		tensile	compressive (no less)	bending					
СГ-Т	2.5	4-5	30-32	9-11	2.8	9.50	*HRC* 70	85-100	4.6
СГ-П	2.4	5-6	42-45	10-12	4.0	12.7	*HRC* 75	130-150	4.2
СГ-М	2.25	2-3	12-15	6-7	2.8	—	*HRC* 50	120	4.6
С-2	2.9	3-4	18-32	9-11	—	—	*HRC* 60	—	4.5
БГС-60	2.7	3-4	50	—	3.7	8.9	*HRC* 80	50	6.0
ЦМ-332	2.9	13-15	40-50	32-45	1.4-5.0	38.0	*HRA* 90	15	8.5

Owing to the structural features of porous graphite, part of the silicon and the graphite remains unbonded. Therefore, siliconized graphite is a monolyte of silicone carbide with inclusions of silicon and graphite. Components made of this material, after impregnation, can be processed only by diamond grinding.

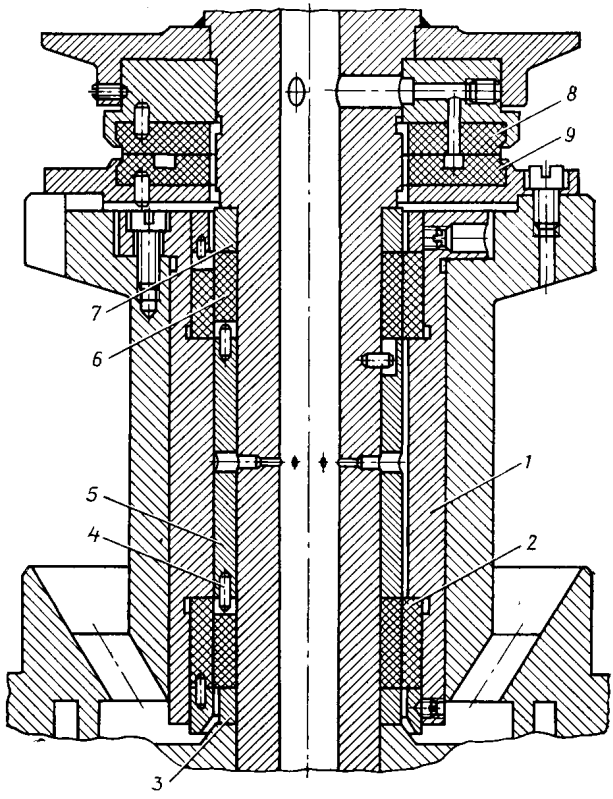

Fig. 11.1. Lower bearing unit of a vertical pump with the sliding components made of ceramic material ЦМ-332

1—sleeve; *2*—bushing (ЦМ-332); *3*—ring (steel 12Х18Н9Т); *4*—pin; *5*—spacer (12Х18Н9Т); *6*—bushing (ЦМ-332); *7*—ring (12Х18Н9Т); *8*—pressure disc (ЦМ-332); *9*—bearing disc (ЦМ-332)

The С-2 silicon carbide contains free silicon, which renders it unfit for use in alkalis. Although it provides high gas impermeability and wear resistance, the material suffers from a substantial disadvantage as compared to siliconized graphite: components from this material are obtained by pressing in moulds, which incurs high production costs where a variety of products are involved.

A distinguishing feature of the БСГ-60 boron-siliconized graphite is that the impregnation of graphite is done with molten silicon and boron, and that provides its increased hardness and wear resistance in liquids with abrasives. These qualities allow the БСГ-60 graphite

to be used as protection against abrasive wear in dryers, separators, centrifuges, etc.

When designing tribological joints with the СГ-М, СГ-П, СГ-Т, БСГ-60 and С-2 materials, it must be taken into account that their linear expansion coefficients are much lower than those of steels and alloys. Parts made of these materials (bushings, rings, etc.) rigidly mounted on metal shafts are liable to breakdown due to the heat generated in friction. Such parts should be fixed (press-fitted, adhesive-bonded) on the outside diameter only.

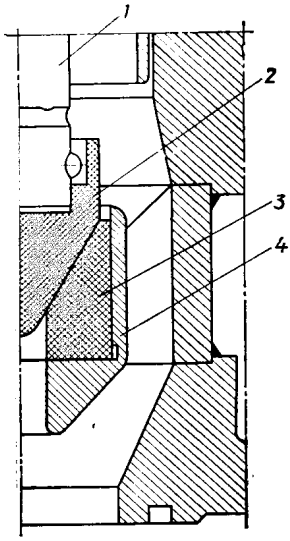

Fig. 11.2. Bearing unit of a sealed centrifugal pump with the sliding components made of ceramic alloy Grade C-8
1—shaft; 2—conical cup; *3*—insert; *4*—insert casing

The ЦМ-332 (sintered Al_2O_3) material provides high chemical stability in acid solutions. It is used for bearing bushings and for seal faces working in contact with various antifriction materials. Unlike the carbides, the ЦМ-332 is prone to cracking from thermal shocks (250-20°C).

In a sliding pair ЦМ-332 against metal the latter wears at a fairly high rate. A much better performance is provided by ЦМ-332 rubbing against ЦМ-332; this arrangement has found industrial use. The lower bearing of a vertical sealed pump, model НЦ-А5-16, handling a 60 percent solution of HNO_3 at 84-99°C, is shown in Fig. 11.1; its bushings are made of ЦМ-332.

The C-8 Grade ceramic material based on boron carbide and silicon carbide resists abrasive wear, does not react to acids (hydrofluoric, nitric, etc.); it is harder, less brittle and less responsive to impact loads than the ЦМ-332 Grade. A bearing assembly using C-8 Grade is shown in Fig. 11.2.

The ceramics are brittle and apt to cracking at sharp temperature changes; for this reason ceramic bushings should be mounted into metal casings and should not be used in applications involving impacts and vibration.

Parts of superhard non-metal materials are ground on conventional grinding machines with diamond grinding wheels, the use of coolant (water or other cooling agents) being indispensable. Since such parts sustain internal stresses, they should undergo natural ageing (about 15 days) prior to finishing, i.e. lapping (as in the case of seal rings for face seals). Seal rings for face seals are lapped after they have been machined to size and mounted in the casings. The lapping is done with the use of diamond pastes and cast iron laps.

In some applications (e.g. paper making), bearing bushes and liners for beaters, defibrators, and acid pumps are manufactured from wood laminated plastics.

11.2.4. Polymer Materials

These are used for sliding bearings in pumps, reactors and other equipment; for seal rings in axial seals; for vacuum-filter components, etc.

Antifriction materials based on fluoroplastics have found application in the last few years because of high chemical stability. The introduction of graphite, coke, molybdenum disulphide, boron nitride, etc., into fluoroplastic-4 improves the strength of resulting materials while retaining the high chemical stability in aggressive media.

Materials based on fluoroplastic-4 are produced in the form of blanks of the following grades (Table 11.9):

Table 11.9

Physico-mechanical properties of commercial antifriction materials based on fluoroplastic-4

Material	Density, g/cm³	Ultimate strength, kgf/mm²		Impact strength, kgf·cm/cm²	Compression modulus $E \cdot 10^{-5}$, kgf/cm²	Hardness *HB*	Thermal conductivity, kcal/m·h·°C	Linear expansion coefficient $\alpha \cdot 10^{-6}$, 1/°C
		tensile	compressive					
Ф4Г21М7	2.1	1.1	1.7*1	40	0.115	5.0	0.92	70
Ф4К20	2.2	1.3	2*2		—	5.0	1.0	
7В-2А	2.0	—	3.5-6.0	—	0.09-0.12	38-40*3	8-10	18-25
АФГМ	2.2	—	0.8-1.6		0.07-0.1	30-35*3	1.0-1.5	40-70

*1 Deformation 2%.
*2 Deformation 5%.
*3 Shore hardness.

Ф4Г21М7 (ФКН-7)—a composition of fluoroplastic-4 with graphite and molybdenum, used in contact with all kinds of materials;

Ф4К20—a composition of fluoroplastic-4 with coke, used for heavier loads than Ф4Г21М7;

АФГМ—a composite material containing graphite and molybdenum disulphide with fluoroplastic-4 used as a binder. The small content of fluoroplastic limits its use in certain aggressive media.

It is advantageous to line rubbing metal bushings with fluoroplastic. The hydrostatic bearing of a pump for handling nitric acid is shown in Fig. 11.3 [6]. A bushing *1* lined with fluoroplastic is press-fitted on the shaft journal. Nitric acid is delivered through chambers *3* in bushing *2*.

All fluoroplastic-base compositions are operable at temperatures of up to 120°C. Above this limit intensive wear of fluoroplastic is observed [4].

The use of fluoroplastic-base materials is justified only in situations where other materials, including carbon-base ones, cannot be used because of their inadequate corrosion resistance.

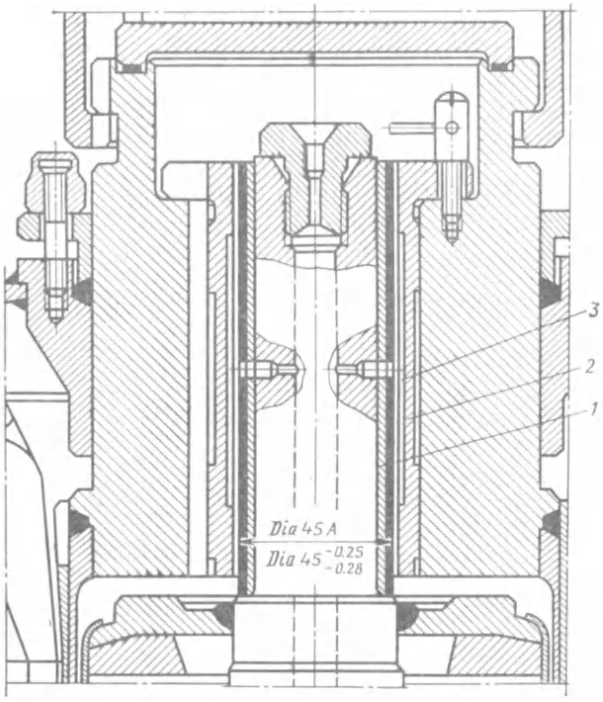

Fig. 11.3. Hydrostatic bearing unit with the sliding pair made of stainless steel and fluoroplastic-4

11.2.5. Silica-Base Coatings (Enamels)

Enameled parts combine the strength of metals and the abrasion resistance of silica-based materials. Only few metals (Pt, Au, Ta) and some nickel-chromium-molybdenum alloys can compete with silicate enamels in resistance to corrosion in aggressive media. The enameled surface has a small surface roughness (0.1 to 0.2 μm *Ra*) and non-uniform waviness having an amplitude of 100 to 200 μm and a spacing of 1 to 5 mm. Hence, the enameled parts have significant dimensional and geometrical form deviation and cannot be used in accurate assemblies without additional processing.

To provide the required dimensional and geometrical accuracy, enameled parts can be ground with synthetic-diamond grinding wheels and subjected to special heat treatment [28].

11.3. HYDROABRASIVE AND EROSIVE WEAR

Hydroabrasive destruction is a mechano-corrosive process which is largely determined by the chemical composition of the ambient medium, its properties and temperature.

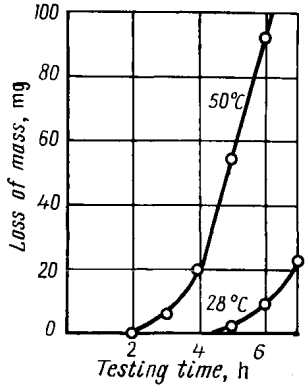

Fig. 11.4. Effect of water temperature on hydroerosion of steel 45

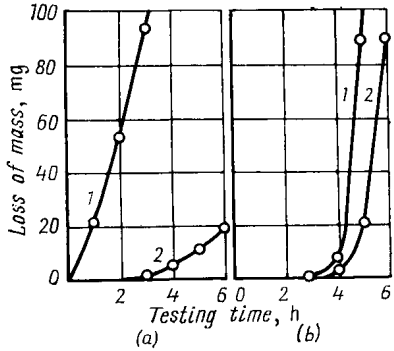

Fig. 11.5. Hydroerosion of steel Grade 45 (*a*) and steel 12X18H10T (*b*) in an acid solution with pH 6.5 (*1*) and tap water (*2*)

The physical properties of a liquid determine the dynamic characteristics of cavitation bubbles, while its chemical properties, the process of corrosion in hydroabrasive wear. The temperature (Fig. 11.4) and acidity (Fig. 11.5) of the medium have a substantial effect on hydroabrasive wear. Even a slight reduction in a hydrogen-ion concentration to pH 6.5 leads to a significantly increased rate of erosion. The heat treatment of carbon steels and cast irons gives no tangible improvement in resistance to abrasive wear in acidic media [18]. Thermodiffusion chrome plating can produce a marked effect. In alkaline media, carbon steels exhibit longer, and stainless steels shorter incubation periods and higher rates of erosion (Fig. 11.6). With a concentration of sodium hydrate in a solution increased from pH 8 to pH 13, the rate of hydroabrasive erosion goes up [19].

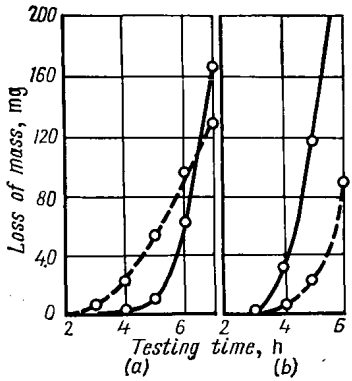

Fig. 11.6. Hydroerosion of steel, Grade 45 (*a*) and steel 12X18H10T (*b*) in water (dash lines) and aqueous solution of sodium hydroxide with pH 11 (solid lines)

Steel parts subject to hydroabrasive action should be produced from steels which comply with the following requirements.

(1) High corrosion resistance. For fresh water as an ambient medium, it is ensured with a chromium content of over 12 percent; for more aggressive media stainless steels of more complex composition need to be used.

(2) The ability to withstand both fatigue and corrosion under microimpact effects. The maximum resistance to abrasive action is provided by stainless steels with martensitic structure, and the minimum resistance, by those with ferritic structure, whose wear resistance hardly differs from that of steels with a stable austenitic

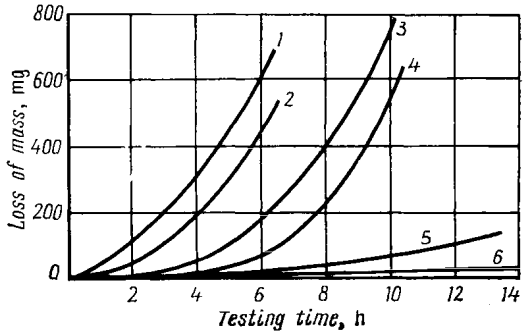

Fig. 11.7. **Cavitation resistance of stainless steels**
1—Grade 12Х18Н8; *2*—10Х18Н3Г3Д2; *3*—10Х12НДЛ; *4*—10Х14АГ10; *5*—10Х14АГ12М; *6*—30Х10Г10

structure; steels with unstable austenite, which through plastic deformation decomposes forming martensite, resist erosion.

(3) Good producibility.

Steels with unstable austenite based on an iron-manganese (Table 11.10, Fig. 11.7) are promising. Under a strong cavitation in

Table 11.10

Cavitation resistance of cast steels

Steel grade	Hardness, *HB*	Loss of mass for 6 h test, mg
30Л	135	1456
20Х13Л	180	870
12Х18Н9Л	180	890
30Х10Г10	200	15

fresh water, the best results are provided by steel 30Х10Г10, and in sea water, by steels 10Х14АГ12 or 10Х14АГ12М [2].

Of grey cast irons, those with large-plates graphite are the least stable, and with globular graphite, the most stable. A high-chromium alloy 130Х16М [25] is very stable in aggressive media.

The erosion resistance of parts used in aggressive media can be substantially increased by hard-facing with stainless steels having a martensitic, austenitic-martensitic, or purely austenitic structure with unstable austenite which is obtained with 12 to 16 percent Cr and 4 to 8 percent Ni [16].

When testing for resistance to hydroabrasive wear, use is normally made of water as a carrier of abrasive particles; the process of erosion of the material is considered as a result of the mechanical action of the abrasive particles and the liquid flow. When abrasive particles are carried by aggressive media, the rate of erosion proves to be completely different. Table 11.11 presents the results of tests of

Table 11.11

Relative wear resistance of some materials in hydroabrasive wear

Material and heat treatment	Medium		
	Aqueous	Acidic, pH 5	Alkaline, pH 12.6
Steels:			
20	0.74	0.90	0.55
45, normalizing	1.0	1.0	1.0
45, hardening and tempering at 200°C	—	—	1.62
У8А	1.36	1.06	—
12Х18Н10Т	1.64	11.50	0.91
20Х13	1.30	10.70	—
40Х13	1.54	12.90	0.99
40Х13, hardening	—	—	1.54
110Г13Л	0.55	0.65	1.36
Cast iron:			
СЧ 12-28	0.30	0.85	0.31
СЧ 18-36	0.36	0.93	0.55
ВЧ 40-10	0.35	0.90	0.68
Alloy 130Х16М	1.81	19.50	1.15
Titanium ВТ1	1.23	11.00	0.63
Bronze БрАЖ9-4	0.96	14.15	0.43
Duralumin Д1	0.19	2.89	—

some materials in various media containing 3 percent of abrasives (quartz sand with a grain size of 0.1 to 0.2 mm) [24]. In acidic media, corrosion processes run at a high rate on the surface of the tested metals, especially iron-carbon alloys. These processes are accompanied with a mechanical action accelerating the rate of the metal erosion. A chemically active medium also produces effect on corrosion-resistant alloys, increasing the wear rate. The hardening of carbon and stainless steels by heat treatment does not improve their wear resistance. High wear resistance in such media is typical of stainless steels, alloy 130Х16М, titanium, copper, and aluminium alloys.

In an alkaline abrasive carrier (sodium hydrate solutions, lime water), the wear rate is much slower, because thin passive films of corrosion products and absorbed OH-ions emerge on the metal sur-

face [24]. The influence of corrosion in alkaline media carrying abrasives is proved by the fact that with the temperature of the medium rising from 15 to 70°C the wear rate grows by approximately 70 percent.

REFERENCES

1. Антифрикционные сульфидированные металлокерамические материалы на основе нержавеющей стали.— В кн.: Повышение износостойкости и срока службы машин, вып. 3, Киев, УКРНИИНТИ, 1970, с. 157-162. Авт.: И. М. Федоренко и др.
2. Богачев И. Н. Кавитационное разрушение и кавитационно-стойкие сплавы. М., «Металлургия», 1972, 189 с.
3. Васильев И. В. К методике испытаний металлов на изнашивание при трении в агрессивной среде.— В кн.: Трение и износ в машинах, т. XV. М., Изд-во АН СССР, 1962, с. 59-77.
4. Виноградов Ю. М., Лазарев Г. С., Кудрявцева Б. М. Исследование новых антифрикционных материалов на основе фторопласта для химического машиностроения.— В кн.: Применение материалов на основе пластмасс для опор скольжения и уплотнений в машинах. М., «Наука», 1968, с. 27-31.
5. Воробьева Г. Я. Коррозионная стойкость материалов в агрессивных средах химических производств. М., «Химия», 1975, 816 с.
6. Воронков Б. Д. Подшипники сухого трения. М.-Л., «Машиностроение», 1968, 138 с.
7. Ганз С. Н., Пархоменко В. Д. Антифрикционные химические стойкие материалы в машиностроении. М., «Машиностроение», 1965, 148 с.
8. Контактные уплотнения вращающихся валов. М., «Машиностроение», 1976, 263 с. Авт.: Г. А. Голубев, Г. М. Кукин, Г. Е. Лазарев, А. В. Чичинадзе.
9. Коробов Ю. М., Прейс Г. А. Электромеханический износ при трении и резании металлов. Киев, «Техніка», 1976, 199 с.
10. Круман Б. Б., Крупицына В. А. Коррозионно-механический износ оборудования. М., «Машиностроение», 1968, 104 с.
11. Лазарев Г. Е. Износостойкость материалов при трении в коррозионно-активных средах.—«Химическое и нефтяное машиностроение», 1974, № 7, с. 38-39.
12. Материалы в машиностроении. Справочник под общ. редакцией И. В. Кудрявцева, т. 3. М., «Машиностроение», 1968, 446 с.
13. Материалы в машиностроении. Справочник под общ. редакцией И. В. Кудрявцева, т. 4, М., «Машиностроение», 1968, 248 с.
14. Материалы для пар трения торцовых уплотнений оборудования химических производств. Инструкция по выбору и применению. М., НИИхиммаш, 1974, 30 с.
15. Мачевская Р. А. и Турковская А. В. Трение и износ нержавеющих сталей в агрессивных средах.—«Химическое машиностроение», 1965, № 4, с. 17-20.
16. Миличенко С. Л. Ремонт кавитационных разрушений гидротурбин. М., «Энергия», 1971, 104 с.
17. Надежность и долговечность машин. Киев, «Техніка», 1975, 405 с. Авт.: И. Б. Костецкий, И. Г. Носовский, Л. И. Бершадский и др.
18. Некоз А. И., Прейс Г. А., Сологуб Н. А. О гидроэрозии металлов в кислой среде.—«Физико-химическая механика материалов», 1970, № 2, с. 109-111.
19. Некоз А. И., Прейс Г. А., Сологуб Н. А. О гидроэрозии сталей в щелочной среде.—«Физико-химическая механика материалов», 1969, № 5, с. 584-587.
20. Пелинский А. А., Тарабанов А. С., Лазарев Г. Е. Результаты испытаний материала СГ-Т.— «Машиноведение», 1971, № 2, АН СССР, с. 92-98.

21. Потенциостатический метод исследования процесса трения металлов в электропроводных средах.— В кн.: Проблемы трения и изнашивания, вып. 6. Киев, «Техніка», 1974, с. 55-60. Авт.: Ю. М. Коробов и др.

22. Прейс Г. А., Сологуб Н. А. Повышение износостойкости деталей оборудования сахарных заводов. Киев, «Техніка», 1966, 139 с.

23. Свойства конструкционных материалов на основе углерода. Справочник. Под ред. В. П. Соседова. М., «Металлургия», 1975, 335 с.

24. Слынько А. И., Прейс Г. А., Сологуб Н. А. Гидроабразивное изнашивание металлов в кислых средах.—«Физико-химическая механика материалов», 1972, № 2, с. 9-13.

25. Тиханович В. И., Кириевский Б. А. Новые литые материалы повышенной износостойкости в условиях трения скольжения и эрозионного разрушения.— В кн.: Повышение износостойкости и срока службы оборудования пищевой промышленности. Москва — Киев, ЦНИИТЭлегпищемаш, 1968, с. 94-101.

26. Томашов Н. Д. Теория коррозии и защиты металлов. М., Изд-во АН СССР, 1960, 590 с.

27. Хрущов М. М., Бабичев М. А. Исследование изнашивания металлов. М., «Наука», 1960, 351 с.

28. Чернявский А. Н., Прейс Г. А., Смирнов Н. С. Алмазное шлифование эмалированных деталей.— В кн.: Теория и практика алмазной и абразивной обработки деталей приборов и машин. М., МВТУ им. Баумана, 1973, с. 117-121.

Chapter 12

ABRASIVE WEAR

12.1. FACTORS AFFECTING THE RATE OF WEAR

Abrasive wear is a major kind of wear for many components of mining, drilling, construction, transport, agricultural and other types of machinery that handle materials containing abrasive particles. Typically, the rate of wear is high (from 0.1 to 100 μm per hour).

This kind of wear is usually caused by hard mineral particles with non-metal interatomic bonds which produce no significant adhesion and seizure phenomena [4, 11]. For this reason the physical processes resulting in wear are relatively simple. On the other hand, a great variety of shapes and mechanical properties of abrasive particles and diverse loading conditions give rise to variable stresses at the contact [11, 15, 22, 24, 27]. Wear debris are separated from the main metal as a result of a single or, generally, multiple action of the abrasive agent, i.e. either microcutting (different in character for tough and for brittle materials) or fatigue (low-cycle in the plastic region and multiple-cycle in the elastic region) takes place. This diversity of wear processes and conditions results in various combinations of the elementary processes involving disintegration and loosening of the surface layers.

The behaviour of the surface layers of materials which are subjected to microscratching is revealed by rubbing their specimens against fixed abrasive particles on a testing machine Х4-Б [24]. For this kind of wear, the relative wear resistance ε_{rel} (expressed as the ratio between the wear of a reference sample and that of the specimen under test) of commercially pure and annealed metals and steels is connected with the Vickers hardness number (HV) by the expression $\varepsilon_{rel} = kHV$, where k is a constant (Fig. 12.1*a*).

For structural steels and tool steels, grades 40, У8, У12 and Х12, hardened and tempered at different temperatures, $\varepsilon_{rel} = \varepsilon'_{rel} + k'(HV - HV_0)$, where ε'_{rel} and HV_0 are, respectively, the relative wear resistance and hardness in the annealed state, and k' is a constant for a given steel (Fig. 12.1*b*). The relative wear resistance ε_{rel} for work-hardened metals and steels, which develop no phase changes during work hardening, does not depend on the hard-

ness obtained after processing or may slightly decrease with its increase (Fig. 12.1*c*).

The relative wear resistance of annealed metals is related to the modulus of elasticity E by the expression $\varepsilon_{rel} = kE^{1.3}$, which holds for commercially pure metals, some alloys, and non-metals. This expression, however, is not valid for heat-treated steels, i.e. the main structural materials used for components subject to abrasion, because their elasticity modulus does not change with the structural changes due to heat treatment.

In testing by this method, the relative wear resistance may depend on the hardness of the abrasive particles. If this hardness is much

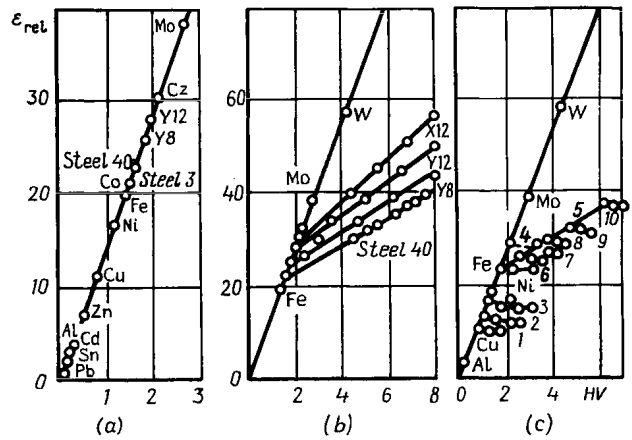

Fig. 12.1. Relative wear resistance ε_{rel} in the rubbing of various metals against fixed abrasive particles, depending on metal hardness (measured before testing) [24]

(*a*) commercially pure metals and carbon steels in annealed condition; (*b*) steels 40, Y8, Y12 and X12 hardened and tempered at various temperatures; (*c*) materials with varying degree of work hardening by plastic deformation: commercially pure metals (Al, Cu, Ni); *1*—brass (20% Zn); *2*—annealed and work-hardened aluminium-base bronze (5% Al); *3*—heat-treated and work-hardened berillium bronze (2% Be); *4*—work-hardened austenitic steel (0.2% C; 18% Cr; 9% Ni); *5*—hardened and tempered steel 40; *6*—steel 40 with different degrees of work-hardening after annealing; *7*—steel 40 with different degrees of work-hardening after normal bardening and tempering at 600°C; *8*—the same, tempering at 450°C; *9*—the same, tempering at 300°C; *10*—the same, tempering at 150°C

higher than that of the steel being tested, the rate of wear will not depend on the difference in hardness between the steel and the abrasive. If, however, the steel is close in hardness to the abrasive grits, a decrease in the hardness difference leads to a reduced wear rate. If the steel is harder than the abrasive grits, the wear rate will be small, and it is smaller with greater difference in the hardness values. The grit size has an effect on the wear rate up to a certain point, beyond which the rate of wear remains constant, with all other things being equal.

The method of testing for wear by rubbing against emery paper provides a high repeatability and accuracy of results (variation

within 2 to 3 percent) under strictly defined conditions (low pressures and sliding speeds, abrasive grits of high strength and hardness, protection against temperature and environmental effects, prevention of abrasive grits from movement and breakage). These test conditions, however, are often inadequate to simulate diverse operating conditions found in engineering practice.

When it slides over a hard stationary abrasive particle, a metal surface develops a scratch. Any mineral particle has rounded edges [11]; these are characterized by the edge angle as well as the rounding radius r. When the ratio of the depth of penetration of the abrasive particle h to its radius r (h/r) reaches a definite critical value, the scratching produces chips (microcutting).

The critical value of h/r depends on the ratio of the shear stress (τ) at the friction contact to the yield point σ_y, i.e. a changeover to microcutting occurs when

$$\frac{h}{r} = \frac{1}{2}\left(1 - \frac{2\tau}{\sigma_y}\right)$$

This relationship determines the "external friction threshold" [15].

Abrasive wear reaches its maximum rate when the ratio between the removed metal and the total scratch volume is greatest [11, 21, 15]; otherwise, no chips are formed, only bulges are left on the scratch edges. The latter are easily destroyed by new abrasive particles coming into action.

The formation of chips in abrasive wear by an abrasive mass having weakly bonded particles seems unlikely. Here [15, 26], the surface layer is subjected to elastic and plastic deformation, or even overdeformation, regular and low-cycle fatigue, and also destruction, which may be intensified by chemical processes brought about by the ambient media.

The destructive action of abrasive particles crushed in clearances between machine components is reduced to making so-called vibrational impact scratches on the metal surfaces. The effect is similar to that observed in a grinding mill. The destructive action is determined mainly by the strength of the particles being crushed. The mating metal surfaces separated by a layer of abrasive particles wear at a rate which is also determined by stresses in the surface layers. Thus, for instance, a very hard mineral may wear more intensively than a much softer steel mating it when hard abrasive particles are present in the clearance between the two. The ratio between the volumes of wear debris of the mating materials depends on the kind of abrasive grits [11, 12].

Wear by the impact of abrasive particles usually involves formation of peculiar chips and elongated lentil-shaped nicks on the metal surface [11] and also fatigue effects due to repeated impacts. The mechanism of wear is complicated by the chemical action of a liquid or gaseous ambient medium, and especially by elevated temperatures. On impacts against monolithic abrasives, dynamic ef-

fects are likely to take place, especially at low test temperatures. In all cases, the penetration of minute abrasive particles into the metal surface may occur, with the resulting change in the running of the wear process.

The most common abrasive is quartz sand, which is a component of various grounds, soils, and dust. It is the main agent that causes wear to machine parts. Because quartz sand grains have a relatively rounded shape and relatively low hardness and strength, their wear action typically involves repeated deformations of the surface-layer microvolumes for separating wear debris [11, 15, 22, 27]. Hence, the need arises to make distinction between several kinds of abrasive wear [24]. These kinds, considered below, are classified according to the intensity of abrasive action, the level of the stresses produced thereby, and the purpose of the components subjected to abrasive wear [9, 22, 28, 29].

Methods of laboratory tests for these kinds of abrasive wear are treated in detail in references [14, 20, 24].

12.2. KINDS OF ABRASIVE WEAR

Wear in an abrasive mass. The main factors determining the rate of wear are abrasive properties of grounds, soils, and moving particles; loads and sliding speeds; and physico-mechanical properties of the materials subjected to wear.

The abrading ability of soils and grounds grows with the increased content, smaller rounding radii, larger size and greater immobility of abrasive particles (mainly quartz ones). Abrasive particles are more immobile in grounds of greater density which, in turn, depends on their dampness and the extent of their freezing-up. Various types of ground have different values of the abrading ability: 1.0 for clays; 1.5 for sands; 1.9 for sandy loam; and 2.3 for sandy soil [3]. To some extent, the rate of wear can be influenced by the chemical activity of the soils and grounds. Wear increases in direct proportion to the load (in the case of earthmoving and agricultural machines, with increased pressure on the flanks of the cutting blades).

The wear life of commercially pure metals and carbon steels as found by testing in an abrasive mass with the use of a testing device IIB-7 [22] is illustrated in Fig. 12.2. The upper part of the chart (*I*) is obtained by wearing in rounded quartz-sand grits, and the lower part (*II*), in sharp hard corundum grits. The lower part (*II*) mainly gives results of testing on an emery paper with sharp hard grits (see Fig. 12.1), where the dominant wear process is microscratching. Here, the relationships $\varepsilon = f(H)$ are linear (Fig. 12.2, *II*). However, they become non-linear in the quartz-sand tests, where $H_{mat}/H_{abr} > > 0.5$ to 0.7 (H_{mat} and H_{abr} are the microhardnesses of the material and the abrasive, respectively), and where the increasing hardness of the metals produces a steeper rise in wear resistance. A higher

content of carbon and carbides in steels of equal hardness increases their wear resistance [19, 24].

The use of isothermal treatment, which results in much lower hardness, makes it possible to achieve the same resistance to abrasive wear as is achieved by means of conventional hardening [19].

The relative values of resistance to wear in an abrasive mass (as referred to a hardened steel, grade Г13Л) for steels with various alloying elements and different microstructures obtained by conventional and isothermal heat treatment are given in Tables 12.1 and 12.2. The variants of the heat treatment are disclosed in Table 12.3.

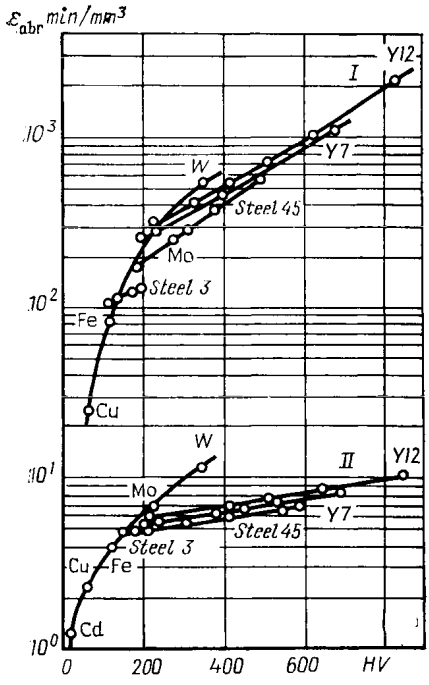

Fig. 12.2. Wear resistance ε_{abr} of pure metals and carbon steels in abrasive mass [22] (*I*—quartz, *II*—corundum)

The wear resistance of plastics in an abrasive mass tends to decrease as their modulus of elasticity rises. It is different with metals, where the inverse relation takes place. Data on wear resistance of some plastics as obtained by tests in an abrasive mass or by other testing methods are given in Table 12.4 (the reference material is polymethyl methacrylate).

For synthetic mineral materials, wear resistance rises with microhardness. Silicon carbide materials exhibit exceptionally high wear resistance when subjected to impactless abrasive action. Data on wear resistance of hard-facing materials are reported in [9, 16].

Wear of rubbing components with abrasive particles in the contact. Despite the continued improvement of protective means (air and oil filters, seals, etc.), it is difficult to prevent completely abrasive particles from getting into clearances between rubbing components. In addition, many machines have mechanisms without enclosures. In some cases, abrasive action is caused by wear debris.

The wear of rubbing parts grows with the amount and size of abrasive particles at the sliding interface. Here, the mechanical strength of the abrasive particles has a key role to play, because they are subject to crushing in the process of wear of heavy-duty joints [8, 11, 27]. The stronger an abrasive particle, the deeper it is pressed into the surface before it is broken, and the heavier is the resulting wear. The mechanical strength, defined by stress, σ, is de-

Table 12.1

Relative wear resistance, ε_{rel}, in abrasive mass for steels heat treated to different hardness values [19]

Steel grades	Variants of heat treatment											
	I		II		III		IV		V		VI	
	HB	ε_{rel}	*HB*	ε_{rel}	*HB*	ε_{rel}	*HB*	ε_{rel}	*HB*	ε_{rel}	*HB*	ε_{rel}
У10	—	—	614	1.78	534	1.61	429	1.43	375	1.28	—	—
У12	—	—	614	1.95	550	1.75	429	1.6	388	1.49	—	—
65	182	0.85	578	1.66	477	1.32	450	1.28	369	1.04	264	0.76
65Г1.5	187	0.99	578	1.39	504	1.27	477	1.21	401	1.12	—	—
65Г2	192	1.12	601	1.31	534	1.26	495	1.17	429	1.16	293	1.07
20Х1.5	131	0.40	415	1.08	388	0.99	362	0.97	302	0.81	229	0.62
20Х2.5	137	0.42	444	1.42	415	1.31	375	1.15	269	0.88	255	0.85
20Х3.5	140	0.44	435	1.77	415	1.71	366	1.57	295	1.23	266	1.14
20Х5	137	0.47	444	2.12	420	2.00	392	1.83	301	1.52	275	1.36
20Х6	143	0.51	444	2.35	426	2.28	383	2.08	302	1.69	269	1.48
35	149	0.49	444	1.08	388	0.94	321	0.75	241	0.59	212	0.50
35Х1.5	174	0.52	514	1.65	477	1.52	429	1.37	363	1.21	262	0.85
35Х2.5	174	0.53	504	1.94	469	1.85	436	1.70	388	1.57	277	1.19
35Х3.5	179	0.56	495	2.45	464	2.29	444	2.20	415	2.08	285	1.40
35Х5	170	0.59	507	3.22	477	2.90	444	2.65	415	2.42	269	1.64
35Х6	179	0.61	514	3.33	477	3.11	444	2.88	401	2.60	269	1.88
55	170	0.69	601	1.55	477	1.32	363	1.04	321	0.89	255	0.74
55Х1.5	187	0.73	601	2.18	534	1.99	514	1.89	363	1.70	293	1.06
55Х2.5	197	0.75	601	2.62	524	2.26	507	2.23	363	1.58	255	1.42
55Х3	187	0.77	589	2.85	567	2.71	477	2.44	388	2.08	285	1.66
55Х4.5	187	0.80	589	3.20	477	2.76	444	2.58	415	2.46	285	2.04
55Х5.5	192	0.84	578	3.68	477	3.19	444	3.05	415	2.86	261	2.13
75	207	1.12	601	1.76	578	1.74	477	1.52	311	1.08	285	0.98
75Х1.5	207	1.15	601	2.42	555	2.23	415	1.78	388	1.63	341	1.42
75Х2.5	201	1.14	601	2.96	578	2.80	514	2.52	415	2.13	321	1.77
75Х3.5	207	1.17	601	3.42	567	3.25	524	3.07	401	2.46	331	2.20
75Х4.5	201	1.18	601	3.88	555	3.65	514	3.44	401	2.94	341	2.68
75Х5	207	1.21	601	4.17	555	3.93	477	3.75	415	3.60	341	2.94
20Х3Г	121	0.46	444	1.68	415	1.60	375	1.50	261	1.19	255	1.16
35Х3Г	170	0.61	495	2.36	477	2.22	461	2.18	429	2.07	293	1.53
55Х3Г	179	0.92	578	2.72	567	2.68	477	2.41	401	2.15	311	1.89
75Х3Г	207	1.25	601	3.35	578	3.26	444	2.75	363	2.43	321	2.31
35Х3Г2	187	0.72	555	2.45	495	2.28	461	2.13	401	1.95	288	1.56
55Х3Г2	241	1.09	601	2.72	555	2.61	514	2.49	477	2.39	363	2.11
75Х3Г2	241	1.33	627	3.33	601	3.28	578	3.16	444	2.80	341	2.52
40ХГС	170	0.64	505	1.58	429	1.35	375	1.25	302	1.14	262	1.03
60ХГС	269	0.81	578	2.70	544	2.54	505	2.45	421	2.31	302	1.63
ХГС	269	1.03	590	3.91	578	3.30	566	3.78	444	3.33	388	3.03
55С2	262	0.75	578	1.10	461	1.00	444	0.97	321	0.90	277	0.84
55Н2	201	0.77	578	1.47	477	1.32	450	1.24	352	1.08	264	0.92

termined as $\sigma = 4N/\pi d^2$, where N is the load producing destruction of a single abrasive grain and d is its diameter. The value of σ rises with reduction in d (because of the scale effect) and in the hardness of the rubbing surfaces (Fig. 12.3). In the contact between steel and plastic, the breaking of the abrasive particles is not observed since

Table 12.2

Relative wear resistance, ε_{rel}, in abrasive mass for steels undergoing isothermal treatment to different hardness values [19]

Steel grades	Variants of isothermal treatment							
	VII		VIII		IX		X	
	HB	ε_{rel}	*HB*	ε_{rel}	*HB*	ε_{rel}	*HB*	ε_{rel}
У10	415	1.65	415	1.63	388	1.60	—	—
У12	415	2.31	415	2.31	401	2.30	388	2.29
65Г1.5	555	1.81	429	1.72	341	1.66	—	—
65Г2	578	1.98	444	1.92	352	1.81	—	—
35Х3.5	—	—	—	—	444	2.78	388	2.67
35Х5	—	—	—	—	461	3.41	444	3.36
35Х6	—	—	477	3.71	444	3.64	—	—
55Х1.5	—	—	514	2.53	477	2.37	429	2.15
55Х2.5	—	—	514	2.82	477	2.66	401	2.36
55Х3	—	—	514	3.14	477	2.87	429	2.63
55Х4.5	514	3.63	477	3.44	461	3.27	444	3.25
55Х5.5	524	4.17	495	4.07	477	4.02	461	3.95
75Х1.5	578	3.12	514	2.82	477	2.65	461	2.60
75Х2.5	555	3.46	514	3.22	495	3.13	461	2.96
75Х3.5	601	4.44	545	4.09	477	3.72	461	3.65
75Х4.5	555	4.57	514	4.32	477	4.12	461	4.01
75Х5	555	4.90	514	4.62	477	4.37	461	4.28
55Х3Г	514	3.26	495	3.15	477	2.94	429	2.91
75Х3Г	601	4.55	545	4.26	477	3.91	461	3.84
55Х3Г2	555	3.48	514	3.32	477	3.18	429	3.06
75Х3Г2	601	4.64	555	4.47	514	4.25	477	4.12
40ХГС	444	2.00	388	1.90	331	1.75	—	—
60ХГС	505	2.88	429	2.66	388	2.51	352	2.45
ХГС	555	4.50	495	4.22	444	4.01	388	3.82

Table 12.3

The variants of heat treatment referred to in Tables 12.1 and 12.2 [19]

Variants of heat treatment	Heat treatment conditions
I	Normal annealing. Heating to 50°C above point Ac_3 or Ac_1, holding for 30 min and cooling with the furnace
II	Hardening at temperature exceeding points Ac_3 or Ac_1 by 50°C and tempering at 170°C
III	Hardening and tempering at 300°C
IV	400°C
V	500°C
VI	600°C
VII	Isothermal quenching from temperature higher than points Ac_1, or Ac_3 by 70°C in a bath heated to 230-240°C
VIII	Isothermal quenching in a bath heated to 270-280°C
IX	310-320°C
X	380-400°C

Table 12.4

Relative wear resistance, ε_{rel}, of plastics
(according to M. M. Tenenbaum)

Material	Relative wear resistance as determined in testing			
	on emery paper	on ПВ-7 apparatus		on grid
		with corundum grits	with quartz grits	
Polymethyl methacrylate	1.00	1.00	1.00	1.00
Fluoroplastic-4	1.09	0.97	3.1-4.9	2.17
Polyethylene ПЭВД	3.57	1.40	1.86-2.15	1.43
Polyethylene ПЭНД	2.33	3.04	3.86-8.05	1.85
Capron	10.00	2.36	9.3-12.6	33.3
Polyamide П-68	2.5-6.25	2.42	7.9-9.9	3.0-83.0
Polystyrene	1.96	0.98	0.69	0.024
Vinylplast	1.41	1.12	1.7-2.8	0.72
Vulcolan	12.50	27.30	84.00	100
Ebonite	1.37	—	2.55	50
Steel 3	25.00	9.70	31.50	—

they almost fully penetrate into the plastic reducing the wear as is the case with rubbing components as dust seals or sliding bearings lined with plastics and rubber [22].

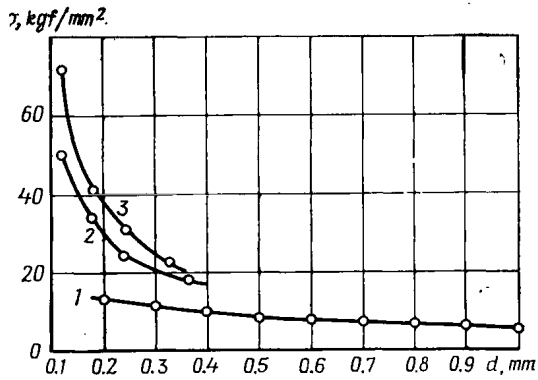

Fig. 12.3. Relation between stress σ and size d of quartz grains compressed between plates of different hardness (according to M. M. Tenenbaum)
1—both plates of cemented carbide ВК-2; *2*—one plate of carbide and the other of glass-filled plastic АГ-4В; *3*—both plates of steel 45 hard to 210 kgf/mm²

The intensive crushing of abrasive particles in gear transmissions, antifriction bearings and heavy-duty universal joints brings about the situation in which wear scarcely depends (and sometimes does not depend at all) on external load, since the contact stresses are determined by the mechanical strength of the particles [5, 27, 28, 29]. For low contact pressures and also in steel-plastic combinations

wear grows substantially with external loads. With such rolling-contact elements as gears and antifriction bearings, the rate of wear varies in direct proportion to slippage. The wear rate is only slightly dependent on the rotational speed of universal joints, antifriction bearings, low-speed and medium-speed gearings [27]. What is important is the hardness of the mating parts: the harder the surface layers, the lower is their wear.

Abrasive wear phenomena in a jet of liquid or that of gas carrying hard particles have much in common. The wear rate depends on the velocity of the particles and the angle at which its vector meets the surface (the angle of incidence α_{in}). In addition, wear is dependent on the concentration of abrasive particles, on their shape, hardness, dynamic strength and also on the physical and mechanical properties of the materials subject to wear.

The loss of mass of the material for 1 kg of the abrasive that strikes it is connected with the speed of the particles by the relationship $I_g = kv^m$, where k is a factor determined by the properties of the abrasive and the material and by the angle of incidence. The exponent m has stable values for $v < 100$ m/s; for higher speeds these values vary within wider limits. The values of m come to 2.3 for steel, Grade 3; 2.5 for hardened steel, Grade 45; 2.8 for white iron; 2.9 for basalt [10, 14, 22, 31]. Relation between the wear and the incidence angle is generally expressed by a curve with the minimum corresponding to the critical angle of incidence ($\alpha_{in,cr}$); its value for brittle non-metallic materials approaches 90°, for metal alloys it decreases with increase in their plasticity and amounts to 30 to 40° for soft steels and 50 to 70° for hardened steels [10, 14, 31]. The values of m and k vary for different operating conditions [14, 22, 32].

An increase in the concentration of the abrasive jet may lead to a reduced wear rate due to a screening effect produced by the particles bouncing from the surface [11]. The exception is rubber, which, with high abrasive concentration, gets heated and wears heavier [14]. The rate of wear in an air jet grows uniformly with the abrasive grain size. However, this relationship holds for abrasive grains measuring up to 150 μm; with larger grains, a variety of relationships can be observed [14].

The presence of moisture intensifies abrasive wear, sharply at the outset (with a moisture content of up to 1 to 1.5 percent) and then slower. In air at +20 to +400°C the rate of wear changes slightly, and in a neutral medium it does not change at all. At temperatures in excess of 400 to 500°C, the rate of wear goes up steeply [11, 14]. For metal alloys, the rate of wear at rising temperatures depends heavily on the chemical activity of the medium.

The described wear behaviour is observed only with small angles of incidence. With greater angles ($\alpha_{in} > 45$ to 55°), the wear patterns change. If, for instance, with small incident angles a hardened steel is normally more wear-resistant than a softer steel, with $\alpha_{in} > 45°$ the opposite is often the case.

Figure 12.4 illustrates the hydroabrasive wear resistance of materials with small angles of incidence ($\alpha_{in} = 10°$), as obtained on a ПВ-12 testing device [22] at $v = 37$ m/s. Data on hydroabrasive wear for various materials are given in Tables 12.5 through 12.8.

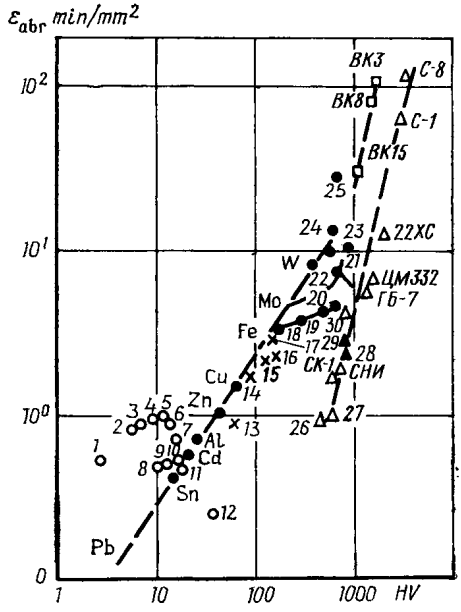

Fig. 12.4. Resistance ε_{abr} of materials to hydroabrasive wear, with incidence [angle of $\alpha_{in} = 10°$ [22]

□—cemented carbides; △—mineral materials; ●—metals; X—non-ferrous alloys; ○—plastics; *1*—polyethylene ПЭВД; *2*—polyethylene ПЭНД; *3*—polypropylene; *4*—capron; *5*—polyamide П-58; *6*—viniplast; *7*—caprolon; *8*—СНП; *9*—polymethyl metacrylate; *10*—polyformaldehyde; *11*—polystyrene; *12*—glass-filled plastic АГ-4В; *13*—silumin АЛ9В; *14*—brass Л62; *15*—brass ЛНМцЖА60-1-2-1-1; *16*—brass ЛМцЖ55-3-1; *17*—bronze АЖ9-4; *18*—grey cast iron; *19*—steel 45 *20*—steel У12; *21*—steel Х12; *22*—white iron; *23*—alloyed cast iron ИЧХ12М; *24*—hard-facing: relite + Sormite-1; *25*—hard-facing ОИ-8М; *26*—china; *27*—silicate glass; *28*—glass ceramic; *29*—basalt; *30*—slag-glass ceramic

The use of very hard metal alloys and hard facing can bring a substantial effect at $H_{mat} > H_{abr}$. Some increase in wear resistance can also be achieved where the hardness of abrasives is only slightly

Table 12.5

Relative wear (by volume) of some alloys and heat-treated steels in a jet of dry quartz sand with a grain size of 0.6 to 1.5 mm, at $v = 82$ m/s (according to I. R. Kleis)

Material	*HB*	Wear at $\alpha°_a$		
		15	45	90
Steel:				
Steel 3 (reference material)	130	1.0	1.0	1.0
25Х2МФА	505	1.4	1.1	0.9
30ХМА	630	1.5	1.4	0.7
45	717	1.6	1.5	0.7
50ХФА	765	1.6	1.4	0.7
60С2А	960	2.1	1.8	0.8
У8	980	2.3	1.9	0.9
Sormite-1	630	1.9	1.3	0.9
White hypoeutectic iron	515	1.6	1.2	0.6

Table 12.6

Relative wear (by volume) of some steels and white irons in a jet of abrasive particles of different hardness 0.3-0.4 mm in size at $v=100$ m/s (according to I. R. Kleis and T. A. Pappel)

Material	*HV*	Quartz ~ 1100 *HV* with α_a°		Glass ~ 500 *HV* with α_a°		Lime ~ 160 *HV* with α_a°	
		30	90	30	90	30	90
Steel:							
45 (reference material)	175	1.0	1.0	1.0	1.0	1.0	1.0
ШХ15	224	1.2	1.3	1.3	1.4	1.6	1.5
ШХ15	463	1.2	0.9	1.7	1.9	3.3	2.3
ШХ15	604	1.2	0.8	2.8	2.4	—	3.8
ШХ15	770	1.3	0.6	13.6	5.6	—	3.0
White hypoeutectic iron	510	0.9	0.5	21.5	9.4	4.6	3.0
White alloyed iron 15-3 (2.8% C; 0.8% Si; 0.8% Mn; 15% Cr; 2.8% Mo)	620	1.0	0.6	41.7	14.7	6.3	3.8
Steel У8	860	1.0	0.7	10.3	6.7	3.4	3.0

Note: Abrading power determined on steel 45 amounts to 1520, 2180 and 6 mg/kg with $\alpha_a = 30°$ and 1003, 1324, and 2.5 mg/kg with $\alpha_a = 90°$ for quartz, glass and lime, respectively.

Table 12.7

Relative wear (by weight) of steels and cast irons in a jet of various abrasives at $v=100$ m/s (according to I. R. Kleis and T. A. Pappel)

Material	*HV*	Quartz sand, grit size 0.6-0.8 mm with α_a°		Lime powder, grit size 0.3-1.3 mm with α_a°		Mixed 90% quartz +10% lime dust with α_a°	
		30	90	30	90	30	90
Steel							
45 (reference material)	177	1.0	1.0	1.0	1.0	1.0	1.0
08Х18Н10Т	195	1.0	0.7	0.8	0.8	1.0	0.8
10Х14Г14Н4Т (ЭИ711)	224	1.1	0.7	1.0	0.8	1.1	0.8
ШХ15	224	1.3	1.1	1.6	1.5	1.3	1.1
15Х25Т	242	1.0	1.0	0.8	0.8	1.0	0.9
08Х17Н5М3	346	1.1	0.7	1.3	1.1	1.1	0.7
White hypoeutectic iron	526	1.4	0.7	4.6	3.0	1.4	0.8
White iron 15-3 (15% Cr, 3% Mo)	614	1.8	0.9	6.3	3.8	2.0	1.2
Steel У8	864	1.5	0.8	3.4	3.0	1.5	1.0

Note: The rate of wear of the reference material in a jet of quartz sand was 820 mg/kg ($\alpha_a = 30°$) and 720 mg/kg ($\alpha_a = 90°$); in a jet of lime powder, 9.3 and 3.0 mg/kg; and in a jet of the abrasives in mixture, 790 and 800 mg/kg, respectively.

Table 12.8

Relative wear (by weight) of sintered cemented carbides of the BK type at an impact speed of 165 m/s (abrasive grit size 0.4-1.0 mm) (according to I. R. Kleis)

Alloy	*HV*	Glass with α_a°		Quartz with α_a°		Electrocorundum with α_a°	
		45	90	45	90	45	90
BK3	1610	420	204	78	47	6.6	6.9
BK6	1480	465	178	91	62	4.7	5.0
BK9	1350	238	143	51	44	3.3	2.4
BK15	1185	193	132	27	19	2.1	1.3
BK25	920	136	51	5.8	4.0	1.4	0.8
Steel 3 (reference material)	130	1.0	1.0	1.0	1.0	1.0	1.0

Note: The rate of wear of the reference material in a jet of glass grits was 278, quartz grits 116, and electrocorundum 256 mm³/kg with $\alpha_a = 45°$, and 155, 84, and 112, respectively, with $\alpha_a = 90°$.

higher than that of the material ($H_{abr}/H_{mat} < 1.6$); here, the structure of the material is of great significance.

The use of rubbers becomes more effective with decreasing impact speeds and abrasive concentrations of the jet and with greater incidence angles [14].

Brittle non-metal materials resist wear fairly well with a small α_{in}, low speeds and fine abrasive grains [11]. They are particularly wear-resistant in chemically active media [14].

A special case is hydroabrasive wear accompanied with cavitation, when the material is subject to a combined action of liquid streams, abrasive particles and cavitational hydraulic impacts. This case is described in [13].

Wear by impacts against a monolithic or loose abrasive material. Data on this type of wear are scarce. The rate of abrasive wear essentially depends on the impact energy: at first the wear rate rises directly with the energy, and then it slows down [6, 20, 24]. Data on relative wear resistance [24] for impact and friction against electrocorundum abrasive paper 4A3 with a grain size of 180, as obtained on testing machines УАМ and Х4-Б, are given in Table 12.9. The reference material was steel 3 hard to *HV* 150.

For friction at small speeds and loads on rigidly fixed strong hard abrasive [24]

$$U_v = k\frac{Nsd_1^2}{HV_0}$$

where U_v = bulk wear, s = sliding distance, N = load, HV_0 = = initial Vickers pyramid hardness of the metal; d = abrasive

Table 12.9

Relative wear, ε_{rel}, of materials by impact (УАМ testing machine) and rubbing (Х4-Б testing machine) against fixed abrasive particles [24]

Material	Heat treatment	*HV*	ε_{rel}, testing machine	
			УАМ	Х4-Б
Copper	—	075	0.51	0.51
Nickel	—	130	0.85	0.85
Molybdenum	—	282	1.84	1.85
Tungsten	—	425	2.83	2.82
St. Grade 3 (0.16% C)	—	150	1.00	1.00
Steel Grade 45 (0.45% C)	Annealed	169	1.13	1.12
	Normalized	212	1.20	1.22
	Hardened, tempered at 150°C	620	1.79	1.79
	Hardened, tempered at 335°C	453	1.51	1.54
	Hardened, tempered at 450°C	370	1.43	1.42
Steel Grade У8 (0.83% C)	Annealed	186	1.25	1.24
	Hardened, tempered at 150°C	795	2.11	2.14
	Hardened, tempered at 300°C	615	1.91	1.86
Steel Grade У12 (1.1%C)	Annealed	210	1.37	1.39
The same	Hardened, tempered at 150°C	840	2.48	2.45
	Normalized at 1050°C	192	1.94	1.26
Steel СН2	Normalized at 1050°C, pressed 72.2%	540	1.90	1.19
Steel Grade 20Х18Н9	Hardened from 1100°C	220	2.27	1.41
Steel Grade ЛГ13	Hardened from 1080°C	256	2.56	1.68
Steel Grade Х12Ф1	Oil hardened from 1050°C	865	2.14	2.85
	Oil hardened from 1200°C	456	3.80	3.01
	Brine hardened (550°C)	468	3.80	3.08
Cast iron Grade СЧ21-40	—	348	1.08	1.17
White iron (3.2% C; 1.07% Si)	—	354	1.74	2.14
Basalt-diabase	—	840	0.11	0.48
Flint*1	—	934	0.63	0.87
Glass ceramic*2	—	845	0.30	1.33

*1 The Izyum deposits.
*2 White.

grain size; k = coefficient determined by the properties of the abrasive surface, by testing conditions, and by the method of specimen holding.

Analysis and evaluation of wear rate (μm/h) for heavy-duty rubbing components (gears, friction transmissions, antifriction bearings) can be done [27] from abrading action conditions A, physico-mechanical properties of materials $M_{1(2)}$, geometrical and kinematic characteristics of a joint $K_{1(2)}$:

$$U_{1(2)} = 4 \times 10^2 \frac{AK_{1(2)}}{M_{1(2)}} \qquad (12.1)$$

where $A = q_a^{2/3} R^{0.5} \sigma^{2.5}$ (q_a = concentration of abrasive particles in air or lubricant, percent; R = average radius of the particles, mm; σ = ultimate strength, kgf/mm^2); $M_{1(2)} = \delta_{1(2)}^{(t)} HB_{1(2)}^{1.5} HB_{2(1)}$ ($\delta_{1(2)}$ = plasticity of the surface layer characterized by the relative elongation at rupture, percent; t = coefficient of frictional contact fatigue); $K_{1(2)} = \sqrt{\rho^*}\, \frac{v_1 - v_2}{v_1 + v_2}\, n_{1(2)}$, where $\rho^* = \frac{\rho_1 \rho_2}{\rho_1 + \rho_2}$ = effective radius of curvature of the rubbing surfaces, mm; v_1, v_2 = sliding speeds of the rubbing surfaces, m/s; $n_{1(2)}$ = the number of loading cycles per minute. In these expressions the subscript 1 designates the surface being tested for wear resistance, and the subscript 2 designates the mating surface. By transforming $K_{1(2)}$ so that it corresponds to the characteristics of a given sliding pair, it is possible to obtain formulas for estimating the wear rate of its components. Values of K for pinions of gear transmissions [27] are given in Table 12.10.

The designations in Table 12.10 are:

Table 12.10

Values of K for toothed gearings

Gearing	K
Involute: spur gears	$[2m(z_1+z_2)\sin\alpha_w]^{0.5}\, y_w n_{1(2)}$
helical gears	$\left[\frac{2m(z_1+z_2)\sin\alpha}{\cos\beta}\right]^{0.5} y_w\, n_{1(2)}$
Novikov's gears	$k_n \left[\frac{2m(i+1)}{f_1 \sin\alpha}\right]^{0.5} f_g f_{lub}\, n_{1(2)}$

m = module, mm; z_1 and z_2 = teeth numbers for pinion and wheel; α and α_w = pressure angles; β = tooth helix angle; k_n = profile coefficient for the Novikov gears, which is the ratio of the tooth profile radius to the module; y_w = geometric factor of wear, which reflects the distribution of wear along the line of action; f_g and f_{lub} = gearing-type factor and lubricant-supply factor for the Novikov gears.

For the pitch-point region, the average value of y_w is found as

$$\bar{y}_w = \frac{y_{w1}\left(\frac{1}{i+1} - \chi_1\right) + y_{w2}\left(\chi_2 - \frac{1}{i+1}\right)}{3(\chi_2 - \chi_1)} \qquad (12.2)$$

The values of χ_1 and χ_2 which determine the points of the beginning and the end of the line of action are found by formulas

$$\chi_1 = 1 - \frac{\sqrt{d_{a2}^2 - d_{b2}^2}}{2a_w \sin\alpha_w}; \quad \chi_2 = \frac{\sqrt{d_{a1}^2 - d_{b1}^2}}{2a_w \sin\alpha_w}, \qquad (12.3)$$

where d_{a1} and d_{a2} = addendum circle diameters; d_{b1} and d_{b2} = base circle diameters; a_w = centre distance. The values of y_{w1} and y_{w2} are determined by substituting χ_1 and χ_2 into formulas:
for enclosed transmissions

$$y_w = \sqrt{\chi(1-\chi)}\,\frac{\chi-(1-\chi)\,i}{\chi} \tag{12.4}$$

for open transmissions

$$y_w = \sqrt{\chi(1-\chi)}\,\frac{\chi-(1-\chi)\,i}{\chi+(1-\chi)\,i}\,\frac{1}{\chi} \tag{12.5}$$

For Novikov's gears

$$f_g = 1 \mp \sqrt{\frac{R}{r}}; \qquad f_{lub} = 1 + \frac{R_1 \sin\alpha \mp ri}{R_1 \sin\alpha \pm r}$$

where R_1 = radius of the pinion pitch circle.

In the formulas for the Novikov gears, the upper signs (plus or minus) apply to the variety where the pinion's tooth flanks are convex and the gear's are concave, the lower signs apply to the variety where the pinion's tooth flanks are concave and the gear's are convex.

To assess the rate of wear by the formulas given above, the values of q_a and R are found by checking samples of the lubricant for abrasives, or ambient air for dust. Some data on q_a and R for gear reducers in various machines can be found in [3, 22, 27]. Data on mechanical strength σ of abrasive particles are given in Fig. 12.3, in literature [8, 11], and can also be determined on a testing device developed by the IMASH R&D Institute. The pertinent geometric parameters and teeth hardness values can be found on the gearing drawings. Data on values of δ and t are given in the literature on the mechanical and frictional properties of materials [1, 15, 23]. The values of δ can also be determined by the non-destructive method described in [25].

Example 10. Find the rate of wear of an involute teeth gearing which has $z_1 = z_2 = 18$; $m = 6$ mm; $\alpha_w = 20°$; $d_{a1} = d_{a2} = 120$ mm; $d_{b1} = d_{b2} = 101.5$ mm; $a_w = 108$ mm. The lubricant contains abrasive particles ($q_a = 1$ percent) of quartz with $R = 0.03$ mm and $\sigma = 25$ kgf/mm^2. Material: Steel 40X; $HB_1 = HB_2 = 300$—320; $\delta_1 = \delta_2 = 12\%$, $t = 1.5$. The frequency of rotation of the gears is 300 rpm.

Solution: First, we determine the tooth geometric characteristics pertaining to wear resistance, i.e. we calculate χ_1 and χ_2 from the formula (12.3), y_{w1} and y_{w2} from the formula (12.4), and $\bar{y}_w$ (for the pitch-point region) from the formula (12.2).

$$\chi_1 = 1 - \frac{\sqrt{120^2 - 101.5^2}}{2 \times 108 \times 0.342} = 0.142$$

$$\chi_2 = \frac{\sqrt{120^2 - 101.5^2}}{2 \times 108 \times 0.342} = 0.858$$

$$y_{w1} = \sqrt{0.142\,(1-0.142)}\,\frac{0.142-(1-0.142)\,1}{0.142} = 1.78$$

$$y_{w2}=\sqrt{0.858\,(1-0.858)}\,\frac{0.858-(1-0.858)\,1}{0.858}=0.26$$

$$\bar{y}_w=\frac{1.78\left(\frac{1}{1+1}-0.142\right)+0.26\left(0.858-\frac{1}{1+1}\right)}{3\,(0.858-0.142)}=0.34$$

Then, using formula (12.1), we find the rate of abrasive wear for the pinion U_1 by substituting the abrasive action characteristics (q_a, R, σ) into the expression for A, and the physico-mechanical characteristics of the materials (δ_1, t, HB_1, HB_2) into the expression for M_1; the value of K_1 for spur gears we determine from the formula given in the Table 12.10 using the values of m, z_1, z_2, α_w, $y_{w1}=y_{w2}$ (for the pitch-point region), and n_1.

And now

$$U_1=4\times10^2\,\frac{1^{2/3}\,0.03^{0.5}25^{2.5}}{12^{1.5}320^{1.5}320}\,[2\times6\,(18+18)\,0.342]^{0.5}$$
$$\times0.34\times300=3.66\ \mu\text{m/h}$$

12.3. IMPROVING THE WEAR RESISTANCE OF MACHINE PARTS

Resistance to abrasive wear is improved by design measures [22, 27], by reducing abrasive action [22], by selecting suitable materials and methods for their strengthening [1, 11, 20, 22, 26]. To reduce wear due to impactless abrasive action, it is necessary in most cases to provide high strength while retaining an adequate plasticity level [2, 15, 22, 24, 26, 27]. The plasticity of surface layers can be determined by the non-destructive method [25].

Steels are strengthened by hardening with a low-temperature tempering. A greater wear resistance, as compared with conventional hardening is achieved by the use of isothermal treatment [19]. Thermochemical treatment (borating, carburizing, etc.) substantially lowers abrasive wear, but here the depth of the case must be taken into account. The conventional hardening of steel significantly reduces its plasticity. The same hardness with a markedly less pronounced change in plasticity is achieved with the aid of high-temperature thermomechanical treatment, and that results in improved wear resistance as compared with conventional hardening [1, 26, 27].

The high-temperature thermomechanical treatment can be applied to various grades of structural and tool steels. The optimum degree of deformation for such steels amounts to 25-40 percent [1, 26]. Of interest is a high-temperature thermomechanical treatment method that involves the heating of the surface layer up to the decalescence point, its deformation, and immediate hardening.

The improvement in wear resistance provided by high-temperature thermomechanical treatment is particularly pronounced in components operating under light loading conditions (friction against the ground, movable joints, etc.). In the heavier conditions (abra-

sive wear in gases or liquids) this effect is hardly felt at all [1, 22, 26].

The structure of a material has a considerable effect on its resistance to abrasive wear. The role of each alloy constituent can be roughly estimated with the aid of the structural diagram (Fig. 12.5) obtained in wear tests of materials used for press-moulds in production of refractory components [17]. The moulds operate at high contact pressures. The coefficient of structural stability k_s, which indicates how responsive is the structure to the martensitic transformation in the process of wear, and the cementite equivalent R (Fe_3C), which indicates the amount and energy capacity of the carbide phase, can be determined as

$$k_c = 240\ C + 45\ Mn + 35\ Cr + 30\ V + 25\ Mo + 10\ W;$$

$$R\ (Fe_3C) = Fe_3C + 0.13\ Cr_{23}C_6 + 0.7\ Cr_7C_3 + 0.79\ Mn_3C + 1.3\ WC + 1.9\ TiC + 2.0\ NbC + 1.8\ VC$$

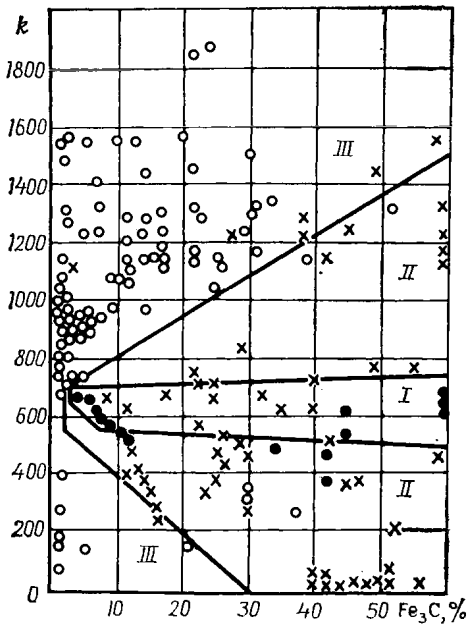

Fig. 12.5. Alloys wear-resistance structural diagram 17]. Wear resistance regions
I—high; *II*—medium; *III*—low

In these equations the chemical symbols designate the percentage of the chemical elements.

According to the diagram of Fig. 12.5, abrasive wear is reduced by those alloy constituents that form carbides of high energy capacity and aid in obtaining an unstable austenitic structure, which turns into a martensitic one during the process of wear. The best wear resistance is exhibited by unstable austenite-carbide and austenite-martensite alloys [2, 17, 22].

Abrasive compositions and stone mouldings (diabase, basalt) provide high resistance to wear in operation without impacts. The costly metal ceramic alloys T5K10, T15K6, T30K4, BK6, BK3 are used under extremely severe operating conditions, where other methods for increasing wear resistance produce no tangible effect. The literature discloses methods for reducing abrasive wear by hard facing [9, 16], electroplating [18], electrical discharge machining and other strengthening techniques [7].

REFERENCES

1. Бернштейн М. Л. Термомеханическая обработка металлов и сплавов, т. II. М., «Металлургия», 1968, 585 с.
2. Богачев И. Н. Кавитационное разрушение и кавитационностойкие сплавы. М., «Металлургия», 1972, 192 с.
3. Боголюбов Б. Н. Долговечность землеройных и дорожных машин. М., «Машиностроение», 1964, 224 с.
4. Богомолов Н. И. Методика и установка для испытаний на абразивное изнашивание.— В сб.: Методы испытания и изнашивание. М., Изд. АН СССР, 1962, с. 12-18.
5. Виноградов Г. В., Вишняков В. А. Абразивный износ при трении качения.—«Известия АН СССР. ОТН. Механика и машиностроение», 1960, № 3, с. 89-98.
6. Виноградов В. Н., Сорокин Г. М., Коротков В. А. Методы испытания на изнашивание при ударе по сыпучему абразиву.—«Заводская лаборатория», 1968, № 6, с. 725-728.
7. Елизаветин М. А., Сатель Э. А. Технологические способы повышения долговечности машин. М., «Машиностроение», 1969, 399 с.
8. Жигаев В. Д. Прочность зерен кварцевого песка.—«Машиноведение», 1971, № 1, с. 11-12.
9. Износостойкость и структура твердых наплавок. М., «Машиностроение», 1971, 95 с. Авт.: Хрущов М. М., Бабичев М. А., Беркович Е. С. и др.
10. Кащеев В. И., Глазков В. М. Изнашивание в потоке движущихся частиц.— В сб.: Методы испытаний на изнашивание. М., Изд-во АН СССР, 1962, с. 24-31.
11. Кащеев В. Н. Абразивное разрушение твердых тел. М., «Наука», 1970, 248 с.
12. Качалов Н. Н. Основы процессов шлифовки и полировки стекла. М., Изд. АН СССР, 1946, 275 с.
13. Козырев С. П. Гидроабразивный износ металлов при кавитации М., «Машиностроение», 1964, 140 с.
14. Клейс И. Р. О некоторых закономерностях ударного изнашивания.— «Вестник машиностроения», 1967, № 8, с. 52-54.
15. Крагельский И. В. Трение и износ. М., «Машиностроение», 1968, 420 с.
16. Лившиц Л. С., Гринберг Н. А., Куркумели Э. Г. Основы легирования наплавленного металла. М., «Машиностроение», 1969, 187 с.
17. Попов В. С., Брыков Н. Н., Дмитриченко Н. С. Износостойкость пресс-форм огнеупорного производства. М., «Металлургия», 1971, 160 с.
18. Прогрессивные методы термической и химико-термической обработки. Под ред. Ю. М. Лахтина и Я. Д. Когана. М., «Машиностроение», 1972, 268 с.
19. Серпик Н. М., Кантор М. М. Исследование изнашивания сталей при трении в свободном абразиве.— В сб.: Износ и трение металлов и пластмасс. М., «Наука», 1964, с. 29-52.
20. Сорокин Г. М. Влияние механических характеристик стали на ее абразивную износостойкость.—«Вестник машиностроения», 1975, № 5, с. 35-38.
21. Ткачев В. Н. Износ и повышение долговечности деталей сельскохозяйственных машин. М., «Машиностроение», 1971, 264 с.
22. Тененбаум М. М. Сопротивление абразивному изнашиванию. М., «Машиностроение», 1975, 271 с.
23. Харач Г. М. Элементы расчета деталей на изнашивание.— В сб.: Износостойкость. М., «Наука», 1975, с. 91-111.
24. Хрущов М. М., Бабичев М. А. Абразивное изнашивание. М., «Наука», 1970, 272 с.
25. Южаков И. В., Ямпольский Г. Я., Калугин Ю. К. Способ контроля качества поверхностных слоев деталей строительных и дорожных машин. Укр. НИИНТИ. Информационный листок № 220, сер. «Дорожное строительство», Харьков, ХПТИ, 1975, 4 с.

26. Южаков И. В., Надточиев А. Б., Андреев Ю. А. Термомеханическое упрочнение режущих органов дорожных машин.— «Строительные и дорожные машины», 1975, № 12, с. 28-29.
27. Ямпольский Г. Я., Крагельский И. В. Исследование абразивного износа элементов пар трения качения. М., «Наука», 1973, 63 с.
28. Avery H. S. Wear resistance. Handbook of mechanical wear, Ann. Arbor. The University of Michigan Press, 1961, p. 17-21.
29. Normann T.E. Abrasive wear of metals. Handbook of mechanical wear. Ann. Arbor. The University of Michigan Press, 1961, p. 17-21.
30. Stauffer W. A. Verschleiß durch sand haltiges Wasser in hydraulischen Anlagen. "Schweizer Archiv für Angewandte Wissenschaft und Technik". Bd. 24, No. 7-8. 1958, S. 218-223, S. 248-263.
31. Wellinger K. und Uetz H. Gleit-Spül-und Strahlverschleiß-Prüfung. "Wear", vol. 1, No. 3, 1957.
32. Siebel E. Handbuch der Werkstoffprüfung. Bd. 2, Berlin, 1955, S. 12-18.

Chapter 13

FRICTION IN VACUUM

13.1. BASIC INFORMATION

In vacuum, operating conditions for rubbing components are mainly characterized by a low rate of regeneration of oxide and adsorption films on their surfaces, and also by a retarded removal of heat from the joint. Depending on the degree of vacuum, these processes run with different intensity. The degree of vacuum or condition of a rarefied gas are distinguished depending on the ratio $\frac{\lambda}{d}$, where λ is the average distance that a gas molecule travels freely between two collisions with other molecules, and d is the molecule size.

Table 13.1

Degrees of vacuum (pressure ranges) [9]

Vacuum		Low $\frac{\lambda}{d} \leqslant 1$	Medium $\frac{\lambda}{d} \approx 1$	High $\frac{\lambda}{d} \gg 1$	Ultra-high
Pressure range	Pa	> 100	$100\text{-}10^{-1}$	$10^{-1}\text{-}10^{-5}$	$< 10^{-5}$
	mm Hg (approximately)	> 1	$1\text{-}10^{-3}$	$10^{-3}\text{-}10^{-7}$	$< 10^{-7}$

Table 13.1 gives four degrees of vacuum relative to $\frac{\lambda}{d}$, each being characterized by a particular pressure range. The lower the pressure, the harder it is to achieve the respective degree of vacuum, and the stricter are the requirements on rubbing components for these conditions.

Various processes in vacuum are considerably influenced by the hydrocarbon compounds, and for this reason there is a tendency to distinguish between "oil" vacuum and "oilless" vacuum. The former is mainly characterized by the presence of the residual gases of hydrocarbon compounds, and the latter, by their absence.

Table 13.2

Main specifications of vacuum pumps

Type of pump	Pressure, Pa		Pump speed l/s
	full	residual	
Steam	100-665 ($\sim$ 10-50)	–	0.1-300
Oil-sealed pumps:			
one-stage	2-6.6 ($1.5 \cdot 10^{-2}$-$5 \cdot 10^{-2}$)	0.27-0.66 ($2 \cdot 10^{-3}$-$5 \cdot 10^{-3}$)	0.5-500
two-stage	0.66-2 ($5 \cdot 10^{-3}$-$1.5 \cdot 10^{-2}$)	10^{-3}-$6.6 \cdot 10^{-2}$ ($1 \cdot 10^{-5}$-$5 \cdot 10^{-4}$)	0.2-50
Double-rotor pumps:			
one-stage	0.66 ($5 \cdot 10^{-3}$)	$6.6 \cdot 10^{-2}$ ($5 \cdot 10^{-4}$)	$15\text{-}4 \cdot 10^{4}$
two-stage	10^{-3}-10^{-2} ($\sim 10^{-5}$-10^{-4})	10^{-4}-10^{-3} ($\sim 10^{-6}$-10^{-5})	5-50
Diffusion pumps, oil-filled:			
high-vacuum	$6.6 \cdot 10^{-4}$ ($\sim 5 \cdot 10^{-6}$)	$6.6 \cdot 10^{-5}$ ($\sim 5 \cdot 10^{-7}$)	$5\text{-}2 \cdot 10^{5}$
ultra-high vacuum	$6.6 \cdot 10^{-7}$ ($\sim 5 \cdot 10^{-9}$)	10^{-9} ($\sim 10^{-11}$)	$100\text{-}2 \cdot 10^{5}$
Turbomolecular pumps	—	10^{-7}-10^{-9} ($\sim 10^{-9}$-10^{-11})	$50\text{-}10^{4}$
Sorption pumps:			
adsorption type	—	10^{-1}-10^{-3} ($\sim 10^{-3}$-10^{-5})	1-10
evaporation type	—	10^{-7}-10^{-11} ($\sim 10^{-9}$-10^{-13})	$2\text{-}2 \cdot 10^{4}$
getter pumps:			
ion-getter type	—	$\sim 10^{-7}$-10^{-11} (10^{-9}-10^{-13})	$2\text{-}5 \cdot 10^{4}$
magnetic discharge type	—	10^{-7}-10^{-9} ($\sim 10^{-9}$-10^{-11})	$2\text{-}10^{4}$
Cryogenic pumps:			
condensation type	—	10^{-7}-10^{-9} ($\sim 10^{-9}$-10^{-11})	$50\text{-}10^{5}$
cryosorption type	—	10^{-10}-10^{-13} ($\sim 10^{-12}$-10^{-15})	$500\text{-}10^{5}$

Notes: 1. Omission in the table signifies that this parameter is not specified.
2. With the elements of sorption and cryogenic type pumps placed on the walls of the vessel being exhausted, the pump speed may reach millions of litres per second.
3. Given in parentheses are pressure values in mm Hg.

The degrees of vacuum defined in Table 13.1 can be obtained using vacuum pumps specified in Fig. 13.1. The main specifications of vacuum pumps suitable for use in friction studies are given in Table 13.2.

In oil-sealed pumps, double-rotor pumps, turbomolecular pumps and diffusion oil-filling pumps extensive use is made of vacuum oils. An oil for use in vacuum must comply with definite requirements

Table 13.3

Some specifications of vacuum oils produced in USSR [9]

Oil type	Application	Molecular mass	Density, kg/m³	Vapour pressure at 20°C, Pa	Residual pressure of steam pump, Pa	Kinematic viscosity at 50°C, 10^{-6} m²/s	Heat of steam, J/K mol
Mineral oils:							
BM-1	Diffusion pumps	450	870	$5.3\cdot10^{-6}$-$2.66\cdot10^{-7}$ ($4\cdot10^{-8}$-$2\cdot10^{-9}$)	$2.7\cdot10^{-4}$ ($2\cdot10^{-6}$)	65-69	$1.15\cdot10^{5}$
BM-2	The same	450	870	$5.3\cdot10^{-6}$-$2.66\cdot10^{-7}$ ($4\cdot10^{-8}$-$2\cdot10^{-9}$)	$\leqslant 4.6\cdot10^{-4}$ $\leqslant 3.5\cdot10^{-6}$	65-69	$1.15\cdot10^{5}$
BM-3	Booster pumps	—	850	$1.3\cdot10^{-2}$-$1.3\cdot10^{-3}$ ($1\cdot10^{-4}$-$1\cdot10^{-5}$)		7-10	$1.13\cdot10^{5}$
BM-4	Mechanical pumps	—	—	$6.6\cdot10^{-4}$-$1.3\cdot10^{-3}$ ($5\cdot10^{-6}$-$1\cdot10^{-5}$)	— —	47-57	—
BM-5	Diffusion pumps	450	870	$1.3\cdot10^{-6}$-$1.3\cdot10^{-7}$ ($1\cdot10^{-8}$-$1\cdot10^{-9}$)	$1.3\cdot10^{-6}$ ($1\cdot10^{-8}$)	—	—
BM-6	Mechanical pumps	—	—	$1.3\cdot10^{-6}$-$4\cdot10^{-5}$ ($1\cdot10^{-8}$-$3\cdot10^{-7}$)	—	30-40	—
BM-7	Diffusion pumps	—	—	$\leqslant 4\cdot10^{-6}$ ($\leqslant 3\cdot10^{-8}$)	$\leqslant 1.3\cdot10^{-4}$ ($\leqslant 1\cdot10^{-6}$)	80-95	—
Г	Booster pumps	350	850	$6.6\cdot10^{-3}$-$1.3\cdot10^{-4}$ ($5\cdot10^{-5}$-$1\cdot10^{-6}$)	—	12.5-15.3	$1\cdot10^{5}$
TM-1	Turbomolecular pumps	—	-	$8.8\cdot10^{-3}$ ($6.6\cdot10^{-5}$)	—	6-9	—
Esters:							
grade ОФ	Diffusion pumps	390	980	$1.3\cdot10^{-5}$ ($1\cdot10^{-7}$)	$\leqslant 1.3\cdot10^{-4}$ ($\leqslant 1\cdot10^{-6}$)	—	—
grade ОС	The same	426	910	$\leqslant 2.7\cdot10^{-6}$ ($\leqslant 2\cdot10^{-8}$)	$\leqslant 1.3\cdot10^{-4}$ ($\leqslant 1\cdot10^{-6}$)	8.5	—
5Ф4Э	The same	446	1200	$1.3\cdot10^{-9}$ (10^{-11})	$\leqslant 9.3\cdot10^{-7}$ ($\leqslant 7\cdot10^{-9}$)	130	—
Organosilicon oils:							
ПЭС-В-1 (ВКЖ-94А)	The same	700	970	$\leqslant 6.6\cdot10^{-6}$ ($\leqslant 5\cdot10^{-8}$)	$2.7\cdot10^{-4}$ ($2\cdot10^{-6}$)	16-33	$1.19\cdot10^{5}$
ПЭС-В-2 (ВКЖ-94Б)	The same	700	970	$1.3\cdot10^{-6}$-$1.3\cdot10^{-4}$ ($1\cdot10^{-8}$-$1\cdot10^{-6}$)	$4\cdot10^{-4}$-$1.3\cdot10^{-3}$ ($3\cdot10^{-6}$-$1\cdot10^{-5}$)	16-33	—
ПФМС-1	Booster pumps	700	1000	$1.3\cdot10^{-3}$-$9\cdot10^{-3}$ ($1\cdot10^{-5}$-$7\cdot10^{-5}$)	—	3.6-4.6	$1.13\cdot10^{5}$
ПФМС-2/5л	Diffusion pumps	700	1050-1070	$6.6\cdot10^{-7}$-$9\cdot10^{-5}$	$2.7\cdot10^{-4}$ ($2\cdot10^{-6}$)	8-13	$1.24\cdot10^{5}$
ФМ-1	he same	546.9	1096	($5\cdot10^{-9}$-$7\cdot10^{-7}$) $1.3\cdot10^{-8}$ (10^{-10})	$1.3\cdot10^{-7}$-$1.0\cdot10^{-6}$ ((1-8)$\cdot10^{-9}$)	35-37	—

Note: Given in parentheses are pressure values in mm Hg.

(the specified kinematic viscosity, evaporation heat, etc.), the principal one being a low vapour pressure. The main specifications of vacuum oils are given in Table 13.3. These oils can be used for lubrication of mechanisms operating under specific vacuum conditions.

The drawback to most of the pumps mentioned above is that oil vapours may get into the vacuum chamber.

Among sorption pumps, the most promising for obtaining ultra-high vacuum, are magnetic-discharge pumps. These are convenient to use for studies of friction in joints with low gassing. Pumps of

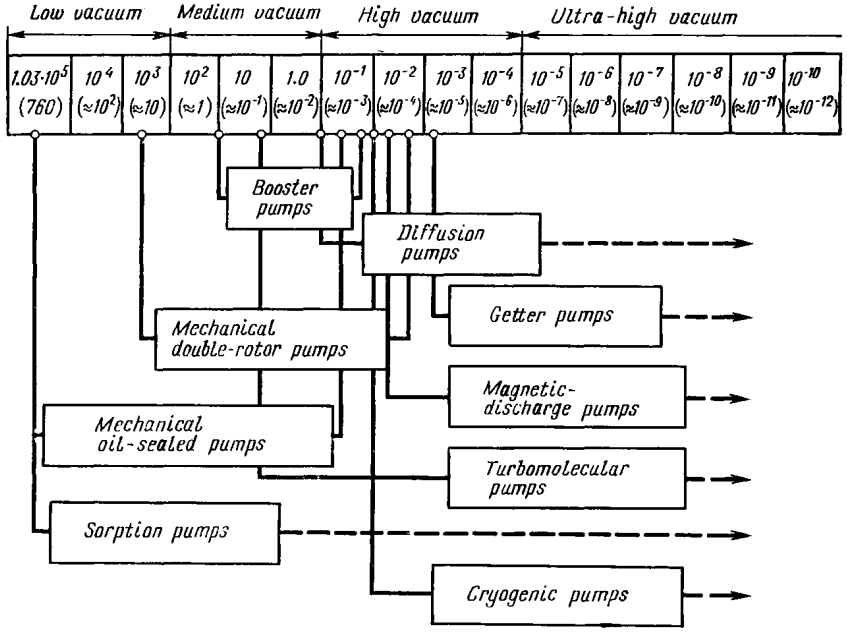

Fig. 13.1. Degrees of vacuum and respective types of vacuum pumps. Given in parentheses are pressures in mm Hg, other values, in Pa

this type are simple and dependable, provide quiet operation, a long service life ($\sim 10^4$ hours) and a high starting pressure (10^{-2} mm Hg), which allows them to be used in combination with adsorption pumps.

Research into the frictional behavior of tribological joints with high gassing in ultra-high vacuum is expedient to carry out using cryogenic pumps.

The main advantage of cryogenic pumps is the speed of evacuation. That makes it possible to achieve ultra-high vacuum without warming-up of the pumping installation and to use rubber seals in separable joints.

13.2. REQUIREMENTS FOR RUBBING COMPONENTS

Distinction should be made between requirements placed on the rubbing components functioning in the vacuum of outer space and those placed on such components functioning in the vacuum created by vacuum pumps in the sealed chambers of vacuum equipment.

This distinction primarily stems from the fact, that the outer space can be regarded as an "ideal pump" with unlimited speed of evacuation, whereas this speed in vacuum pumps is limited. In addition, requirements for space applications are determined by specific operating conditions, such as various radiations, ultra-low or ultra-high temperatures, etc.

Requirements for the rubbing components of vacuum equipment are formulated with regard to the fact that it is difficult to obtain and keep vacuum, especially high and ultra-high, and that the vacuum pumps and control equipment are very costly.

These requirements can be classified into those on the materials, construction, and operational conditions.

Materials. Materials used in tribological joints of vacuum equipment should have the minimal gassing and porosity, low vapour pressure, high thermal stability and resistance to corrosion.

Gassing. In vacuum, materials and workparts release considerable amounts of gases and vapours present on their surfaces and inside. The amount and composition of the gases depend on the past of the materials. Gases can be absorbed by the material during its processing and contact with the environment. In order to assess the overall flow of outgoing gases it is necessary to know the specific gassing rate for a given material. This is the amount of gas liberated from a unit surface area or mass per unit time. The specific gassing rate is usually expressed in 1 mm Hg/cm^2·s. Values of this rate for various materials are given in Table 13.4 [9].

It should be noted that for the same material different sources may cite widely differing values of the specific gassing rate because of different methods of its measurement.

The overall flow Q of gases from the walls of a joint can be determined by the formula $Q = qA$, where q = specific outgassing rate; A = surface area exposed to vacuum.

If a sliding pair is made of different materials, the overall flow comprises the flows from each material. Account must also be taken of increased gassing from the walls of a joint periodically exposed to the air and of the influence of preliminary treatment of the surface (etching, electrical polishing, degassing, etc.). On the basis of specific gassing rates, it is possible to evaluate the range of pressure in which a given material is expedient to use for a tribological unit of vacuum equipment, and the cost of evacuation. As an example, Table 13.5 presents the rate of evacuation provided by a vacuum pump to ensure pressure p in a sealed vacuum chamber where various

Table 13.4

Rate of specific gassing from metal surfaces at room temperature

Material	Preliminary treatment	Specific gassing rate		Time of evacuation before measurement, h
		$m^3 \cdot Pa/(m^2 \cdot s)$	$\frac{l \cdot mm\ Hg}{(cm^2 \cdot s)}$	
Low-carbon steel	—	$4.1 \cdot 10^{-4}$ $7.3 \cdot 10^{-5}$	$3.09 \cdot 10^{-7}$ $5.5 \cdot 10^{-8}$	1 6
	Annealed in vacuum at 420°C	$1.2 \cdot 10^{-8}$-$4 \cdot 10^{-8}$	$9 \cdot 10^{-12}$-$3 \cdot 10^{-13}$	Practically constant
Stainless steel	—	$2.4 \cdot 10^{-4}$ $4.1 \cdot 10^{-5}$	$1.8 \cdot 10^{-7}$ $3.09 \cdot 10^{-8}$	1 6
	Untreated	$1.7 \cdot 10^{-4}$ $2.0 \cdot 10^{-5}$	$1.27 \cdot 10^{-7}$ $1.48 \cdot 10^{-8}$	1 5
	Annealed in vacuum at 400°C	$1.2 \cdot 10^{-8}$-$4 \cdot 10^{-10}$	$9 \cdot 10^{-12}$-$3 \cdot 10^{-13}$	Practically constant
Copper	Untreated	$1.97 \cdot 10^{-4}$ $6.45 \cdot 10^{-5}$	$1.48 \cdot 10^{-7}$ $4.85 \cdot 10^{-8}$	1 5
	Annealed in vacuum at 400°C	$9.3 \cdot 10^{-9}$ $1.07 \cdot 10^{-10}$	$7 \cdot 10^{-12}$-$8 \cdot 10^{-14}$	Practically constant
Brass	Etched, cleaned in benzol and acetone	$1.97 \cdot 10^{-5}$ $1.54 \cdot 10^{-6}$	$1.48 \cdot 10^{-8}$ $1.16 \cdot 10^{-9}$	1 5
	Cleaned in benzol and acetone	$2.24 \cdot 10^{-4}$ $9.0 \cdot 10^{-5}$	$1.69 \cdot 10^{-7}$ $6.75 \cdot 10^{-8}$	1 5
	Untreated	$3.38 \cdot 10^{-4}$ $1.21 \cdot 10^{-4}$	$2.54 \cdot 10^{-7}$ $9.1 \cdot 10^{-8}$	1 5
Duralumin	Etched, cleaned in benzol and acetone	$4.77 \cdot 10^{-5}$ $3.92 \cdot 10^{-6}$	$3.59 \cdot 10^{-8}$ $2.95 \cdot 10^{-9}$	1 5
	Cleaned in benzol and acetone	$2.82 \cdot 10^{-4}$ $1.41 \cdot 10^{-4}$	$2.12 \cdot 10^{-7}$ $1.06 \cdot 10^{-7}$	1 5
	Untreated	$5.64 \cdot 10^{-4}$ $1.92 \cdot 10^{-4}$	$4.24 \cdot 10^{-7}$ $1.44 \cdot 10^{-7}$	1 5
Aluminium Nickel Molybdenum Tantalum Tungsten	—	$(4\text{-}9) \cdot 10^{-6}$ $(7\text{-}8) \cdot 10^{-6}$ $(4.5\text{-}8.5) \cdot 10^{-6}$ $6.0 \cdot 10^{-6}$ $1.3 \cdot 10^{-6}$	$(3\text{-}7) \cdot 10^{-9}$ $(5\text{-}6) \cdot 10^{-9}$ $(3.5\text{-}6.5) \cdot 10^{-9}$ $4.5 \cdot 10^{-9}$ $1 \cdot 10^{-9}$	2

materials, with a total surface area of 1 cm^2 are placed. The gassing rate for plexiglass, Teflon*, stainless steel, and stainless steel annealed at 400°C in vacuum was taken to be 4×10^{-4}; 3×10^{-7}; 2×10^{-7}; and $9 \cdot 10^{-12}$ l·mm Hg/(cm^2·s), respectively. As seen from

Table 13.5

Pump speed required for exhausting various materials with total surface area of 1 cm^2 to pressure p

Pressure in vacuum chamber mm Hg	Pump speed, l/s, for materials			
	plexiglass	Teflon	stainless steel	stainless steel heated in vacuum at 400°C
10^{-6}	$4 \cdot 10^2$	$3 \cdot 10^{-1}$	$2 \cdot 10^{-1}$	$9 \cdot 10^{-6}$
10^{-7}	$4 \cdot 10^3$	3	2	$9 \cdot 10^{-5}$
10^{-8}	$4 \cdot 10^4$	$3 \cdot 10$	$2 \cdot 10$	$9 \cdot 10^{-4}$
10^{-9}	$4 \cdot 10^5$	$3 \cdot 10^2$	$2 \cdot 10^2$	$9 \cdot 10^{-3}$

Table 13.5, with a plexiglass specimen having a surface area of 1 cm^2, a pump speed of 400 l/s is required for evacuation to a pressure of 10^{-6} mm Hg. To provide this speed, it would take two high-vacuum "oil"-type pumping installations BA-05-4. With the "oilless" method, two turbomolecular pumps TMH-200 or two magnetic-discharge pumps NORD-250 would have to be used, the cost of each of these units being four to six times that of the BA-05-4.

Gas emission from solid lubricants. The principal characteristics of solid lubricants to be used in vacuum are the rate of specific gassing and the chemical composition. Oil and grease are disqualified for use in most vacuum applications for their chemical composition and relatively high rate of gassing.

A low gassing rate typical of solid lubricants allows them to be used in high and ultra-high vacuum at high temperatures.

Under these conditions the rubbing surfaces are gradually cleaned of films through gassing and friction, and that facilitates interaction between the juvenile metal surface and vapours released by the solid lubricant. Such an interaction is provided by sulphur, selenium, and hydrogen. In some cases this effect reduces friction and wear, in others it may lead to embrittlement of the surface layer and increased wear.

Figure 13.2 shows gas-emission curves for some solid lubricants and self-lubricating materials [14]. Tungsten and niobium diselenides not only give off the smallest amounts of gases but also provide the best thermal stability among the other solid lubricants.

Gas emission in friction. Various kinds of mechanical interaction between solids in vacuum, including friction, increase gassing and, consequently, pressure, and change the composition of the

* Trade name.—*Tr.*

residual gaseous medium in the vacuum chamber. The charts in Fig. 13.3 indicate that gassing during friction is unstable [14]. Three stages can be distinguished on the charts: the initial, where gassing gradually mounts; the transitional, where gassing shows sharp variations; and the steady-gassing stage.

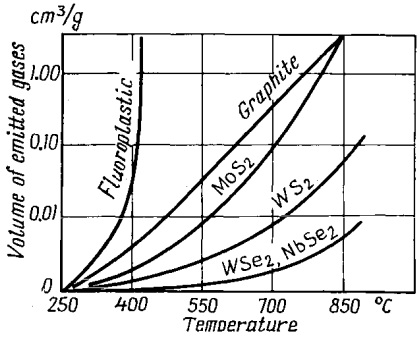

Fig. 13.2. Gag-emission characteristics of lubricants in a vacuum of 10^{-6} mm Hg

The friction force chart is similar in character to the gassing chart, i.e. it also has three stages: the initial, where the friction force shows a gradual rise; the transitional, where the friction force has sharp variations; and the stable-friction stage. The wear of the rubbing surfaces increases as the process proceeds to the third stage. Comparison of the actual wear observed on the rubbing surfaces with the character of the charts allows the conclusion that the initial stage involves gradual wear of protective oxide films on the metal surface. The wear and destruction of the films lead to an increase in the rate of gas flow from the metal and in the friction force and wear.

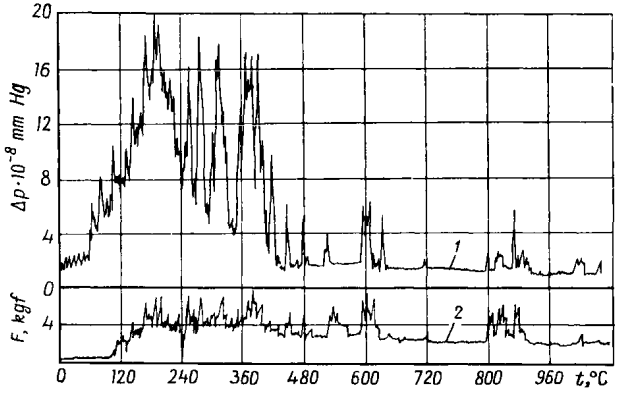

Fig. 13.3. Gassing in friction of steel Grade 45 (sliding speed 0.24 m/s, vacuum 10^{-7} mm Hg)

1—variation of hydrogen mass-spectrum peak height in time; *2*—variation of friction force

Gassing from molybdenum disulphide as varied with frictional temperature can be observed in metal-ceramic materials having a layer of this solid lubricant. The latter (MoS_2) is contained by the metal-ceramic base in "pure" form, i.e. without any binder (be-

cause the materials used as binders usually give off great amounts of gas and have a complex spectrum).

Figure 13.4 depicts the effect of temperature on the average residual pressure p (ϑ), the coefficient of friction in high vacuum, and the partial pressure measured when the rubbing elements are in relative motion or at rest. Temperatures near the sliding interface are plotted on the axis of abscissas; along the axis of ordinates are plotted: on the right—the friction coefficient, on the left—the mean residual pressure and the height of the mass-spectrum peak (A), which characterizes the partial pressure of individual components of the residual gases.

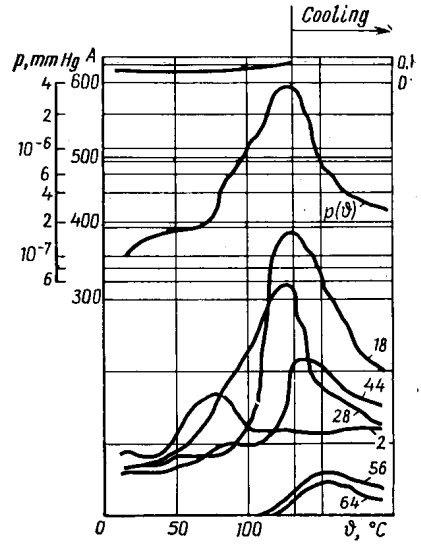

Fig. 13.4. Variation of friction coefficient, gas flow and gas composition with temperature in friction of metal-ceramic materials with a layer of MoS_2

As seen from the graphs of Fig. 13.4, friction is accompanied with gas emission. The spectrum of the gases is defined by masses 2, 18, 28, and 44, corresponding to H_2, H_2O, $N_2 + CO$, and CO_2. These gases are absorbed within the bulk and on the surface of the specimens while they are held in air. As the frictional temperature rises on the surface of the specimen, it gives off more gases, generally through water evaporation. The spectrum also shows mass 64, which represents sulphurous-acid anhydride SO_2. As is known, MoS_2 readily and quickly oxidizes in air in the presence of water vapours.

In the course of friction the previously formed sulphur oxide is liberated. It has been found that during the initial stage of heating of a non-degassed material, the peak of mass 64 rises to the point corresponding to 300°C. As heating continues, the peak of mass 64 drops to the initial value, but at 800°C it quickly rises again. Here, however, the peak goes up because MoS_2 begins dissociating into sulphur and molybdenum.

A study into the combined effect of friction and ultra-high vacuum on gas emission from Teflon filled with 25 percent black soot was reported in [26]. Here, the vapours were analyzed for chemical composition (Table 13.6) and for the kinetics of their adsorption and condensation, with pressure changes recorded during the process.

All molecular masses observed during the friction of Teflon can be ascribed to the fragments of Teflon molecules; it was found that mass 69 (CF_3) lasted longer by an order of magnitude than the other masses. Calculation of the speed and the time of formation of a

Table 13.6

Composition of gases emitted in friction of Teflon

Molecular mass	Emission peak height in relative units	Composition	Molecular mass	Emission peak height in relative units	Composition
31	6.0	CF	69	2.5	CF_3
50	1.5	CF_2	81	0.2	C_2F_3
51	0.5	HCF_2	100	0.3	C_2F_4
62	0.7	C_2F_2			

monolayer of gas molecules indicates that such a layer forms in one hour at a distance of 10 cm from a Teflon bearing during friction at a sliding speed of 60 cm/s. Contaminant films with a thickness smaller than that of a single monolayer can bring about considerable changes in the physical properties of the surface of a solid. For this reason Teflon, despite its excellent lubricity, cannot be used in high vacuum in the proximity of cooled surfaces sensitive to contamination.

The mass-spectrometry of gases emitted by solid lubricant coatings indicates that in friction the latter give off specific decomposition products which result from thermomechanical destruction of the coating material.

Porosity. Porous materials are not recommended for use in vacuum. They readily absorb liquids used for cleaning the rubbing components to be placed into a vacuum chamber. These liquids may contain various impurities dissolved in the process of this indispensable operation. The impurities stay in the pores and comprise a source of gas emission. In addition, porous materials adsorb gases at atmospheric pressure and then gradually liberate them during evacuation. As a rule, porous materials can be used in low and medium vacuum, but not in high vacuum.

Vapour pressure. A principal characteristic of materials that determines the possibility of their use in vacuum is the pressure of vapours at the maximum temperature occurring during their service or heating for degassing. According to reference [1] this pressure must be lower by two to three orders of magnitude than the residual pressure within the vacuum installation. The vapour pressure determines the rate of evaporation of a material, which can be found from the formula [5]

$$W = 5.833 \times 10^{-2} p \sqrt{\frac{M}{\vartheta}}$$

where W = rate of evaporation, g/cm^2·s; p = vapour pressure, mm Hg; M = molecular mass, g/mol; ϑ = temperature, K.

The evaporation of the material and its condensing on the walls of the components of vacuum equipment may damage the electrical insulators, observation windows and reflectors. It must be borne in

mind that the firmly bound constituents of alloys evaporate in vacuum as well as pure metals.

Thus, for instance, zinc can be almost fully vaporized from brass by prolonged heating in high vacuum. Such metals as Cd, Zn, Mg, Bi, Sb, featuring high-pressure evaporation at the heating temperatures typical of high-vacuum installations, are not recommended for tribological units in vacuum applications. Vapour pressures for various metals at different temperatures are given in Table 13.7.

Table 13.7

Metal vapours pressure (mm Hg) at different temperatures (°C)

Metal	Melting temperature, °C	Pressure, mm Hg							
		10^{-7}	10^{-6}	10^{-5}	10^{-4}	10^{-3}	10^{-2}	10^{-1}	10^{0}
Bi	271	(350)	(400)	474	536	609	698	802	934
Cd	321	(95)	(120)	148	180	220	264	321	—
P	—	—	—	—	—	—	(195)	(220)	(270)
Pb	328	(360)	(420)	483	548	625	718	832	975
Sn	232	(640)	(730)	823	922	1042	1189	1373	1609
In	157	(520)	(590)	667	746	840	952	1088	1260
Sb	630	(340)	(395)	466	525	595	678	779	904
Zn	419	(140)	(175)	211	248	292	343	405	—
B	2027	—	—	1687	1827	1977	2157	2377	2657
Ti	1800	—	—	1321	1431	1558	1703	1877	2083
V	1857	—	—	1432	1551	1687	1847	2037	2287
Cr	1903	—	—	1062	1162	1267	1392	1557	1737
Co	1495	—	—	1162	1262	1377	1517	1697	1907
Ni	1452	—	—	1142	1247	1357	1497	1667	1887
Cu	1084	—	—	942	1032	1142	1272	1427	1622
Ga	37	—	—	757	842	937	1057	1197	1372
Mo	2577	—	—	1987	2167	2377	2627	2927	3297
Ag	961	—	—	757	832	922	1032	1167	1337

Note. Figures in parentheses are obtained by extrapolation.

Thermal stability. Materials for the rubbing components to be used in high-vacuum applications should possess thermal stability, i.e. the ability to stand repeated heating to high temperatures. Vacuum installations are heated at a pressure from 10^{-3} to 10^{-6} mm Hg to reduce the emission of gases from the materials. The heating temperature may be as high as 450°C, the duration of heating being up to 50 hours. To obtain ultra-high vacuum, the heating is done after each exposure of the vacuum chamber to the air at atmospheric pressure.

Corrosion resistance. Rubbing components for use in high vacuum and, particularly, in ultra-high vacuum are expedient to manufacture from materials with improved corrosion resistance, because such materials feature low gas emission.

When materials are intended for use in space applications, they must also be resistant to the action of factors typical of the space environment (various kinds of radiation, meteoric particles, etc.). In recent years, solid lubricants, self-lubricating materials, and metals with a low shear strength have found extensive application in mechanical engineering and instrument making. This is a new class of materials which provide low friction and wear without fluid lubricants and greases (see Chapter 9).

Design requirements for tribological units. The design of a tribological unit intended for use in vacuum should meet the following requirements:

—the unit should be easy to mount and dismantle, its elements should be easily accessible for cleaning;

—it should preferably have no hard-to-exhaust chambers connected with the main vacuum volume, since these involve a significant increase in the time required to obtain a specified degree of vacuum, and sometimes make this vacuum impossible to achieve;

—it should give off the minimum flow of gases in operation as well as in its stationary condition;

—it should provide high reliability, since its failure may not only result in the irreparable damage to the workpiece or material but also involve downtime of costly vacuum equipment;

—its gases should comply in composition with the residual gases permissible for vacuum installations.

The latter requirement is particularly important in some manufacturing processes and scientific experiments. For instance, the ingress of hydrocarbons into electrovacuum instruments in the process of evacuation results in unstable functioning of the cathodes, in shorter life and in reduced reliability of the instrument. Hydrocarbons are also impermissible in experimental studies of nuclear reactions and various physical phenomena occurring on the surface of solids.

The main requirements placed on vacuum processing conditions are as follows [3].

(1) The rooms where vacuum tribological units are manufactured must be free of suspended particles (dust, soot, etc.) or vapours of oils, acids, alcalis or other chemicals and volatile fluids in the air.

(2) All machined or otherwise processed components must be carefully cleaned of impurities (chips, oil, paint, oxide films, etc.).

(3) Before final assembly, all the components must be degreased. The degreasing procedure to be used is as follows:

(a) rinsing in benzine Б-70 at least twice, each time changing it, until the used benzine contains no impurities. Its cleanness can be checked by applying a drop on a piece of filter paper. Clean benzine should leave no greasy spots on the paper;

(b) drying at 80 to 100°C in a drying chamber or by blasting with hot cleaned air until the smell of benzine has vanished.

(4) Assembly should be carried out in gloves made of napless fabrics.

(5) Assembled units must be mounted into vacuum equipment as soon as possible. When prolonged storage is required, the units are advisable to place into special vacuum containers.

13.3. STATIC FRICTION

13.3.1. Advantages of Tribological Joints with Static Friction

Owing to small displacements in joints with static friction, their heat generation, wear, and, what is particularly important, gas emission are negligible.

Units of this type for operation in the static friction regime in vacuum without lubrication were initially used in mechanisms for transmitting intermittent motion from the atmosphere into vacuum [4]. The static friction regime is effected as the elements of the tribological unit move along a closed path and interact in a definite sequence. The motion diagram for such a unit is shown in Fig 13.5. A driving element *1* (a grip) moves from the initial position *I* into position *II* where it clamps the driven element *2* (a rack) and moves with it into position *III*, thereby providing feed motion. In the positions *II* and *III* the elements form a tribological unit where static friction takes place. The driving element *1* is then retracted into an intermediate position *IV* and brought back to the initial position *I*, and after that the cycle is repeated.

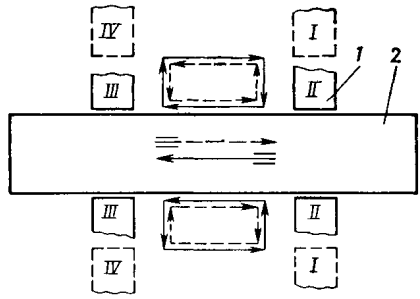

Fig. 13.5. Principle of an intermittent motion mechanism
1—driving element (clamp); *2*—driven element (rack)

This mode of operation provides high reliability without lubrication in an ultra-high vacuum (up to $5 \cdot 10^{-12}$ mm Hg) and heating up to 500°C for degassing.

13.3.2. Determining the Coefficient of Static Friction

The installation whose general layout is shown in Fig. 13.6 allows investigation into static friction in a vacuum created by the "oil" (up to $5 \cdot 10^{-7}$ mm Hg) or "oilless" (up to $5 \cdot 10^{-10}$ mm Hg) methods of evacuation, at atmospheric or higher (up to 5 atm) pressure in inert

or some other gases with controlled chemical composition, and also at elevated temperatures (up to 450°C). The specimens can be made of materials with different physical and mechanical properties and can have different shapes (sphere against flat surface, cylinder

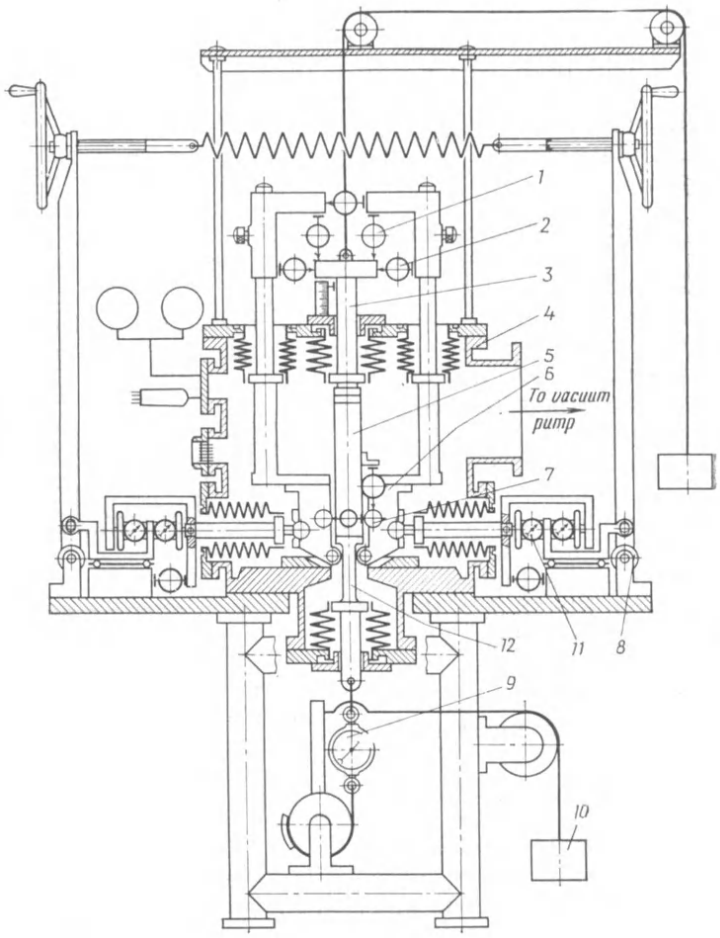

Fig. 13.6. Schematic diagram of a high-vacuum apparatus for studying static friction

1—tangential displacement sensor; *2*—indentation sensor; *3*—measuring rod; *4*—vacuum chamber; *5*, *7*—specimens under test; *6*—pivoting member; *8*—normal-load application mechanism; *9*—dynamometer; *10*—weight; *11*—dynamometer; *12*—tangential-load application mechanism

against cylinder, cylinder against flat surface). A specimen *5* is at one end connected to the tangential loading mechanism, which applies a load of 1,000 kgf, and at the other to the measuring rod *3*, which contacts the measuring tips of a tangential displacement sensor *1* and an indentation sensor *2*.

Table 13.8

Values of friction parameters τ_0 and β for steel grade 12X18H10T in combination with other steels in vacuum

Steel grade	Pressure, mm Hg	Evacuation method	Temperature, °C	τ_0, kgf/mm²	β
P9	$5 \cdot 10^{-6}$	Oil type	20	6.43	0.232
У7				2.54	0.32
40X13				3.95	0.26
ШХ15	$5 \cdot 10^{-3}$	Oilless type		5.75	0.156
P9	$5 \cdot 10^{-9}$			9.65	0.575
P9	$3 \cdot 10^{-7}$		200	9.65	0.545

To obtain the values of the friction parameters τ_0 and β in the formula for calculating f (cf. Chapter 2), each shape combination of

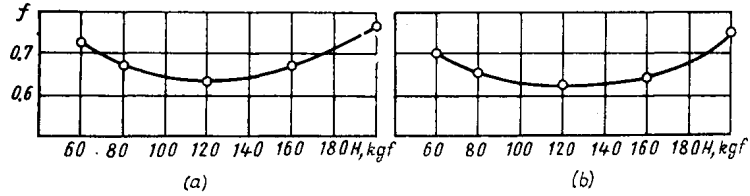

Fig. 13.7. Relation between static friction coefficient (f) and normal load (N) for a stainless steel 12X18H10T/steel P9 combination in "oilless" vacuum at different temperatures:
(*a*) ultra-high vacuum ($5 \cdot 10^{-9}$ mm Hg) at normal temperature (20°C); (*b*) high vacuum ($3 \cdot 10^{-7}$ mm Hg) at 200°C

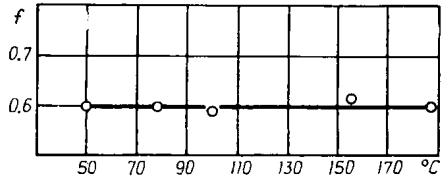

Fig. 13.8. Relation between static friction coefficient (f) and temperature (°C) for a stainless steel 12X18H10T/steel P9 combination at normal load of 80 kgf in high vacuum (10^{-6}-10^{-7} mm Hg) achieved by "oilless" evacuation

specimens should be tested at different mean pressures p_r. With an elastic contact between the specimens, the deformation component can be neglected. Then the friction parameter τ_0 can be determined

from the formula

$$\tau_0 = \frac{(f_1 - f_2)\, p_{r_1} p_{r_2}}{p_{r_2} - p_{r_1}}$$

where f_1 and f_2 = coefficients of static friction corresponding to p_{r_1} and p_{r_2}.

With the value of τ_0 being thus found, the parameter β can be determined from the equation for the friction coefficient. The values of τ_0 and β calculated in this way from experimental data are given in Table 13.8.

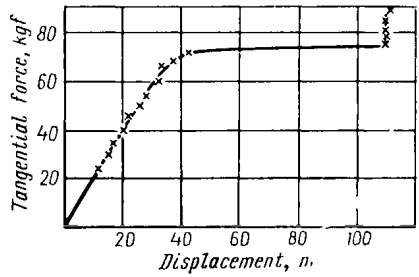

Fig. 13.9. Displacement (μm) as function of tangential load (friction force) for a steel 12X18H10T/steel 40X13 combination at normal load of 80 kgf in high vacuum ($5 \cdot 10^{-5}$ mm Hg)

The effect of normal loads and temperatures on the static friction coefficient is illustrated in Figs. 13.7 and 13.8.

Figure 13.9 shows a typical relationship between the tangential load and axial displacement in vacuum.

13.3.3. Wear Behaviour of Rubbing Components in Prolonged Operation in the Static Friction Regime

This is an important aspect of the studies of tribological joints in vacuum. The results of wear tests for rubbing components made of various materials are given in Table 13.9.

Figure 13.10*b* is a micrograph of a rubbing surface after 250 hours of continuous operation in high vacuum under a load of 15 kgf. Initially, the surface had a finish of 0.63-0.32 μm Ra. The micrograph shows a considerable improvement in surface finish as a result of the run. Comparison with a surface roughness specimen (Fig. 10*a*) having a finish of 0.04-0.02 μm Ra indicates, that the surface under test has a roughness smaller than that of the specimen.

What is also noteworthy is that after a 250-hour run the microhardness of the surface has increased three times.

Table 13.9

Wear (by mass) of the clamp of the intermittent motion device under different operating conditions

Sliding pair: steel 12X1810T on steel ХВГ

Test stage	Operating time, h	Number of working cycles	Rack's length of path, m	Clamp wear, g
High vacuum ($p = 2 \cdot 10^{-7}$ mm Hg) *obtained by means of an oil-filled diffusion pump*				
Tangential load 0.1 kgf, mass of clamp before tests 13.9342 g				
1	146	318158	2228	0
2	100	150956	1057	0.0001
3	100	154492	1061	0
4	100	146484	1025	0.0001
5	100	149552	1047	0
Total	546	919642	6418	0.0002
Tangential load 15 kgf, mass of clamp before tests 11,2844 g				
1	50	78208	547	0
2	50	78000	546	0
3	50	87650	589	0.0001
4	50	89100	599	0.0001
Total	200	332958	2281	0.0002
Ultra-high vacuum ($p = 5 \cdot 10^{-11}$ mm Hg), *"oilless" evacuation*				
Tangential load 0.1 kgf, mass of clamp before tests 13,9869 g				
1	50	81848	573	0
2	50	78988	553	0
3	50	70064	560	0
4	47	75946	548	0
Total	197	306846	2234	0

Note: 1. For operation in ultra-high vacuum, steel 12X1810T clamp was sulphidized.
2. Normal load ∽ 20 kgf.
3. Contact area ∽ 1.5 mm².

Shown in Fig. 10*c* is a micrograph of a rubbing surface tested in high vacuum under the same load but in the sliding friction regime. In a short time (about 30 min) the surface develops deep furrows and other kinds of surface damage typical of severe wear.

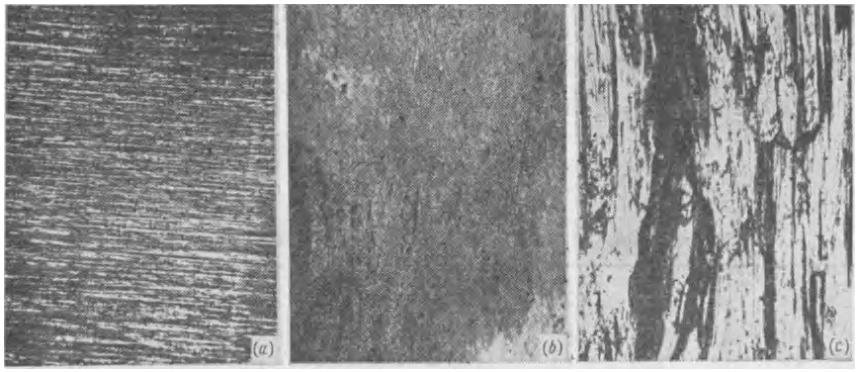

Fig. 13.10. Surface micrographs (×115)

(*a*) surface roughness specimen of the 12th Class according to standard; (*b*) rubbing surface of clamp after 250 h ($4 \cdot 10^5$ cycles) of operation under static friction conditions at 15 kgf load in high vacuum ($4 \cdot 10^{-7}$ mm Hg); (*c*) rubbing surface of clamp after 30 min operation under sliding friction conditions at 15 kgf load in high vacuum ($2 \cdot 10^{-7}$ mm Hg) obtained through «oil» evacuation

13.4. SLIDING FRICTION

Sliding friction in vacuum without lubrication is characterized with high values of the friction coefficient and seizure of the rubbing surfaces, heavy wear, and often by the jamming of the joint.

Tests of a stainless steel specimen in rubbing against a counterface of the same material at different levels of vacuum revealed the following coefficients of friction [21]:

Pressure in vacuum chamber (mm Hg)	760	760	$4 \cdot 10^{-7}$	$1.4 \cdot 10^{-8}$	$8 \cdot 10^{-9}$
Coefficient of friction	0.47	0.82	1.22	2.74	2.94

The coefficients of friction in the air, at the beginning and after two hours of the test run (the first two values) are given for comparison. The tested specimen was a semi-spherical slider rubbing against a flat surface at a low sliding speed (0.076 m/s) and a small load ($N = 20$ g).

Bushings of steel 20X13 (HRC 32-35) were tested in combination with shafts of metal-ceramic bronze in a vacuum of 10^{-7} mm Hg at $p_a = 2$ kgf/cm^2 and a sliding speed of 0.8 m/s. After 20 minutes from the beginning of the run the coefficient of friction began to increase, which was accompanied by a rise in temperature, vibrations of the unit and seizure of the rubbing surfaces. The coefficient

of friction reached 0.8, two times the value obtained during similar tests in air.

The results of tests [17] in air and in vacuum ($3 \cdot 10^{-6}$ mm Hg) of rubbing components made of different materials are given in Table 13.10.

Table 13.10

Coefficients of friction of metals in air and in vacuum

Sliding pair	Load, kgf	Coefficient of friction					
		in air			in vacuum		
		Start	10 min	60 min	Start	10 min	60 min
Aluminium-aluminium	3.1	0.50	0.78	0.78	1.10	1.57	1.57
	6.3	0.57	0.59	0.59	0.61	0.75	0.59
Berillium bronze-berillium bronze	3.3	0.46	0.57	0.58	0.71	0.87	1.10
	6.5	0.44	0.89	0.70	—	—	—
Brass-brass	3.3	0.31	0.31	—	0.43	0.50	0.70
	6.5	0.37	0.39	—	0.40	0.55	0.60
Copper-copper	3.3	0.26	1.04	1.04	0.32	1.22	2.0
Stainless steel-stainless steel		0.29	0.47	0.51	0.32	0.62	0.93
Steel IIIX15-copper	6.5	0.13	0.66	0.70	0.25	0.41	0.45
Stainless steel-aluminium	3.3	0.29	0.39	0.40	0.38	0.39	0.34
Stainless steel-brass		0.21	0.32	0.39	0.32	0.67	0.84
Berillium bronze-brass		0.28	0.34	0.38	0.49	0.62	0.90
Brass-berillium bronze	6.5	0.26	0.28	0.36	0.50	0.77	0.89
Copper-steel IIIX15		0.32	0.38	0.55	0.77	0.97	0.96
Steel IIIX15-copper		—	—	—	0.58	0.79	0.85
Cadmium-cadmium (coating)		0.26	0.44	0.39	0.43	0.43	0.31
Nickel-nickel (coating)	3.3	0.33	0.33	0.30	—	—	—
Silver-silver (plating)	6.5	—	—	—	0.28	0.41	0.39
	—	0.26	0.28	0.36	0.50	0.77	0.89

When parts of the same metal slide on each other in vacuum, the coefficient of friction depends on their hardness. The diagram in Fig. 13.11 indicates that the coefficient of friction of pure metals in vacuum decreases as their hardness increases. The difference in the friction coefficients for specimens of the same metal can be explained mainly by different degrees of surface cleaning. Careful degassing leads to increased coefficients of friction, as is illustrated by the upper curve in Fig. 13.11.

Values of the friction coefficient for single-run tests in air and in vacuum (10^{-5} mm Hg) of specimens made of various pure metals are given in Table 13.11 [2].

Frictional characteristics of rubbing components are improved by the use of self-lubricating materials, solid lamellar lubricants and thin metal coatings. Plain bearings made from self-lubricating materials reduce the weight of equipment while retaining its strength and, often, dimensions.

Table 13.11

Friction coefficients for pure metals in a single-stroke sliding in air and in a vacuum of 10^{-5} mm Hg

Sliding pair	Friction coefficient		Sliding pair	Friction coefficient	
	in air	in vacuum after outgassing		in air	in vacuum after outgassing
Cu-Ni	0.45	1.50	Cu-Fe	0.51	0.75
Ta-Ni	0.23	0.90	Ta-Cu	0.44	0.43
W-Ni	0.21	1.36	W-Cu	0.34	0.41

Self-lubricating materials can be exemplified by the AMAH family (cf. Ch. 11).

The stability and low coefficients of friction of materials AMAH-2 and AMAH-4 in vacuum allow them to be used for sliding bearings operating at average loads of 2 to 10 kgf/cm^2 and sliding speeds of up

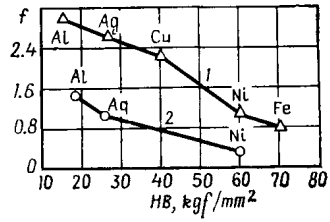

Fig. 13.11. Effect on hardness on friction coefficient for sliding pairs of the same materials

1—vacuum 10^{-2} mm Hg with outgassing; *2*—vacuum $3 \cdot 10^{-6}$ mm Hg without outgassing

to 4 m/s in high-vacuum applications. With sliding speeds reduced to 1 m/s, the loads can be increased from 50 to 150 kgf/cm^2. Sliding bearings made of AMAH are used in combination with shafts made of steel 20X13 hardened to HRC 35 and finished to 0.16-0.32 μm Ra. The AMAH bearings should be finished to 1.25-2.5 μm Ra. The radial clearance used should take 0.6-0.8 percent of the shaft diameter. Fig. 13.12 shows relationships between the coefficient of friction and frictional temperature for AMAH-2 in air and in high vacuum. As is seen, the coefficient of friction in air is twice that in vacuum. The tests were run at a specific load of 2 kgf/cm^2 and a sliding speed of $v = 4$ m/s [14].

New grades of the АСП-type plastics, namely ТЕСАН and ЭСТЕРАН, developed in the USSR, have a low coefficient of friction which is stable over a wide range of temperatures (Fig. 13.13). The wear resistance of some of these materials, e.g. ЭСТЕРАН, is lower by an order of magnitude than that of AMAH [16]. The results of studies on frictional behaviour of a large group of self-

lubricating materials used for sliding bearings in a vacuum of 10^{-5}-10^{-6} mm Hg at temperatures of up to 500°C are reported in [13].

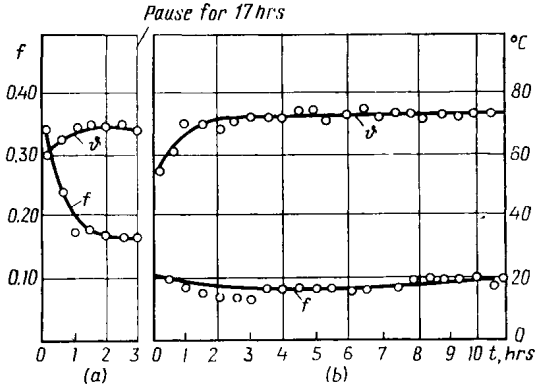

Fig. 13.12. Friction coefficient of AMAH-2 as function of testing time
(*a*) in air; (*b*) in high vacuum

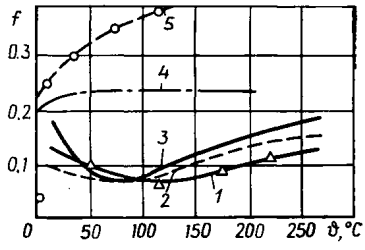

Fig. 13.13. Friction coefficient as function of temperature for diverse materials
1—ТЕСАН, *2*—ЭСТЕРАН; *3*—AMAH; *4*—fluoroplastic-4; *5*—cloth laminate with antifriction fillers

Figure 13.14 shows comparative data on the working temperature ϑ, wear life T, and pv for sliding bearings of different self-lubricating materials. These materials are divided into two groups. One group

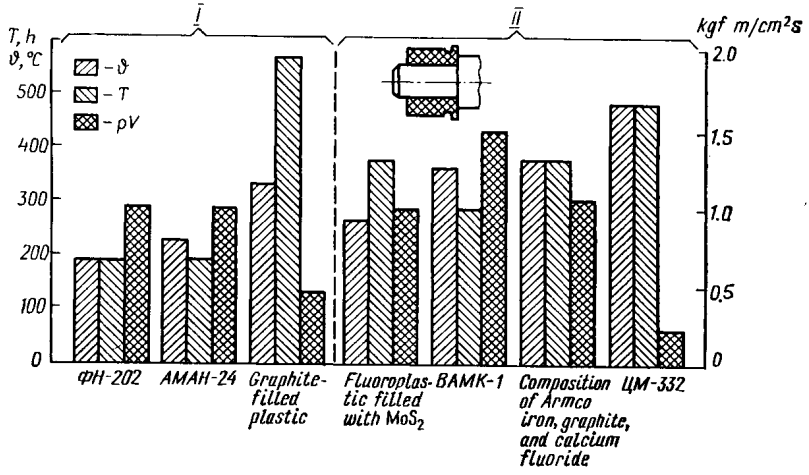

Fig. 13.14. Characteristics of self-lubricating materials as found by testing of sliding bearings

(I) includes materials recommended for use in vacuum as low-loaded self-aligning inserts and as solid-lubricant inserts in bearings with transfer lubrication. Group II includes materials for high tempera-

tures, loads and speeds. These materials provide long wear life (except metal-ceramic material ЦМ-332). Metal-fluoroplastic band with MoS_2 and material ВАМК-1 do not wear the shaft, but the former is subject to intensive wear itself. The materials based on Armco with graphite and calcium fluoride and metal-ceramic material ЦМ-332 wear little but inflict wear on the shaft [14].

Solid-lubricant coatings can be effected by means of suspensions ВНИИ НП-209, ВНИИ НП-212, ВНИИ НП-213, and ВНИИ

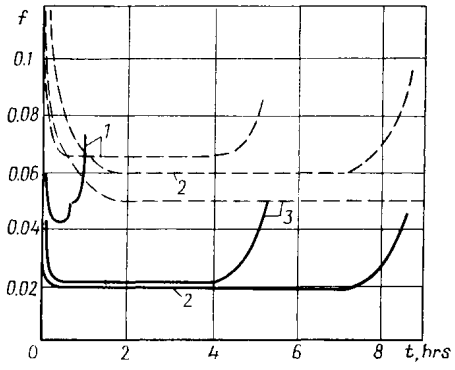

Fig. 13.15. Friction coefficient (f) of solid lubricant coatings as function of testing time (t) in air (dash lines) and in high vacuum (solid lines)
1—ВНИИ НП-213; *2*—ВНИИ НП-212; *3*—ВНИИ НП-230

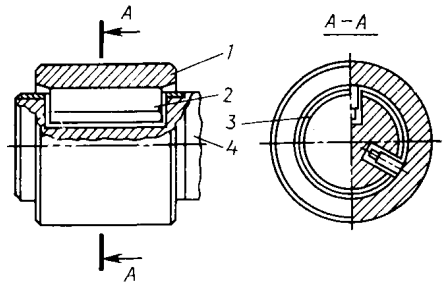

Fig. 13.16. Bearing with solid-lubricant inserts in the shaft

НП-230 (cf. Chapter 10). Fig. 13.15 illustrates the frictional behaviour of various solid-lubricant coatings in air and in ultra-high vacuum ($2 \cdot 10^{-8}$ to $5 \cdot 10^{-9}$ mm Hg). The longest wear life is exhibited by ВНИИ НП-212 and ВНИИ НП-230.

The wear life of tribological units in vacuum can be effectively increased by using the so-called transfer method, in which the applied lubricant is transferred from the lubricating element to the rubbing surfaces. This method has found use in vacuum engineering and in many general engineering applications.

A sliding bearing (Fig. 13.16) comprises an inner sleeve *3* secured to shaft *4*, an outer sleeve *1*, and three lubricating inserts *2* arranged at 120° to each other. The inserts can freely move radially in slots of the shaft that coincide with openings in the inner sleeve. As the shaft rotates, the inserts are pressed against the surface of the sleeve *1* under the action of the centrifugal force, thereby providing lubrication of the rubbing surface. The pressing is aided by leaden pads placed under the inserts. Some designs with solid-lubricant inserts are shown in Fig. 13.17 [10].

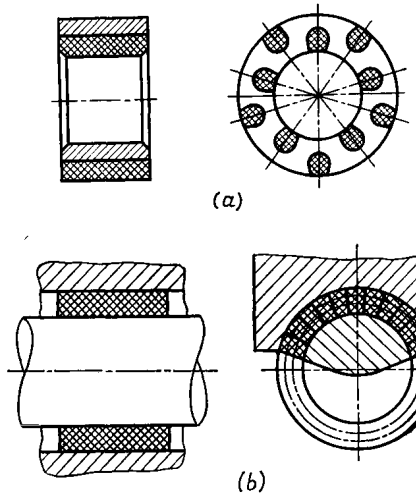

Fig. 13.17. Sliding bearings with transfer lubrication by inserts
(*a*) pressed into the bearing bushing; (*b*) moulded into an elastic annular frame

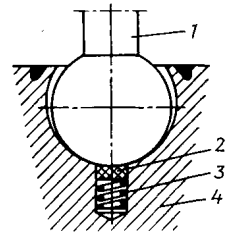

Fig. 13.18. Ball socket with transfer lubrication

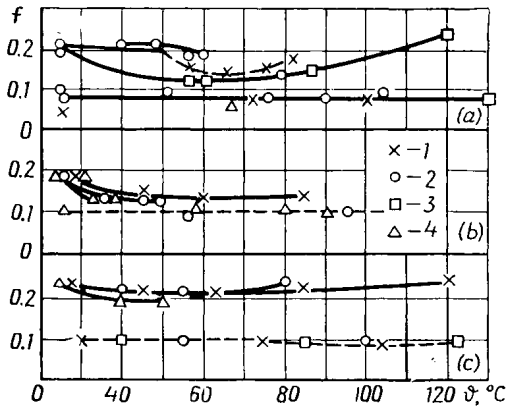

Fig. 13.19. Effect of vacuum and friction temperature on frictional characteristics of the diselenides of refractory metals
(*a*) niobium diselenide; (*b*) tungsten diselenide; (*c*) tantalum diselenide; *1*—load 1000 gf; *2*—load 500 gf; *3*—load 2000 gf; *4*—load 200 gf; – – – in vacuum $5 \cdot 10^{-7}$; —— in air

Figure 13.18 shows a spherical thrust bearing [12], the spherical end of the shaft *1* being in contact with a lubricating insert *2* pressed to it by a spring *3* arranged in the housing *4*. For such an arrangement used in vacuum, the spring is made of berillium bronze БрБ2, the shaft is made of steel ШХ-15, and the housing is made of the same or softer steel. That makes it possible to widen the range of working temperatures, which can be from —150 to +400°C depending on the grade of self-lubricating materials; with the use of molibdenum diselenides and high-temperature metals, the upper limit can be increased to 800°C.

The reliable functioning of tribological units in high vacuum can also be secured by the use of thin solid-lubricant and soft-metal coatings deposited on the rubbing surfaces (cf. Chapters 9 and 10). The effect of vacuum, load and temperature on the friction coefficient of diselenides is shown in Fig. 13.19 [14].

13.5. ROLLING FRICTION

Much effort has been made in recent years to develop new and improve current designs of rolling bearings for operation in high vacuum [6, 8, 10]. Normal operation of high-speed bearings without fluid lubricants can be achieved by the use of retainers made of polymeric and metal-ceramic materials which provide adequate strength, high wear resistance and thermal stability, and low friction and thermal expansion coefficients.

Rolling bearings with retainers made of AMAH-24 proved to have the best service properties in vacuum at elevated temperatures (up to 300°C).

In rolling bearings use can also be made of some other self-lubricating materials (fluorine-containing ФН-202, ФН-3, АФГ-80ВС, Fluoroplastic-4, epoxy resin compounds, АСП-plastics, etc.). Lubrication in such bearings is effected through the transfer of the retainer material to the balls and the raceways.

A ball bearing with a retainer made of an AMAH-type material [7] is shown in Fig. 13.20. The reinforced retainer provides increased strength and thermal stability for use at elevated temperatures.

Data on operation of rolling bearings with retainers from self-lubricating materials in vacuum are given in Table 13.12 [2].

In some cases the raceways of bearings are coated with molybdenum disulphide.

The diselenides of refractory metals (WSe_2, $NbSe_2$, $TaSe_2$, $MoSe_2$) and some soft metals (Au, Ag, In), which are used as thin coatings on the rubbing surfaces, provide the minimal evaporation. The results of comparative tests of rolling bearings coated for lubrication with thin films of soft metals are given in Tables 13.13 and 13.14.

In tribological units of vacuum equipment (the bearings of wire feeders in titanium sorption pumps, bearings in intermittent motion drives, etc.) operating without lubrication in ultra-high vacuum at

Table 13.12

Operation in vacuum of rolling bearings with ratainers made of self-lubricating polymeric materials and stainless-steel races

Retainer material	Bearing inner diameter, mm	n, rpm	Axial load, kgf	ϑ, °C	Vacuum pressure mm Hg	Operation time, h
Teflon, glass fibre	4.7	8000	0.100	70-85*1	$4 \cdot 10^{-6}$-$6 \cdot 10^{-8}$	3810
				70-90*1	$3 \cdot 10^{-7}$-$3 \cdot 10^{-8}$	3300*2
				80-90*1	$9 \cdot 10^{-7}$-$2 \cdot 10^{-8}$	3883
Duroid 5813 (Teflon-based)				Room 90*1	$1 \cdot 10^{-3}$-$4 \cdot 10^{-6}$	62
				80-95*1	$3 \cdot 10^{-7}$-$3 \cdot 10^{-8}$	5110
				Room-95*1	760-$4 \cdot 10^{-7}$	90
Teflon, glass fibre, MoS_2	20	1800	0.225	Room	10^{-6}-10^{-7}	50
Epoxy resin, MoS_2					10^{-7}	9000

*1 Outer race temperature.
*2 Still operative after this run.

low speeds and loads, use is often made of some standard types of rolling bearings. Such, for instance, are single-row ball bearings

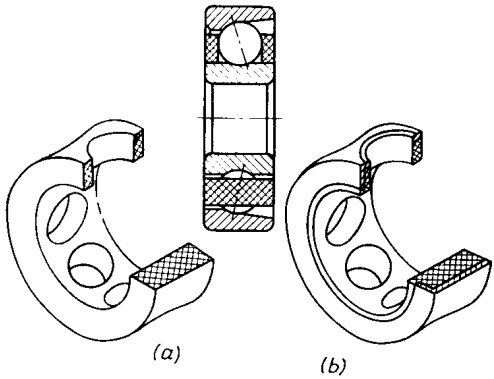

Fig. 13.20. Angular-contact ball bearing with retainer made of self-lubricating material AMAH
(*a*) plain retainer; (*b*) reinforced retainer

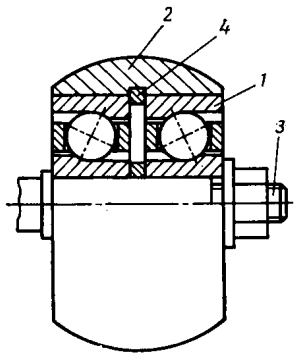

Fig. 13.21. Bearing unit for intermittent motion drive
1—ball bearing; *2*—casing; *3*—shaft; *4*—retaining ring

made of stainless steel (GOST 8338-75) and trust ball bearings made of high-temperature steel (GOST 831-75).

An example of use of such bearings is shown in Fig. 13.21. This is a bearing unit for an intermittent motion drive [4] with angular-

Table 13.13

Wear life of rolling bearings with solid-lubricant coatings [23]

Coating	Wear life, h	Bearing condition
Gold	140	Bearing failure
Silver	405	Test stopped because of increased friction moment
Silver-molybdenum disulphide	360	
Silver-sulphide film	360	
Lead	1000	Bearing failure
Lead-base bismuth	1650	
Bismuth		Test stopped after 1240 h of run, with bearing in good condition

Table 13.14

Comparative tests of rolling bearings in vacuum (10^{-9} mm Hg) [25]

n, rpm	Friction moment, gf·m		Coating	Note
	before testing	after testing		
5	1.72		No coating	Scuffing, high friction moment
93	1.36	11.5		
280	1.41	Seizure		
3350	1.41			
5	0.64		Gold plating	No tangible rise in friction moment
25	0.61			
93	1.41	—		
280	1.72			At 120 rpm slight noise with no effect on performance
600	1.36			
1200	1.36			

Note. Tested bearings of size 4.6 mm ID and 12.5 mm OD. Bearings without coating radially loaded to 6.75 gf, and with gold plating to 19 gf.

Table 13.15

Frictional characteristics of rolling bearings in starting

Pressure, mm Hg	Friction force, kgf	Friction moment, kgf·cm	Effective coefficient of friction	Preparatory treatment
760	0.04	0.05	0.011	No heating
$1 \cdot 10^{-2}$	0.04	0.05	0.011	
$5 \cdot 10^{-5}$	0.035	0.04	0.01	
$2 \cdot 10^{-7}$	0.03	0.04	0.01	
$1 \cdot 10^{-8}$	0.03	0.04	0.01	Heating in vacuum to 250°C for 15 h
$3 \cdot 10^{-9}$	0.04	0.04	0.01	
$5 \cdot 10^{-9}$	0.05	0.06	0.014	Heating in vacuum to 400°C for 15 h
$5 \cdot 10^{-10}$	0.05	0.06	0.014	

contact ball bearings. The bearings have solid stainless-steel retainers and the races are made of high-speed steel P18. Such bearing units show reliable operation without any lubricant in a vacuum of 10^{-10} to 10^{-12} mm Hg during 1000 hours with periodical heating to 450°C for degassing. The working load and speed were within 10 kgf and 1 m/min, respectively.

The bearing unit was tested by the inclined plane method under different conditions after 1000 hours of operation in ultra-high vacuum. The results are given in Table 13.15.

REFERENCES

1. Балицкий А. В. Технология изготовления вакуумной аппаратуры. М., «Энергия», 1974, 312 с.
2. Вайнштейн В. Э., Трояновская Г. И. Сухие смазки и самосмазывающиеся материалы. М., «Машиностроение», 1968, 180 с.
3. Данилин Б. С., Минайчев В. Е. Основы конструирования вакуумных систем. М., «Энергия», 1971, 392 с.
4. Данилов К. Д. Сверхвысоковакуумный ввод поступательного движения. Электронная техника, сер. 1, «Электроника СВЧ», 1973, вып. 4, с. 112-114.
5. Дэшман С. Научные основы вакуумной техники. М., «Мир», 1964, 715 с.
6. Бобров Д. П., Нусинов М. Д., Папко В. М. Исследование величин пороговых давлений, ограничивающих воздействие разряженной среды на работоспособность шарикоподшипников.— В сб.: Теория трения, износа и смазки. Ташкентский политехн. ин-т, 1975, с. 149-151.
7. Опоры осей и валов машин и приборов. Под ред. Спицына Н. А. и Машкова М. М. М., «Машиностроение», 1970, с. 520.
8. О работоспособности подшипников сухого трения с учетом условий эксплуатации.— В сб.: Теория трения, износа и смазки. Ташкентский политехн. ин-т, 1975, с. 151-153. Авт.: В. К. Гончаров, А. Т. Кудряшев, В. А. Хрусталев, Л. Н. Семенова и др.

9. Основы вакуумной техники. М., «Энергия», 1975, 416 с. Авт.: Б. И. Королев, В. И. Кузнецов, А. И. Пипко, В. Я. Плисковский.

10. Пацов Г. М. Конструктивные направления повышения износостойкости опор вакуумного типа. «Труды МИЭМ. Детали машин и приборов». Вып. 18, 1972, М., МИЭМ, с. 153-171.

11. Работоспособность твердых смазочных покрытий.— «Вестник машиностроения», 1962, № 12, с. 25-27. Авт.: Г. В. Курилов, В. Ф. Удовенко, Н. И. Вионцек, Л. Н. Сентюрихина и др.

12. Спицын Н. А. Кузнецова Т. И. Одношариковые подшипники с ротапринтной твердой смазкой. «Труды МИЭМ. Детали машин и приборов». Вып. 18, 1972, М., МИЭМ. с. 28-38.

13. Спицын Н. А., Пацов Г. М. Конструкции и применение подшипников скольжения.— «Вестник машиностроения», 1970, № 9, с. 16-19.

14. Трение и износ в вакууме. М., «Машиностроение», 1973, 216 с. Авт.: И. В. Крагельский, И. М. Любарский и др.

15. Трояновская Г. И. Применение самосмазывающихся материалов при ротапринтной смазке.— «Вестник машиностроения», 1974, № 4, с. 51-54.

16. Шембель Н. Л., Сагалаев Г. В. Сравнительные данные о свойствах графитопласта АТМ-2.— В сб.: Фрикционные и антифрикционные пластмассы. Материалы семинара. М., МДТП им. Ф. Э. Дзержинского, 1975, с. 50-57.

17. Beller W. Friction research grinds to halt (in space environment) — "Missiles and Rockets", 1960, vol. 7, No. 9, p. 23-25.

18. Boes D. I. Long term operation and practical limitations of dry self-lubricated bearings from 1.10^{-5} torr to atmospheric. "Lubricat. Eng.", 1963, vol. 19, No. 4, p. 137-142.

19. Bowden F. P., Tabor D. The Friction and Lubrication of Solids. Oxford (a. o.), University Press, 1950, pp. 90-121.

20. Brown R. D., Burton R. A., Ku P. M. Long duration lubrication studies in simulated space vacuum.— "ASLE Transact", 1964, vol. 7, No. 3, p. 236-248.

21. Bruescke E. E., Eckman B. Device for the measurement of friction at ultrahigh vacuum.— "Rev. Scient. Instruments", 1963, vol. 34, No. 9, p. 978-980.

22. Evans E. H., Flatley W. T. Bearing for vacuum operation—retainer material and design.— "Transact. ASME", 1963, vol. 85, ser. B. No. 2, p. 129-134.

23. Lubricant evaluation for bearing systems operating spatial environments. "ASLE Transact", 1963, v. 6, No. 1, p. 67-77. Auth.: P. Lewis, S. F. Murray, M. B., Peterson, H. Esten.

24. Lubrication and wear in space system. In Transactions of the tenth National Vacuum Symposium of the American Vacuum Society, 1963, p. 3-13. Auth: R. W. Parcel, F. I. Clause, C. F. O'Hara, W. C. Joung.

25. Westmoreland R., Reed I. D. Vacuum testing bearings without contamination.— "Space/Aeronautics", 1962, vol. 37, No. 6, p. 175-183.

26. Wilkens W., Kranz O. The formation of gases due to the sliding friction of Teflon on steel in ultrahigh vacuum. "Wear", Vol. 15, No. 3, 1970. p. 215-227

Chapter 14

FRICTION AT LOW TEMPERATURES

14.1. TRIBOLOGICAL UNITS AND MATERIALS FOR USE AT LOW TEMPERATURES

Low temperatures constitute an extensive range from 0 K to 273.15 K. Temperatures under 120 K are called cryogenic, and those under 0.3 K are called super-low temperatures.

The general trend in cryogenic engineering is towards placing tribological units beyond the low-temperature areas to increase reliability and reduce losses of cooling efficiency. Such an arrangement, however, can be cumbersome, and in some cases impossible. With the rapid advance in cryogenic engineering and, particularly, in electrical machines with superconductive windings cooled with liquified gases, the number of low-temperature tribological units is steadily growing.

Units of this type can work with lubrication, e.g., in a cryogenic fluid or with the use of a special fluid lubricant, or without any lubricant at all. In the latter case use is made of self-lubricating materials.

The field of application. The following kinds of tribological units are used at low temperatures:

—axial and radial shaft seals in cryogenic pumps, rotary regenerators, rectifiers, expansion turbines, and electric generators with superconductive rotors;

—piston seals in cryogenic pumps, helium refrigerators, piston-type low-temperature air-driven engines;

—radial rolling bearings in mechanisms and machines working in various media and in vacuum at low temperatures.

Low-temperature axial seals can be exemplified by the double-side bellows-type metal-graphite seal unit of a submersible liquid-oxygen pump used in spacecraft [8]. The unit is mounted on the shaft of the drive motor, which is placed in a sealed container filled with helium compressed to 5.5 kgf/cm^2. The motor, which is separated from the liquid oxygen by the seal, rotates at a speed of 11,000 rpm. The stationary graphite ring is made of graphite P5N and the rotating ring, of stainless steel 440C chromium-plated after lapping, the plating thickness being over 25 μm.

Structural materials. *Metals.* A number of carbon steels and metals with body-centred cubic lattices (Fe, Cr, Mo, Ta, W) are subject to brittleness at low temperatures, and therefore they cannot be recommended for use over a wide range of temperatures. In low-temperature units and machines use should be made of metals with face-centred cubic lattices (Al, Ni, Pb, Cu, Ag) or with hexagonal close-packed lattices (Ti, Zn, Mg, Co), steels with fine-grained structures (used at up to —45°C), hardened and tempered low-alloy ferritic steels with fine-grained martensitic structures (used up to —100°C), stainless steels with austenitic structures (up to —200°C), and nickel steels with ageing martensite (up to —240°C). Most widely used in low-temperature applications are copper, nickel, magnesium, titanium, and aluminium alloys.

In tribological joints where one of the rubbing components is made of metal, the metal generally used is stainless steel. In combination with graphite, annealed stainless steel 440C (made in USA) with hard chromium plating gives good results. Use is also made of steels 40X, Г13Л, 38ХМЮА, У8, 12Х18Н9Т, 45 (heat treated), etc.

When one of the rubbing parts is made of steel 40X, improved wear resistance can be achieved by gas cyaniding at 860°C with quenching in oil. The surface hardness obtained can be as high as HRC 61. However, the influence of heat treatment on wear resistance is complex and far from being direct [16]. The results of research into wear resistance of materials under the action of abrasives at low temperatures are reported in [10].

Non-metals. Graphite is a common material used in graphite-graphite and graphite-steel combinations at low temperatures. It is also used as an addition to various plastics, e.g., for making compositions (such as 15 percent graphite +85 percent fluoroplastic-4, or 5 percent graphite +95 percent nylon) used in liquid nitrogen and liquid hydrogen (according to some foreign sources). Graphite can be used for retainers of ball bearings operating at very low temperatures. However, it is fluoroplastics and their derivatives that have found the widest application as antifriction materials for low-temperature rubbing components.

Unlike many plastics, fluoroplastics retain their elasticity at low temperatures. They are used straight and in composition with other plastics, metals, and solid lubricants (MoS_2, Pb, etc.). The addition of 30 to 50 percent bronze by volume to fluoroplastic-4 reduces the linear expansion coefficient by a factor of 2, increases the thermal conductivity three times, and sharply reduces the rate of wear (according to some foreign sources).

The wear resistance, mechanical strength, and thermal conductivity of fluoroplastic-4 can also be improved by filling it with fine-grain powders of solid lubricants.

The following fluoroplastic-base materials have found use in cryogenic machines: ФН-202, which is fluoroplastic-4 filled with

10 percent nickel and 3 percent molybdenum disulphide; АМИП-15М, fluoroplastic-4 filled with 15 percent glass ceramic and 3 percent molybdenum disulphide; Ф4Ж-20 (filled fluoroplastic); compositions ФКД-5Б; ФСД-5Б; Ф4К20; ФСД5; ФКД5.

In the USA, the retainers of ball bearings operating in liquid nitrogen are manufactured from Teflon (fluoroplastic-4) filled with glass fibres; retainers made from a composition comprising fluoroplastic-4, glass fibres, and WSe_2 have been found to wear only slightly in a vacuum of 10^{-8} mm Hg at temperatures of from —185 to +235°C.

Good antifriction properties and wear resistance in a vacuum of up to 10^{-9} mm Hg at temperatures ranging from —195 to +230°C have been exhibited by the following fluoroplastic-base compositions tested in the USA: 70 percent Ag + 20 percent Teflon +10 percent WSe_2, and 60 percent Cu + 30 percent Teflon +10 percent WSe_2.

Efficient operation in liquid-oxygen and liquid-nitrogen pumps has been shown by sliding bearings having three layers: a steel backing, a layer of porous bronze impregnated with a mixture of 20 percent lead and 80 percent of fluoroplastic-4, and a layer of fluoroplastic-4 25 μm thick. Satisfactory results have been obtained with bearings made of tin bronze having a layer of fluoroplastic-4 mixed with lead within the temperature range from —200 to +200°C.

Sliding bearings for operation at low temperatures are also made of polymeric materials, such as cloth laminate ПТ; polyamides П-68, АК80-20, capron; glass-filled capron, glass-filled polyamide

Table 14.1

Properties of fluoric polyethers

Characteristics	E-1	E-2	E-3	E-4
Degree of polymerization	1	2	3	4
Molecular mass	286.03	452.08	618.12	784.15
Boiling point, °C	39	101	153	193
Compressibility at 25°C and 500 kgf/cm², percent	8.20	6.48	5.64	5.18
Vapour heat in boiling, kJ/kg	960	730	610	520
Setting point, approximately (ν = = 0.2 m²/s), °C	—154	—123	—107	—94
Density at 25°C, kg/m³	1580	1660	1710	1760
Specific heat, c_p, kJ/(kg·°C)	1.025	1.02	1.015	1.0
Coefficient of thermal conductivity, W/(m·°C)	0.086	0.086	0.086	0.086
Volumetric expansion coefficient, m³/(kg·°C)	$1.12 \cdot 10^{-6}$	$0.96 \cdot 10^{-6}$	$0.73 \cdot 10^{-6}$	$0.67 \cdot 10^{-6}$
Absolute vapour pressure at 52°C, kgf/cm²	1.64	0.14	0.016	0.006
Kinematic viscosity coefficient at 25°C, m²/s	$0.3 \cdot 10^{-6}$	$0.6 \cdot 10^{-6}$	$1.3 \cdot 10^{-6}$	$2.3 \cdot 10^{-6}$

П-68 and their compositions with molybdenum disulphide. Polyamides of П-68 and АК80-20 types develop cold brittleness at —30 to —70°C. Glass-filled polyamides can be used at much lower temperatures.

Low-temperature lubricants. The wear life of tribological units working at low temperatures can sometimes be improved by the use of special fluid lubricants. The main requirements placed on such lubricants are a low solidification point (which must be considerably lower than the working temperature), a high boiling point, low evaporation at maximum possible working temperatures, chemical neutrality, low moisture adsorption, and good heat-transfer properties. Lubricants of this kind can be exemplified by organo-silicone oil No. 3, grease ЦИАТИМ-221 (based on oil No. 3), and hydrocarbon grease ЦИАТИМ-205. Experiments have shown that fluid lubricants are good for use up to a definite temperature, which is dependent on the solidification point, under which the coefficient of friction is higher than that in sliding without the lubricant. For rubber СКМС-10 sliding on metal, these temperatures came to 100°C with oil No. 3 and ЦИАТИМ-221 and to 50°C with ЦИАТИМ-205.

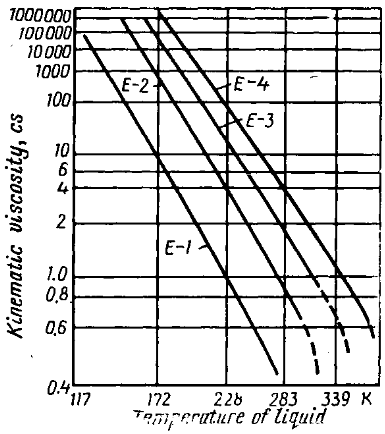

Fig. 14.1. Kinematic viscosity of fluoropolyethers as function of temperature [6]

A much wider range of working temperatures is typical of fluoropolyethers, which are distinguished by the degree of polymerization:

$$F(\underset{\displaystyle CF_3}{\underset{|}{C}}FCF_2O)_n \cdot CHFCF_3$$

where n = 1, 2, 3 or 4. The liquids that correspond to the different indices n are designated as E-1, E-2, E-3 and E-4. They differ in viscosity, which grows with n. The properties of fluoropolyethers are given in Table 14.1 [6].

Relationship between the kinematic viscosity of fluoropolyethers and temperature is shown in Fig. 14.1.

Studies on fluoropolyethers have shown that they can form hydrodynamic films at low temperatures, and within a range of from —45 to —185°C their lubricating efficiency is comparable to that of mineral oils at 40 to 150°C.

14.2. EXPERIMENTAL TECHNIQUES

The coefficients of friction and the wear of various combinations of materials, as measured in experiments, differ considerably from those observed in low-temperature service conditions. This can be explained on the one hand by widely varying operating conditions (temperature pressure, sliding speed, working medium, type of motion, etc.), and on the other, by a great diversity of investigations and experimental procedures. The available test data are insufficient for clear understanding of the frictional behaviour of materials at low temperatures, because such studies have been done on a relatively small scale, which fact is partly explained by the technical difficulties involved in conducting low-temperature tests with a fair degree of confidence.

Keeping the specimen surface clean during testing.

During low-temperature friction tests, the specimen is cooled, and the vapours of water, carbon dioxide, oil and other substances present in the ambient medium may condense, freeze out, or get adsorbed on the carefully prepared specimen surfaces. Even the traces of condensate on the rubbing surfaces sharply change the coefficient of friction, because the process of friction is greatly dependent on the cleanness of the surfaces. One method for keeping them clean during tests is a preliminary blasting with a dry gas that will not condense at the test temperature. In specimens immersed into liquid nitrogen directly from the surrounding air, a hard film of adsorbed moisture formed on their surfaces [25]. To prevent this, the measuring chamber of the testing device was blasted with dry helium for 15 min. The blasting reduced the wear of graphite specimens sliding on stainless steel 304 (USA) by a factor of ten thousand. Some investigators [20] recommend that the test chamber should be blasted with gas twenty times and evacuated prior to testing. Another effective method for keeping the specimen surfaces clean is conducting the tests in vacuum [4]. In some cases it has proved expedient to combine the evacuation of the measuring chamber to 10^{-5} mm Hg with a simultaneous heating of the specimens to 300°C before testing [22]. The best means for preventing the contamination of the specimen surface is believed to be an ultra-high vacuum of 10^{-9} to 10^{-10} mm Hg [4]. It is well to provide for after-test warming of the specimens to the ambient temperature while it is inside the apparatus [25] so that no condensate appears on their surfaces on opening the vacuum chamber.

Strict control of the medium where friction tests are carried out, the absence of substances that can condense on the specimen surfaces (water, carbon dioxide, lubricants, etc.) and the prevention of condensate from forming on the specimen after testing—these are indispensable conditions for securing accurate experimental results. These conditions can be met only with the use of an apparatus which is completely sealed.

Stabilizing the temperature of specimens. In studies of the effect of low temperature on friction and wear, there is always the need of maintaining a constant temperature of the specimens during the tests. Otherwise, due to friction the temperature of the rubbing surfaces may become much higher than the initial temperature.

The simplest solution seems to be the running of tests at temperatures corresponding to the boiling or sublimation points of some substances. For instance the tests may be run at —196°C (77 K) in liquid or gaseous nitrogen [19], at —183°C (90 K) in liquid oxygen, and also at temperatures of —78°C (195 K) and 0°C (273 K).

In frictional tests with very low sliding speeds, e.g., with translation at 2 to 3 mm/s or even at $2 \cdot 10^{-5}$ mm/s, it is not difficult to maintain the specimen temperature. With high sliding speeds, however, it is much more difficult to stabilize the temperature, because the cooling system of the test apparatus has to deal with frictional heat whose intensity varies in the course of the test (it is equal to zero at the beginning). A strong dependence of the friction coefficient on temperature [7, 22] and sliding speed [21] necessitates, for a more adequate and detailed picture of the process, such a cooling system for the apparatus that will allow the tests to be run at different temperature steps, with the specimen temperature reliably stabilized.

Maintaining the stability of friction-force sensors. At low temperatures strain-gauge sensors and the elastic elements on which the sensors are placed change their characteristics. Hence they need to be calibrated over the whole range of test temperatures. Strain gauges are normally located outside the apparatus for ease of handling [25]. The transmission lever is usually sealed with the aid of a bellows. In low-temperature friction-test apparatus [25], the maximum deflection of the transmission lever in measuring the friction force does not exceed 0.075 mm, and therefore the error due to the bellows resilience is negligible.

The absense of lubricant in movable joints inside the measuring chamber. The study of dry friction, e.g., in rotary motion, presents difficulties for two reasons: first, the drive-shaft bearings must be capable of functioning without any lubricant, and second, the apparatus must be completely sealed.

The first problem can be solved by the use of bearings with gas lubrication or ball bearings with fluoroplastic retainers [19]. Ball bearings with retainers made of fluoroplastic-3 can normally function at —196°C for a long time (up to 200 hours). The balls and races for such bearings should be made of stainless steel 9X18.

The problem of complete sealing can be solved in a number of ways, e.g., by the use of shaft seals of the bellows type, which are widely employed in vacuum technology at low and high pressures. The drawback to such designs is the need for planetary gears and a considerable number of bearings, which require lubrication.

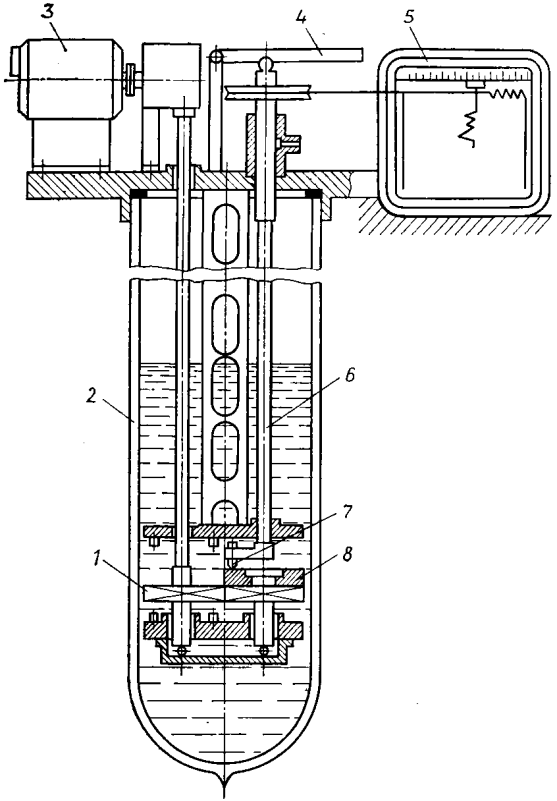

Fig. 14.2. Tribometer for studying friction in cryogenic liquids [9]

1—gear transmission; *2*—Dewar flask; *3*—electric motor; *4*—lever; *5*—recorder; *6*—bar; *7*—indenter; *8*—ring

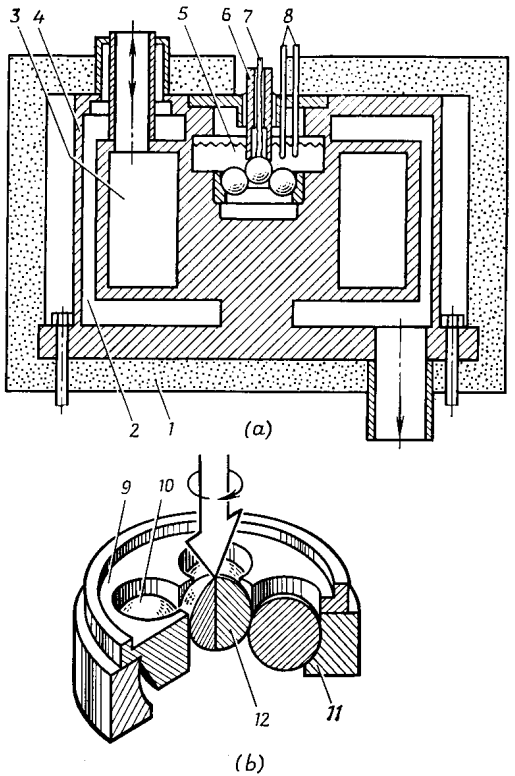

Fig. 14.3. Tribometer for studying friction in fluid low-temperature lubricants [6]

(*a*) general layout; (*b*) five-ball test assembly device; *1*—foamed plastic; *2*—vacuum jacket; *3*—liquid nitrogen chamber; *4*—body; *5*—test chamber; *6*—drive shaft; *7*, *8*—thermocouples; *9*—cage; *10*—lower ball; *11*—race; *12*—upper ball

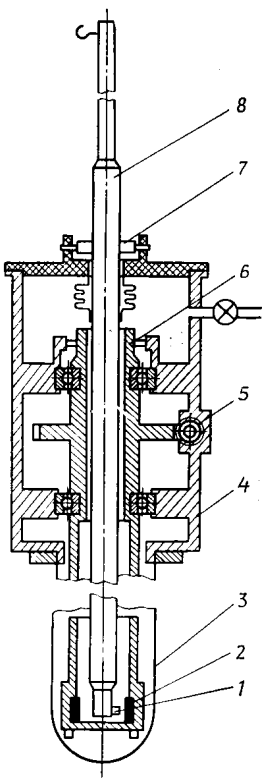

Fig. 14.4. Tribometer for studying friction in gaseous media [20]

1—wear pin; *2*—bushing; *3*—vessel; *4*—housing; *5*—worm gearing; *6*—tube; *7*—pivot; *8*—shaft

Cryogenic tribometers. An apparatus for experimental studies of dry friction at low temperatures must provide strict control of the environment, clean surfaces of the specimens, stable temperature of

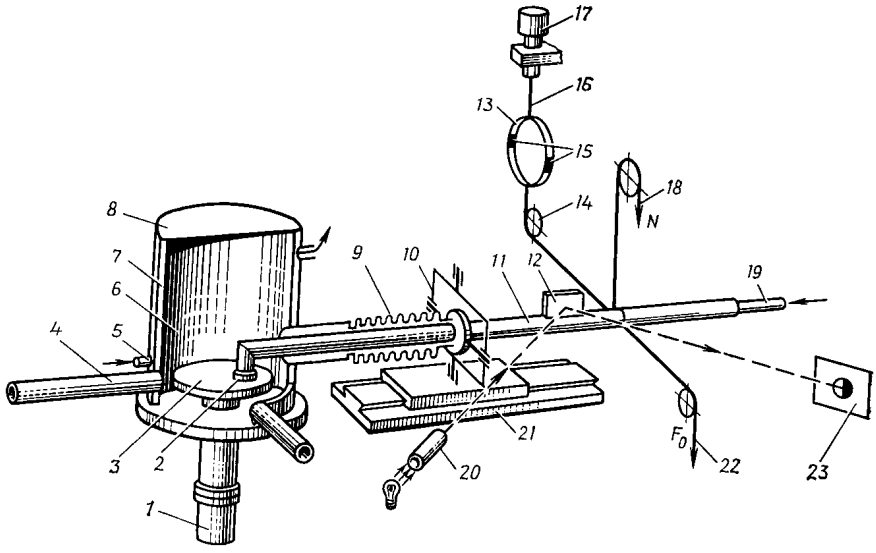

Fig. 14.5. Cryotribometer KT-1 for studying friction in gases and in vacuum [2]

1—electric drive; *2*—specimen; *3*—rotary counterface; *4, 8*—observation windows; *5*—fitting; *6*—chamber; *7*—insulation; *9*—bellows; *10*—pivot; *11*—lever; *12*—mirror; *13*—elastic member; *14*—roller; *15*—strain gauges; *16*—string; *17*—screw; *18, 22*—load; *19*—tube; *20*—optical system; *21*—slide; *23*—screen

the specimens, complete sealing, and stability of the strain-gauge sensors. Such tribometers are described in references [2, 4, 5, 6, 9, 19, 20] and illustrated in Figures 14.2 to 14.5.

14.3. COEFFICIENTS OF FRICTION AT LOW TEMPERATURES

The coefficient of friction can be determined by the analytical and experimental method described in Chapter 2. Experimental data are given below.

Friction in cryogenic liquids. Values of the coefficient of friction in cryogenic liquids (liquefied nitrogen and hydrogen) for various combinations of materials are given in Tables 14.2 and 14.3.

In liquid nitrogen and, particularly, hydrogen the retention of oxide films on rubbing surfaces is impossible. As a result, the rubbing surfaces of metals cleaned of oxide films in the course of friction show a tendency to seizure and intensive wear. In liquid oxygen the

Table 14.2

Coefficients of friction in cryogenic fluids for materials sliding on stainless steel

Material	Liquid medium	
	nitrogen	hydrogen
Graphite + fluoric metal	0.18	0.22
Graphite + phenol	0.04	0.06
Graphite (15%) + fluoroplastic-4 (85%)	0.09	0.16
Graphite (5%) + nylon (95%)	0.06	0.15

Table 14.3

Coefficients of friction in liquid nitrogen

Sliding pair		f	Source (reference number)
I	II		
Steel 304	Steel 304	0.4	—
Steel 440C	Steel 440C	0.34	
Steel 52100	Steel 52100	0.34	
Al	Steel 30XMIOA	0.853	[12]
Ti		0.734	
Nb	Nitrided GOST 4543-61	1.016	
Mo		0.879	
W		1.068	
Fe		1.023	
Co		0.537	
Ni		1.037	
30XMIOA		0.897	
Al	Al	0.718	
Ti	Ti	0.692	
Nb	Nb	0.990	
Mo	Mo	0.831	
W	W	1.006	
Fe	Fe	0.841	
Co	Co	0.512	
Ni	Ni	0.879	
Polystyrene	Steel 45 Heat-treated	0.33-0.35	[9]
Rigid PVC		0.20-0.22	
Cloth laminate		0.31-0.34	
Fluoroplastic-4		0.09-0.10	
Wood (beech)		0.32-0.38	
Ebonite		0.30-0.48	
Graphite		0.68-0.72	

friction of metals involves vigorous formation of oxide films and severe corrosion of the surfaces. Another feature of friction in cryogenic liquids is their low viscosity, which leads to scoring and considerable heat generation. There is also a possibility of formation of the gaseous phase, which leads to the cavitation and destruction of the rubbing surfaces.

Although cryogenic liquids have poor lubricity, their presence in the friction zone sometimes makes it possible to increase the wear life of tribological components over the life of these components in vapours of the same liquids at the same temperatures. In liquid nitrogen the process of friction and wear is stabilized and the coefficient of friction is to some extent reduced for combinations of hard metallic surfaces or that of a hard metallic surface with a non-metallic one [9].

The data of Table 14.3 indicate that in liquid nitrogen metals with different electronic and crystalline structures behave differently: the couples of metals with cubic crystal lattices wear intensively and have a higher coefficient of friction than that in the couples of metals with hexagonal lattices [12].

Friction in gaseous media. Values of the coefficient of friction in gaseous media at low temperatures for various materials combinations are given in Tables 14.4 to 14.7. Table 14.4 gives friction coefficients for pure metals, determined by means of a cryotribometer; the coefficients of kinetic friction are measured at a sliding speed of 0.25 mm/s and normal load of 2 gf.

Table 14.4

Static f_{st} and sliding f_{sl} coefficients of friction in gaseous helium [20]

Material of sliding pairs	Temperature, K					
	300		80		20	
	f_{st}	f_{sl}	f_{st}	f_{sl}	f_{st}	f_{sl}
Fe (99.9%) Fe (99.99%)	1.09	0.92	1.04	0.90	—	—
Al (99%) Al (99%)	1.62	1.43	1.60	1.41	—	—
Cu (99.95%) Cu (99.95%)	1.76	1.56	1.70	1.45	1.66	1.42
Au (99.98%) Au (99.98%)	1.88	1.60	1.77	1.60	2.03	1.79
Pt (99.98) Pt (99.98%)	1.92	1.70	1.93	1.68	—	—
Ni (99.95%) Ni (99.95%)	2.11	1.78	2.00	1.68	2.02	1.68
Au (99.98%) Al (99%)	1.42	1.22	1.50	1.16	—	—
Fe (99.9%) Cu (99.95%)	1.99	1.80	2.03	1.80	—	—
Ni (99.95%) Cu (99.95%)	2.34	2.13	2.35	2.12	—	—
Cu (99.95%) Fe (99.9%)	0.43	0.43	0.40	0.40	—	—
Cu (99.95%) Ni (99.95%)	0.85	0.85	0.85	0.85	—	—

An interesting fact is low coefficients of friction for sliding pairs where the pin (stationary specimen) is made of soft metal (Fe, Ni); in pairs with both specimens of the same material the coefficient of friction is approximately twice as high. It can be seen from

Table 14.5

Coefficient of friction in gases

Sliding pair I	Sliding pair II	Medium	Temperature, K	f	Source
12X18H9T	ATM-1	Air	233 (293)	0.16 (0.125)	After A. P. Nesterova
	Fluoroplastic-4			0.075 (0.06)	
Steel У12	Plastic-133			0.12 (0.1)	
АГ-4	Steel 45			0.2 (0.2)	
АГ-4	Brass ЛС-59-1			0.19 (0.18)	
Steel 45 heat-treated	Polystyrene	Nitrogen vapours	77	0.35-0.37	[9]
	Rigid PVC			0.21-0.24	
	Cloth laminate			0.32	
	Fluoroplastic-4			0.11-0.14	
	Wood (beech)			0.40	

Table 14.6

Coefficients of friction for fluoroplastic-stainless steel combinations in gaseous helium [3]

Temperature, K	f for sliding pairs				
	Ф-3 / 12X18H9T	ФН-202 / 12X18H9T	АМИП-15М / 12X18H9T	Ф4Ж-20 / 12X18H9T	Ф-3 / Ф-3
110	0.255	0.135	—	0.20	0.26
130	0.27	0.130	0.32	0.18	0.26
150	0.26	0.120	0.22	0.19	0.26
170	0.27	0.115	0.27	0.21	0.26
190	0.29	0.120	0.345	0.32	0.275
210	0.32	0.160	0.2	0.25	0.28
230	0.33	0.22	0.19	0.22	0.30
250	0.38	0.25	0.21	0.215	0.325
270	0.425	0.26	0.25	0.225	0.36

Table 14.4 that generally the coefficient of friction for pure metals is practically constant over a temperature range from 20 to 300 K.

Additional information on the coefficient of friction of pure metals in gaseous media can be found in [15].

A ring 70 mm in diameter, made of steel 40X was hardened at 850°C and tempered at 200°C; a pin, 10 mm in diameter, made of steel Г13Л, after hardening by heating to 1050°C and quenching in water, had an austenitic structure. The test conditions were as follows: sliding speed 0.11 m/s, normal load 5.2 kgf, and surface roughness 0.32-0.16 μm Ra. The coefficients of friction in air at 83 and 293 K proved to be 0.56.

Table 14.7

Values of coefficients a and b in Formula (14.1)

Sliding-pair materials		Temperature range, K	$a \cdot 10^3$	b
I	II			
Ф-3	Steel 12Х18Н9Т	93-173	0	0.25
		173-273	1.5	0.005
ФН-202		103-193	0	0.125
		193-273	2.19	—0.297
Ф4Ж-20		93-168	0	0.19
		169-188	6.75	—0.662
		188-223	—3.2	0.928
		223-273	0	0.213
АМИП-15М		123-168	3.45	—0.945
		168-196	6.25	—0.849
		196-213	—11.4	2.6
		213-263	0.9	—0.011
АМИП-15М	Steel 12Х18Н9Т chromium-plated	20-100	0.74	0.04
Ф-3	Ф-3	90-173	0	0.255
		173-273	1.25	0.039

Values of the coefficient of friction in gaseous media at low temperatures for some non-metals are presented in Tables 14.5 and 14.6.

Relationship between the coefficient of friction and temperature for the materials given in Table 14.6 can be described by an equation

$$f = aT + b \qquad (14.1)$$

where T = absolute temperature of a rubbing surface; a and b = = constants given in Table 14.7.

Friction in vacuum. Tables 14.8 and 14.9 provide values of the coefficient of friction in vacuum at low temperatures for various combinations of materials.

For some plastic materials a monotone change in the friction coefficient is observed with decreasing temperature. It is noteworthy that with polyethylene, as the temperature goes down from 233 to 213 K, the coefficient of friction rises against its general trend observed within the temperature range of from 293 to 193 K. A monotone character of change of the friction coefficient with temperature is also disturbed in helium for the combinations Ф4Ж-20-12Х18Н9Т at 168 to 223 K and АМИП-15М — 12Х18Н9Т at 168 to 213 K (see Table 14.7).

Table 14.8

Coefficients of friction for metals in vacuum at low temperatures

Sliding-pair materials		Pressure, mm Hg	Temperatures, K	f	Source (reference number)
I	II				
Al	Al	10^{-10}	5	2.2-2.4	
		10^{-8}	77	2.5-2.8	
Cu	Cu	10^{-10}	5	$\geqslant 5$	[17]
Cu*1	Cu*1	10^{-8}	77-300	$\geqslant 5$	
		$5 \cdot 10^{-10}$	73	3	
			273	4	[4]
Pb	Pb	10^{-10}	5	$\geqslant 6$	
		10^{-8}	77-300	$\geqslant 6$	
Fe	Fe	10^{-10}	5	1.1-1.2	[17]
			77	1.1-1.3	
		10^{-8}	300	1.5-1.8	
Zn	Zn	10^{-10}	5	0.25-0.36	
			77	0.35-0.40	
		10^{-8}	300	0.5-0.55	
Steel 40X *2	Steel 40X *2	$5 \cdot 10^{-7}$	83	0.4-0.5	[16]
Steel 110Г13Л	Steel 40X	$5 \cdot 10^{-7}$	293	0.6-0.7	[15]
			83	0.95	

*1 — Copper electrolytic.
*2 — Steel 40X cyanided.

Table 14.9

Coefficients of friction for non-metals in vacuum of 10^{-5} mm Hg [22]

Sliding-pair materials		Temperature, K				
I	II	193	213	233	253	273
Polyethylene	Polyethylene	0.33	0.4	0.38	0.42	0.53
Fluoroplastic-4	Fluoroplastic-4	0.2	0.2	0.7	0.11	0.1
Fluoroplastic-3	Fluoroplastic-3	0.3	0.31	0.35	0.41	0.48
Polymethyl methacrylate	Polymethyl methacrylate	0.45	0.45	0.46	0.48	0.54

14.4. ANALYTICAL STUDY OF TEMPERATURE FIELD IN AXIAL SEALS

Generation of heat in tribological joints located near the main low-temperature units of a machine can affect its characteristics, such as the cooling rate, the efficiency, the maximum attainable temperature level, and the duration of the start-up stage. The tribological components of cryogenic machines are usually made of materials with low thermal conductivity, and, therefore, the emerging temperature field greatly determines their performance, reliability, wear resistance, and frictional losses. In axial seals of cryogenic machines where the coefficient of mutual overlapping is actually equal to 1, the frictional heat, temperature, and temperature gradient are important factors that have an effect on the performance.

The problem of an unstable temperature field which develops in rotary axial seals has been treated in references [18, 23] with allowance for variation of the friction coefficient with temperature. For the initial stage of operation characterized by a temperature field of maximum intensity, the axial seal may be regarded as a system of two like cylindrical rods of annular cross-section, whose end faces are pressed against each other. When one of the rods rotates round the common axis, frictional heat is generated at the contact. The amount of heat depends on the sliding speed, the normal force creating the pressure, and the coefficient of friction. The latter itself generally depends on the temperature at the sliding interface, which changes in time. The problem is formulated on the following assumptions: it is one-dimensional, the frictional heat is generated uniformly over the whole contact area, there is no heat transfer to the ambient atmosphere, the thermal resistance at the contact is small and can be neglected, the coefficient of friction is a known function of the temperature at the sliding interface, and the thermal properties of the materials do not depend on temperature. The mathematical model of the process is expressed by a system of two differential equations

$$\frac{\partial \vartheta_i (x_i, t)}{\partial t} = a_i \frac{\partial^2 \vartheta_i (x_i, t)}{\partial x_i^2}$$

where $i = 1, 2$; $t > 0$; $0 < x_i < \infty$.

The initial conditions are $t = 0$; $\vartheta_1 (x_1, 0) = \vartheta_0$, $\vartheta_2 (x_2, 0) = \vartheta_0$.

The boundary conditions on the rubbing surface (with $x_1 = x_2 = 0$):

$$\vartheta_1 (0, t) = \vartheta_2 (0, t) = \vartheta (t); \; q (\vartheta (t)) = q_1 (\vartheta (t)) + q_2 (\vartheta (t)),$$

where

$$q_1 (\vartheta (t)) = -\lambda_1 \frac{\partial \vartheta_1}{\partial x_1}; \quad q_2 (\vartheta (t)) = -\lambda_2 \frac{\partial \vartheta_2}{\partial x_2}$$

At an infinitely remote distance from the rubbing surface, where $x_1 = x_2 = \infty$

$$\vartheta_1(\infty, t) = \vartheta_0; \ \vartheta_2(\infty, t) = \vartheta_0$$

With a linear relation between the coefficient of friction and temperature [cf. Formula (14.1) and Table 14.7], the temperature in the i-th member of the sliding couple ($i = 1; 2$) can be calculated by the formula

$$\vartheta_1(x_i, t) = \vartheta_0 + \frac{f_0}{a} K_i I_i \tag{14.2}$$

here

$$I_i = \frac{2}{\sqrt{\pi}} \int_0^{\sqrt{\mathrm{Fo}_i}} \exp\left[K_i^2(\mathrm{Fo}_i - \tau^2) - \frac{1}{4\tau^2}\right] \times \left[1 + \frac{2}{\sqrt{\pi}} \int_0^{K_i\sqrt{\mathrm{Fo}_i - \tau^2}} \exp(-\xi^2)\, d\xi\right] d\tau \tag{14.3}$$

$$\mathrm{Fo}_i = a_i t / x_i^2, \quad K_i = \beta\, dx_i / \sqrt{a_i}, \quad i = 1; \ 2 \tag{14.4}$$

$$\beta = \frac{\sqrt{a_1 a_2}}{\lambda_1\sqrt{a_2} + \lambda_2\sqrt{a_1}}, \quad d = \frac{anN(r_2^3 - r_1^3)}{45(r_2^2 - r_1^2)^2}, \quad f_0 = a\vartheta_0 + b \tag{14.5}$$

In these formulas t = time; x = distance from the rubbing surface in the i-th member of the sliding couple; ϑ_0 = initial temperature of the sliding couple; a_i = thermal diffusivity of the material of the i-th member; λ_i = thermal conduction coefficient of the material of the i-th member; n = rotational frequency; N = normal load; r_1 and r_2 = radii of the outer and inner circles defining the seal rings; a and b = coefficients from Formula (14.1).

To facilitate calculations, the coefficient I, depending on two dimensionless sets of quantities K and Fo, has been determined with the aid of a computer for a wide range of parameters; some of the data are given in Table 14.10.

With a linear relationship between the coefficient of friction and temperature, the temperature at the sliding interface in the initial unstable regime can be found by the formula

$$\vartheta(0, t) = \vartheta_0 + \frac{f_0}{a} \beta\, dI_{in} \tag{14.6}$$

where

$$I_{in} = \frac{1}{\sqrt{\pi}} \int_0^t \exp\left[\beta^2 d^2 (t - \xi)\right] \left[1 + \frac{2}{\sqrt{\pi}} \int_0^{\beta d\sqrt{t-\xi}} \exp(-\tau^2)\, d\tau\right] \frac{d\xi}{\sqrt{\xi}} \tag{14.7}$$

Table 14.10

Coefficient I as function of K at some values of Fo

K	I_{in} at Fo					
	1	5	10	15	20	25
0.002	0.3998	1.654	2.671	3.465	4.140	4.738
0.004	0.4004	1.660	2.685	3.488	4.172	4.779
0.006	0.4010	1.666	2.699	3.510	4.203	4.820
0.008	0.4015	1.672	2.713	3.533	4.236	4.861
0.010	0.4021	1.678	2.727	3.557	4.268	4.904
0.012	0.4026	1.684	2.742	3.580	4.301	4.946
0.014	0.4032	1.690	2.757	3.604	4.335	4.990
0.016	0.4038	1.696	2.771	3.628	4.369	5.035
0.018	0.4043	1.702	2.786	3.653	4.404	5.080
0.020	0.4049	1.709	2.801	3.678	4.439	5.125
0.040	0.4107	1.773	2.960	3.941	4.816	5.623
0.060	0.4167	1.842	3.134	4.238	5.250	6.207
0.080	0.4228	1.915	3.326	4.575	5.753	6.897
0.100	0.4291	1.994	3.539	4.957	6.339	7.720

Table 14.11

Coefficient I_{in} as function of time

Time, s	I_p at βd			
	0.0	0.0001	0.001	0.01
60	8.740	8.746	8.800	9.377
120	12.361	12.373	12.482	13.677
180	15.139	15.157	15.320	17.138
240	17.481	17.505	17.723	20.192
300	19.544	19.574	19.848	22.985
360	21.409	21.446	21.774	25.596
420	23.125	23.167	23.551	28.073
480	24.722	24.770	25.209	30.445
540	26.221	26.275	26.770	32.734
600	27.639	27.700	28.250	34.956
660	28.988	29.055	29.661	37.121
720	30.277	30.350	31.012	39.239
780	31.518	31.592	32.310	41.317
840	32.703	32.788	32.562	43.361
900	33.851	33.942	34.772	45.375
960	34.961	35.058	35.944	47.363
1,020	36.037	36.140	37.082	49.329
1,080	37.082	37.191	38.189	51.276
1,140	38.099	38.213	39.267	53.206
1,200	39.088	39.208	40.320	55.120
1,260	40.054	40.180	41.347	57.022
1,320	40.996	41.128	42.352	58.912

ϑ (0, t) = temperature at the sliding interface depending on time;

$$\beta d = \frac{\sqrt{a_1 a_2}\, anN\,(r_2^3 - r_1^3)}{(\lambda_1 \sqrt{a_2} + \lambda_2 \sqrt{a_1}) \cdot 45\,(r_2^2 - r_1^2)^2}$$

The values of I_{in} depending on integration limits and on the set of quantities βd have been determined for a wide range of parameters using a computer; some of the data are given in Table 14.11.

Example 1. Find the temperature at the interface of an axial seal after 10 min of run from the start. The rubbing materials are fluoroplastic-4 and stainless steel 12X18H9T.

Given: $n = 5{,}000$ rpm, $N = 0.6$ kgf, $a = 1 \cdot 10^{-3}$ K^{-1}, $b = 0.027$, $r_1 = 0.02$ m, $r_2 = 0.03$ m, $\vartheta_0 = 273$ K, $\lambda_1 = 15.6$ W/(m·K), $C_1 = 0.462$ kJ/(kg·K), $\rho_1 = 8{,}130$ kg/m^3, $\lambda_2 = 0.279$ W/(m·K), $C_2 = 0.973$ kJ/(kg·K), $\rho_2 = 2{,}150$ kg/m^3 (subscript 1 pertains to the stainless steel).

Solution: Thermal diffusivity coefficients $a_1 = 4.15 \cdot 10^{-6}$ m^2/s; $a_2 = 0.133 \times 10^{-6}$ m^2/s; coefficient $\beta = 1.19 \cdot 10^{-4}$ [formula (14.5)]: coefficient $d = 8.46$ [formula (14.5)]; the value of $\beta d = 0.001$; the value of $I_{in} = 28.25$ (Table 14.11); the value of $f_0 = 0.3$ [formula (5)]; the interface temperature $\vartheta = 281.5$ K [formula (6)].

Example 2. Find the temperature of the rubbing components of Example 1 at a distance of 8 mm from the sliding interface after 7 min of run from the start.

Given: The data of Example 1.

Solution: Coefficient $\beta = 1.19 \cdot 10^{-4}$ [formula (14.5)]; coefficient $d = 8.46$ [formula (14.5)]; the values of $K_1 = 3.95 \cdot 10^{-3}$; $K_2 = 21.9 \cdot 10^{-3}$ [formula (14.4)]; the values of $\mathrm{Fo}_1 = 27.2$, $\mathrm{Fo}_2 = 0.87$ [formula (14.4)]; the values of $I_1 = 4.9$, $I_2 = 0.4$ (Table 14.10); the temperature inside the stainless steel member $\vartheta_1 = 278.8$ K; the temperature inside the fluoroplastic-4 member $\vartheta_2 = 275.6$ K, the temperature at the interface $\vartheta = 280$ K.

REFERENCES

1. Алексеев В. И., Ковальченко М. С. Некоторые закономерности изнашивания металлов и металлоподобных карбидов в вакууме при низких температурах.— «Физико-химическая механика материалов», 1971, № 3, с. 38-42.

2. Архаров А. М., Воронин Г. И., Харитонова Л. Д. Прибор для исследования сухого трения при низких температурах.— «Приборы и техника эксперимента», 1971, № 4, с. 235-236.

3. Архаров А. М., Харитонова Л. Д. Экспериментальное исследование антифрикционных свойств материалов на основе фторопласта при низких температурах.— «Известия вузов. Машиностроение», 1973, № 7, с. 122-126.

4. Браун и Бартон. Прибор для измерения трения и адгезии в сверхвысоком вакууме.— «Приборы для научных исследований», 1966, № 12, с. 61-63.

5. Брюшке и Экман. Прибор для измерения трения в сверхвысоком вакууме.— «Приборы для научных исследований», 1963, № 9, с. 17.

6. Дитрих, Таунсенд, Зарецкий. Усталость тел качения при низких температурах и смазке фтористыми полиэфирами.— «Проблемы трения и смазки», 1971, № 3, с. 50-58.

7. Карагусов И. Х. Влияние температуры на антифрикционные свойства поршневого манжетного уплотнения из ФН-202.— «Кислородное и автогенное машиностроение», 1965, вып. 1, с. 10-11.

8. Кислик В. Ж. Применение гелиевого торцового уплотнения в насосе для жидкого кислорода. Пер. с англ.— «Проблемы трения и смазки», 1969, № 4, с. 75-81.

9. Кулеба В. И., Любарский И. М. Исследование процесса трения и изнашивания материалов в среде жидкого азота.— «Проблемы трения и изнашивания», 1976, № 9, с. 71-75.

10. Ларионов В. П., Ковальчук В. А. Хладостойкость и износ деталей машин и сварных соединений. Новосибирск. Сибирское отделение изд-ва «Наука», 1976, 206 с.

11. Новицкий Л. А., Кожевников И. Г. Теплофизические свойства материалов при низких температурах. М., «Машиностроение», 1975, 216 с.

12. Самсонов Г. В., Запорожец А. А. Развитие электронных представлений о процессе изнашивания переходных металлов в среде жидкого азота.— «Физико-химическая механика материалов», 1970, № 6, с. 43-48.

13. Смирнов Е. Н., Кудрявцев Е. А., Смирнов Е. В. Применение антифрикционных материалов в насосах для сжиженных газов высокого давления.— «Химическое и нефтяное машиностроение», 1973, № 10, с. 39-40.

14. Справочник по физико-техническим основам криогеники. Под ред. М. П. Малкова. М., «Энергия», 1973, 387 с. Авт.: М.П. Малков, И. Б. Данилов, А. Г. Зельдович, А. Б. Фрадков.

15. Трение и износ при низких температурах.— «Металловедение и термическая обработка металлов», 1971, № 3, с. 9-12. Авт.: Г. Н. Преснякова, И. М. Любарский, В. Ф. Удовенко, Е. И. Марьяхина, С. С. Черняк.

16. Трение цианированной стали 40Х в вакууме при температурах —190 и +20°С.— В сб.: Поведение материалов в условиях вакуума и низких температур. Харьков, 1972, с. 42-46. Авт.: Г. Н. Преснякова, И. М. Любарский, В. Ф. Удовенко, Е. И. Марьяхина.

17. Установка для исследования процесса высшего трения и смазывания в сверхвысоком вакууме при температурах от 500 до 5 К.— «Проблемы трения и изнашивания», 1972, № 2, с. 68-73. Авт.: С. С. Карапетян, В. С. Оськин, А. Н. Пономарев, А. А. Силин.

18. Харитонова Л. Д. Расчет температурного поля в узлах трения низкотемпературных машин.— «Известия вузов. Машиностроение». 1973, № 12, с. 105-110.

19. Элконин Б. В. О работоспособности сепараторов шарикоподшипников при низких температурах.— «Вестник машиностроения», 1968, № 2, с. 34-36.

20. Burton R. A., Russel J. A., Ku P. M. Metallic friction at cryogenic temperatures.— "Wear", 1962, No. 5, p. 60-68.

21. Flom D. G., Porile N. T. Friction of teflon sliding on teflon.— "Journal of applied physics", 1955, No. 9, p. 1088-1092.

22. King R. F., Tabor D. The effect of temperature on the mechanical properties and the Friction of Plastics.— "The Proceeding of the Physical Society", 1953, vol. 66B, p. 728-734.

23. Schaaf S. A. On the superposition of a heat source and contact resistance. — "Quarterly of applied mathematics", 1947, vol. 5, p. 107-111.

24. Swenson C. A. Mechanical Properties of teflon at low temperatures.— "Review of Scientific Instrument", 1954, No. 8, p. 834-835.

25. Wisander, Johnson. Wear and Friction in liquid nitrogen with austenitic stainless steel having various surface coatings.— "Advancing Cryogenic Engineering", 1960, vol. 4.

Chapter 15

FRETTING

15.1. BASIC INFORMATION

The useful life of many tribological joints is limited by wear or failure of the rubbing components due to fretting, which occurs with oscillatory relative displacements of the rubbing surfaces. Such displacements may result from vibrations, reciprocating motion, periodic bending or twisting of mating components, etc. Slip between joint faces is an indispensable condition for fretting to arise. Intensive wear of the components involves the loss of the design dimensions beyond the tolerances. Fretting also tangibly downgrades the surface layer quality, producing increased surface roughness, micropits, subsurface microcracks, which reduce the fatigue strength of the components.

According to GOST 5272-68 *fretting* is defined as corrosion of rubbing surfaces oscillating relative to each other in presence of a corrosive medium. GOST 16429-70 gives a definition of *fretting wear* as a mechano-corrosive wear of rubbing surfaces having small relative oscillatory displacements. The term 'fretting', or 'fretting wear', is sometimes applied to the phenomena that occur in the rubbing of precious metals or non-metals, and also in that of chemically active metals in high vacuum or dry inert gases. The term 'fretting' can also be found as referred directly to the oscillatory relative displacements of rubbing parts pressed against each other.

Fretting is a specific kind of wear that has the following differences in character and origination conditions from the conventional wear observed in non-oscillatory rubbing:

—wear debris are hard to remove from the friction zone owing to a small amplitude of oscillations, and surface damage is clearly confined to real-contact areas;

—the rate of relative motion of the rubbing surfaces is much lower than that of plain non-oscillatory motion. For instance, with a sliding amplitude of 0.025 mm and a frequency of oscillation of 30 Hz, the maximum rate of sliding equals 4.7 mm/s, and the mean rate, 3 mm/s;

—the presence of oxygen may reduce wear in plain sliding friction, whereas in fretting it aggravates surface damage. Wear debris in fretting are mainly metal oxides.

Typically, fretting develops in various forced fits on rotating shafts, in the attachment of turbine and compressor blades, in splined, keyed, threaded and riveted joints. Subject to fretting are also cables and cable pulleys; contact surfaces of antifriction bearings that transmit loads without rolling; couplings; contact surfaces of compression springs, leaf springs, safety valves and machine governors; cams and linkages; electrical contacts, etc.

Surface damage caused by fretting appears in the form of wear scars, pick-up of metal particles; tearing or pitting, with the pits often filled with powdery wear debris; bands or grooves of local wear and also surface microcracks. On the surfaces subject to fretting, such phenomena can be observed as seizure, microcutting, and fatigue failure in microvolumes accompanied with oxidation and corrosion. Depending on loading conditions, materials and ambient media, one of these processes can be dominant and the other complimentary. The first visual indication of fretting on rubbing surfaces is the presence of coloured spots where compacted oxides accumulate.

In addition to the changes in geometry and appearance of the component, fretting can bring about another harmful effect, such as a loss of dimensional accuracy. This may develop in two ways. If the wear debris can to some extent escape from the contact zone, the character of the initial fit will change and the interference in the joint will become weaker. If the debris is trapped, the joint is liable to seizure or even jamming, which is all the more likely because the volume of the wear debris is usually greater than that of the metal oxides formed. This situation is particularly critical in applications where the parts in contact have from time to time to disengage during operation (as, for instance, in safety valves and governors).

15.2. FRETTING TESTS

The testing methods are reviewed in detail in [1, 2, 3].

Experimental practice indicates that fretting wear tests give the best results when performed on specimens with flat annular contacts.

Resistance to fretting can be assessed by mass wear ΔU_m or linear wear U, or by these quantities related to a unit sliding distance.

The mean linear wear is determined by recording the profile of the sliding track. Although it provides a general picture of surface damage, the method sometimes may prove to be inaccurate. For instance, deep local micropits may be more harmful than those of the same volume but of smaller depth. The mass wear evaluation method is ineffective in situations where the extent of wear is small and, particularly, the transfer of material from one rubbing surface to the other is likely. Surface damage due to fretting can also be assessed by multiplying the area of the wear spot by its depth.

Before testing, the specimens are carefully cleaned and degreased. After the tests, the oxides on the rubbing surfaces are removed either

by mechanical action or by means of solvents. For all practical purposes the following solutions provide the required cleaning effect:

No. 1 (for 100 ml of aqueous solution): 4 g hydroquinone, 22 ml ortho-phosphoric acid (concentrated), 20 ml alcohol;

No. 2: 70 ml liquid glass (density 1.2 to 1.25) and 100 ml hydrochloric acid. The liquid glass is added to the acid, and the solution is hold for 24 h before using.

15.3. FACTORS INFLUENCING THE DEVELOPMENT OF FRETTING

The rate of fretting wear depends on the mechanical characteristics of contact interaction, the nature of the materials in contact, the chemical composition of an ambient medium (gaseous or liquid), and other factors.

Amplitude of slip. Relative oscillatory displacements of the mating surfaces are essential for fretting to occur. A very small amplitude (8×10^{-7} mm) of slip is believed to be sufficient to cause a conspicuous surface damage. As the amplitude grows, the effects of fretting become increasingly similar to plain sliding wear.

Normally, the rate of fretting wear is in direct proportion to the amplitude of slip, but some findings have revealed a parabolic relation as well (Fig. 15.1). A particularly sharp rise in the wear of steel is observed with an amplitude of 0.10 to 0.15 mm, when seizure develops to a considerable degree. With very small amplitudes, the friction is rolling rather than sliding in nature, because the oxide particles function as rolling elements, and that checks the development of seizure. The character of relation between the wear rate and the slip amplitude varies depending on the material of the parts in contact, and on the testing methods and conditions.

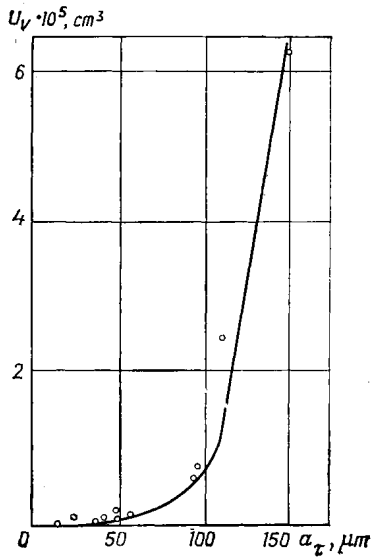

Fig. 15.1. Wear volume U_v as function of slip amplitude a_τ for a low-carbon steel—duralumin combination at $N = 19$ kgf; $N_c = 10^6$ cycles (according to O.N. Muravkin, A.V. Ryabchenkov and N. Panafidin)

Contact pressure. Tangible damage due to fretting may arise at very small pressures (in unloaded rolling bearings, in loose threaded assemblies, etc.). The effect of load on the development of fretting is rather difficult to evaluate, because the actual contact pressure in

the joint does not remain constant during operation. The reason is the changes in the initial microprofiles of the mating surfaces and the formation of a wear debriis layer at the interface.

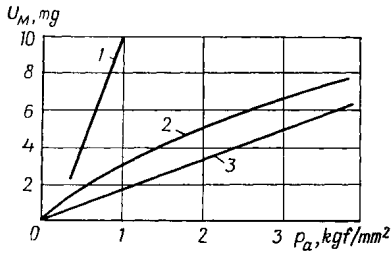

Fig. 15.2. Wear of carbon steel as function of specific load (a_τ = 0.09 mm; N_c = 67 800 cycles; f = 38 Hz)
1—according to Read and Butter; *2*—according to I. Pheng and G. Ulig; *3*—according to K.G.R. Wright

The relation between the wear rate and normal load can be linear or parabolic depending on the testing method and conditions, properties of the materials, surface damage criteria, slip amplitudes, and load ranges (Figs. 15.2 and 15.3).

If the drive system of the test rig is not rigid enough, an increase in the normal load may result in a decrease in the oscillation amplitude and in the rate of wear. However, this decrease in wear achieved on reaching a certain critical load value should not be attributed entirely to the reduction in amplitude, because a similar effect is also observed when the amplitude is maintained constant (Fig. 15.4).

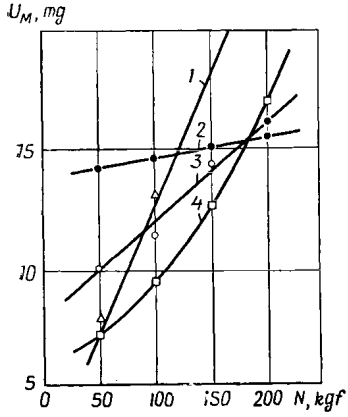

Fig. 15.3. Wear of steels 20(4), 18Х2Н4МА (3), 30ХГСА (2); and alloy aluminium Д16 (1), as function of normal load (counterface of steel 30ХГСА, a_τ = 0.3 mm; N_c = = 27·10⁴ cycles, f = 25 Hz) according to B.D. Shipilov *et al.*

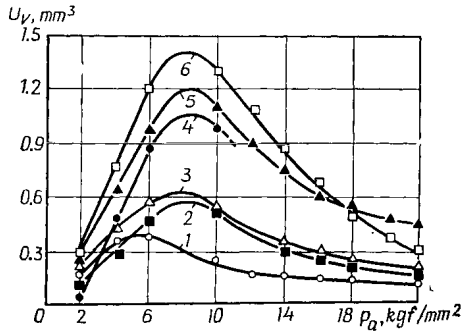

Fig. 15.4. Wear by volume as function of specific load at a_τ = 0.05 mm: f = 25 Hz; N_c = 250·10³ cycles
1—hardened steel 45; *2*—steel 12Х18Н9Т; *3*—bronze; *4*—alloy Д16Т; *5*—Armco iron; *6*—normalized steel 45

Here, the amount of wear grows up to a load of 600 to 800 kgf/cm² and then goes down. The observed wear behaviour signifies that different basic phenomena underlying fretting come into play. At the loads corresponding to the rising portions of the curves, the corro-

sion fatigue processes, particularly typical of fretting, run on the mating surfaces, which still can relatively easily be reached by atmospheric oxygen. The decrease of wear at loads exceeding the critical values is brought about by more intensive seizure and mutual metal transfer on the joint faces. Although the overall amount of wear declines, the depth of surface damage at individual points grows with the rise of the specific load. As this takes place, an increase in the friction force slows down owing to the plastic flow of the metal and to the growing intensity of thermal effects.

Oscillation frequency. Variation in oscillation involves the changing of the cycle period, the speed of the relative oscillatory motion,

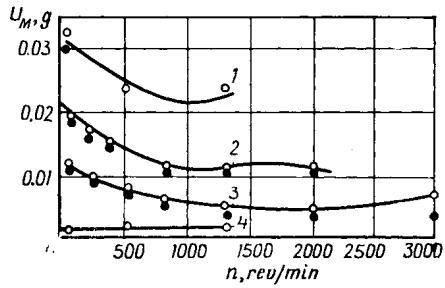

Fig. 15.5. Wear of low-carbon steel in dry air as function of oscillation frequency and amplitude at $p_a = 3.7$ kgf/mm²
1 — $a_\tau = 0.23$ mm; $N_c = 67\,800$ cycles; 2 — $a_\tau = 0.091$ mm; $N_c = 457800$ cycles; 3 — $a_\tau = 0.091$ mm; $N_c = 67\,800$ cycles; 4 — $a_\tau = 0.01$ mm; $N_c = 67\,800$ cycles; ○ — referred to 25°C; ● — temperature of test (from Pheng and Ulig)

and the contact temperature. Typically, fretting wear in air decreases with rising oscillation frequency, and then it tends to level off (Figs. 15.5 and 15.6). In nitrogen, wear does not depend on oscillation frequency. The formation and rupture of oxide films determine the amount of wear to a considerable degree. As lower oscillation frequencies at a constant amplitude prolong the time of exposure of metal surfaces in contact to oxidation, a respective increase in the amount of wear may result.

Apparently, the critical frequency at which wear reaches its peak and the rate of this wear for different materials must depend on their oxidation stability. This is confirmed by the fact that steels that resist oxidation (e.g., steel 18Х2Н4МА) scarcely respond to frequency changes (Fig. 15.7). The abnormal wear behaviour of aluminium alloy Д16 is usually attributed to the predominance of abrasion. It follows from Fig. 15.5 that the effect of frequency on wear grows with the slip amplitude, contact pressure, and testing time.

The change of wear rate with oscillation frequency in fretting can also be accounted for by a marked decrease in the fatigue life of metals at lower loading frequencies.

The number of loading cycles. Damage to the surfaces in contact from fretting spreads with the increase of testing time. However, the character of fretting progress may change depending on properties of the material, oscillation amplitude, and specific load. Normally, the wear rate for steel grows particularly fast during the running-in stage, and then it slows down. It is interesting to note, however, that a low-gradient portion may be observed on the wear curve near its origin (Fig. 15.8), which reflects repeated transfer of the metal from one mating surface to the other.

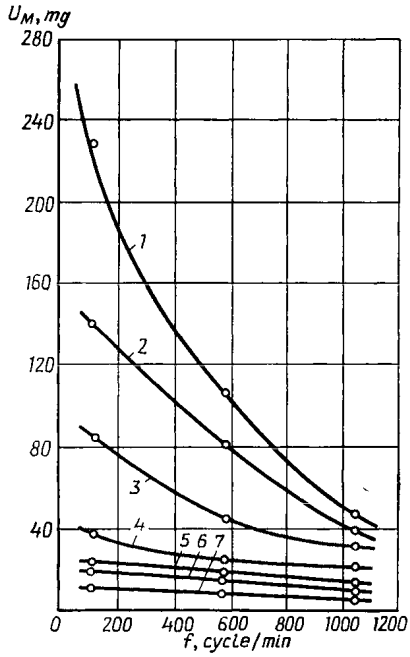

Fig. 15.6. Effect of oscillation frequency (cycles/min) on fretting wear of steel 15 (p_a = 5 kgf/mm², a_τ = 0.524 mm)
1—N_c = 103 550 cycles; *2* — N_c = 70 850 cycles; *3*—N_c = 38 150 cycles; *4*—N_c = 16 350; *5* – N_c= 10 900; *6*–N_c = 5450; *7* –N_c=2 725 (from A. N. Ryabchenkov and O. N. Muravkin)

With small amplitudes and moderate contact loads, the wear curve may at some testing stage become decaying in character; with high amplitudes and specific loads the extent of wear is generally proportional to the number of test cycles.

In some situations where fretting involves the formation of very hard wear debris (e.g., for aluminium and its alloys), the wear grows linearly straight from the beginning, which indicates the predominant role of microcutting. If the relative tangential oscillations of the mating surfaces are accompanied with pulsations of the normal load, precipitate wear may result.

Ambient medium. The intensity of fretting is strongly dependent on the corrosive activity of the gas medium and on the chemical activity of the metal. In air, fretting wear is greater than in vacuum, nitrogen, and helium. In oxygen all metals are damaged by fretting harder than in air.

Data on the effect of humidity on the development of fretting are discrepant. Some authors report a 50 to 60 percent reduction in the wear of steel with humidity rising up to 100 percent as compared with the wear observed in dry air. Others report still greater change of wear with humidity, their relation not always being monotone (Fig. 15.9). One of the factors contributing to the reduction of wear in humid air is a change of frictional characteristics due to adsorption or capillary condensation of water vapours on the joint faces.

Wear in atmospheric conditions is usually several times greater than in liquids (e.g., distilled water, sodium hydrate solution). Apparently, in liquids protective oxide films form faster than in

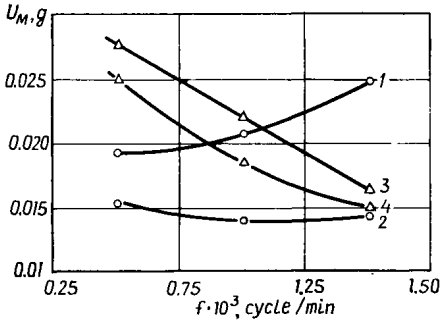

Fig. 15.7. Effect of oscillation frequency on (fretting wear of alloy Д16(1); steel 18Х2Н4МА (2); steel 20 (3); and steel 30ХГСА (4) at $a_\tau = 0.3$ mm; $p_a = 1.25$ kgf/mm²; $N_c = 2.7 \cdot 10^5$ cycles (from V.L. Shipilov [*et al.*)

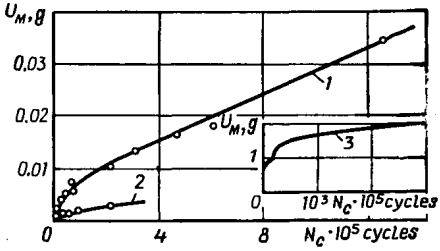

Fig. 15.8. Fretting wear of low-carbon steel as function of the number of loading cycles at $a_\tau = 0.097$ mm; $f = 9$ Hz; $p_a = 3.72$ kgf/mm²; *1* — in air; *2*—in nitrogen; *3*—the initial portion of the curve *1* (according to I. Pheng and G. Ulig)

air. In addition, in liquids wear debris are less hard, and they are partly washed out of the contact zone, thereby reducing abrasive wear.

Lubrication. Although lubrication usually cannot give full protection from fretting, any lubricant in the joint is better than none at all. *Fluid lubricants*, such as mineral and fatty oils, provide the maximum effect when the surfaces in contact are immersed in the oil delivered to the friction zone so that the surfaces are protected from oxygen. The best results are obtained with the oils in which oxygen dissolves poorly and has a low diffusion coefficient. In addition, the oi s should have good tackiness, withstand high pressures, resist oxidation, and provide high stability of the properties in time. For example, polyglycol ethers and diesters are more effective than mineral oils of the same viscosity. Of all synthetic oils for instrument applications, the maximuam resistance to fretting is achieved with oils having high lubricity: ВНИИ НП-6, МН-60, and ВНИИ НП-223. Oils based on silicone fluids, such as

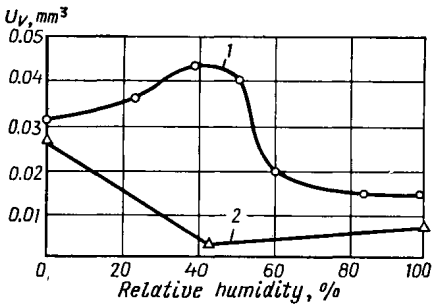

Fig. 15.9. Bulk wear of steel as function of relative humidity
1—according to N. Soda and A.Aoki; *2*—according to K.G.R.Wright

МП-601, МП-610, ВНИИ НП-274, ВНИИ НП-293 do not provide adequate fretting stability. Thin mineral oils (transformer oil, spindle oil) are ineffective for protection from fretting, whereas thin synthetic diester oils blended with additives like tricresyl phosphate (e.g. oil ВНИИ НП-50-1-4Ф) are capable of considerably retarding the progress of fretting. Some non-metal films, for instance those formed by phosphating and anodizing, provide good retention of an oil film on the mating surfaces and thereby reduce fretting effects.

The application of fluid lubricants involves the problem of keeping them in place by sealing; despite various solutions to this problem, fluid lubricants are often, under severe conditions of fretting, incapable of separating effectively the mating surfaces and preventing them from direct contact. For this reason, in certain circumstances it is advantageous to use *greases*. With greases, however, the antifretting properties are heavily dependent on the mechanical stability, consistency, soap content, additives, etc. Greases similar in chemical composition and consistency may have different fretting stability, depending on their shear strength. Generally, the effect of fretting is more pronounced with the use of greases having high shear strength. The initial consistency of greases as such cannot define their antifretting properties. Diluting to lower consistencies improves the ability of greases to prevent fretting. In some cases, however, a grease of lower consistency exhibits much poorer antifretting properties because of its soap content.

In some cases solid lubricants, both metals (lead, indium) and non-metals (graphite, molybdenum disulphide), can be effectively used for the prevention of fretting. On the other hand, molybdenum disulphide, graphite, and zinc oxide added to greases produce little or sometimes even negative effect.

Good results can be achieved by the use of calcium greases with extreme-pressure additives. Typically, a lubricated surface with greater roughness shows better resistance to fretting. The reason for it is that surface irregularity valleys serve as natural lubricant collectors which regenerate boundary lubricant films; in addition, wear debris accumulate there. For softer metals, however, increased surface roughness results in greater wear.

Fretting resistance of various materials. All materials (metals and non-metals) in any combination are to some extent subject to fretting. Depending on contact pressure, slip amplitude, testing time, and lubricant, some combinations of materials under certain conditions can be damaged more than others and under different conditions may prove to be less sensitive to fretting. Three groups of the combinations of materials according to their resistance to fretting are given in Table 15.1.

No positive relation between the hardness of metals and their resistance to fretting has been established. Only the materials that do not oxidize in fretting (quartz, ruby, glass, mica, etc.) exhibit the

Table 15.1

Fretting resistance of various materials combinations (testing in dry air without lubrication)

Combinations of materials with fretting resistance		
Good	Medium	Poor
According to Mc Dowell		
Cast iron/cast iron: with phosphate coating with rubber gaskets with rubber cement adhesive with tungsten sulphide with powdery molybdenum disulphide Cast iron/stainless steel with powdery molybdenum disulphide	Cast iron/cast iron (with smooth, rough and unmachined surfaces) Cast iron/copper coating Cast iron/amalgamated copper coating Cast iron/silver plating	Cast iron/cast iron coated with shellac Cast iron/chromium plating Cast iron/tin plating
Cold-rolled steel/cold-rolled steel Hardened tool steel/tool steel	Copper/cast iron Brass/cast iron Zinc/cast iron	Hardened tool steel/stainless steel Aluminium/stainless steel Aluminium/cast iron Magnesium/cast iron Bakelite/cast iron Laminated plastic/cast iron
Laminated plastic/gold plating	Magnesium/copper plating Circonium/circonium	Gold plating/gold plating Chromium plating/chromium plating
According to Gray and Jenny		
Sand-blasted lead-coated steel/steel (very good) Steel/steel with nylon gasket 1.6 mm thick (very good) Bonderized (Zinc-and-Iron) steel/steel (good with adequately thick coating)	Sand-blasted steel/steel Sulphide-coated bronze/steel Cast bronze/phosphated steel Magnesium/steel	Steel/steel Sand-blasted copper-, tin- or silver-plated steel*1/steel Sand-blasted steel coated with aluminium foil/steel Nitrided steel/chromium-plated steel*2 Steel/steel with beryllium-bronze gasket

*1 Silver-plated steel can be effective with small loads and plating thicknesses (0.1 mm).

*2 Some improvement in fretting resistance is gained with heating the chromium-plated steel to 538°C for 1 hour.

Continued

Combinations of materials with fretting resistance		
Good	Medium	Poor
According to Sackman and Rightmire		
Lead/steel Silver plating/steel Phosphated steel/steel	Zinc/steel Cadmium/steel Copper alloy (phosphorous bronze)/steel	Steel/steel Nickel/steel Aluminium (or its alloy)/steel Tin/steel Antimony/tin
Silver plating/aluminium coating	Zinc/aluminium Copper coating/aluminium Nickel plating/aluminium Silver plating/aluminium Iron coating/aluminium	Aluminium/aluminium Zinc plating/aluminium Iron-coated steel/aluminium

increase of resistance to fretting with hardness. Apparently, damage to surfaces from fretting is largely related to the abrasive properties of the wear debris. Besides, resistance to fretting depends on the ability of the material to withstand dynamic loads (cyclic strength), its corrosion resistance, and its plasticity and toughness.

In some cases, an important part in fretting is played by the electrochemical factor. It follows from Fig. 15.10 that the higher the positive electrode potential of a material relative to that of steel 45 which it contacts, the less is its damage by fretting and, in turn, the greater is the wear of the steel itself. Sometimes this factor is outweighed by a specific mechanical property: a material with low corrosion stability but high cyclic strength (e.g., steel 30ХГСНА) resists fretting well. On the other hand, high corrosion stability with a relatively low cyclic strength also provides adequate resistance to fretting. Considering materials chemically active to approximately the same degree, it can be inferred that surface damage from fretting correlates with the cyclic strength of the materials. The electrochemical factor comes into play when dispersed-phase oxides emerge in the friction zone; these oxides can actively absorb moisture and oxygen from air and retain them on the surface.

Table 15.2. gives information on fretting resistance of some materials.

Ambient and contact temperatures. It has been observed in practice, that in winter fretting is generally much stronger than in summer. Experimental findings indicate that fretting wear of carbon

Table 15.2

Fretting resistance of steels ($a_t = 50$ μm, $f = 30$ Hz)*1

Steel grade	Heat treatment	Fretting resistance at pressure, kgf/cm², $Q \cdot 10^3$ cycle/μm		
		100	300	500
30ХГСА	Oil hardening from 870-890°C, tempering at 400°C, cooling in oil	125	100	71.4
30ХГСНА	Oil hardening from 890-900°C, tempering at 200°C	250	167	125
40ХНМА	Oil hardening from 850°C, tempering at 600°C	200	125	83.3
38ХА	Oil hardening from 860°C, tempering at 520°C	125	83.5	62.5
12Х2Н4А	Oil hardening from 780-810°C, tempering at 150-170°C in air	83.4	45.5	14.1
12ХН3А	Oil hardening: 1st stage from 840±20°C, 2nd stage from 780-810°C, tempering at 150-170°C in air	100	71.5	43.2
14ГСН2МА(ДИ-3А)	Oil hardening from 820±20°C, tempering at 190°C in air	114	91	57.5
18ХНВА	Carburizing at 980-1030°C, hardening from 950°C in air, tempering at 200°C	62.5	50	45.5
38ХМЮА	Nitriding: 1st stage 500-520°C for 18 h, 2nd stage 540-560°C for 25 h, cooling with furnace	125	83.3	62.5
16ХГТА	Oil hardening from 790-860°C, tempering at 160-180°C	125	41.7	22.7
08Х18М10Т	Air hardening from 1050°C	253	16.2	117
ХН38ВТ(ЭИ703)	Water hardening from 1140°C	250	83.3	71.4
14Х17Н2	Oil hardening from 1020°C, tempering at 300°C, cooling in air	278	167	125
13Х12Н2В2МФ	Oil hardening from 1020°C, tempering at 700°C, cooling in water	200	135	91
40Х12Н8Г8МФБ	Water hardening from 1150±10°C (heating for 1.75-2 h), two stage ageing at 670°C (16 h) and 790±±10°C (16 h), cooling in air	250	167	106.3
ХН77ТЮР*2	Air hardening from 1080±10°C (8 h), ageing at 700±10°C (16 h), cooling in air	334	200	116
ЖС6-К*2	Air hardening from 1210-1220 °C (4 h)	227	167	79.4
ШХ15	Oil hardening from 835-860°C, tempering at 150°C	83	23.8	15.6
ХВГ	Oil hardening from 820-840°C, tempering at 160-180°C	55.5	31.3	23
45	Hardening from 830-850°C, tempering at 300°C	143	71.4	58.8

*1 Reference material was heat-treated steel 45 (hardening at 830-840°C, tempering to *HV* 600).
*2 Alloy.

steel steadily grows with its temperature lowered to—140°C, whereas within the range of from +50 to 150°C its rate remains practically unchanged. At low temperatures the metal may become brittle, and the adsorption of gases increases, which may change the speed of the chemical reactions.

The oscillatory contact interaction may itself result in substantially increased temperatures in surface layers. The contact temperature varies depending on the oscillation amplitude, specific pressure

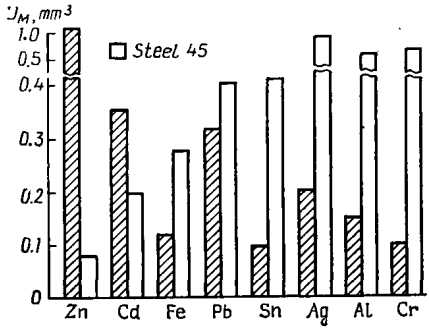

Fig. 15.10. Histograms of fretting wear (by volume) of electrodeposited and thermodiffusional coatings in contact with steel 45 at $p_a = 5$ kgf/mm²; $N_c = 0.5 \cdot 10^6$ cycles

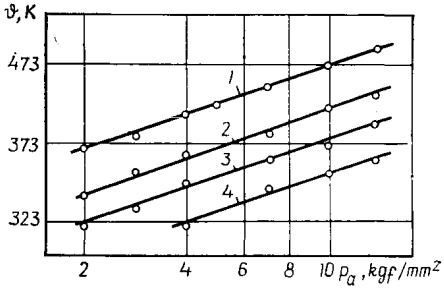

Fig. 15.11. Mean temperature of surface layer for steel Grade 45 as function of specific load at $f = 25$ Hz; *1*—$a_\tau = 0.02$ mm; *2*—$a_\tau = 0.03$ mm; *3*—$a_\tau = 0.05$ mm; *4*—$a_\tau = 0.08$ mm

and thermal properties of the surfaces in contact (Fig. 15.11). High instant temperatures (up to 700 to 800°C) may occur on the contact surfaces at moderate as well as at high loads. These are localized temperatures at the spots of real contact. For materials of lower thermal conductivity, all other things being equal, contact temperatures produce a stronger effect, which may lead to surface-layer structural changes and a stronger tendency to seizure.

15.4. MECHANISM OF FRETTING

Generally, the process of fretting for steel under dry friction conditions can be divided into three main stages. At the first stage, the strengthening of the surfaces in contact and a cyclic flow of the surface layers are observed; most asperities forming the spots of real contact interact plastically. This is aided by the seizure of juvenile metal at the spots of contact after the rupture of the natural oxide films. The asperites disintegrated due to fatigue and the disrupted cold-weld junctions produce primary wear debris, part of which oxidizes. But most of the wear debris at this stage is metal particles. Transition of the surface layers into a highly dispersed state speeds up the process of oxidation.

The second stage of fretting involves continued accumulation of fatigue damage in the subsurface layers. Simultaneously, a corrosive medium is formed in the friction zone through the adsorption of oxygen and moisture on the oxides. The rate of wear at this stage is not high; this wear is mainly associated with the destruction of oxide films in the friction zone. Here the amount of the wear debris levels off because its departure from the contact is balanced by the formation of new wear particles. These conditions give rise to a specific (mechano-chemical) mechanism of increasing the oxidation of metal surfaces. This mechanism involves the development, under cyclic loading conditions, of a chemically responsive highly-dispersed surface-layer structure. This is a mixed structure (consisting of the metals and their oxides), which may perform as a protective factor, reducing wear. The second stage of fretting may be called the incubation phase. Under the optimal conditions of the stabilized contact, the previously strengthened surface layers carry somewhat reduced cyclic loads and accumulate fatigue intensified by corrosion processes.

Being semiconductors, the highly-dispersed oxides formed in fretting serve as catalysts in the process. They increase the adsorption of oxygen and moisture in active radical and ion-radical forms, developing an active electrolytical medium between the mating surfaces.

The third stage of fretting is characterized by a final disintegration of the affected areas loosened by the fatigue and corrosion processes. Since electrochemical processes are likely to run at this stage, it can be called fatigue-and-corrosive destruction. At this stage the surface layers, which have long been subjected to cyclic deformations, become so weakened that they lose stability and rapidly disintegrate. This is manifested by increased wear rate.

15.5. QUANTITATIVE ESTIMATION OF FRETTING

In its present state, the theory of fretting has yet to be further developed to allow purely analytical calculations of wear rate for various materials. The current methods of experimental wear-rate analysis can be divided into two groups depending on the adopted criterion of fretting resistance.

The first group can be exemplified by the method suggested by A. S. Akhmatov and M. S. Ostrovsky. Here, the fretting-resistance criterion used is the duration of the latent period of fretting (τ), after which the boundary lubricant film is broken, and tearing in depth occurs on the contact surface

$$\tau = k_1 R_a \exp(-k_2 A N f / R_a)$$

where A = amplitude of slip; f = oscillation frequency; k_1 and k_2 = empirical coefficients determined from experimental data.

The second-group methods involve calculations of the amount of wear. The equation used is based on the fatigue-and-corrosion mechanism of fretting:

$$\Delta F_n = k_1 N a_\tau N_c + (k_2 + k_3 N + k_4 N^2) \frac{N_c}{f}$$

where k_1, k_2, k_3, and k_4 = constants determined by the chemical activity, specific surface energy, and fatigue strength of the material; N_c = number of cycles. The values of the coefficients are found from experimental data on ΔF_n for several (no less than four) sets of N, N_c, f, and a_τ.

15.6. PROTECTION FROM FRETTING

Damage to contact surfaces is generally determined by the main processes, such as fatigue, corrosion, seizure, and microcutting. These processes develop in the surface layers simultaneously, but,

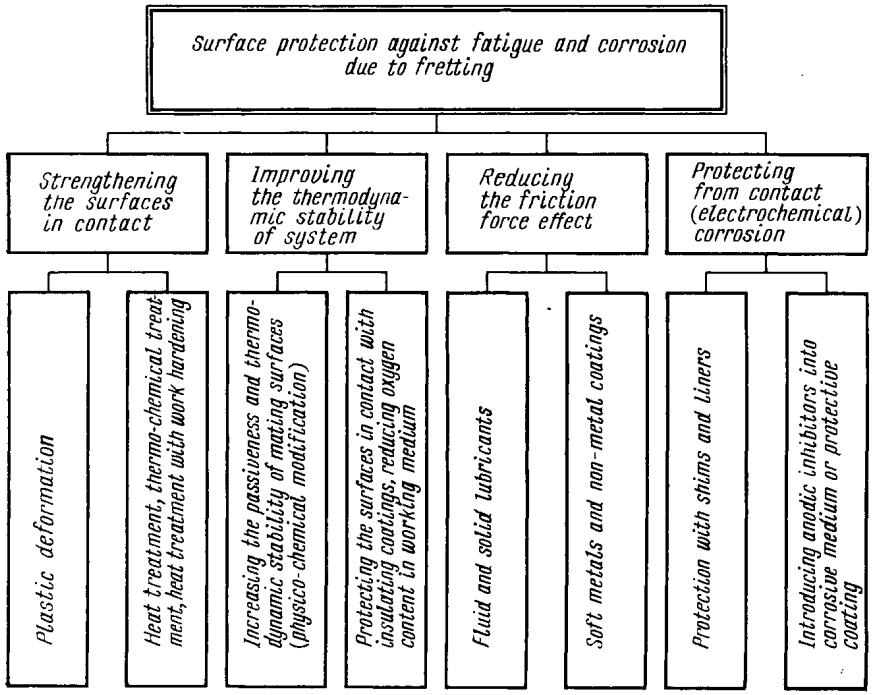

Fig. 15.12. Choice of methods of protection against corrosion and fatigue due to fretting

depending on the materials' properties and loading conditions, one of them becomes the principal process that limits the life of the joint. The differentiation of the processes running in the surface layer in

the course of fretting allows for a rational classification of measures for fretting prevention. Fig. 15.12 shows a diagram of methods selected for the protection from the most typical fretting process, that is, corrosion combined with fatigue.

A complex interplay of physical and chemical phenomena in fretting along with a great number of factors that determine the intensity of these phenomena in a given situation makes it difficult to

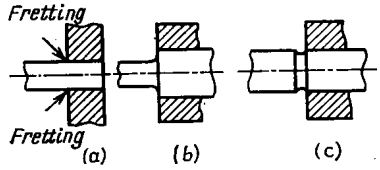

Fig. 15.13. Elimination of fretting in a shaft/hub assembly
(*a*) initial arrangement; reducing stress concentration by enlarging shaft diameter (*b*) and by introducing relieving groove (*c*)

work out universal protection methods. Therefore, most of the proposed methods have been developed and proved for specific applications, so that the same method in different conditions may give a different effect.

Design and manufacturing methods. Slip and fretting are prevented by such design measures as increased interference in forced fits, the use of special devices for damping vibrations, improved lubrication, and rational design of mating parts. For instance, an increase in the diameter of a shaft where it fits into a hub or a relief groove (Fig. 15.13) holds back the development of fretting. The groove (Fig. 15.13*c*) should be so dimensioned that the equilibrium between the stresses in the fretting region and in the groove bottom is achieved. Interferences in excess of 25 to 30 μm practically prevent the initiation of fretting. On the other hand, geometry errors of the mating surfaces (taper, ovality, etc.) make way for fretting.

The oscillatory displacements of mating surfaces can be eliminated by reducing the tangential force through coating one or both surfaces with films having a low elasticity modulus. The limitation here is that at a given slip amplitude the tangential force must not be as high as the maximum friction force.

Specific design solutions can be recommended for protection from fretting, e.g. non-contact labyrinth seals, spherical locating surfaces rather than cylindrical, rolling friction rather than sliding, tightly fitted prismatic and Woodruff keys.

Wide possibilities are offered by fretting-resistant materials for parts in contact (see Table 15.2). The use of such materials as Teflon and rubber in shaft-and-bushing assemblies sometimes makes it possible to exclude fretting completely. A Teflon film is sprayed onto the shaft, heat-treated and greased before assembly. Variations are

possible in which Teflon and rubber are used as liners interposed between mating surfaces.

The solution of Rubrax*, adhesives ВДУ-3 and БФ-2, and zinc plating also provide high protective properties, without any significant detriment to the contact of the mating surfaces.

The use of fluid and solid lubricants also holds promise as a means for protection from fretting. Graphite and molybdenum disulphide can markedly retard the development of fretting (Table 15.3). Where

Table 15.3

Effect of solid lubricants on fretting resistance of steel
(according to E. E. Veismantel)

Solid lubricant	Friction coefficient	Number of cycles $n \cdot 10^{-6}$	Extent of damage
Water paste of MoS_2	0.055	5	1
Varnish emulsion of MoS_2	0.115	15	2
Zinc chromate	0.070	15	4
Suspension of 25% powdery zinc chromate and 75% MoS_2 in a paint	0.090	5.2	2
		9	3
		15	5
Suspension of 10% powdery zinc chromate and 90% MoS_2 in a paint	0.062	15	2
MoS_2	0.048	15	1
Suspension of MoS_2 in black treacle	0.045	15	2
Mixture of fine-grain graphite with silicone resin	0.058	15	2
Colloidal graphite	0.040	15	1
Mixture of colloidal graphite with epoxy resin	0.085	15	3
Mixture of colloidal graphite with silicone resin	0.104	15	4

Designation of damage: 1 — negligible; 2 — slight; 3 — moderate; 4 — substantial; 5 — severe.

service conditions may involve ejection of the lubricant (by an air flow, centrifugal forces, etc.), the best solution is the use of lubricants filled with binders. Compounds of silicone resin and fine-flake graphite, and also molybdenum disulphide with 10 percent zinc chromate have proved effective in such applications.

Methods for protection from the main fretting processes. These are primarily manufacturing methods for the physico-chemical modification of mating surfaces; their aims are to strengthen the surfaces, to protect them from corrosive action of the medium, to increase the

* Trade name of vulcanized bitumen.—*Tr.*

thermodynamic stability of the system and reduce the effect of the friction force, etc.

Good results are achieved by cold working, heat treatment, thermochemical treatment, electroplating, chemical coating, deposition of plastics and polymer films.

Table 15.4 gives data on the fretting resistance of steel 45 treated by various methods. The greatest effect in each of the groups is provided by hydraulic shot blasting, tinning, and composite borating, respectively.

Table 15.4

Effect of surface treatment on fretting resistance of steel 45

Kind of treatment	Fretting resistance*1 $Q \cdot 10^3$ cycles/μm at pressures ($a_\tau = 0.05$ mm, $f = 30$ Hz), kgf/mm²		
	1	3	5
Steel 45 in basic condition	45.5	40	38.2
Cold working:			
hydraulic shot blasting	155	111	83.4
air shot blasting	143	100	66.6
vibrogrinding with strengthening	125	91	58.8
Thermal and thermochemical treatment:			
composite borating	1150	820	700
aluminizing	273	185	114
borating with copper plating	217	116.2	86
siliconizing	185	114	86.3
nitriding	125	83.3	62.5
induction hardening	120	83.4	62.5
impregnating with vanadium	104	69.5	55.6
furnace hardening	102	71.4	58.5
borating	74	59	55.7
Electroplating and chemical coating:			
tinning	125	100	55.6
silver plating	83.2	62.5	50
cadmium plating	67.4	53.7	43.8
phosphating	52.6	45.3	41.7
zinc plating	43.1	28.6	24.2
lead coating	62.5	28.4	33.4

*1 Fretting resistance (Q) was assessed as the number of test cycles required to obtain wear of unit depth (indenter — steel 45 hardened to HV 600).

When selecting a protective coating for parts subject to fretting, it must be taken into account that the coating may affect the fatigue strength of the material, since the deposition process involves the immersion of the part into an acidic medium. The surface layer becomes hydrogenated, and that leads to reduced fatigue strength. This effect may reduce the fatigue strength even stronger than fret-

ting itself. For this reason most electrodeposited coatings must be used in combination with a surface strengthening treatment. Electroplatings are recommended for use on spacers and bushings as a means for protection of the main parts.

REFERENCES

1. Голего И. Л., Алябьев А. Я., Шевеля В. В. Фреттинг-коррозия металлов. Киев, «Техніка», 1974, 269 с.
2. Рябченков А. В., Муравкин О. Н. Фреттинг-коррозия и защита металлов. М., ЦБНТИ, 1957, с. 4.
3. Уотерхауз Р. Б. Фреттинг-коррозия. Л. «Машиностроение», 1976, 270 с.
4. Филимонов Г. Н., Балацкий Л. Т. Фреттинг в соединения судовых деталей. Л., «Судостроение», 1973, 294 с.

Chapter 16

FRICTION AND OSCILLATIONS

Friction and oscillations are closely interconnected: friction is capable of generating oscillations, and oscillations have influence on friction.

To simplify analysis of the phenomena taking place in the friction contact, the following discussion is based on the concept that the friction force is mainly formed by a load normal to the rubbing surface and by the corresponding normal contact deformation (Amonton's law).

Important is also the concept that the oscillations in complex elastic systems, i.e. the actual tribological joints, are interdependent [10, 12]. That means, that the normal and tangential (both longitudinal and transverse) oscillations of a slider cannot arise irrespective of one another. When one kind of oscillation occurs, the others usually take place too.

This interdependence is determined by how close the natural frequencies of the respective oscillations are and by the character of their relation.

16.1. NORMALLY DIRECTED OSCILLATIONS GENERATED BY FRICTION OF SURFACES WITHOUT LUBRICATION OR WITH BOUNDARY LUBRICATION

If a sliding body (further referred to as the *slider*) has a height that is not much greater than its transverse dimensions, i.e. this slider is other than a rod sliding on its end face, the elastic compliance of the slider in the normal direction is dozens of times lower than the compliance of the contact layer, the latter being a layer formed by the peaks and valleys of microirregularities of the rubbing surfaces. In this case, the slider is roughly similar to an absolutely rigid body that rests on a number of minute springs which simulate the peaks of surface irregularities. Some of these are in contact and carry the nor-

mal load, while others, the smaller ones, are out of contact. Any casual normally directed pulse acting on the slider will cause its free oscillations in the normal direction. These oscillations are nonlinear and asymmetrical, because more and more new smaller peaks come into contact as the slider moves downwards, and because the contact rigidity is variable: it rises when the slider moves down and drops when the slider moves up. An increase in the amplitude of these oscillations causes the mean level of the slider over the counterface to rise and thereby the total real contact area to decrease.

As the slider moves along the counterface, its surface asperities receive micropulses from the asperities of the counterface. The normal components of these micropulses continuously generate the oscillations of the slider as a whole in the normal direction. It has been shown by experiments [17], that these micropulses, chaotic as they are, maintain permanent quasiperiodic sustained oscillations of the slider in the normal direction. Because the amplitude of these oscillations is small (micrometres or their fractions), the fundamental oscillation frequency is very near the natural frequency of linear oscillations:

$$\nu = \frac{1}{2\pi} \sqrt{\frac{k}{m}} \tag{16.1}$$

where k = contact rigidity coefficient and m = mass of the slider

The oscillations considered, being asymmetrical, lift the slider. and reduce the friction force [9].

The higher the speed of sliding, the more intensive are the normal components of the micropulses between the surface asperities, and hence the greater is the amplitude of the oscillations, the higher is the mean level of the slider movement, the smaller is the real contact area, and the weaker is the friction force. That may explain the drooping of the friction force-speed characteristic, i.e. reduction in the friction force with increase in the speed of sliding in the absence of lubrication. Oscillograms of the oscillations (which henceforward will be referred to as *contact oscillations*) show, that their amplitude grows linearly with the sliding speed.

To sum up, the force of dynamic sliding friction is always somewhat weakened by the contact oscillations generated by this friction, and the force of static friction is also always weakened by the contact oscillations generated by microseisms with amplitudes of tenths to hundredths of micrometres, which always take place [18, 19].

16.2. THE EFFECT OF FORCED OSCILLATIONS ON FRICTION FORCE

Normal forced oscillations. To reduce friction, use is made of normally-directed forced oscillations whose frequencies are usually very different from the contact resonant frequency. For this reason

a tangible reduction of friction force requires the application of powerful vibrators.

It must be borne in mind that in actual tribological joints the character of the normal oscillations is determined, strictly speaking, not only by the contact rigidity of the rubbing interface ("frictional rigidity"), but also by the rigidity of the joint's components, their arrangement, etc. [10]. Therefore resonance effects sometimes can be observed at various frequencies.

The optimum frequency of normal forced oscillations must be near the value found from formula (16.1). Due to the non-linearity of

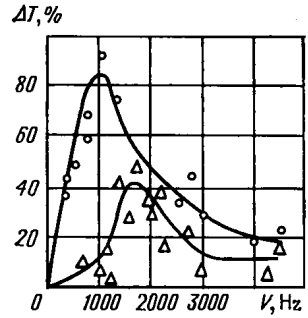

Fig. 16.1. Variation of relative decrease of friction force with frequency of forced normal oscillation at constant mass of slider and different loads exerted by vertical spring. Unhardened steel, surface roughness 0.6 μm Ra, slider mass m = const; ○ — N = 250 gf; △ — N = 1050 gf

contact oscillations, the resonant frequency can be shifted off this value by about 10 percent [17].

Formula (16.1) is applicable not only to multiple contacts, but also to a single contact, exemplified by a smooth sphere with a fairly smooth spherical socket. In the former case the contact rigidity has to be found by experiments, and in the latter it can be calculated by the Hertz formulas.

The selection of a vibrator is determined by the construction of the tribological joint and by the mass of the vibrating element. Piezoelectric vibrators are convenient to use for small masses, whereas electrodynamic vibrators are used for large masses. The quantitative problem of power rating of the vibrator depending on the slider mass and the rubbing surface properties has yet to be solved. It can be said, however, that the power of the vibrator must increase with an increase in its mass.

An example of the effectiveness of reducing the friction force by normally-directed forced oscillations is given in Fig. 16.1 in the form of a graphically represented relation between the oscillation frequency and the friction force. Piezoelectrical vibrators are attached symmetrically to the top surface of the slider so that they extend radially from this surface far enough to provide the coincidence of their natural bending oscillation frequencies with the resonance frequency of the contact oscillations and, at the same time, with that of the vibrator. That increases the magnitude of the friction-force resonance minimum without changing its frequency. The frequencies

causing the extreme drop of the friction force coincide with a 10 percent error with the frequency of contact oscillations calculated by formula (1). Similar diagrams obtained from tests on a vibration table are shown in Fig. 16.2. The calculated and experimental results as compared with each other are presented in Fig. 16.3. Figs. 16.1

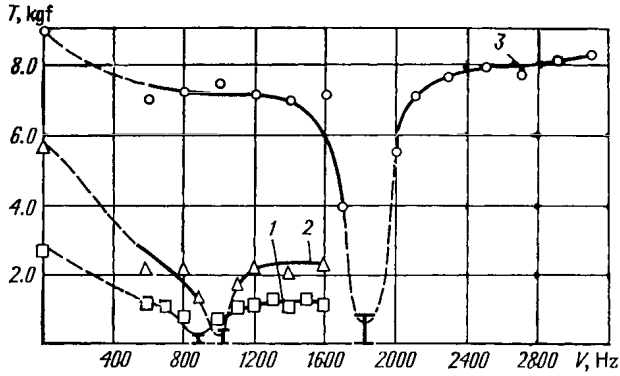

Fig. 16.2. Variation of friction force with frequency of forced oscillation of slider on counterface placed on vibration table. Slider mass and table oscillation amplitude are constant with loads
1—3.0 kgf; *2*—4.0 kgf; *3*—10.0 kgf

and 16.2 illustrate a new application of the slider's forced oscillations for friction-force control, i.e. the changing of the friction force by controlling the frequency of the forced oscillations. If this frequency is changed within the range near the resonance value, the friction force will be very responsive to it. For gradual control, the forced oscillation frequencies should be farther from the resonant frequency.

Tangential forced oscillation. Another example of the resonance method for reducing the friction force given in the paper [4] is a single-point contact of a horizontal cemented-carbide pin supported by two through-hole synthetic sapphire bearings with polished bearing surfaces. The aim of the work was to verify the foregoing concepts and their effectiveness for reducing friction in precision instruments. The pin was subjected to forced axial oscillations so that in addition to the above-mentioned effect of contact oscillations, another effect could take place. It consists in that transverse tangential oscillations at instantaneous velocities v_t produce the friction force vector that is always directed opposite the instantaneous values of the resultant sliding velocity. The latter makes an angle $\alpha = \arctan \frac{v_t}{v}$ with the vector of the transverse displacement velocity v. Therefore, the instantaneous values of the force which resists the transverse displacement is $T_{inst} = fN \cos \arctan \frac{v_t}{v}$. Hence

$$T_{inst} = fN \frac{v}{v^2 + v_t^2}$$

or

$$T_{inst} = fN \frac{v}{\sqrt{v^2 + \omega^2 a^2 \cos^2 \omega t}} \tag{16.2}$$

$$T_{inst\,min} = fN \frac{v}{\sqrt{v^2 + \omega^2 a^2}} \tag{16.3}$$

As seen from formulas (16.2) and (16.3), effective resistance to sliding at a = const must drop monotonously with the rise of the frequency of the forced transverse tangential oscillations, i.e. no resonance minimum of the friction force should have taken place if the described effect of resonance with normal contact oscillations had not been brought into play.

Let us consider the way the tangential oscillations, either transverse or longitudinal, induce normal contact oscillations. Normal

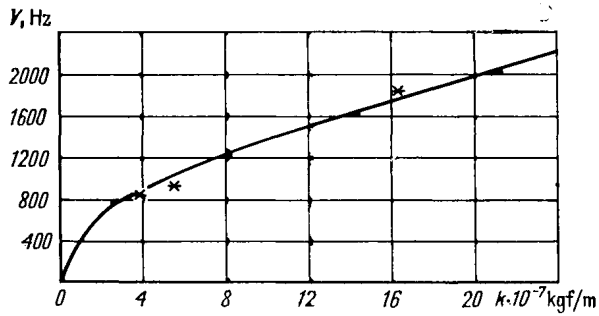

Fig. 16.3. Analytical relation between resonance frequency and rigidity of contact in normal direction as found by formula (1). The points indicate magnitudes of resonant frequency obtained experimentally (cf. Fig. 16.2)

micropulses are proportional to the speed of sliding. With tangential oscillations at work, the normal micropulses reach its maximum twice for one period of the tangential oscillations. As there is the natural frequency of the normal oscillations, the frequency of the forced tangential oscillations, which is half that of the normal oscillations, must act as a resonance frequency for inducing the maximum-amplitude normal oscillations.

Such, then, is the mechanism of reducing the friction force by forced tangential oscillations, both transverse and longitudinal. Each of them can be used for the purpose, if that is more convenient than the use of normal oscillations. Here, however, the condition of the friction-force minimum will be other than (16.1):

$$\nu_t = \frac{1}{4\pi} \sqrt{\frac{k}{m}} \tag{16.4}$$

By the way, the trivial effect of reducing the friction force through jerks of the slider at $\omega^2 a > g$ also has a monotone dependence on frequency and produces no resonance whatever.

In the course of the work [4], a sharp (tenfold) resonance drop of the friction force was observed at forced axial oscillation frequencies whose values were very close to half the normal-oscillations resonance frequency value found from the Hertz formulas for contact rigidity. The typical results are given in Table 16.1, where ν is calculated

Table 16.1

Frequencies of natural normally directed oscillations and resonant frequencies of axial oscillations

m, g	ν	ν/2	$\nu_{t_{res}}$
	Hz		
2.5	8.6	4.3	5.5
7.5	6.0	3.0	3.8
23.5	4.1	2.05	2.75

by formula (16.1), $\nu_{t_{res}}$ being the forced oscillation frequency which gives a sharp resonance drop of the friction force. The quantity $(\nu\sqrt{m})$ is not constant here, because contact rigidity in formula (16.1) depends on load, i.e., mass in this case. However, $k \sim N^n$ according to the Hertz formula, where $n < 1$, and thereby the effect of mass on frequency prevails over the effect of rigidity on it, and resonance frequency decreases with a rise in mass.

The influence of tangential forced oscillations upon the friction force has also been discussed in [10, 24], but irrespective of the effect they give through inducing normal contact oscillations.

16.3. FRICTIONAL SELF-EXCITED OSCILLATIONS

A non-uniform sliding of solids rubbing against each other under a constant reactive force may involve more or less periodic halts. This non-uniformity is called *frictional self-excited oscillations* [5, 7, 10].

A possible explanation for non-uniform sliding is a drooping sliding speed-friction force characteristic. In this case a casual acceleration of sliding reduces the friction force and leads to a further acceleration until the slider has slipped into the position where its external elastic constraints develop a reaction force which causes the slider to slow down. The slow-down increases the friction force and therefore leads to a further slow-down. In some cases the slider slows down to a stop, and then the pull of the elastic drive rises until it dislodges the slider by causing it to skip once again.

The non-uniformity occurs when the gradient of the drooping characteristic, i.e. a negative derivative of the friction force with respect to the sliding speed, becomes greater than the coefficient of damping of the drive's oscillating system. The greater this gradient, the more intensive oscillations take place and the higher is the speed below which the slider oscillations are attended with halts. It follows from the foregoing, that the main practical recommendation for eliminating the non-uniformity of sliding is to increase the damping capability of the slider drive and to lower the gradient of the friction force-sliding speed characteristic or to remove completely the factors which give rise to a drooping characteristic. For lubricated surfaces such a factor is [9] the hydrodynamic effect of the lubricant (in the region of mixed-mode friction).

However, practical experience and special experimental studies do not prove the conclusions made from the above explanation. For instance, the use of low-viscosity lubricants reduces the gradient of the characteristic, but such lubricants considerably increase the non-uniformity instead of reducing it. The reasons for this phenomenon as well as the significance of the drooping of the characteristic as a consequence of normal contact oscillations generated by friction [18, 19] will be discussed later. 4

Some authors [5, 7, 8, 10] believe a so-called jump ΔT of the friction force during the transition from a standstill to sliding to be the cause of frictional self-oscillations. This jump is capable of generating frictional self-excited oscillations with halts irrespective of the sign of the friction-force derivative with respect to sliding speed, i.e. even when the friction force rises with the speed. According to this view, there is a critical speed of sliding that rises with ΔT, i.e. with an increase in the duration of a halt. At the speeds higher than the critical speed, halts disappear. The main difficulties in carrying into practical effect recommendations based on this view stem from the lack of dependable data on the magnitude of the friction-force jump for different sliding conditions.

A more general understanding [10] of frictional self-excited oscillations is aided by the foregoing concepts about the significance of complex movement of a slider as part of an elastic system which includes constrained oscillations with a positively determined relationship between the friction force and the normal load. In accordance with this understanding, a casual change in sliding conditions (the friction force, speed, acceleration, etc.) gives rise to tangential displacements due to deformations of the drive. These tangential deformations, being somewhat interconnected with normal deformations, produce the deformations normal to the rubbing surfaces. That leads to a change in the friction force (or its projection on the direction of movement) and to a further change in the tangential deformations of the drive's elastic system. At certain phase relationships between the tangential and normal displacements (oscillations), conditions are created for changes in the magnitude of the friction

force in unison with the tangential longitudinal oscillations of the slider, i.e. the non-uniformity of its movement. Generally, there are three kinds of constraints: the elastic or coordinate constraint; the speed constraint, or that expressed in terms of the first derivative of coordinate with respect to time; and the inertial constraint, expressed in terms of the second derivative of coordinate with respect to time. The coordinate constraint arises from the fact that the direction of action of the friction force does not coincide with the axes of rigidity of the elastic system that carries and moves the slider (including the contact interaction of the rubbing surfaces). In this case, the friction force varies owing to an additional loading caused by the elastic forces. Such conditions, for instance, can be found in some types of shoe brakes, on the side surfaces of slideways in various machines, etc. Such a system with a coordinate constraint has been treated independently in studies [21, 22, 23, 25], as applicable mainly to the sliding of the end faces of inclined rods on a plane.

According to R. T. Spurr, a rod, fixed at its upper end in an elastic joint and inclined back from the normal at an angle approximating arctan f (where f is the sliding friction coefficient) and producing no tension in the joint, receives a tangential force applied to its lower end and directed against its speed:

$$T = \frac{fG}{1 - f \tan \theta} \tag{16.5}$$

where G = mass of the slider fixed on the lower end of the rod, and θ = angle of the backward deviation of the rod from the normal (i.e. the upper end of the rod is shifted in the direction opposite that of its sliding). As the upper end moves forward with the lower end being stuck, angle θ grows. With $\tan \theta \to \frac{1}{f}$ we have $T \to \infty$. If the elastic joint at the rod's upper end had no freedom of vertical elastic deflection, the whole moving system would completely wedge at this angle. However, the joint is attached to the other, very stiff horizontal rod, which now begins to deflect upwards. Force T reaches its maximum at $\theta = \arctan \frac{1}{f}$ and then changes the sign, and the rod's lower end is forced forward by the moment of the joint recoil. The phase of jamming changes over to the phase of slipping when the joint's moment changes its sign and again begins to press the rod against its counterface. Angle θ grows again, and the cycle repeats.

R. Courtel considers both positive and negative deviations of a rod from the normal at an angle of 3° and demonstrates mathematically that the lower end of the rod must oscillate and jam if the rod is so loaded axially that, owing to interdependence between contact rigidity and load, the natural frequency of its axial oscillations is twice the natural frequency of its bending oscillations. The axial and the bending oscillations produce resonance, the amplitude of the

axial oscillations grows, and the friction drops. "The Courtel front bulge" [21], formed in front on the rod's lower end at each initial displacement preceding its skip, serves as a brake.

Of practical importance is the action of the hydrodynamic force of lubrication as an instance of the speed relationship between tangential and normal oscillations [9, 10, 11]. Under the action of this force which increases with sliding speed, the slider "floats up", i.e. receives a displacement normal to the surface of friction. That results in a lower contact load and contact deformation, and hence, in a lower friction force. This effect can explain why the friction force falls as the sliding speed goes up, i.e. the drooping of the friction-speed characteristic. If the speed changes in the course of longitudinal oscillations, the hydrodynamic force then periodically changes, too, and so does the friction force. However, with rapid speed variations the slider fails to float up because of its inertia and also because it is difficult for the lubricant to penetrate into or to be forced from a narrow space between the surface irregularities of the slider and the slideway. Consequently, the contact friction force varies much less during oscillations than it does during a stable movement at speeds corresponding to the maximum and minimum speeds of the movement with oscillations. This factor, which is very important for analyzing the slider's slow-down with a sharp change in its speed, as is the case with accurate positioning in machine tools, implies that the drooping friction-force characteristic is here a very insignificant cause of non-uniform movement and so for practical purposes can be left out of consideration.

The inertial constraint arises mainly in sliding movement of objects whose centre of gravity is situated far from the surface of sliding (high uprights, overhanging structures moving along vertical ways, etc.). Any variation in sliding speed generates an inertial force due to acceleration, and that gives rise to the wobbling of the slider in its ways. As a result, the contact deformation and friction force vary and thereby bring about variations in the deformation of the drive and in the sliding speed.

As a rule, all kinds of constraints are found in actual tribological systems. It should be noted that, depending on design features and frictional conditions, the coordinate constraint may result not only in non-uniform sliding but also in wedging of the slider in its ways, where the contact deformations and friction force rise faster than the thrust of the slider drive, and the slider is impossible to shift.

The mechanism of a non-uniform sliding due to the described features of a sliding system is illustrated in Fig. 16.4. In a plane perpendicular to the plane of sliding, two translatory oscillations, for instance those along axes ξ and ν, can be distinguished, which are somewhat shifted relative to each other in time, i.e. in phase. Since oscillations take effect on different coordinate axes, the resultant motion has a path of the relative sliding of two rubbing bodies (which is superposed on the specified movement) in the form of a closed curve,

theoretically an ellipse. Motion along such a path, which is shown in the diagram as successive positions of the frictional contact, involves variations in the normal contact deformation of the rubbing bodies. The normal contact deformation and hence the friction force T, which is determined by it, vary in such a way that when sliding takes place along the friction-force line of action, the contact deformation is greater than it is during sliding in the opposite direction.

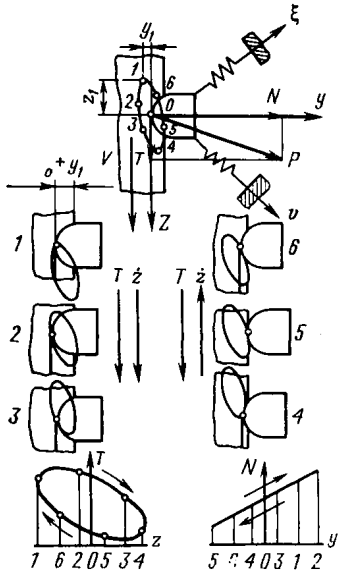

Fig. 16.4. Path of motion and variation of friction force in process of oscillations

In the diagram the magnitudes of friction force T and load N are taken to be proportional to the amount of normal contact deformation. The area confined within the curve depicting variation of the friction force during sliding represents the work of the friction force in the course of oscillations that is expended further on generating the oscillations. Self-excited oscillations set in, when the energy brought in this way becomes equal to the energy dissipated by resistance to motion (with regard to non-linearity of the system).

Another kind of relation between the tangential and normal oscillations which are produced during sliding by asperity interaction [18, 19] is described on pp. 4-115.

A casual acceleration of sliding increases the amplitude of contact oscillations, reduces the friction force and leads to a further acceleration until the slider skips forward by inertia into a position where external elastic constraints develop a recoil which slows down the slider. The slow-down reduces the amplitude of the normal contact oscillations, raises the friction force and, consequently, brings about a further slow-down. In some cases such a slow-down results in a halt, wherein the pull of the drive builds up until the slider skips forward again.

During each skip the amplitude of normal asymmetrical contact oscillations grows and the slider rises over the counterface. Therefore, the self-oscillatory skips are always not merely dashes forward but jumps along two axes. This behaviour is inevitable with any primary cause of non-uniform sliding, because the cause just discussed always combines with other possible sources of the non-uniformity.

16.4. THE ROLE OF TANGENTIAL SELF-EXCITED FRICTIONAL OSCILLATIONS AND THE PROVISION OF MOTION UNIFORMITY

The main adverse effects of the oscillations of this kind are, first, a non-uniform movement of tool slides in their ways resulting in a periodic micropattern on the machined surfaces and, second, errors of positioning [10, 16].

A great variety of factors conducive to generation and damping of self-excited oscillations and also the possibility of their simultaneous action make it hardly possible to offer quantitative recommendations for eliminating these oscillations.

The simplest situation is found with friction without lubrication or with boundary friction, when the rate of feed is within the region of a sharply drooping friction-speed characteristic, which corresponds to very slow feeds. Here, the main cause of non-uniform sliding is exactly a fall in the friction force with an increase in sliding speed; as we have seen, this factor is governed by normal contact oscillations generated by friction.

Hence, two seemingly contradictory measures can be taken.

The first is to eliminate normal contact oscillations by damping them in the normal direction. Adequately-intensive damping removes self-excited oscillations, although the friction force grows significantly. This measure, however, is difficult to realize in actual constructions.

Much simpler is the opposite measure, namely, forced oscillations of the slider in a contact-resonance regime, when the amplitude of the normal contact oscillations is so great that the slider "floats" at the maximum level. This method is very effective and is simpler to realize. It has been successfully used in [6], where recordings of frictional self-excited oscillations show their sharp disappearence at the resonance frequency of the forced normal oscillations of the slider. Tangential oscillations whose frequencies are half the frequencies of the normal oscillations can also be used for the purpose in accordance with formula (16.4).

Some other general qualitative recommendations can be given for attaining a uniform motion [5, 10, 12]. These are as follows:

1. To increase the stiffness of the drive without giving rise to, or strengthening, the detrimental coordinate constraint and without reducing the damping ability.

2. To lower the friction coefficient by all available means, including the forced oscillation mentioned above, i.e. by using appropriate materials for the rubbing surfaces (such as fluoroplastics, for instance), lubricants with high boundary-film properties, and antifriction joints (rolling guideways, ballscrews, etc.); denser lubricants

to provide mixed-mode friction with a lower friction coefficient, and wedge-like chamferings on sliding surfaces; etc.

3. To reduce the total friction force in complex tribological joints with several sliding surfaces (guideways) by relieving measures (delivering oil under pressure to the guides, using spring-controlled rollers that take up part of the load, etc.); by eliminating misalignments in the joint due to errors in design, machining, and assembly; and by reducing excessive tightness created by gibs and wedges used sometimes to increase the contact stiffness of movable joints.

4. To increase the damping ability of a system by rational use of fixed joints or special damping materials and devices.

5. To eliminate or modify constraints in a system by re-orienting the axes of stiffness of the elastic system and by changing the relative magnitudes of stiffness; by bringing into coincidence as fully as possible the vector of the resultant friction force and that of the drive forces, and also the centres of gravity of the sliding member and the system's stiffness centre.

6. To provide conditions which prevent seizure of the rubbing surfaces.

Design analysis of non-uniform motion conditions that takes into account a complex interaction of the rubbing surfaces forming a system with many degrees of freedom is a special problem, which can be solved approximately with the use of computer techniques [10].

In practice, use can be made of very simple calculation methods which give approximate values of the parameters that determine limiting conditions under which non-uniform motion takes place.

The critical speed v_c, above which no jumps of the slider occur, [5, 16] is evaluated from the formula

$$v_c = \frac{\Delta f N}{\sqrt{\psi k m}} \tag{16.6}$$

where $\psi = 4\pi\theta$ = relative dissipation of energy in oscillations; Δf = difference between the static and sliding friction coefficients; k = slider drive rigidity, kgf/μm; m = slider mass.

Given below are approximate values of the difference between the static and sliding friction coefficients for machine-tool slideways [15]:

Cast iron-cast iron	0.08	Cloth laminate-cast iron	0.12
Steel-cast iron	0.05	Teflon-cast iron	0.04
Bronze-cast iron	0.02		

The critical value of the ratio between the total friction force and the drive stiffness at the minimum specified speed of sliding can be evaluated by the formula suggested in [20] and recommended by ENIMS* [13]:

$$\frac{T}{k} \leqslant \frac{1}{n_s}\left[\frac{T}{k}\right] \tag{16.7}$$

* Experimental Machine-Tool R & D Institute, Moscow.

where $n_s \approx 1.5$ = safety factor; $\left[\frac{T}{k}\right]$ = parameter determined for machine-tool slideways from the chart in Fig. 16.5.

With a known relation between the friction force and the sliding speed for given sliding conditions, it is possible to find the critical speed using the limiting values of $\left[\frac{T}{k}\right]$.

We have not yet touched upon the question of rolling, although in many cases a drooping speed characteristic and self-excited oscillations can also be found there. However, they are easier to dispose

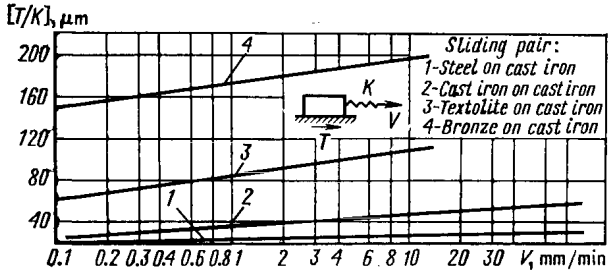

Fig. 16.5. Parameter $\left[\frac{T}{k}\right]$ as function of sliding speed. Surface roughness 0.32-0.63 μm, *Ra* oil, И-20А

of, because a small coefficient of friction makes it possible to remove self-oscillations by increasing the drive stiffness to a much smaller extent than in sliding.

16.5. THE EFFECT OF OSCILLATIONS ON WEAR OF RUBBING SURFACES

Few studies have been conducted as yet to clarify the question of whether or not the normal forced oscillations that lower the friction force have any effect on wear. In one of them [14], destruction of a sphere and a plane in contact under only a normal periodic load has been investigated. The destruction was observed in a narrow annular contact zone, and it could be ascribed to Reynolds' periodic slip, which accompanies a mutual normal deformation of contact surfaces of different curvature, rather than to normal periodic deformations. A. V. Chichinadze et al. [1] investigated the effect of both tangential and normal oscillations on the performance of power transmissions in tracked and wheeled vehicles. They found that normal oscillations with amplitudes of 5 to 50 Hz cause increased wear to the friction elements and lead to an unstable braking torque.

Table 16.2

Coefficient of friction (f) and resistance to fretting (τ) as measured in testing instrument oils used for a sliding pair: sphere (steel ШХ15, 0.04-0.08 μm R_a) against a flat (synthetic sapphire, 0.02-0.04 μm R_a); $N = 20$ gf; $\nu = 260$ Hz

Oil grade	GOST, TU	Working temperature range, °C	Viscosity, cSt, at temperature limits		Lubricant effect	
			upper	lower	f	resistance to fretting
МН-60	GOST 8781-71*1	—60 - +150	50 000	11-12	0.106	> 5000
ВНИИ НП-6	ТУ НП 55—64	—50 - +150	5 200	3	0.112	> 5000
МП-714	ТУ 38-1-258—69	—10 - +150	—	8-14	0.120	3000
НИИЧП-40-60П	ТУ 25-07-693—73	—60 - +60	17 800	20	0.126	2000
ПЭС-С-1	GOST 10957—74	—60 - +100	5 000	7	0.140	950
ВНИИ НП-1-4МО	GOST 13374—67	—60 - +170	7 000*1	30	0.170	200
ОКБ-122-3	GOST 18375—73*1	—60 - +100	5 720	7.5	0.180	170
МП-605	ТУ 38-1-01-78—70	—60 - +200	6 500	12	0.270	39
НИИЧП-41-60	ТУ 25-07-693—73	—60 - +60	5 350	18	0.280	42
МП-610	ТУ 38-1-01-120—71	—60 - +250	3 300	57	0.290	32
МП-601	ТУ 38-1-259—69	—60 - +150	2 500	10	0.286	35

*1 At −40°C.

Table 16.3

Coefficient of friction (f) and resistance to fretting (τ) as measured in testing instrument greases used for a sliding pair: sphere (steel ШХ15, 0.04-0.08 μm R_a) against a flat (synthetic sapphire, 0.02-0.04 μm R_a); $N = 20$ gf; $\nu = 260$ Hz

Oil grade	GOST, TU	Working temperature range, °C	Viscosity, p, at temperature limits		Lubricant effect	
			upper	lower	f	resistance to fretting
ВНИИ НП-223	GOST 12030-66	—50 - +100	4000	2	0.115	> 5000
ВНИИ НП-271	TU 38-1-299—69	—60 - +130	3000	4	0.140	800
ОКБ-122-7	МРТУ 38-1-230—66	—60 - +80	20000	50	0.172	230
ЦИАТИМ-201	GOST 6267-74	—50 - +100	11000	50	0.158	390
ЦИАТИМ-221	GOST 9433-60*1	—60 - +150	8000	50	0.260	120
ВНИИ НП-270	TU 38-1-299—69	—60 - +130	400	10	0.122	3000
ВНИИ НП-274	TU 38-00154—71	—80 - +170	2000	9	0.290	20
ВНИИ НП-257	GOST 16105-70*1	—60 - +150	2900*1	9	0.300	< 10

*1 At −40°C

Most work on the influence of oscillations on wear dealt with tangential oscillations. These questions have been treated in detail in Ch. 15.

In practice, it is important to test miniature tribological joints in instruments, watches, etc., for resistance to fretting. The testing method [3] consists in that a miniature part is secured to a tuning-fork prong and is pressed against a miniature counterpart by the normal component of the weight. The normal load can be changed to a minimum by changing the inclination of the entire fork-part-counterpart complex. With the fork turning in a vertical position, the normal load approximates zero. The coefficient of friction, whose changes make it possible to determine the latent period of fretting, i.e. resistance to fretting, can be calculated from a period of oscillation decay produced by the friction of the tested part during the free oscillations of the fork as well as during its oscillations induced by an electromagnet.

The result of testing various lubricants for their effect on fretting resistance τ (a latent period of fretting) are given in Table 16.2 (for instrument oils) and in Table 16.3 (for instrument greases).

REFERENCES

1. Алексеев Г. Ф., Чичинадзе А. В., Борисов С. Г. Трение и износ фрикционных пар при наложенных вибрациях. Теория трения, износа и смазки 1975, Ташкент, Ташкентский политехн. ин-т, с. 172-173.
2. Ахматов А.С. Молекулярная физика граничного трения. М., Физматгиз, 1963, 472 с.
3. Ахматов А. С., Мавдютова Р., Островский М. С. Исследование контактного взаимодействия металл-минеральных пар в условиях вибраций: Тезисы докладов Всес. научн. технич. семинара по контактной жесткости в машиностроении. Тбилиси, Грузинский политехн. ин-т, 1974, с. 4.
4. Буданов Б. В., Хандельсман Ю. М., Ускова С. Г. О влиянии вибрации на трение в камневых опорах скольжения.— В сб.: Часы и часовые механизмы. «Труды НИИЧаспрома», вып. 13. М., НИИЧаспром, 1973, с. 77-83.
5. Дерягин Б. В., Пуш В. Э., Толстой Д. М. Теория фрикционных автоколебаний с периодическими остановками. «Труды III Всесоюзной конференции по трению и износу в машинах», т. II. М., Изд-во АН СССР, 1960, с. 132-152.
6. Григорьева С. Р., Толстой Д. М., Чичинадзе А. В. Об устранении фрикционных автоколебаний. ДАН СССР, т. 202, № 1, 1972, с. 76.
7. Ишлинский А. Ю., Крагельский И. В. О скачках при трении. ЖТФ, т. XIV, вып. 4-5, 1944, с. 276-283.
8. Крагельский И. В. Трение и износ. Изд. 2-е, перераб. М., «Машиностроение», 1968, с. 480.
9. Кудинов В. А. Гидродинамическая теория полужидкостного трения.— В сб.: Сухое и граничное трение. Фрикционные материалы. «Труды III Всесоюзной конференции по трению и износу в машинах», т. II. М., Изд-во АН СССР, 1960, с. 161-170.
10. Кудинов В. А. Динамика станков. М., «Машиностроение», 1967, 359 с.
11. Кудинов В. А. и Лисицын Н. М. Основные факторы, влияющие на равномерность перемещений столов и суппортов станков при смешанном трении.— «Станки и инструмент», 1962, № 2, с. 1-5.

12. Кудинов В. А. Природа автоколебаний при трении.— В сб.: Исследование колебаний металлорежущих станков при резании металлов. М., Машгиз, 1958, с. 251-273.
13. Методика расчета узлов металлорежущих станков на плавность медленных перемещений. М., ЭНИМС, 1972. Авт.: Кудинов В. А., Кочинев Н. А., Брухимович М. И., Ломако И. П. 21 с.
14. Пинегин С. В., Орлов А. В.'и Гудченко В. М. Разрушение материалов под действием пульсирующей нагрузки.— «Машиноведение», 1966, № 1, с. 76-83.
15. Пуш В. Э. Конструирование металлорежущих станков. М., [«Машиностроение», 1977, 392 с.
16. Пуш В. Э. Малые перемещения в станках. М., Машгиз, 1961, с. 124.
17. Толстой Д. М., Борисова Г. А. и Григорова С. Р. Роль собственных контактных колебаний нормального направления при трении.— В сб.: О природе трения твердых тел. Минск, «Техника», 1971, с. 116.
18. Толстой Д. М. и Каплан Р. Л. К вопросу о роли нормальных перемещений при внешнем трении.— В сб.: Новое в теории трения. М., «Наука», 1966, с. 42-59.
19. Толстой Д. М. Собственные колебания ползуна, зависящие от контактной жесткости и их влияние на трение. ДАН СССР, т. 153, № 4, 1963, 820 с.
20. Филипов Д. Б. Расчет плавности перемещений узлов подач станков. Экспресс-информации. Сер. «Автоматические линии и металлорежущие станки», 1969, № 37.
21. Baglin R., Rongier P. et Courtel R. Sur la rigidité de contact entre deux surfaces solides et son role dans le frottement en présence des vibrations. C. R. Acad. Sc. Paris, t. 268, 1969, 686 pp.
22. Courtel R. Sur l'observation de certains dommages periodiques causés a surfacés par le frottement et leur interprétation. C. R. Acad. Sc. Paris, t. 253, 1758 p.
23. Courtel R.Normal vibration in contact friction.—"Wear", 11, 1968, p. 77.
24. Lenkiewicz W.The sliding friction process—effect of external vibrations.— "Wear", 13, 1969, No. 2, p. 99-108.
25. Spur R. T. Frictional Oscillations.— "Nature", vol. 169, 1961, p. 50.

Chapter 17

SELECTIVE TRANSFER

17.1. PHYSICO-CHEMICAL MECHANISM OF SELECTIVE TRANSFER

17.1.1. Main Terms and Definitions

Selective transfer is a kind of frictional interaction characterized primarily by the molecular component of the friction force. It arises as a result of chemical and physico-chemical processes taking place on the rubbing surfaces and involves the phenomena of self-compensation for wear and those of reducing friction. The most typical phenomenon is the formation of a protective film wherein a diffusion-vacancy mechanism of deformation is realized without accumulating the effects typical of fatigue processes.

The systems of self-compensation for wear and of reducing friction or, shorter, of reducing wear and friction are physico-chemical processes or phenomena that facilitate relative displacement of rubbing surfaces or protect them from wear or provide self-compensation for wear.

Wear and friction reducing systems other than selective transfer, can be exemplified by the formation of a boundary layer of adsorbed lubricant or a run-in surface under boundary-friction conditions.

The following selective transfer systems can spontaneously arise under selective transfer conditions:

—reduction of pressures due to selective dissolution of the surface irregularity peaks under load and due to formation of a plastic surface film (similar to a run-in layer);

—facilitation of relative displacement and reduction of wear of the rubbing surfaces due to a diffusion-vacancy mechanism of deformation of the surface film that excludes deformation of the main material;

—protection of the rubbing surfaces against oxidation due to a reducing lubrication medium;

—collection of the dispersed metal particles by a double-layer electric field and their deposition in the contact zone, which significantly reduces their outflow with the lubricant;

—formation on the rubbing surfaces of polymeric films from lubricant decomposition products, which reduce friction and increase wear protection [13].

A definite characteristic of selective transfer in its variations is the formation of a protective metallic film which, depending on the initial lubricant medium, has a varying ability to reduce friction and wear.

Different changes taking place during the initial stage of friction determine four main variations of selective transfer: plasma-forming lubrication, metal-plating lubrication, traverse lubrication, and ion lubrication. Hence, the very concept of lubrication becomes transformed (excepting, of course, the action of applying a lubricant) and takes several forms different in content:

—lubricant as an initial substance before changes in the friction zone, e.g. a plasma-forming lubricant;

—lubricant as the products of change of the initial substance, e.g. surface-active agents resulting from chemical reactions directly on the rubbing surfaces;

—lubricant as a protective metallic film formed on the rubbing surfaces, which features a very low resistance to their relative displacement.

Let us give definitions relating to the main variations of selective transfer:

Plasma-forming lubricants are a group of hydrocarbon lubricants which provide selective transfer through tribodestruction of part of their constituents during friction in the contact zone, through chemical sorption of the destruction products on the anodic components of the alloys used in the tribological joint, and through the formation of surface-active agents and a protective metallic film. Lubricants of this type give rise to selective transfer only on the rubbing surfaces containing a film-forming material, such as bronze and copper.

Servovital film* is a protective metallic film in which a diffusion-vacancy mechanism of displacement takes place in friction. It appears at the initial stage of friction when anodic components of the surface layer of the rubbing metal or alloy undergo selective dissolving. The film is subject to the action of surface-active agents [7, pp. 12-19; 16].

Diffusion-vacancy mechanism of displacement is a process running when shearing occurs in the servovital film. The film features a high concentration of vacancies and a low density of dislocations; for this reason the diffusive process of disruption and formation of metallic bonds therein runs with increased intensity.

Nubial film (Latin *nubium*—skin) is a protective tribopolymeric film formed from the products of tribodestruction of lubricant hydrocarbons. Unlike the tribopolymeric films formed from special additives to mineral oils, the nubial film acts on real contact areas which are greater by two orders of magnitude than the contact microareas

* This and other terms pertaining to the protective films described in this chapter have been proposed by A. A. Polyakov. *Tr.*

usual in boundary lubrication conditions, and, respectively, at pressures which are lower by two orders of magnitude [14].

As distinct from the metal-plating lubricants below, the plasma-forming lubricants can function under selective transfer conditions only in tribological joints whose materials are capable of forming protective films. Actually, however, such lubricants are fairly acceptable for 'hybrid' conditions, i.e. for boundary friction combined with selective transfer.

A servovital film formed from the cathodic component of the antifriction alloy on its rubbing surface is transferred to the steel counterface in the course of friction. The film fills the valleys of surface irregularities on the steel surface and thereby forms an adjoining film on it. The alloy particles are transferred in a colloidal or ion form. The colloidal particles provide lubrication and, as they become discharged, they give up metallic particles and molecules of the surface-active agents to the film.

The diffusion-vacancy mechanism of displacement is the most representative, inherent only in selective transfer, process of lubrication by a metallic film saturated by surfactants whose molecules occupy its micropores, reduce its strength and so promote the outcrop of dislocations accumulated during its deformation. This mechanism is treated in greater detail in [16].

The formation of the nubial film has been discovered experimentally. However, its role in reducing friction and wear has yet to be studied.

To utilize selective transfer in tribological couples which do not have film-forming materials, e.g. steel against steel, steel against cast iron, use is made of metal-plating lubricants.

Metal-plating lubricants are a group of greases and liquids which contain powder of a film-forming material subject to selective dissolving, or a metallic oxide, or an organometallic compound. All these constituents undergo reducing or destruction in the zone of friction and release metal, which forms the metal-plating film. Here, surface-active agents must be either in the basic lubricant or formed in the destruction of the organometallic compound [6, pp. 94-103; 15, pp. 59-95].

Metal-plating film is a protective film in which the diffusion-vacancy mechanism of displacement takes place. The film is formed at the initial stage of friction from a metal-plating lubricant containing a metallic powder or metal oxide which is added to a plasma-forming lubricant (activating selective dissolving [15] or reducing), or it is formed by tribodestruction of organometallic compounds which give up the metal. The film is under the action of surface-active agents.

The metal-plating film substantially differs from the servovital film not only in the mode of formation, but also in quality. The absence of selective dissolving of the surface roughness peaks has to be compensated for by filling the surface roughness valleys with the

film material, which makes a difference. The surface-active agent formed in the selective dissolving process is replaced either by the surface-active agent contained in the lubricant or by that formed from anions remaining after the tribodestruction or dissociation of the organometallic compounds.

Metal-plating lubricants (e.g. based on grease ЦИАТИМ-201) containing bronze or brass powders are used in heavily loaded assemblies, such as screw-and-nut mechanisms, where conventional lubricants produce little effect [15].

Wear resistance of the metal-plating film varies considerably owing to a wide diversity of its components and variations in their properties. In an extreme case where lubrication is effected by a medium having no surface-active agents, e.g. an aqueous solution of sulphuric acid for chemical engineering applications or aqueous solutions of salts used in well drilling, it can be classed as ion lubrication.

Ion lubrication is based on the property of metal ions formed in an electrochemical process to be drawn into the clearance between the rubbing surfaces and to be discharged there. The discharge produces a protective metallic film (dividing film). Metal ions can also be obtained from a solution of the lubricant and be deposited in the contact zone.

Dividing film is a protective metallic film formed during friction in the contact zone as a result of the discharge of metal ions (ion lubrication). The diffusion-vacancy mechanism is not realized there. The film has mainly a dividing function.

The formation of ions in the course of electrochemical interaction between a lubricant and a metal placed therein is described in [15]. The formation of a dividing film from solutions of cuprous salts is described in [15, pp. 120-127], where the film was found to show high effectiveness compared with instances where no such film was present. The phenomenon in which ions from an aqueous salt solution used as lubricant are drawn into the clearance between the rubbing surfaces of rubber and glass is treated in reference [20].

The wear resistance of rubbing surfaces in the presence of salt brines significantly grows if the products of destruction of plastics or solid hydrocarbons are introduced in between the surfaces. For instance, specially designed joints with inserts of those materials working in sea water have substantially increased wear life [15]. The products of destruction of solid plastics in contact behave similarly to those of liquid hydrocarbons, i.e. they initiate an oxidation-reduction process and form surface-active agents, which markedly reduces wear. The reason for this is that the relative movement of the rubbing surfaces sets the particles in motion and so brings them in contact, as is the case with their behaviour in a liquid. Because of its combination with the ion or the plasma-forming lubrication types (where there is a part made from a film-forming or metal-polymer material), such a lubrication system is called traverse lubrication.

Traverse lubrication is therefore lubrication with products of plastics tribodestruction (combined with the ion lubrication) or one in a pair formed by a metal polymer and steel, or one in friction between a film-forming material with polymer inserts and steel. This type of lubrication involves the transfer to the contact zone of not only charged metallic particles, but also the polymer tribodestruction products equally charged and adsorbed on the contact.

An indispensable element of the traverse lubrication is the presence of metal particles reacting with tribodestruction products in the polymer film being formed. It should be noted that only those metal polymers that contain film-forming materials, such as copper and bronze, are capable of providing the traverse lubrication.

Selective transfer by means of the traverse lubrication is used for marine applications [6, pp. 53-58] and for applications where metal-polymer materials contain film-forming components.

Sometimes it may be difficult to identify the type of lubrication that involves selective transfer (which is revealed by the formation of copper or some other film on the rubbing surface). However, the very phenomenon of the spontaneous formation of a protective metallic film that sharply reduces friction and wear is indicative of selective transfer as such.

17.1.2. Preparatory Physico-Chemical Processes of Selective Transfer

These are tribodestruction of the lubricant or an additive, selective dissolving, and passivation. At the initial stage, these processes prepare transition from a disordered friction where considerable disturbances or even scoring are likely to occur to the orderly, stable conditions of selective transfer, where those disturbances are excluded.

In sliding pairs bronze-steel with the use of a plasma-forming lubricant, the processes preparing the surface to friction are the tribodestruction of the lubricant, and consequently, the selective dissolving of alloy components in a thin surface layer of bronze and the formation of a servovital film and surface-active agents.

In steel-steel or steel-cast iron sliding pairs using a metal-plating lubricant, the preparatory process is the release of atoms or ions of the metal from the decomposing lubricant and their deposition together with molecules of the surface-active agents in the contact zone during friction. As they form metallic bonds, the metal atoms leave some superfluous amount of vacancies. The ligands left over from the complex compounds can constitute surface-active agents. The latter can also be represented by the active components of the lubricant, by compositions of the tribodestruction products, and by complex compounds themselves. For example, if the atoms of the metal are reduced from its oxide, the surface-active

agent should be contained in the basic lubricant; the same holds for additives of a metal powder, e.g. copper and bronze. In this case the surface-active agents facilitate its deformation and dissolving. The sediment of the metal powder fills the irregularities of the steel or cast-iron surface, thereby forming a metal-plating film.

In extreme cases, where lubrication is effected, for instance, by a flow of a sulphuric-acid solution, as in chemical production processes, the deposition of a protective metallic dividing film may occur. Although such a film cannot withstand wear, and its coefficient of friction is about 0.1, it readily recuperates and tangibly reduces the wear and friction that take place when it is absent.

Tribodestruction of the lubricant. For a fluid lubricant in boundary-friction conditions this is an adverse process because it involves corrosion, a change in lubricant viscosity, etc.

In selective transfer conditions, the tribodestruction of the lubricant provides the active parts of the desintegrated molecules which are necessary to initiate a chain of processes leading to selective dissolving and formation of the servovital film. For this reason it is desirable to use, as lubricants, organic compounds with a low energy of dissociation and decomposition.

The elementary chemical processes in a low-temperature plasma are placed into two classes: (1) the processes running with neutral particles and (2) those running with charged and excited particles.

The first class includes the reaction of molecule dissociation, e.g. $CH_4 \rightarrow \dot{C}H_3 + H$. The formation of atoms and radicals leads to the reactions of exchange $RH + \dot{C}H_3 \rightarrow \dot{R} + CH_4$, of dehydrogenation $RH + H \rightarrow \dot{R} + H_2$ and to some other reactions. This promotes the development of radical-and-chain transformations which run at high speeds and low activation energies. The second class of reactions includes the excitation $H + e \rightarrow H^* + e$ and ionization $H + e \rightarrow H^+ + 2e$ of atoms by electrons; the dissociation of molecules in their collisions witb electrons $H_2 + e \rightarrow 2H + e$; $H_2O_2 + e \rightarrow 2OH + e$; $O_2 + e \rightarrow 2O + e$; dehydrogenation $C_2H_2 + e \rightarrow C_2H + H + e$; $C_2H_4 + e \rightarrow C_2H_2 + H_2 + e$; dissociative recombination $AB^+ + e \rightarrow A + B + e$; and recombinative ionization in the collision of three particles $N + N + K + e \rightarrow N_2 + K^+ + e$ [8].

Such processes have often been observed in lubricants. These quick-running intermediate processes, as well as catalytic, electrochemical and others, result in destruction products which, as a rule, have a reduced molecular mass.

In investigation of the selective transfer mechanism as applied to tribological couples copper alloy-steel working in glycerine, the surface tension of the latter at the interface with air has been found to decrease. Hence, it has been assumed that the mechano-chemical reactions and the dissolving of the more active components of the

copper alloy result in the formation of surface-active agents and other decomposition products.

These products are mostly made up of deoxidizing agents. By reacting with oxides, they reduce an oxide film on the surface.

The elimination of the oxide film lowers the energy of electron emission, facilitates the running of the chemosorption processes and the loosening of the surface layer.

As said above, organometallic compounds are formed from the interaction of the destruction products with the impurities and alloying elements:

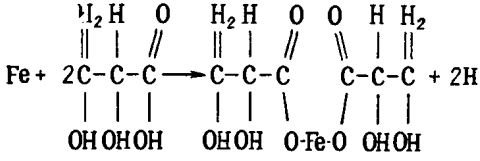

The presence of polar and polarized substances in the gap between the rubbing surfaces gives rise to electrokinetic processes, which is of great importance where charged metal particles formed on dispersion of the surface layers get into the gap. These particles are held there by an electric field and, as there is no oxidation of the metal, they can once again adhere to the metal surface, thereby reducing its wear.

Selective dissolving is a physico-chemical process running between lubricant tribodestruction products and alloy components in a thin surface layer of the friction zone; the process is activated by friction and pressure on the contact. This process runs spontaneously and results in:

—formation of a metallic protective servovital film with increased concentration of vacancies, which determines the diffusion-vacancy mechanism of its deformation; the film is formed from the metal surface layer left after selective dissolving;

—formation of a new organometallic compound which is a surface-active agent, that is, a product of reaction between the alloying elements and destruction products; as it is adsorbed on the film, the surface-active agent reduces the film's strength thereby reducing its resistance to shearing strain; as is known, such compounds are used as antiwear additives to oils [12];

—reduction of contact pressure due to an increase in the real contact area by several orders of magnitude as a result of selective dissolving of the asperities being under load [15].

Passivation. The preparatory processes spontaneously come to an end owing to reduced contact pressure and lower potential difference between all galvanic pairs on the surfaces in contact, since the latter become covered with a film, excepting the contact and gap areas. The passivation takes place in stable friction conditions and

promotes the transfer of charged particles to the contact zone. In extreme cases, where the lubricant is an aggressive medium (e.g. solutions of acids, salts, or sea water), the same processes take place; that, however, does not exclude corrosive action of the lubricant on the rubbing surfaces [11, 18].

17.1.3. Physico-Chemical Essentials of the Wear and Friction Reducing Systems

Boundary friction and dry friction comprise systems which involve heat dissipation and irreversible changes in the metal: oxidation, dispersion, fatigue failure or failure due to structural changes. A thin oxide film and layers of the lubricant or a mixture of oxygen and moisture adsorbed on it are incapable of protecting the metal surface layer from deformation, strengthening, and breaking, and they produce considerable friction.

Although metal and chemical films artificially created on the rubbing surfaces prolong service life of the surface layer, their effect is often inadequate. The principal drawback to such films is lack of compensation for damage and wear, and for unbalanced processes leading to failure.

Selective transfer involves two processes: (a) the formation of organometallic compounds which reduce the strength of the adsorbent, i.e. the main metal providing the reduction of wear, and (b) the formation of superfluous vacancies in the surface layer which also aid in reducing its strength in deformation without breaking.

The oxidation of the lubricant and metal is used in selective transfer for reducing wear and friction losses.

The analysis of the physico-chemical mechanism of wear reduction by selective transfer [13] and the revealing of other factors conducive to higher wear resistance have lead to the conclusion that wear reduction is brought about by the action of the above-mentioned individual wear and friction reducing systems.

Actually, various combinations of materials and lubricants can create a variety of the wear and friction reducing systems. Accordingly, their ability to reduce wear and friction will be variable. Several of such systems can be singled out which are possible not only in the selective transfer regime but also in the boundary-friction regime (e.g. based on electrophoresis or polymerization on the contact). Here, the effect of these systems differs markedly from that in the selective transfer regime.

The system of reducing the specific load. In the selective transfer regime, upon selective dissolving of the alloying components by tribodestruction products in a thin surface layer, a servovital film with a self-lubricating capability is formed on the surface. The surface-active agents developing here directly on the cathodic element, i.e. on the material of the emerging servovital film, permeate

it, reduce its bulk strength and facilitate its dispersion. The latter leads to the formation of colloidal particles, which develop micelles owing to the presence of surfactants, whose concentration should exceed the critical value required for micelle formation.

Simultaneously with these processes, the servovital film is transferred onto the steel counterface, where it fills the valleys of surface irregularities, levels out the profile and so reduces the pressure.

When the real contact areas grow up to the size of the nominal surface and the pressure sharply drops, the dispersion and selective dissolving will come to an end, and friction will then take effect on the servovital film containing the surface-active agents, lubricant and micelles.

In steel-steel and steel-cast iron tribological couples, pressure is reduced as the metal from the lubricant is deposited on the rubbing surfaces, filling the asperities with a metal-plating film.

If there is no surface-active agent in the lubricant or in the products of chemical reactions, its function can partly be performed by the inactive hydrocarbons. If the latter are absent (for instance, in lubrication by a sulphuric-acid solution), the formation of a protective film goes slow. The film thus formed (dividing film) may easily oxidize, and for this reason the film formation in the stable regime goes on without stopping. As this takes place, the specific loads decrease but slightly.

Reduced pressures make it possible to increase the reliability of joints and their load capacity, specifically in aircraft applications. Here, studies have been undertaken on the range of selective transfer application with regard to critical specific loads, temperature effects, and design characteristics of tribological joints. The use of selective transfer makes it possible to load the joints heavier without increasing their mass and overall dimensions [15].

The system of compensating for surface-layer deformation effects produced by friction and of reducing the resistance to shear. The servovital and metal-plating films have the ability to reduce the amount of dislocations developed during friction to the level found in an annealed material. That is sufficient to prevent fatigue and destruction processes in the surface layer. This phenomenon is based on the diffusion-vacancy mechanism, whose principle is as follows.

It has been found [16] that the protective film has a high concentration of point defects, or vacancies. Indeed, it is known [1] that selective dissolving of the alloying components of a copper alloy (consisting in that atoms of the alloying elements leave their places in the crystal lattices of solid solutions and chemical compositions) produces superfluous vacancies. In addition, vacancies develop as the film is deformed and when dislocations come to the surface. A film 1 μm thick has porosity, which additionally reduces its thickness to the magnitude commensurable with the dislocation stress fields. A surface-active agent which occupies the pores

reduces the strength of their walls. A high mobility of dislocations in the film is therefore provided by the combined assistance of such favourable factors as a high superfluous vacancy concentration, the Rebinder adsorption effect, and the thin walls of the film pores.

At the same time, the increase of the real contact area to a value near the nominal contact area on the one hand, and the reduction of friction by about an order of magnitude on the other, give us

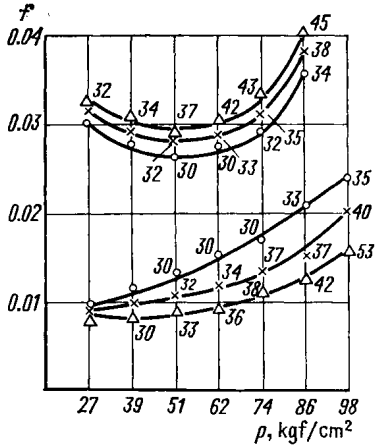

Fig. 17.1. Variation of friction coefficient with load (lubrication with oil MC-20—the upper curves, and with glycerine—the lower curves) for sliding speeds
○—0.6 m/s; ×—1 m/s; △—2 m/s. The figures indicate temperatures

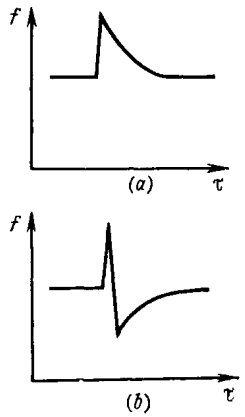

Fig. 17.2. Change of friction coefficient with time at suddenly applied additional pressure
(a) boundary friction; (b) selective transfer

the reason to believe that friction runs between weakly bonded individual particles rather than between solid surfaces. This condition of the film is difficult to investigate because it exists in the process of friction attended by pressure, heat, and tribochemical action, and it ends when the friction is stopped.

In friction, the servovital film differs from the boundary-lubrication film only in magnitudes of friction and wear. Fig. 17.1 shows relationships between the friction coefficient and pressure for boundary lubrication (upper curves) and for selective transfer (lower curves). The tests were carried out in the AE-5 friction testing machine on specimens made of bronze БрАЖМц 10-3-1,5 rubbed against steel 45.

Comparing the curves for oil MC-20 (boundary friction) and glycerine (selective transfer), it can be seen that in the first case the increased temperature and speed of rubbing cause a rise, whereas in the second case, a fall in friction. Such a phenomenon in the selective transfer regime indicates an improvement in the lubricity and a decrease in the toughness of the film due to chemosorption processes,

which is excluded for boundary friction. The temperature range for lubricant operation in the selective transfer regime is markedly widened.

A similar effect is observed in the selective transfer regime with a sharply increased loading. Fig. 17.2 illustrates a change in the friction coefficient in time with a suddenly applied additional pressure for boundary friction (Fig. 17.2*a*) and for selective transfer (Fig. 17.2*b*). At the beginning of loading the coefficient of friction grows in both cases, and the rubbing surfaces get heated. When the additional load is removed, the friction with boundary lubrication gradually decreases to the initial level. In the selective transfer regime, the removal of loading sometimes produces a sharp fall in friction which then gradually mounts to its initial level. This behaviour as well as that observed at rising temperatures has essentially the same reasons, which are the change from adsorption to chemisorption, additional dissolving, and the formation of surface-active agents.

It has been found that the ability of the servovital film to reduce wear and friction depends on the features of the copper alloy used, namely, on the quantity and properties of alloying elements, on the alloy composition regularity, on the number of the alloying elements with regard to the alloy solution limit, and on the properties of the surface-active agents formed in friction.

The system of wear compensation by the use of electrical phenomena for collecting and depositing the dispersed particles of metal in the friction contact zone. Under selective transfer conditions, electrical phenomena may have a significant part to play in reducing wear and friction.

When selective transfer changes over to a steady-state regime, a double electrical layer is found at the interface of the servovital film (or metal-plating film) and the lubricant.

When one or both rubbing components are dielectrics, a double electrical layer can be generated on their surfaces by triboelectrification. Therefore, a more or less intensive electric field is always present in the gap between the rubbing surfaces. This field creates electrokinetic processes which assist in reducing wear and friction through the adsorption of the contacts of ions, colloidal particles or cathodic metal particles present in the lubricant [5].

The process of electrophoresis compensates for the loss of the film's dispersed particles returning them to the contact area. These are colloidal particles which make up the bulk of the particles in the steady-state regime.

A very important case is the transfer of ions and larger charged particles to the contact zone in the electrochemical process running between the contact zone and the other surfaces (which even may not take part in friction). This pertains to all electroconductive lubricants, such as solutions of acids, salts, and hydrocarbons containing electroconductive additives. This also includes the adsorp-

tion of copper particles in the friction contact zone in refrigerating machines, the particles being conveyed by a flow of freon from the areas where corrosion dissolves the material of copper tubing.

During friction in a steady regime, the double electrical layer undergoes a cyclic change in the concentration of anions and cations in the diffusive and dense parts of the film. The process of friction depolarizes the polarized surface layers and so promotes the surface 'dressing'. As a result, most particles get discharged, adsorbed, compressed under load, and turned into the metal of the servovital film. As this takes place, the molecules of a surface-active agent adsorbed by a metal particle are drawn by the latter into the film. These molecules eventually provide porosity and elasticity of the film, additional lubrication, and, what is the most impotrtant, adsorptive action on the film. It is more than probable, tha the molecules prolong the life of vacancies as they adsorb on the latter.

In the absence of organic compositions the dividing film is formed which, as it wears, recovers again during the steady-state friction regime, and prevents the rubbing surfaces from direct contact. Actually, such wear consists most likely in oxidation, because only in this way a metal ion (an atom or a component of an oxide molecule) can, on getting discharged, go out of the contact zone. If the source of ions is some non-rubbing surface, this wear can go on infinitely. Since the ions are solvated and the sediment generated is loose enough, the friction force is lower than it is in friction of steel against steel.

The diverse rubbing conditions, lubricants, and materials combinations used in engineering practice influence the effectiveness of the electrical phenomena in reducing wear and friction.

Some examples of the use of different materials under conditions typical of the discussed system are presented in Table 17.1. The first line of the Table gives the results of an experiment disclosing the effect of ions collected by the double electrical layer field on the coefficient of friction, which was here reduced by a factor of 2. The other lines contain data on the industrial use of the system in the selective transfer regime, where the effect of the system is the most prominent.

It should be noted that the deposition of particles in the gap alone is not sufficient to form the servovital film capable of deformation without destruction, because it aslo requires organic compositions and surface-active agents in the lubricant. Table 17.1 gives only three instances where the lubricants contain organic compositions. In the other cases, however, where the dividing film is formed, the lack of organic compounds is somewhat compensated for, because the electrokinetic collection system restores the film as this wears out. When the wear resistance of a tribological joint needs to be increased, organic molecules can be delivered to the contact zone by the transfer method or some other methods.

The system of preventing the metal from oxidation in rubbing. The wear of the oxide film accounts for most of the metal surface

Table 17.1

Application of electrical phenomena for reducing wear and friction

Material of sliding pairs	Fluid lubricant	Source of ions or particles	Field of application	Notes, reference
Glass/rubber	Aqueous solutions of salts or alkalis	Aqueous solutions of salts or alkalis	Experiments	Friction reduced [20], no selective transfer
Glass + cuprous oxide/steel	Water + crude oil	Cuprous oxide	Oil wells drilling	Friction reduced by 80% [15, pp. 120-127] [17]
Wood impregnated with complex compounds/steel	Glycerine + complex compounds	Complex copper compounds	Textile machinery bearings	
Steel/steel	Aqueous solution of sulphuric acid	Copper alloy	Tribological joints in chemical equipment	[15, pp. 176-180]
	Cutting fluids with addition of salt or copper	Copper salt	Metal cutting	[15, pp. 196-201]
	Freon + oil	Copper	Refrigerator machines	—

wear in dry and boundary friction. The oxide film forms a barrier that prevents the metals of the rubbing components from seizure. The latter is typical of metals only; it involves the integration of crystal lattices of the rubbing surfaces at real contact areas. In high-load friction conditions, the rupture of oxide film and the development of local seizure result in rapid wear. The thickening of oxide films and increased wear rate are observed at elevated bulk temperatures (caused by external heating and inadequate heat removal).

In the selective transfer regime, oxidation and seizure are prevented by the dense layers of an adsorbed surface-active agent. As mentioned above, a surface-active agent is formed mainly at the initial stage of friction, where the products of destruction of the alloy's anodic components undergo selective dissolving [1, 7, pp. 6-9]. As these layers are transferred to the cathodic surface, they block it from the molecules of oxygen. At the same time they reduce the strength through the adsorptive action and facilitate the dispersion of the metal. The dispersion gives rise to colloidal particles, which are drawn by the double electrical layer into the contact zone, where they get discharged and join the film metal. In this way seizure turns into a useful phenomenon, because it prevents the dissipation of particles and replenishes the film material.

Reducing conditions on the rubbing surfaces are also provided by the tribodestruction and oxidation of the lubricant hydrocarbons which yield a number of reducers, including hydrogen.

The removal of the oxide film reduces the energy of electron emission and thereby facilitates the running of chemisorption processes and the loosening of the surface layer.

With a lubricant having no organic compounds, the dividing film during friction operates in reducing conditions and does not oxidize. However, when the friction stops, oxidation takes its course as usual. To protect the dividing film, use is made of lubricating inserts which supply the film surface with organic compounds [6].

The system of forming a protective polymer film. A lubricant containing substances that polymerize on the contact was proposed in the 1950s [19]. The resultant film provides much higher resistance to deformation and penetration than the carrier liquid does.

A number of oil-soluble additives have been proposed [9], e.g. a mixture of methyl ether of a polybasic acid and polyamines that gives a polyamide polymer, which effectively reduces seizure on a Rider gear-type testing machine.

However, both the cases have the drawbacks typical of boundary lubrication, i.e. high specific pressures due to a small real contact area and the presence of oxide films. In addition, the oxide film on steel is a poor catalyst of polycondensation and polymerization reactions.

Unlike boundary friction, the selective transfer regime at the beginning of friction involves processes which provide favourable con-

ditions for a strong bond of the polymerization products with the metal, low pressures commensurable with the film strength and free chemical bonds arising in the selective dissolving of the alloy components, these bonds being available for interaction with the polymer formed on the surface. The absence of the oxide film on the surface also makes for this interaction. The free radicals of organic substances that are formed in the process of decomposition during friction can form polymeric chains, which adhere by the active end to the metal surface and thereby produce polymeric formations. These were observed in the selective transfer regime [1, 18].

Chemical and mass spectrophotometric analyses have shown that as a result of mechano-chemical processes at the sliding interface between brass and steel lubricated by glycerine, the latter is oxidized into aldehyde glycerine, acrolein, glyceric acid, and other products with the molecular weight lower than that of glycerine [7]. These products, often being unsaturated hydrocarbons, can be polymerized by triboactivation.

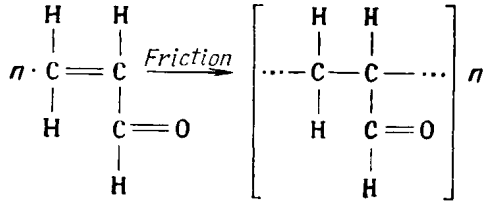

The resulting structure formed from the polymerized molecules complements the action of the other wear and friction reducing systems. In addition, the polymeric formation, which has been found to be in a semiliquid state [1], has a coefficient of friction which approximates that for fluid friction.

As mentioned in the foregoing, the absence of individual systems from the whole complex of the wear and friction reducing system leads to losses in its effectiveness. On the other hand, selective transfer can be utilized in some tribological joints by methods not mentioned above, which, however, do not change the nature of the processes. Such methods are: brass-plating, the use of bronze inserts [2, 10] and of cemented carbide materials in a copper matrix [6]. These methods are based on the combined action of the wear and friction reducing systems modified by losses due to the intrinsic drawbacks, such as the use of bronze inserts instead of solid bronze part, etc. However, these losses are in most cases negligible and are offset by the advantages offered by these methods.

17.2. UTILIZING SELECTIVE TRANSFER IN TRIBOLOGICAL JOINTS

Practical experience makes it possible to indicate several ways of utilizing the selective transfer phenomena:
—to develop wear-resistant bronze-steel sliding pairs, working in the selective transfer regime;
—to use metal-plating lubricants providing the selective transfer regime in steel-steel sliding pairs;
—to develop wear-resistant metal-ceramic, metal-polymer, and other materials working in the selective transfer regime;
—to develop cutting fluids providing a copper film on the cutting edge in the course of machining for increased tool life;
—to develop new techniques for processing rubbing surfaces, e.g. frictional bronze- or copper-plating, for improved antiscuff properties, reduced run-in wear, and reduced fretting;
—to speed up the running-in process for sliding pairs with the initial point contact (e.g. gear mesh in globoidal reduction gears);
—to prolong the life of weak-current electric contacts [15], etc.

The use of selective transfer in tribological units involves some increase in the mass of the steel component, since the material of the bronze component is transferred to it during the initial period of friction when the bronze wears at a somewhat increased rate. However the unit as a whole hardly loses any mass.

17.2.1. High-Load Pin Joints

Pin joints in the aircraft landing gear operate in short-cycle swing-motion conditions at frequencies of 0.5 to 10 Hz, low sliding speeds (0.005 to 0.1 m/s), and high specific pressures (2 to 15 kgf/mm^2), with inadequate lubrication, and often with no lubrication at all [15]. A study of selective transfer was undertaken with the use of a special testing device (see Fig. 17.3) simulating the operation of an aircraft landing-gear pin joint.

The experiments revealed critical pressures (p_{cr}) and critical temperatures (ϑ_{cr}) of the unit at which the operation of the bronze-steel pair changes over from the selective transfer regime (zone *I*, Fig. 17.4) to the regime of intensive wear of the bronze bushing (zone *II*). The rubbing surfaces were lubricated with grease ЦИАТИМ-201 periodically through 4×10^3 swinging cycles.

In testing within the range of pressures and temperatures defined by zone *I* in Fig. 17.4 the rubbing surfaces of the bronze bushings were found to have a surface roughness of 0.08-0.32 μm *Ra* and the loaded areas of the bushings to be coated with a thin copper film. The steel pin was covered with copper only when cadmium-plated; the chromium-plated pins had no copper film. At these pressures, the bronze-steel pair exhibited a low wear rate; here the bronze bushings only were subject to wear, whereas the steel pins remained intact.

At the pressures and temperatures within zone *II*, operation of the bronze-steel pair was characterized by a high wear rate of the bronze bushings, by seizure, by tearing in depth of bronze and by the smearing of bronze particles on the friction surfaces.

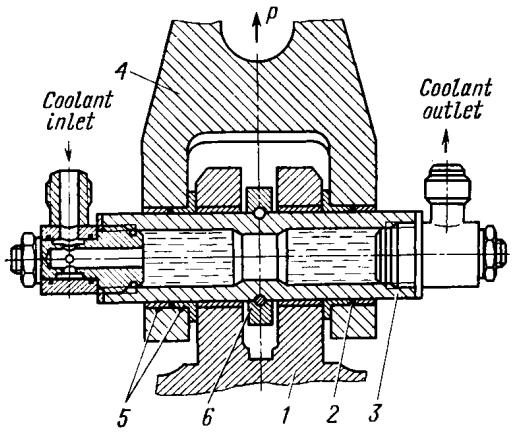

Fig. 17.3. Sliding components
1, *4*—hinges; *2*—bronze bushings; *3*—steel pin; *5* - thermocouples; *6*—rocking bar

As seen in Fig. 17.4, the region of selective transfer relative to pressure is substantially limited by the bulk temperature of the unit.

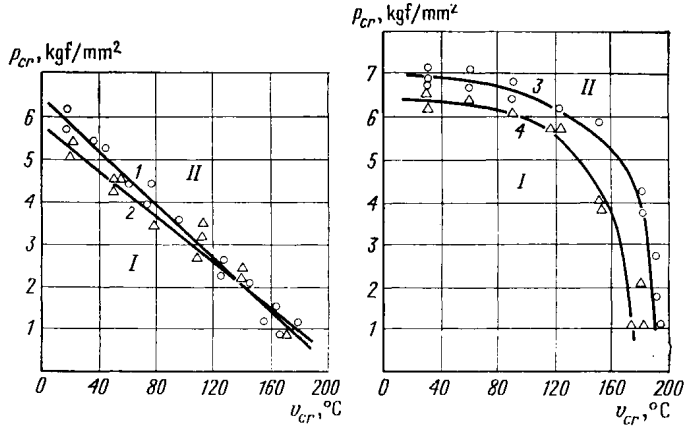

Fig. 17.4. Critical loads and temperatures for bronze/steel sliding couples
1—bronze БрАЖН10-4-4/chromium-plated steel; *2*—bronze БрАЖМц10-3-1.5/chromium-plated steel; *3*—bronze БрАЖН10-4-4/cadmium-plated steel; *4*—bronze БрАЖМц 10-3-1.5/cadmium-plated steel

With the rise of the bulk temperature, the critical pressure and hence the load-carrying capacity of the joint decrease.

It was established that when the joint that had been operated for a long time at pressures exceeding the critical value was switched

over to operation at pressures below the critical value, the selective transfer regime was restored.

The experiments have shown that the pressure and temperature of the joint also have a significant effect upon the friction coefficient. Relationships between the friction coefficient for bronze-steel combinations and the parameter p/p_{cr} (where p = pressure on the bushing and p_{cr} = critical pressure at the respective temperature) are shown in Fig. 17.5. The curves are constructed for steady-state

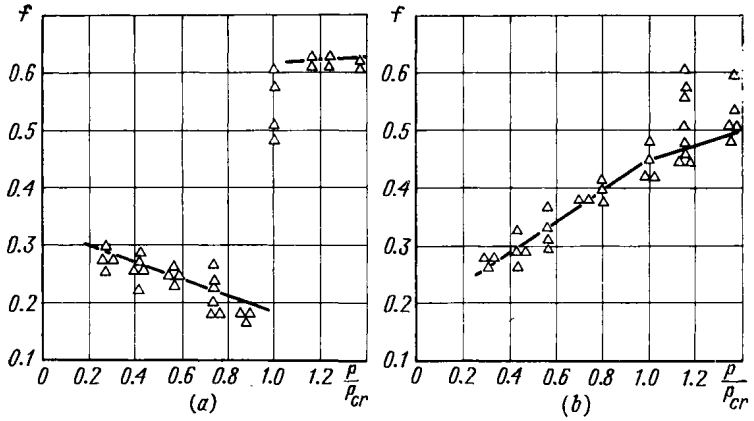

Fig. 17.5. Coefficient of friction as function of parameter p/p_{cr}
(*a*) bronze БрАЖН10-4-4/cadmium-plated steel; (*b*) bronze БрАЖН10-4-4/chromium-plated steel

wear conditions. As seen from the charts, the character of the relationship depends on the rubbing materials, on the kind of pins coating, and on the temperature regime through the critical pressure value. As specific pressures exceed the critical value in the bronze — cadmium plated steel combination, the friction coefficient sharply grows, which indicates that the sliding couple changes its frictional regime from selective transfer to one of intensive wear of the bronze bushings. In the bronze — chrome plated steel combination this transition shows a milder change in the friction coefficient.

17.2.2. Automotive Running Gear

Prolonged service life of automotive running gear units and parts can be achieved by the use of lubricants containing fine powders of copper, copper alloys or their oxides [15]. In the course of friction, the oxides reduce to pure copper and coat the rubbing surfaces with a thin metal layer, which markedly increases their wear resistance and antiscuff properties. Only 1 percent (by mass) of copper powder added to greases УС-2 and 1-13 made it possible to obtain nearly a two-fold increase of the seizure load limit.

Laboratory tests on friction machines with reciprocating and rotary motion showed that with 5 percent of powder and over, the selective-transfer phenomena took place as early as at the initial stages of friction. With a powder concentration of 10 percent and over, the copper is transferred onto the steel surfaces. The copper layer thus formed remains constant and effective up to the extreme load provided by the friction machine. An insignificant variation in the layer thickness and the absence of tangible wear over the whole period of testing imply that the entire plastic deformation in given loading conditions is taken up by the copper layer 0.6 to 1.7 μm thick.

A series of tests with recording the bulk temperature showed that the antiscuff properties of lubricants with added powders remained at temperatures in excess of 150°C (the dropping point for grease 1-13 is 120°C and for grease УС-2 is 100°C). The maximum temperature fixed for grease 1-13 with a 10 percent powder content was 186°C. Further loading of the specimens raised the friction coefficient to 0.2-0.3 and caused the lubricant to smoke, but no surface scoring was observed. That proves that the main load in the extreme friction conditions was taken by the copper layer, which is important for emergency conditions.

Special tests were carried out to simulate the operation of a truck wheel hub used in the ЗИЛ-130 truck. The hub with a loading device and recording instruments was mounted on revolving drums. The load on the wheel hub was 1125 kgf, which corresponds to the truck's full loading capacity, with a rotational frequency of 500 rpm and a test run of 500 hours.

Performance data, such as wear of the mating surfaces of the bearing and the swivel axle spindle, the copper film thickness, the lubricant viscosity and temperature, were fixed during the test run. The metal-plating lubricants shown in Table 17.2 were tested. These

Table 17.2

Composition of metal-plating lubricants

Lubricant grade	Powder filler	Filler content, %	Powder grit size, μm
1-13	Cuprous oxide	10	15-20
УС-2	Powder of БНК-brass	15	5-10
ЦИАТИМ-201	Copper powder	15	10-15

lubricants were found to reduce wear substantially. The rubbing surfaces were covered with a thin layer of copper. The growth of the layer lasted for 60 to 65 hours and then stopped. The copper layer covered all loaded surfaces of the bearing: its outside and inside diameters, the rollers and the tracks.

Field tests of metal-plating lubricants were undertaken for three years on 29 trucks (twelve ЛАЗ-695Е units, five ЛАЗ-699А units, and twelve ЗИЛ-130 units). To assess the effectiveness of the metal-plating lubricants, the left-hand wheel hubs were filled with grease 1-13 and the right-hand ones with the same grease containing copper powder. The hubs were inspected after every 12000 km of running. The processes within the hubs were also permanently recorded with the aid of strain gauges and recorders installed in two sample vehicles run in the same conditions.

The results obtained are given in Table 17.3.

Table 17.3

Results of service tests of automobile wheel assemblies

Test run, km	Right-hand wheel hubs, metal-plating lubricant, wear, μm	Left-hand wheel hubs, grease 1-13, wear, μm
2000*1	⩽ 0.29	70
12000	⩽ 0.29	27*2
24000	⩽ 1.3	19*2
36000	⩽ 1.25	25*2
48000	⩽ 0.6	33*2
60000	⩽ 0.3	37*2

*1 Running-in.
*2 Before lubricant change.

The use of the metal-plating lubricants in the wheel hubs made it possible to establish the optimum period between lubricant changes at 36000 km and to reduce the specific cost of these operations by 60 percent.

17.2.3. Leadscrew-and-Nut Assembly

Studies of selective transfer in a leadscrew-and-nut assembly were conducted on experimental installations which make it possible to simulate operating conditions similar to those in machine tools [15]. The test specimen was a plain leadscrew-and-nut assembly having a trapezoidal thread of 50 × 8, a thread surface finish of 1.25-2.5 μm *Ra* and accuracy within the 3rd tolerance grade.

Friction and wear in the assembly were studied using a metal-plating lubricant, grease ЦИАТИМ-201 containing copper powder. Since the antifriction properties of a metal-plating lubricant depend on the character of interaction between the filler (copper powder) and the rubbing surface, the filler concentration is important for the lubricant service properties. Fig. 17.6 shows a relationship between the nut wear rate and the copper powder concentration in ЦИАТИМ-201.

The metal-plating lubricant formed by grease ЦИАТИМ-201 plus 10 percent (by mass) of copper powder drastically reduces friction and wear as compared with oil И-20А and grease ЦИАТИМ-201 without the filler (Figs. 17.6 and 17.7). That can be attributed to a thin film typical of selective transfer, which is formed on the thread flanks as these come in contact. The film creates favourable operating conditions and reduces friction by localizing deformations within itself. The thin copper film has a lower yield point and shear strength than the leadscrew and nut materials.

Industrial tests of the metal-plating lubricant ЦИАТИМ-201 + + 10 percent copper powder were effected in the leadscrew-and-nut

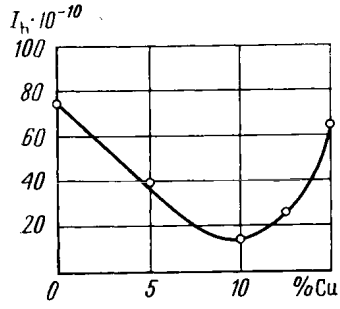

Fig. 17.6. Relation between the rate of wear of nut (bronze БрОЦС5-5-5) and the concentration of copper powder in grease ЦИАТИМ-201

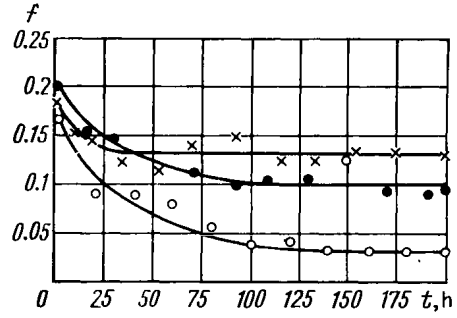

Fig. 17.7. Variation of friction coefficient in time

leadscrew (steel 45)—nut (БрОЦС5-5-5); n= =60 rpm; axial load 250 kgf; ×—oil И-20; ● — ЦИАТИМ-201; ○—ЦИАТИМ-201 + 10% copper

pairs of the longitudinal feed drives in horizontal and vertical milling machines, models 6М82 and 6М12П. The machines were used in mass and small-lot production under identical operating conditions [15].

It was found that the wear life of leadscrews lubricated with the metal-plating lubricant ЦИАТИМ-201 + 10 percent copper was 3 times longer than that of leadscrews lubricated with oil И-30А.

The estimated economic effect of utilizing the selective transfer regime in the leadscrew-and-nut pair of a horizontal or vertical milling machine amounts to no less than 160 roubles per annum for one unit.

17.2.4. Metal-Plating Lubricants in Production Equipment

The automated lubricating systems of production equipment can deliver metal-plating lubricants to the rubbing surfaces [15]. Wear and friction investigations were performed on low-power presses equipped with automatic lubrication systems and on casting machines, models 5924 and 5922, where the centralized lubrication systems

delivered metered quantites of lubricant to the rubbing surfaces during the opening of the mould. The lubricant under test was grease ЦИАТИМ-201 with 10 percent (by mass) of cuprous oxide.

In operation, measurements were taken of power consumption and temperature in movable joints. The power consumption of the press using the metal-plating lubricant was found to drop by 15 to 20 percent against that with conventional lubricants. The temperature varied with the power consumption.

The tests were carried out in different modes of lubrication, i.e. the lubricant was fed by fixed quantities but at variable time intervals. The tests showed that the metal-plating lubricant can be supplied less frequently than conventional lubricants, which implies its lower consumption.

Unlike operation with conventional lubricants, no scoring was observed with the metal-plating lubricant.

The use of metal-plating lubricants in production equipment can reduce lubricant consumption by 25 to 30 percent and power consumption by 10 to 15 percent, and prolong service life 1.5 to 2 times.

17.2.5. Wear-Resistant Materials for Submersible Pump Seals

Such a material is basically tungsten carbide in the form of moulded grains measuring 0.18 to 0.28 mm with the addition of copper

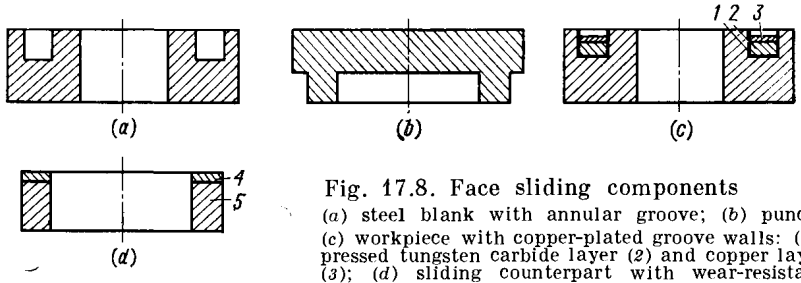

Fig. 17.8. Face sliding components
(*a*) steel blank with annular groove; (*b*) punch; (*c*) workpiece with copper-plated groove walls: (*1*), pressed tungsten carbide layer (*2*) and copper layer (*3*); (*d*) sliding counterpart with wear-resistant layer (*4*) on steel backing (*5*)

[6]. Sliding face seals utilizing this material are manufactured as follows. An annular groove of rectangular cross-section is machined on the end face of a steel blank (Fig. 17.8*a*). The walls of the groove are electroplated with a thin coating of copper. The groove is then filled with a uniform layer of tungsten carbide grains which is pressed with a punch at 3000 to 4000 kgf/cm^2. The pressed grains are then covered with a uniform layer of copper powder and pressed again under the same pressure. The workpieces thus obtained (Fig. 17.8*c*) are placed in a vacuum furnace, where the pressed layer is impregnated with molten copper at 1150 to 1200°C. The residual pressure inside the vacuum furnace is maintained at 10^{-2} to 10^{-3} mm Hg.

The molten copper fills the voids between the grains, forming a hard layer of tungsten carbide and copper firmly bonded to the steel base (Fig. 17.8*d*). The workpiece then undergoes machining operations which include grinding the working face with a diamond wheel and lapping with diamond powder or paste on a cast-iron surface plate. The working layer of this new compound has a thickness of 1 to 5 mm and over. A layer of 1.5 mm thick requires that tungsten carbide grains should be put into the groove in a layer 2.8 to 3 mm thick, with the groove depth being 5 mm.

The face seal thus obtained exhibits high wear resistance and good antifriction properties. The copper content in the working layer usually comes to 11-12 percent. The material comprises carbide grains (eutectic W_2C + WC) bonded by copper layers, the eutectic structure being distinctly differentiated and mostly fine-grained, which provides its higher strength.

The composite material offers advantages over metal-ceramic tungsten-cobalt cemented carbides, such as grades BK-3, BK-8, BK-15. It is less brittle and has no tendency to thermal cracking owing to the copper bond.

Laboratory tests of the face seals used in a ПЭД-type submersible electric motor for oil-field applications were carried out at a sliding speed of 7.5 m/s (n = 3000 rpm) and a pressure of 2 kgf/cm^2. Inside the sealed chamber there was oil MC-20, and outside, saline water, with a pressure difference of 2 kgf/cm^2. The seal wear after 2000 hours of operation was found to be 0.027 mm. Similar results were obtained in laboratory tests of the face seals in water pumps ГНОМ 100-25. The seals were tested with oil MC-20 and clayey water separated without any pressure difference, at a sliding speed of 7.1 m/s and a pressure of 3 kgf/cm^2. The average total wear of the seal for 500 hours of operation amounted to 0.01 mm, with the coefficient of friction being 0.082 to 0.095.

In the seals that separate oil from water, the latter, as it gets on the sliding interface, initiates the selective transfer process.

17.2.6. A Wear-Resistant Material for Oil Pump Seals

The material has been developed to increase the service life of powerful oil pumps, whose downtime due to wear of sliding pairs accounted for 40 to 50 percent of the total downtime [15]. The material is obtained by sintering the powders of tungsten and cobalt carbides with copper-nickel alloys. The sintering is carried out in a hydrogen medium. The production process is similar to that used for the seals described above.

Cobalt and nickel provide for secure bonding of tungsten carbide grains since tungsten readily dissolves in these metals. Copper, which is uniformly dispersed in the alloy micropores, creates prerequisites for selective transfer. The latter begins as water and oil

come in contact with the seal interface. The composite material was designated TM-1.

Investigations showed that the content of tungsten carbide grains in the material in excess of 80 percent is undesirable, because the compound becomes harder to press and has an increased brittleness.

The TM-1 was laboratory tested. When operated in crude oil, the combinations TM-1 against TM-1 and TM-1 against bronze БрОЦС 5-5-5 exhibited a 1.5-2 times increase in load capacity over the sliding pair formed by case-hardened steel 16ХГТА and bronze БрОЦС 5-5-5 (Fig. 17.9).

The TM-1 against TM-1 pair can operate in a medium with abrasive particles. The sliding pair has high hardness and good antifriction properties which make it possible for the seal to operate without stopping for over 9000 hours. This is four to five times longer than the wear life of the seals utilizing bronze against graphite.

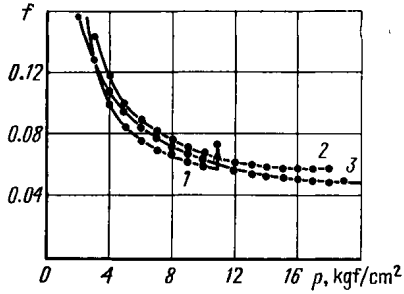

Fig. 17.9. Coefficient of friction as function of contact pressure between sliding components in crude oil at sliding speed 15 m/s
1—steel 16ХГТА/bronze БрОЦС5-5-5; *2*—alloy ТМ1/alloy ТМ1; *3*—alloy ТМ1/bronze БрОЦС5-5-5

Of much interest is the sliding pair TM-1 against БрОЦС 5-5-5 when used in diesel fuel. It operates in the selective transfer regime. A copper film is formed on both the bronze and the carbide counterfaces, providing the lowest coefficient of friction (0.05 to 0.07) and high load capacity.

17.2.7. A Glass-Metal Sliding Pair

The glass coatings of casing pipes are used in oil-field applications as protection against paraffin sedimentation and corrosion [15].

A difficulty arising in their use is that drill collars are moved along their surface, being pressed against the pipe walls with variable force. As a result, the glass coating is rubbed away down to the pipe metal and completely destroyed. That brought forward the problem of increasing the glass coatings wear life.

The maximum effect was obtained by introducing 1 to 1.35 percent of cuprous oxide (Cu_2O) into industrial grades of glass. The rate of wear was substantially reduced and brought to that of carbon steel 40 for given testing conditions (Fig. 17.10). A significant difference in the sliding surfaces of a conventional and the cuprous-oxide filled glass was obversed. The conventional-glass surface was found to have a great number of cracks, whereas the surface of the glass filled with cuprous oxide proved to be smooth and crackless.

The studies revealed that the wear behaviour of glass coating differs from that of glass plates made of the same grade of glass. The reason for it is that the process of glass coating involves substantial compressive stresses which under definite conditions cause the change in the character of wear; a uniform abrading changes to the scaling of glass particles from the sliding surface, which ought to be regarded as its complete wear.

The addition of cuprous oxide has made it possible to substantially shift away the region of scaling owing to reduced cracking of the

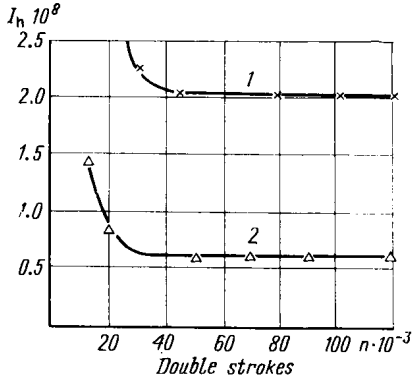

Fig. 17.10. Wear rate for glass coatings as function of the number of sliding double strokes
1—unfilled glass; *2*—glass filled with 1.5% Cu_2O

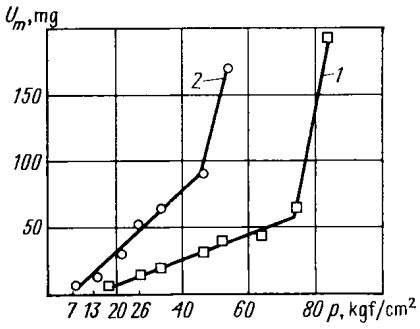

Fig. 17.11. Wear of glass coatings as function of pressure
1—glass filled with 1.5% Cu_2O; *2*—unfilled glass

sliding surface. The wear of glass coatings unfilled and filled with Cu_2O as a function of the nominal pressure by a steel specimen is shown in Fig. 17.11.

In order to explain this wear decrease effect, the rubbing surfaces of the glass coating and the steel specimen were studied after testing. The surface of the steel specimen was found to have a thin film of copper. This film became visible after prolonged test runs.

All that makes it possible to conclude that friction between cuprous-oxide filled glass and metal involves the selective transfer phenomenon, which extends the wear life and the field of application of the glass coatings.

17.2.8. Tribological Joints Working in Corrosive Media

A great number of tribological joints in chemical engineering applications operate in corrosive media. The use of the selective transfer phenomenon in friction in chemically-active media presents difficulties, because the thin layer of copper formed on the rubbing surfaces is dissolved and eventually not restored, and copper alloys

(bronze, brass) do not provide corrosion resistance in most aggressive media.

A method for depositing a layer of copper on the rubbing surfaces during friction in corrosive media has been proposed in [15], whereby the copper layer is obtained with the aid of a thermoelectromotive force created by placing the rubbing parts in contact with stainless steels containing copper.

The parts under test were the rings of a face seal made of cemented carbide, grade BK6. The rings were mounted in holders made of stainless steel 08X18H10T containing 0.24 percent Cu. The tests were carried out in a 5 percent solution of H_2SO_4 and in a 10 percent solution of NaOH. These media were selected with regard to the maximum and minimum corrosion resistance of the cemented carbide BK6: high resistance (grade 2 to GOST 13819-68) in NaOH, and low resistance (grade 8) in H_2SO_4. The tests were performed in a face friction machine (Fig. 17.12).

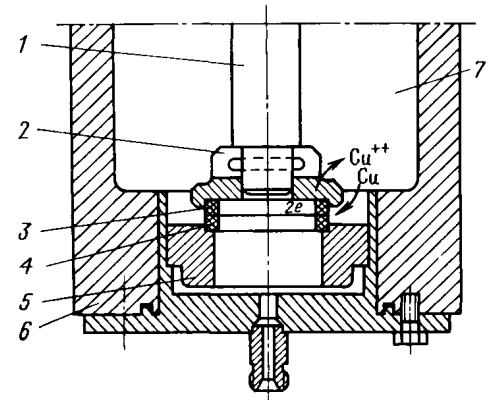

Fig. 17.12. Schematic diagram of face friction machine

1—shaft; *2*—holder of upper specimen; *3*, *4*—specimens; *5*—holder of stationary lower specimen; *6*—housing; *7*—electrolyte

The testing conditions were: specific load 3.86 kgf/cm^2, sliding speed 7.3 m/s, coefficient of mutual overlap $K_{ov} = 1$, ambient temperature 20°C, test duration 183 hours.

Analysis of the testing results showed that the linear wear of the rings in the 10 percent solution of NaOH amounted to 0.02 mm with slight traces of spot corrosion on the rubbing surfaces. In the 5 percent solution of H_2SO_4 no linear wear was found. A copper film 0.04 mm thick was formed on the rubbing surfaces.

The rings were also tested in H_2SO_4 in rotation without contact to exclude friction and wear; the gap between the rings was 3 mm. After 307 hours of run the rings were found to have lost their mass from corrosion at a rate of 1.9117 g/(m^2 h) and 2.074 g/(m^2 h), respectively, or 1.1 to 1.2 mm per annum, which corresponds to wear grade 8. No copper layer was observed on their surfaces.

The loss of mass without friction in the 5 percent solution of H_2SO_4 should be fully attributed to corrosion, whereas during friction the formation of a copper film on the rubbing surfaces protects them against wear. Friction in NaOH gives no rise to a copper film. The copper film on the rubbing surfaces excludes wear of the parent materials of the sliding pair.

17.2.9. Water-Lubricated Tribological Joints

The utilization of selective transfer for increasing the wear life of tribological joints operating in water resulted in a wear-reducing method reported in [15]. To embody the method, a new composite material was developed, which made it possible to discard the use of greases and to design movable joints that require no servicing.

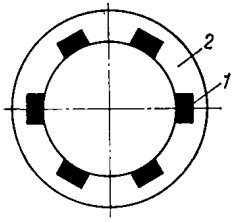

Fig. 17.13. Bearing with lubricating inserts
1—insert; *2*—metal bushing

The rubbing surface of the composite material (Fig. 17.13) consists of metal *1* and polymer *2* elements arranged in alternating order. The metal base is made of copper alloys. The polymer inserts are made of fluoroplastic filled with graphite. During operation, the wear debris of the fluoroplastic inserts is transferred by the counterface to the metal portions. Here, favourable conditions are created for the selective transfer process. Selective dissolving of the copper alloy is activated by water and is greatly accelerated by friction. However, the copper film formed from metal particles undergoes rapid oxidation under the action of water, and the wear rate rises.

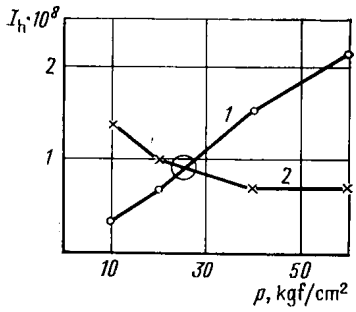

Fig. 17.14. Effect of load applied to lubricating element on wear of inserts (*1*) and metal (*2*)

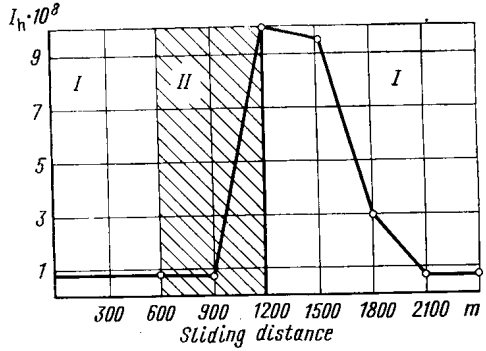

Fig. 17.15. Increase in wear after cutting off water from friction zone
I—water is delivered; *II*—water is cut off

The character of the process changes, if the contact zone is supplied with substances which shift the chemical balance to reducing processes, and that provides for a steadier selective transfer regime. These substances are included in the insert material. The servovital film formed during friction has a high load capacity.

The load capacity of this film depends on the rate of delivery of the wear products to the contact zone, which is determined by the ratio of the insert and metal areas. The pressure at which the wear

of the metal is equal to that of the insert is defined by the point of intersection of the curves in Fig. 17.14. In water, the servovital film builds up gradually, resulting in increased contact area and reduced wear rate. The film can for some time retain its properties after the delivery of water to the friction zone has been stopped, exhibiting a slow rate of wear. The run of the process of wear is depicted by the graph in Fig. 17.15. The tests were performed in the МФТ-1 testing machine at a pressure of $P_0 = 100$ kgf/cm^2 and a sliding speed of 0.05 m/s. After the water had been shut off the wear rate remained at the same level over 300 m of sliding. Then it began to rise and mounted up more than 10 times. With the delivery of water resumed, the friction surfaces gradually levelled off, and the wear decreased to the initial-rate level.

17.2.10. Cutting Tools

The wear of cutting tools in machining steel can be reduced by creating conditions for selective transfer phenomena at the contact of the tool and the workpiece. A thin film of copper is formed on the tool surfaces, which exhibits a considerable compressive strength and a low tangential shear strength [15]. Such a lubricating film can be obtained through chemosorptive interaction between some copper-containing substances (e.g. $CuSO_4$), a surfactant (e.g. glycerine, a mixture of glycerine and alcohol, oleic acid, sulphanole), and the rubbing surfaces.

If these components are delivered to the friction zone during cutting, the film formed will be present on the tool over the whole period of operation. The film reduces the coefficient of friction, the possibility of direct contact between the cutting edge and the workpiece, the cutting temperature and hence the tool wear.

In the case of copper sulphate as a copper-containing agent, water is used as its carrier. The concentration of $CuSO_4$ in the solution varies from 1.5 to 20 g per litre, depending on cutting conditions. The amount of oleic acid or sulphanole in the overall volume of the solution is 0.5 percent and 0.06 percent, respectively. An addition of up to 60 g per litre of sodium tripolyphosphate is recommended to prevent corrosion.

17.2.11. Frictional Plating of Steel Surfaces by Brass, Bronze, and Copper

The frictional plating method is used for steel parts to prevent their seizure during running-in and to reduce their wear during normal operation. Before assembly, the parts are coated by the frictional method with thin layers of brass, bronze or copper [4, 10]. Selective transfer can be induced in such layers.

The process is carried out in two stages: preparation of the surface and frictional plating as such.

The preparation begins with degreasing, which is done twice by cleaning with pure benzine without any additives. The first cleaning consists in wiping the surface with cloth soaked in benzine for complete removal of visible grease films, especially slushing compounds. Then the surface is treated with a brush in fresh benzine and dried.

After the cleaning, thick oxide films are removed from the surface. The removal is effected by sand paper whose grain size is determined by the required surface finish, bearing in mind that the

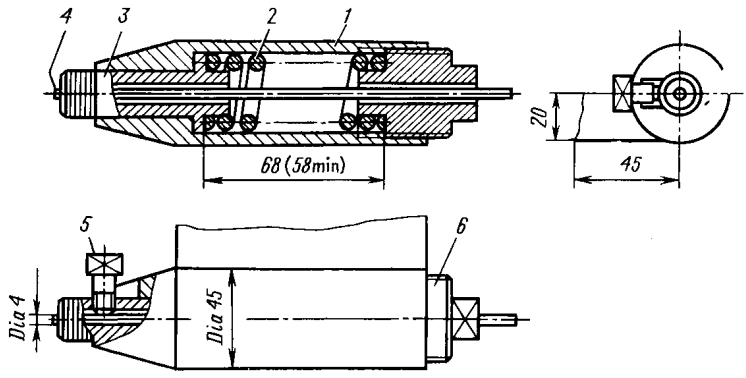

Fig. 17.16. Frictional brass-plating device

latter is not impaired by frictional plating. The best results are attained when the surface is ground to a finish of from 1.25-2.5 μm *Ra* to 0.08-0.16 μm *Ra*. Treating with sand paper can be done on the workpiece loaded in a machine tool where the frictional plating operation is to be performed immediately after.

The process is carried out in a lathe. The workpiece is held between centres or in the chuck with the back centre, and a friction plating device is clamped in the tool holder.

The device (Fig. 17.16) has a body *1* which is provided with a lateral extension for clamping in the tool holder. A piece *4* of brass, bronze or copper bar 4 mm in diameter is passed through the bores of bushings *3* and *6*, both bores being 4.2 mm in diameter. The bar is fixed in position by a screw *5*. Spring *2* provides the necessary working pressure. In operation, the bar is moved by the carriage along the workpiece and pressed against its surface by the spring. The working pressure (10 to 12 kgf/mm^2) is checked through special marks provided on bushing *3*.

The frictional plating is done with the use of glycerine, which is applied with a brush to the surface being coated.

The process was initially developed for coating carbon steels [10]. When tried on chromium-nickel steels, it failed. The coating material was found to cover only individual areas of the surfaces spaced far apart from each other. The reason is that glycerine is not capable of loosening and reducing the denser and more complex oxides of the main material, which contain compositions of chrome and other alloying elements (Si, Ni, Mo, Ti).

Hence, use is now made of media containing glycerine with additives, such as zinc chloride, ortho-phosphoric acid mixed with aniline, hydrochloric acid, sulphuric acid.

Unlike electrodeposits, the platings produced by the friction method are free from hydrogen, which is an advantage. They are used as running-in coatings for aircraft landing-gear pin joints and also for fuel-metering equipment components.

17.2.12. Globoidal Worm Gearings

Globoidal worm gearings, produced in the USSR, with the worm made of steel 40X, heat treated to *HRC* 32-35, and the wormwheel made of bronze БрОНФ 10-1-1, operate at a sliding speed in mesh of 6 m/s and pressure of 1000 kgf/cm^2. These conditions allow the selective transfer effect to be used for self-generating the rubbing surfaces in the globoidal gearing [15].

With the point contact, the copper film formed is readily squeezed out of the contact zone, which facilitates formation of the bearing surface in mesh. This was the premise for testing the globoidal worm gearings.

The tests were carried out on a testing machine which made it possible to determine frictional losses with high accuracy (the accuracy of measurement at the wormwheel shaft is 0.2 percent and at the worm shaft 0.4 percent).

The worm gearing tested was a РГУ-80 reduction gear unit, with A^* = 80 mm, i^{**} = 37, n = 1500 rpm. The worm material was alloy steel 40X, *HRC* 32-35. The wormwheel was made of bronze БрОНФ 10-1-1, it had 37 teeth cut by a Hindley hob. The unit had no preliminary running-in. It was filled with industrial grade glycerine. In the course of testing, the following parameters were fixed at one-hour intervals: efficiency, load M_2, worm rotational frequency, glycerine temperature, and ambient temperature. The testing machine was stopped each 8 hours to check the wormwheel teeth, the contact-pattern size and the backlash. The gearing was loaded stepwise in order to determine the maximum load capacity, using running-in in the selective transfer regime. The results are presented in Fig. 17.17. At a 40 kgf/m load, which amounts to 150 percent of the rated value, the efficiency dropped and the temperature rose.

---

* Centre distance.
** Ratio.

The tests were stopped. On inspection, the contact pattern was found to have spread over 70 percent of the tooth area. The axial displacement of the worm did not increase, the leading flank of the worm helix was covered with a thin layer of copper. The overloading did not affect the condition and the rate of wear of the teeth. The test showed that the gearing, working in the selective transfer regime at the initial stage, had run-in rapidly (for 40 min) and then could take heavy loads.

Another eight reduction gear units of different makes were tested in the selective transfer regime. In all the cases, the initial 45-min period of running-in made it possible to achieve efficiency that surpassed the rated values, which are usually obtained in 80 to 100 hours of operation. It was found that the selective transfer phenomena

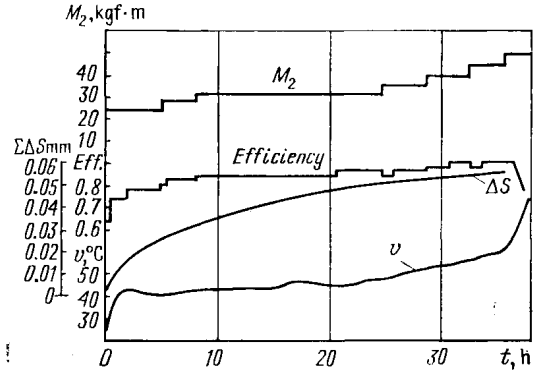

Fig. 17.17. Testing a reduction gear unit lubricated with glycerine. Test results chart

had begun after 2 to 3 min of loading and reached a steady condition in 10 to 15 min; the main rise of efficiency took place in this period. The contact pattern area spread over 35 to 40 percent of the tooth surface, the wear came to from 0.02 to 0.03 mm.

After the gear unit run in with glycerine had been changed over to operation with cylinder oil, the copper film disappeared in 25 to 30 min of run; the efficiency dropped by 8 percent, and the contact pattern ceased growing. These tests have signified that the optimal contact conditions in the gear pair are achieved rather rapidly in the initial period of operation with selective transfer. These conditions provide for reliable operation of the gearing with high efficiency and load-carrying capacity.

In all, 80 reduction gear units were run in under selective transfer conditions, and not a single one developed scoring, although in some of them the initial pressure was as high as 1500 kgf/cm^2.

The rapid running-in of the worm and wormwheel can be accounted for by the fact that the copper film is easily forced from the contact

zone under the contact load; in addition, part of the film is transferred to the worm through plastisizing action of the surface-active agents.

REFERENCES

1. Гаркунов Д. Н., Крагельский И. В., Поляков А. А. Избирательный перенос в узлах трения. М., «Транспорт», 1969.
2. Гаркунов Д. Н., Красиков С. Г. Оценка антифрикционных свойств материалов в тройном сочетании.— В сб.: Методы испытаний и оценка служебных свойств материалов подшипников скольжения. М., «Наука», 1972, с. 10-13.
3. Гаркунов Д. Н., Поляков А. А. Повышение износостойкости деталей конструкций самолетов. Изд. 2-е. М., «Машиностроение», 1974.
4. Гаркунов Д. Н., Снитковский М. М., Соломко В. А. О применении избирательного переноса в узлах трения в судовых механизмах. М., ЦБНТИ Минморфлота СССР, 1975.
5. Духин С. С., Дерягин Б. В. Электрофорез. М., «Наука», 1976.
6. Избирательный перенос при трении и его экономическая эффективность. (Сборник статей). М., МДНТП им. Дзержинского, 1972, с. 22-28, 53-58, 91-103, 183-188, 209-212, 229-232. Авт.: К. П. Волков, Д. Н. Гаркунов, С. С. Гриденок и др.
7. Избирательный перенос при трении. М., «Наука», 1975, с. 6-9, 12-24. Авт.: А. А. Поляков, Л. М. Рыбакова, Ю. С. Симаков и др.
8. Кокурин А. Д. Химия плазмы. Л. «Знание», 1948.
9. Лебедевская В. Г., Бродский Е. С., Заславский Р. Н. Состав и структура полимеров трения.— «Химия и технология топлив и масел», 1976, № 4, с. 53-57.
10. Лозовский В. Н. Фрикционное латунирование стальных деталей. Передовой научно-технический опыт. М., ЦИТЭИН, 1961.
11. Мельниченко И. М., Поляков А. А. Исследование электронного потенциала медно-цинкового сплава в зависимости от его фазового состава и структуры.— В сб.: Проблемы трения и изнашивания, № 8, Киев, «Техніка», с. 69-74.
12. Оловоорганические производные алкилфенолов — противоизносные присадки к смазочным маслам.— «Химия и технология топлив и масел», 1977, № 4, с. 54-57. Авт.: В. Л. Лашхи, О. Н. Цветков, Ф. Н. Ермолов и др.
13. Поляков А. А., Гаркунов Д. Н., Крагельский И. В. Физико-химическая механика подавления износа в явлении избирательного переноса. ДАН СССР, 1970, т. 191, № 4, с. 821-823.
14. Поляков А. А., Гаркунов Д. Н., Крагельский И. В. Проявление эффекта безызностности в условиях избирательного переноса.— В сб.: Избирательный перенос в узлах трения. М., МДНТП им. Дзержинского, 1971, с. 4-8.
15. Повышение износостойкости на основе избирательного переноса. Под ред. Д. Н. Гаркунова. М., «Машиностроение», 1977.
16. Рыбакова Л. М., Куксенова Л. И. Об изменении периода кристаллической решетки в приповерхностных слоях меди и латуни при трении.— ФММ, т. 39, вып. 2, 1975, с. 362-366.
17. Трение и износ материалов на основе полимеров. Минск, «Наука и техника», 1976, 431 с. Авт.: В. А. Белый, А. Н. Свириденок, М. И. Петроковец и др.
18. Электрохимические процессы при трении и использование их в борьбе с износом. Тезисы докладов. М., Изд-во ВСНТО, 1973, с. 136-137, 159-161, 122-124, Авт.: Б. Д. Воронков, Б. И. Лебедев, И. М. Мельниченко и др.
19. Furey M. J., The formation of polymeric films directly on rubbing surfaces to reduce wear, "Wear", vol. 26, 1973, p. 369-392.
20. Mortimer T. P., Ludema K. C. Rubber friction in aqueous solutions. "Wear", vol. 28, No. 2, 1974, p. 197-206.

Chapter 18

THEORY OF ELASTOHYDRODYNAMIC LUBRICATION

The elastohydrodynamic lubrication theory gives an explanation of the phenomena that occur in the contact area of two elastic solids separated by a liquid film. Formulas relating to this theory make it possible to determine the thickness of the lubricating film, frictional stresses, and temperature for heavily loaded contacts at pressures $\geqslant 3 \times 10^3$ kgf/cm^2. The film thickness has effect on the performance of tribological components in the elastohydrodynamic operating conditions, that is at $h \geqslant Ra$. The frictional stress τ determines the energy losses in a contact, and the performance of the lubricant depends essentially on its temperature ϑ. The main elastohydrodynamic parameters are necessary for the calculation of dynamics, stiffness, temperature fields, and stress conditions in complex elastohydrodynamic systems, such as, for instance, rolling bearings.

The theory of elastohydrodynamic lubrication is applicable to rolling and sliding bearings, mechanical transmissions, metalforming lubrication, and biomechanics. It offers methods for calculation of parameters for parts in lubricated contact and recommendations on the choice of their geometry, materials, and operating conditions.

18.1. PHYSICAL PHENOMENA IN ELASTOHYDRODYNAMIC CONTACT

The coordinate system is referred to the point or line of contact. The axes x and y lie in a plane tangent to the bodies in contact, and the axis z is directed normally to them. The lubricant adheres to the rubbing surfaces and is drawn into the clearance between the bodies because of their rolling and (or) sliding motion. A high contact pressure deforms the bodies, enlarges the area of the small clearance, and makes it almost planoparallel; the viscosity of the lubricant grows by several orders of magnitude. The clearance becomes smaller near the boundary of the elastohydrodynamic contact, and the highly viscous lubricant escapes with great difficulty out of the nar-

row clearance, which is nearly closed on all sides except that from which the lubricant is supplied. An elastohydrodynamic lubricant film of about 0.1 to 10 μm is formed. Fig. 18.1 depicts clearance level lines *1* in a typical contact. The arrows *2* indicate the lubricant flow. The shape of the clearance, the distribution of pressure and the thickness of the film can be determined experimentally [10] by numerically solving the appropriate equations of elastohydrodynamics [2, 8, 11], or by using approximate semi-asymptotic methods

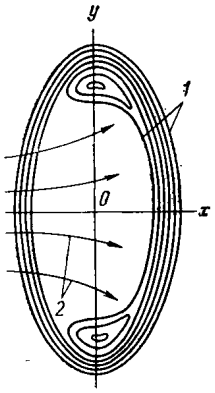

Fig. 18.1. Elastohydrodynamic contact

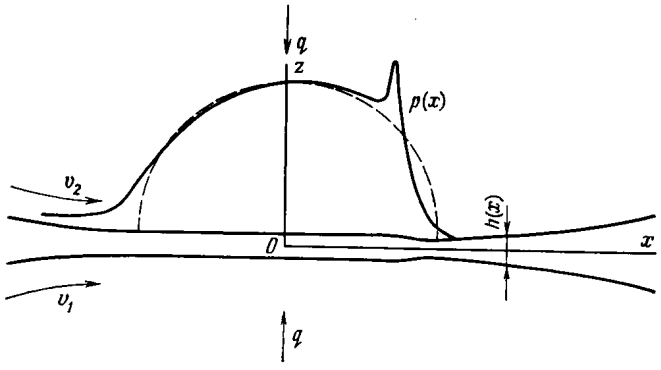

Fig. 18.2. Distribution of pressure in contact of two cylinders

[4]. Fig. 18.2 shows a typical distribution of pressure p (x) in a contact of two cylinders [2, 8, 11]. Here h (x) is the film thickness, v_1 and v_2 are the velocities of the surfaces, q is the load per cylinder unit length: the dash line designates the Hertzian distribution of pressure.

Large pressure gradients and sliding in the contact cause the lubricant to work at high speeds of displacement. The heat generation due to displacement raises the temperature of lubricant by tens and even hundreds of degrees and increases the temperature of the bodies near the contact area. The temperature field in this area, which is variable both through the depth and across the plane of the film, can be determined by solving the system of two equations: one for the motion and energy of the lubricant, and the other for the thermal conductivity of the bodies. Fast motion of the lubricant (about 10^{-5} s) is similar to explosion phenomena.

High pressures and displacement speeds (about 10^7 1/s) result in a very complex behaviour of lubricant: they cause, in particular, non-linear viscous properties and relaxation effects to show up. With an increased loading and temperature or lower rolling velocities, the surface roughness becomes a factor that markedly affects the frictional and thermal conditions in the contact area. In the region of the contacting surface asperities, the film thickness becomes

Table 18.1

Variation of viscosity and piezo-coefficient of different oils with temperature

Type of oil	Viscosity $\eta \cdot 10^3$ kgf s/m² (upper line) and piezo-coefficient α 10^8 m²/kgf (lower line) at temperature °C						
	50	60	80	100	120	140	150
МС-20	11.4 22.3	7.60 20.7	3.40 17.6	1.84 14.5	1.05 11.3	0.70 8.3	0.57 6.8
75% МС-20+25% transformer oil	5.84 20.6	4.00 19.2	1.91 16.5	1.08 13.7	0.67 10.9	0.47 8.2	0.39 6.8
50% МС-20+25% transformer oil	2.85 19.2	2.06 18.0	1.05 15.4	0.64 13.0	0.41 10.5	0.30 8.1	0.26 6.8
25% МС-20+75% transformer oil	1.46 17.6	1.08 16.5	0.60 14.4	0.39 12.3	0.27 10.2	0.21 8.0	0.19 6.9
Spindle oil 2	1.16 12.8	0.86 12.3	0.47 11.4	0.31 10.5	0.22 9.5	0.17 8.7	0.16 8.2
МК-8	0.74 15.9	0.55 15.0	0.30 13.2	0.20 11.4	0.16 9.6	0.13 7.8	0.12 6.9
Transformer oil	0.74 15.9	0.55 15.0	0.32 13.2	0.22 11.4	0.16 9.6	0.14 7.8	0.13 6.9
МН 7.5	0.310 12.8	0.214 12.3	1.14 11.1	0.70 10.1	0.49 9.0	0.36 7.9	0.32 7.4
ВНИИ НП-7	2.24 12.3	1.69 12.0	1.01 11.2	0.64 10.5	0.46 9.9	0.34 9.2	0.31 8.8
Б-38	2.32 8.4	1.63 8.3	0.83 8.3	0.52 8.2	0.35 8.1	0.26 8.1	0.22 8.1
ЛНМЗ-36/1-К	1.01 9.4	0.74 9.1	0.43 8.4	0.29 7.7	0.22 7.1	0.17 6.4	0.15 6.1
50-1-4Ф	0.68 0.92	0.55 9.1	0.38 8.4	0.28 7.8	0.21 7.3	0.16 6.8	0.15 6.5

very small and variable. With local film thicknesses of the order of 10^{-8} m [7], transition to boundary friction is possible. As a rule, the elastohydrodynamic frictional conditions are effective at $h \approx Ra$.

18.2. LUBRICANT FILM THICKNESS

The average thickness h of the lubricant film occurring in a contact of two cylinders is given by the formula [8, 4]

$$\frac{h}{R} = 1.65 \left(\frac{\eta\alpha v}{R}\right)^{0.73} \left(\frac{p_0}{E'}\right)^{-0.18} \qquad (18.1)$$

where $R = R_1R_2/(R_1 \pm R_2)$ = effective radius; R_1 and R_2 = radii of the cylinders, $R_1 > R_2$; the sign "plus" is taken for external, and the sign "minus" for internal contact; η and α = dynamic viscosity and piezo-coefficient of the base oil contained in the lubricant, respectively, at the inlet temperature (Table 18.1); p_0 = maximum contact pressure according to Hertz: $E' = E/(1 - \mu^2)$; $v = (v_1 + v_2)/2$, where v_1 and v_2 = cylinder-surface velocities in the coordinate system referred to the cylinder axes (see Fig. 18.2).

The film thickness in an elliptical contact is found by the formula

$$\frac{h}{R_x} = (1.82 - 0.68\chi) \left(\frac{\eta\alpha v}{R_x}\right)^{0.75} \left(\frac{p_0}{E'}\right)^{-0.25} \qquad (18.2)$$

where $R_x = R_{1x}R_{2x}/(R_{1x} \pm R_{2x})$; R_{1x} and R_{2x} = curvature radii of the surfaces in the plane passing through the direction of rolling or sliding motion (axis x) and a normal common to both surfaces (axis z); $R_{1x} > R_{2x}$; $\chi = R_x/R_y$; $R_y = R_{1y}R_{2y}/(R_{1y} \pm R_{2y})$; R_{1y} and R_{2y} = curvature radii of the surfaces in the section yz (see Fig. 18.1); $R_{1y} > R_{2y}$; $0 \leqslant \chi \leqslant 1$; $v = (v_1 + v_2)/2$; v_1 and v_2 = surface velocities in the direction x. The results of the calculation by formula (18.2) are in good agreement with numerical solution of the elastohydrodynamic equations obtained so far only for one set of parameters. Comparison between the results obtained by the calculation with formula (18.2) and those obtained experimentally [1] is given in Table 18.2. In [1], $E = 9.8 \times 10^9$ kgf/m^2; the comparison is made for $v = 0.5$ m/s. Subcripts 0, 1, and 2 refer to the experiment, formula (18.2), and the Archard formula, respectively.

In the design calculation of lubricated tribological units, the film thickness can in some cases be used as an approximate criterion of performance. The larger the thickness h, the higher the contact fatigue life and lower the wear, lubricant temperature, and energy losses. Larger values of h can be achieved by increasing η and α through the choice of an appropriate lubricant or improvement in cooling conditions, by increasing the rolling speed, dimensions and rigidity of the mating parts, and by reducing the contact pressure.

At high rolling velocities v, the values derived from the formulas (18.1) and (18.2) should be multiplied by the coefficient $\varphi =$

Table 18.2

Comparison of calculated results with experimental data

$R_{2x}=R_{2y}$, mm	R_{1y}, mm	P, kgf	η kgf s/m²	$\left(\frac{h}{R_x}\right)_0 10^4$	$\left(\frac{h}{R_x}\right)_1 10^4$	$\left(\frac{h}{R_x}\right)_2 10^4$
2.6	∞			3.08	2.75	2.58
3.2	∞	0.49	0.056	2.60	2.43	2.26
2.6	∞	0.98	0.057	2.96	2.62	2.58
3.2	∞		0.056	2.50	2.28	2.16
2.6	∞	2.94		2.65	2.40	2.32
3.2	∞		0.057	2.34	2.13	2.02
2.6	∞			2.50	2.30	2.23
3.2	∞			2.19	2.04	1.96
2.6	4.37	4.9	0.053	3.27	3.02	2.56
3.2	4.37		0.057	2.81	3.14	2.54

Note. Coefficient $\alpha = 2.58\times10^{-7}$ m²/kgf

$= 3.94/(3.94 + \psi^{0.62})$, where $\psi = \eta\delta v^2/k$ (k = lubricant's thermal conductivity; δ = temperature coefficient of viscosity [3]). With insufficient lubrication, the film thickness in a contact of two cylinders can be estimated by the formula

$$\frac{h}{R} = 6.6\varepsilon^{5/6}\left(\frac{\eta\alpha v}{R}\right)^{1/3}\frac{p_0}{E'} \qquad (18.3)$$

which holds true if $\varepsilon \ll (\eta\alpha v/R)^{1/2}\,(p_0/E')^{-3/2}$, where ε = distance from the meniscus boundary to the Hertzian region.

18.3. FRICTIONAL STRESSES, HEAT FLOW, AND TEMPERATURE

Let the viscosity of oil, η, depend on pressure p and temperature ϑ in accordance with the formula

$$\eta = \eta_0 \exp\left[\alpha p/(1 + \beta p) - \delta^* (\vartheta - \vartheta_0)\right]$$

where

$$\delta^* = \delta + \gamma p/(1 + \beta p) \text{ or } \eta = \eta_0 \exp\left[\alpha p/(1 + \beta p)\right] \times \left[1 + \delta (\vartheta - \vartheta_0)\right]^{-1}$$

Then, regarding the lubricant as a non-linear Maxwellian fluid with a high-frequency shear modulus G, we can obtain equations for

frictional stress

$$\frac{\tau}{1-(\tau/G)^2} = \eta \frac{v_2 - v_1}{h} \frac{\operatorname{arsinh} \Lambda}{\Lambda \sqrt{1+\Lambda^2}} \tag{18.4}$$

where

$$\Lambda = \left\{ \Lambda_0^2 [1 - (\tau/G)^2] + \sinh^2 \left[\frac{\delta^* (\vartheta_2 - \vartheta_1)}{4} \right] \right\}^{1/2}$$

here $\Lambda_0 = (\eta\delta^*/8k)^{1/2} \mid v_2 - v_1 \mid$; ϑ_1 and ϑ_2 = surface temperatures: $\vartheta = (\vartheta_1 + \vartheta_2)/2$; $G = 10^6$ to 10^7 kgf/m^2, and

$$\frac{\tau}{1-(\tau/G)^2} = \eta \frac{v_2 - v_1}{h} \frac{\arctan \Lambda^0}{\Lambda^0} \tag{18.5}$$

where

$$\Lambda^0 = \Lambda^* [1 - (\tau/G)^2]^{1/2}$$

$$\Lambda^* = \frac{\mid v_2 - v_1 \mid}{2[1 + \delta(\vartheta - \vartheta_0)]} \left\{ \frac{\eta_0 \delta \exp [\alpha p/(1+\beta p)]}{k} \right\}^{1/2}$$

Example 1. Calculate τ with the equation (18.4) for a sphere with a radius of 15.9 mm in contact with a plane. Assume $p_0 = 10^8$ kgf/m^2; $v_1 = 1.4$ m/s; $v_2 = 0$; $\vartheta_0 = 50$°C; $\vartheta_1 = 75$°C; $\vartheta_2 = 115$°C; $E_1 = 2 \times 10^{10}$ kgf/m^2; $E_2 = \infty$; $\mu = 0.3$; the lubricant consists of 50 percent MC-20 and 50 percent transformer oil; inlet temperature $\vartheta = 30$°C; $G = 4 \times 10^6$ kgf/m^2; $k = 0.013$ kgf/(s °C). From Table 18.1 $\eta_0 = 2.85 \times 10^{-3}$ kgf s/m^2; $\delta = 3 \times 10^{-2}$ 1/°C; $\beta = 0$; $\alpha = 1.92 \times 10^{-7}$ m^2/kgf; $\gamma = 1.24 \times 10^{-9}$ m^2/(kgf °C). From the formula (2) $h \approx 2.8 \times 10^{-7}$ m. The equation (4) is solved by the trial method, rendering $\tau \approx 3.9 \times 10^6$ kgf/m^2. The coefficient of friction at the centre of the contact area $f \approx 0.04$.

Semi-empirical formulas for the mean coefficient of friction are obtained in [5]. In operation at high rolling speeds, the effect of tangential stresses on the kinematics of the contact needs to be considered [13]. If slipping occurs over the whole contact area, the local sliding is determined by the formula

$$s = s_0 (1 + \varkappa\xi) \tag{18.6}$$

where s_0 = sliding without regard to tangential deformations; $\xi = x/a$ (a = half-axis of the contact ellipse); $\varkappa = 2fp_0 [B - \mu (D - C)]/s_0 G_0$; G_0 = shearing modulus for the material of the rubbing components; $B = D - e^2C$; $2D = K + e^2C$; $E = (2 - e^2) D - e^2C$; K and E = elliptic integrals of the first and the second kind; e = eccentricity of ellipse. For cylinders $\varkappa = 4fp_0/s_0E' \leqslant 1$.

Local heat flows are determined by the expressions

$$q_{1,2} = \frac{\tau (v_2 - v_1)}{2} \left[1 \pm \frac{1}{2\Lambda_0'^2} \sinh \frac{\delta^* (\vartheta_2 - \vartheta_1)}{2} \right] \tag{18.7}$$

where

$$\Lambda_0' = \Lambda_0 [1 - (\tau/G)^2]^{1/2}$$

For maximum temperature in the lubricant film, the following approximate formula is valid

$$\vartheta_{max} = \frac{\vartheta_1 + \vartheta_2}{2} + \frac{1}{\delta^*} \ln \left[\cosh \frac{\delta^* (\vartheta_2 - \vartheta_1)}{2} + \Lambda_0'^2 + \frac{1}{4\Lambda_0'^2} \sinh^2 \frac{\delta^* (\vartheta_2 - \vartheta_1)}{2} \right] \tag{18.8}$$

18.4. SERVICE LIFE OF ROLLER BEARINGS

The ratio of the lubricant film thickness to the mean surface roughness, called parameter λ, can serve as a criterion for the assessment of service life of high-speed roller bearings [9]. With $\lambda > 1$, the actual bearing life normally exceeds the rated life [12] because a comparatively thick film reduces tangential stresses in the contact. The parameter $\lambda = h/\sqrt{R^2a_1 + R^2a_2}$; here h is computed by formulas (18.1) and (18.2).

The parameter λ for the most heavily loaded roller in a cylindrical roller bearing should be found by the formula

$$\lambda = \frac{11.3s}{1+s} \frac{d_1}{\sqrt{R^2a_1 + R^2a_2}} \frac{[\eta_0 \alpha n (1+2s)]^{0.73}}{p_0^{0.18} s^{0.73}} \qquad (18.9)$$

where $s = d_r/d_1$, d_r = roller diameter, m; d_1 = raceway diameter for the inner ring, m; η_0 = lubricant viscosity at the inlet temperature, kgf s/m^2; n = rotational frequency of the inner ring, 1/s; $p_0 = 5.67 \times 10^4 [F_r (1 + s)/lZd_1 s]^{1/2}$ kgf/m^2; here F_r = radial load

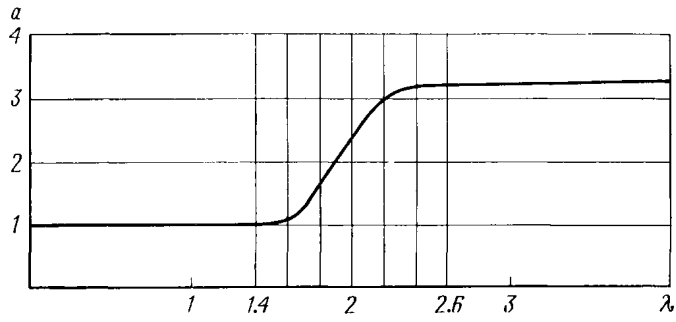

Fig. 18.3. Effect of parameter λ on service life of rolling bearings

on the bearing; l = effective length of the roller (the length of its line of contact with the raceway); Z = number of rollers. After finding λ by the formula (9), the graph in Fig. 18.3 should be used, where a is the ratio of the bearing life L' that takes into account the effect of lubricant on the bearing life L. The graph is obtained from the results of the work [9] and experiments conducted at the Bearing Research Institute.

Example 2. Estimate the service life of a 6-32208 ДТ$_2$ bearing with $d_r = 10^{-2}$ m; $d_1 = 5 \times 10^{-2}$ m; $l = 7.8 \times 10^{-3}$ m; $Z = 14$; $Ra_1 = Ra_2 = 1.6 \times 10^{-7}$ m, running at $n = 83.3$ 1/s; $F_r = 1070$ kgf; $\vartheta = 65.5$°C; the lubricant composition is 50 percent MC-20 and 50 percent transformer oil; the inner race is rotated.

From Table 18.1 we find η_0 and α by interpolation: $\eta = 1.78 \times 10^{-3}$ kgf s/m^2; $\alpha = 1.59 \times 10^{-7}$ m^2/kgf. Now, we determine s; compute p_0, $\sqrt{Ra_1^2 + Ra_2^2}$, and

λ. The values found will be: $s = 0.2$; $p_0 = 1.96 \times 10^8$ kgf/m^2; $\sqrt{Ra_1^2 + Ra_2^2} = 2.6 \times 10^{-7}$ m; $\lambda = 1.92$.

By the graph in Fig. 18.3 we determine a, it will be 2.2. The bearing life $L = 4.26 \times 10^7$ revolutions, and $L' = 9.4 \times 10^7$ revolutions.

18.5. DESIGN CALCULATION OF BALL BEARINGS

The thickness of oil film for a ball in contact with the raceways can be estimated by using formula (18.2) and the values of R_x, v, and p_0 appropriate for the given type of bearing. With precision bearings, however, reliable values of h and, in addition, the kinematic

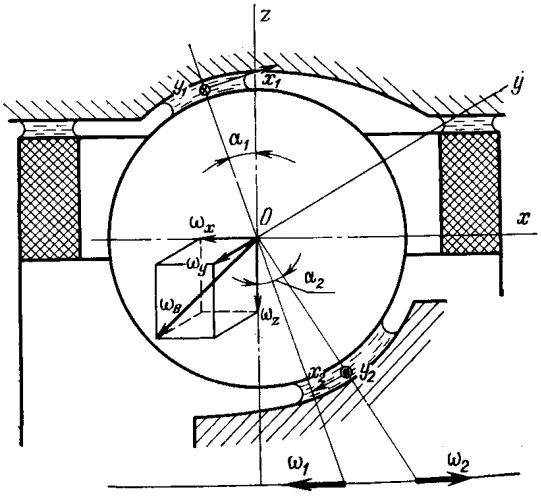

Fig. 18.4. Design diagram for ball bearing

and load characteristics of the bearing need to be obtained. A considerable axial preload is typical of high-precision bearings. In this case (Fig. 18.4), the equations have the form [3]

$$
\left.\begin{aligned}
&Q_1\cos\alpha_1 - F_{x1}\sin\alpha_1 - Q_2\cos\alpha_2 + F_{x2}\sin\alpha_2 - F_c = 0\\
&Q_1\sin\alpha_1 + F_{x2}\cos\alpha_1 - Q_2\sin\alpha_2 - F_{x2}\cos\alpha_2 = 0\\
&F_{y1} - F_{y2} = F_c'\\
&M_{y1} + M_{y2} - M_{gy} = 0\\
&M_{x1} + M_{x2} + M_{1k}\cos\alpha_1 + M_{2k}\cos\alpha_2 = 0\\
&M_{z1} + M_{z2} - M_{gz} + M_{1k}\sin\alpha_1 + M_{2k}\sin\alpha_2 = 0\\
&Q_2\sin\alpha_2 + F_{x2}\cos\alpha_2 - F_a/Z = 0\\
&(R_1 - 0.5D + \delta_1 - h_1)\cos\alpha_1 + (R_2 - 0.5D + \delta_2\\
&- h_2)\cos\alpha_2 = (R_1 + R_2 - D)\cos\alpha_{0]}^{e}\\
&(R_1 - 0.5D + \delta_1 - h_1)\sin\alpha_1 + (R_2 - 0.5D + \delta_2\\
&- h_2)\sin\alpha_2 = \delta_x + (R_1 + R_2 - D)\sin\alpha_0
\end{aligned}\right\} \quad (18.10)
$$

$m = 1, 2$; subscript 1 relates to the outer race, and subscript 2 to the inner race; α_m = contact angles; F_a = axial load; Z = number of balls; R_m = raceway radius; D = ball diameter; δ_m = elastic approach between ball and raceway; α_0 = initial angle of contact; δ_x = axial displacement of the inner race.

All the quantities in the equations (18.10) are functions of unknown variables α_m, δ_m, δ_x, ω_x, ω_y, ω_z and ω_c, where ω_x, ω_y and ω_z = components of the ball's angular velocity in a coordinate system rotating together with the ball centre; ω_c = angular velocity of the cage.

$$Q_m = K_m \delta_m^{3/2}; \quad K_m = (E'/3\varkappa_m^{1/2})\,(2/n_{\delta m})^{3/2};$$

$$\varkappa_m = R_{xm}^{-1} + R_{ym}^{-1}; \; R_{xm}^{-1} = 2D^{-1} - R_m^{-1};$$

$$R_{ym}^{-1} = 2[D\,(1 + c_m\gamma \cos\alpha_m)]^{-1}; \quad \gamma = D/d;$$

$$d = d_0 - 2\,(R_1 - 0.5D)\cos\alpha_0 + 2X_2;$$

$$\cos\alpha_1 = X_2\,(X_1^2 - X_2^2)^{-1/2};$$

$$\cos\alpha_2 = [(R_1 + R_2 - D)\cos\alpha_0 - X_2]/(R_2 - 0.5D + \delta_2 - h_2);$$

$c_1 = 1$; $c_2 = -1$; R_{xm} and R_{ym} are substituted into formula (18.2) for R_x and R_y; $0.5d_0 = 0.5D_2 + R_2 - (R_2 - 0.5D)\cos\alpha_0$, where D_2 = inner raceway diameter; $n_{\delta m} = \bar{K}\,(e_m)\,\{(4/\pi^2)\,[1 + (R_{xm}/R_{ym})]^{-1}\bar{D}^{-1}\,(e_m)\}^{1/3}$; $R_{ym}/R_{xm} = (1 - e_m^2)\,\bar{D}\,(e_m)/[\bar{K}(e_m) - \bar{D}\,(e_m)]$; $\bar{K}\,(e_m)$ and $D\,(e_m)$ = elliptical integrals of the first and the second type; $p_{0m} = 3Q_m/2\pi a_m b_m$; $a_m = \eta_m\,(3Q_m/E'\varkappa_m)^{1/3}$; $b_m = \mu_m\,(3Q_m/E'\varkappa_m)^{1/3}$; $\eta_m = \{(2/\pi)[1 + (R_{xm}/R_{ym})]\,\bar{D}(e_m)\}^{1/3}$; $\mu_m = \{(2/\pi)\,[1 + (R_{ym}/R_{xm})]\;[\bar{K}\,(e_m) - \bar{D}\,(e_m)]\;(1 - e_m^2)^{1/2}\}^{1/3}$; $u_m = (D/4)\,\{\omega_m\;[(1/\gamma) + c_m\cos\alpha_m] + \omega_x\cos\alpha_m + \omega_z\sin\alpha_m$ with the rotating inner race $\omega_1 = -\omega_c$; $\omega_2 = \Omega - \omega_c$; Ω = angular velocity of the inner race; $(v_{xm}^2 + v_{ym}^2)^{1/2}$ should be inserted into formula (18.4) in place of $v_2 - v_1$; $v_{xm} = \omega_{sm}y_m + \omega_y r_m$; $v_{ym} = -\omega_{sm}x_m + \omega_m\,(d/2 + c_m r_m\cos\alpha_m) - (\omega_x\cos\alpha_m + \omega_z\sin\alpha_m)r_m$; $\omega_{sm} = \omega_x\sin\alpha_m - \omega_z\cos\alpha_m - c_m\omega_m\sin\alpha_m$; $r_m = D/2 - \delta_m/2 - x_m^2/2R_{xm}^* - y_m^2/2R_{ym}^*$; R_{xm}^* and R_{ym}^* = curvature radii for the surfaces in contact [12]; local pressure $p_m = p_{0m}\,[1 - (x_m/a_m)^2 - (y_m/b_m)^2]^{1/2}$; $F_{xm} = \int\limits_{\Omega_m}\int \tau_{xm}d\Omega_m$; $F_{ym} = \int\limits_{\Omega_m}\int \tau_{ym}d\Omega_m$; τ_{xm}, τ_{ym} = components of vector τ; $M_{ym} = \int\limits_{\Omega_m}\int \tau_{xm}r_m d\Omega_m$; $M_{xm} = \int\limits_{\Omega_m}\int [\tau_{ym}\,(r_m\cos\alpha_m + x_m\sin\alpha_m) - \tau_{xm}y_m\sin\alpha_m]d\Omega_m$; $M_{zm} = \int\limits_{\Omega_m}\int [\tau_{ym}\,(r_m\sin\alpha_m - x_m\cos\alpha_m) + \tau_{xm}y_m\cos\alpha_m]d\Omega_m$; $F\,(c) = M\,(d/2)\omega_c^2$; $M_{gy} = I\omega_c\omega_z$; $M_{gz} = I\omega_c\omega_y$; $I = MD^2/10$; M = ball mass; $F_c =$

$= \pi l_c (\eta_0 \omega_c d_{c1}^3)/(2h_c Z d)$; l_c = width of the region of contact between the cage and the race shoulder; d_{c1} = outer diameter of the cage; h_c = locating clearance; $M_{mk} = tu_m Q_m$, t = retardation time for steel.

The system of equations (18.10) is solved by the Newton method, and appropriate programmes can be used for the purpose. The input data are: the geometry of the bearing, the operating conditions and the characteristics of the lubricant.

Example 3. A rotor runs in type 1076097 bearings; $\Omega = 3142$ 1/s; $D = 2.381$ mm; $\alpha_0 = 12°$; the raceway temperature in the outer and the inner ring is 100°C and 120°C, respectively; $t = 5 \times 10^{-8}$ s; the base oil is MC-14, and its parameters at $\vartheta_0 = 100$°C are: $\eta_0 = 4 \times 10^{-3}$ kgf s/m²; $\alpha = 10^{-7}$ m²/kgf; $\beta = 3.3 \times 10^{-9}$ m²/kgf; $\delta = 5.8 \times 10^{-2}$ °C; $k = 2.5 \times 10^{-2}$ kgf/(s °C) and $G = 8 \times 10^5$ kgf/m². Some calculation results are given in Table 18.3.

Table 18.3

Results of calculation for three magnitudes of preload [3]

F_a, kgf	α_1	α_2	$p_{01} \times 10^{-8}$	$p_{02} \times 10^{-8}$	h_1	h_2	$\frac{\omega_c}{\Omega}$
	radians		kgf/m²		μm		
0.342	0.211	0.235	1.18	1.16	0.4	0.18	0.4025
1.52	0.230	0.240	1.56	1.56	0.37	0.17	0.4034
2.4	0.238	0.246	1.72	1.73	0.36	0.16	0.4037

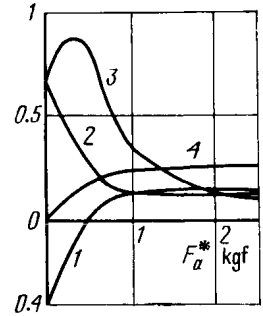

Fig. 18.5. Results of kinematic calculation
1—ω_{s1}/Ω; 2—ω_{s2}/Ω; 3—$\omega_y \times 10^2/\Omega$; 4—$\omega_z/\omega_x$

The results of calculation of the kinematics are presented in Fig. 18.5.

18.6. CALCULATION OF GEAR TRANSMISSIONS

Gear transmissions are calculated according to USSR Standard 21354-75. For the calculation of the lubricant film thickness use may be made of formulas (18.1) and (18.2) or formulas given in [6, 8]. Let us consider, by way of example, the calculation of a spur gear transmission.

Example 4. The pitch circle radii $R_1 = 85$ mm; $R_2 = 385$ mm; the pressure angle $\alpha = 20°$; angular velocity $\omega_1 = 125.6$ 1/s; the load per tooth unit length $q = 2 \times 10^5$ kgf/m; the oil used is MC-20, and the input contact temperature is 50°C. Compute the film thickness for the contact at the pitch point.

The effective radius of curvature $R = 23.8$ mm; $\eta = 10^{-2}$ kgf m/s^2; $\alpha = 2.3 \times 10^{-7}$ m^2/kgf; the rolling speed $v = 3.6$ m/s; $p_0 = 1.75 \times 10^8$ kgf/m^2; and $h = 1.8 \times 10^{-6}$ m.

Using the formulas (18.4) and (18.5), it is also possible to calculate the coefficient of friction and the maximum film temperature.

REFERENCES

1. Бакашвили Д. Л. Исследование качения шарика в шарикоподшипнике. Труды 1-й Всероссийской конференции «Контактно-гидродинамическая теория смазки и ее практическое применение в технике». Куйбышев, КуАИ им. С. П. Королева, 1973, с. 75-84.

2. Галахов М. А., Заппаров К. И. Распределение давления в упругогидродинамическом контакте цилиндров.— ДАН СССР, 1977, т. 232, № 1, с. 54-57.

3. Галахов М. А., Заппаров К. И., Яковлев Н. И. Кинематика и динамика радиально-упорного шарикоподшипника при осевой нагрузке — «Изв. АН СССР. Механика твердого тела», 1977, № 3, с. 53-57.

4. Грубин А. Н. Основы гидродинамической теории смазки тяжело нагруженных цилиндрических поверхностей.— «Труды ЦНИИТМАШ», кн. 30, 1949, с. 126-184.

5. Дроздов Ю. Н., Рещиков В. Ф. О коэффициенте трения и толщине масляной пленки в тяжело нагруженном контакте — «Вестник машиностроения», 1968, № 12, с. 9-12.

6. Коднир Д. С. Контактная гидродинамика смазки деталей машин. М., «Машиностроение», 1976, 303 с.

7. Коровчинский М. В. О некоторых вопросах эластореологии, имеющих приложение в теории трения.— В сб.: Трение и износ в машинах. М., Изд-во АН СССР, 1962, № 17, с. 68-165.

8. Петрусевич А. И. Основные выводы из контактно-гидродинамической теории смазки. М., Изд-во АН СССР, ОТН, 1951, № 2, с. 209-223.

9. Скурка И. С. Упругогидродинамическая смазка роликовых подшипников.— «Проблемы трения и смазки», 1970, № 2, с. 110-122.

10. Cameron A., Gohac R. Theoretical and Experimental Studies of the Oil Film in Lubricated Point Contact. Proc. Roy. Soc. Ser. A. N 1427, vol. 291, 1966, p. 1021-1034.

11. Dowson D., Higginson G. R. Elastohydrodynamic Lubrication. New York, 1966. 235 p.

12. Harris T. A. Rolling Bearing Analysis. New York, 1966, 481 p.

13. Kalker I. I. On the Rolling Contact of Two Elastic Bodies in the Presence of Dry Friction, Thesis, Delft, 1973, 283 p.

Chapter 19

ROLLING BEARINGS

19.1. GENERAL DATA ON ROLLING BEARINGS

19.1.1. Classification

By the direction of the load sustained, rolling bearings are classified as radial, angular-contact, thrust, and angular-contact thrust bearings, and by the shape of rolling elements, as ball and roller bearings (Table 19.1).

By the width-to-diameter ratio, rolling bearings come in the extra-light, very light, light, light broad, medium broad, and heavy series. Light and medium-series bearings are applied most commonly. Along with standard types, custom-designed bearings are manufactured.

19.1.2. Accuracy Classes

USSR St. Std. GOST 520-71 establishes five classes of accuracy for bearings: 0, 6, 5, 4, and 2. The accuracy classification according to former GOST 520-55 was different (see Table 19.2).

The 2nd class bearings are designed for use in ultraprecision machine tools and measuring instruments.

19.1.3. Designation

The main bearing designations are stipulated by GOST 3189-75 (Table 19.3).

Along with the main numerical character in the designation of a bearing, there may also be additional signs that characterize alternative grades of material in the component parts, special design, or specific requirements (Table 19.4).

The accuracy class according to GOST 520-71 is indicated on the left of the main numerical code. Just before the accuracy class, an appropriate figure may be placed to denote the range of radial clearance in accordance with current standards.

Table 19.1

Classification of rolling bearings according to USSR St. Std. GOST 3395-75

Radial bearings		Angular-contact bearings		Thrust and angular-contact thrust bearings	
Ball type	Roller type	Ball type	Roller type	Ball type	Roller type
Single-row	Single-row, with short cylindrical rollers	Single-row	Single-row, with tapered rollers	Thrust single-row	Thrust, cylindrical rollers
Same, with snap-ring groove	Same, double-row	Single-row, with separable rings, three- or four-point contact	Same, with flanged outer ring	Thrust double-row	Thrust, tapered rollers
	Single-row, spherical rollers			Angular-contact, with 60° contact angle	
Same, with shouldered outer ring	Double-row, spherical	Single-row, two-piece rings	Double-row tapered rollers	—	Thrust, spherical rollers
Same, with flange-mounted outer ring	Same, shielded	Double-row	Four-row, tapered rollers		
Same, shielded	Single-row, needle rollers				
Same, sealed	Needle rollers, composite roller-guiding raceway				
Same, self-aligning					
Double-row, self-aligning					

Table 19.2

Bearing grades of accuracy

GOST 520-55 and TU 5434-ST	GOST 520-71	Accuracy characteristic	GOST 520-55 and TU 5434-ST	GOST 520-71	Accuracy characteristic
H and П	0	Normal	C	4	Precise
ВП, B and AB	6	Improved	T and CT	2	Ultra-precise
A and CA	5	High			

Table 19.3

Bearing designation

Place of digits in designation (from right to left)	Signification of digits	Place of digits in designation (from right to left)	Signification of digits
First and second	Bore diameter	Fourth	Type
Third and seventh	Series	Fifth and sixth	Special design features

Table 19.4

Additional characters in bearing designation

No.	Design features	Additional characters	
		for basic make	for modification
1	Rings and rolling elements from stainless steel	Ю	Ю1, Ю2, etc.
2	Rings and rolling elements from heat-resistant steel	Р	Р1, Р2, etc.
3	Rings and rolling elements from carbonized steel	Х	Х1, Х2, etc.
	Heavy cage		
4	from bronze	Б	Б1, Б2, etc.
5	from brass	Л	Л1, Л2, etc.
6	from aluminium	Д	Д1, Д2, etc.
7	Textolite cage	Е	Е1, Е2, etc.
8	Heavy cage from graphitized steel	Г	Г1, Г2, etc.
9	Special heat-treating requirements	Т, Т1, Т2, Т3	—
10	Grade of lubricant put into shielded or sealed bearing	С1, С2, С3, С4, etc.	—
11	Noise requirements	Ш, Ш1, Ш2, Ш3, etc.	—

Note: The characters according to Nos. 1-8 are indicated in bearing drawings, and those according to Nos. 9-11 are additional to the former and can be indicated in the specifications.

19.1.4. Materials for Components

Races and rolling elements of standard bearings are made from steels ШХ15, ШХ15СГ or ШХ20СГ, 18ХГТ, and 20Х2Н4А. Races and rolling elements for stainless bearings are made from chromium steels 11Х18М and 95Х18, and those for heat-resistant bearings, from tungsten-vanadium steel 8Х4В9Ф2 (ЭИ347Ш). The hardness of the components should range from 58 to 65 *HRC* depending on the grade of steel.

Stamped steel cages are produced from cold-rolled strip, thin-sheet carbon steel, and quality steel plate. Heavy cages are turned from brass, bronze alloys БрАЖМц 10-3-1.5 and БрАЖН 10-4-4, aluminium alloys Д1Т and АК-4, and tubular textolite.

19.2. CHOICE AND DESIGN OF ROLLING BEARINGS

19.2.1. General Suggestions on Choice of Bearings

A rolling bearing suitable for the specified operating conditions is chosen with regard to the following factors:
—the magnitude and direction of load which can be radial, axial, or a combination of both; momentary loading is also possible;
—the character of load application (continuous, variable, vibrational, or impact);
—the rotational frequency of one or both races;
—the required bearing life (that is, service life expressed in working hours or millions of revolutions);
—the operating environment (air, vacuum, water, aggressive liquid or gas), temperature, dust content, and so on.

Specific requirements to be placed on bearing units may include:
—self-alignment of the shaft or bearing housing to make up for their unavoidable misaligning in operation;
—shaft axial displacement capability in response to temperature variations;
—location of the bearing on a plain shaft by means of an adapter sleeve or the use of special accessories for easier assembly;
—specification of frictional moment for start-up or steady-state rotation;
—stiffness and true rotation.

When considering a bearing application, priority should be given to ball bearings which have lower energy losses compared with more labour-intensive and costly roller bearings. Wherever practicable, use must be made of the class 0 normal accuracy bearings; the higher-accuracy and precision bearings should be employed only where especially accurate rotation is needed.

Tentative choice of rolling bearing type and series

Load	Rotational frequency and speed parameter				
	Static load $n = 0$	Slow rotation $d_m n < 1 \times 10^5$	Medium-speed rotation $1 \cdot 10^5 < d_m n < 3 \cdot 10^5$	High rotational frequency $3 \times 10^5 < d_m n < 15 \times 10^5$	Extra-high rotational frequency $d_m n > 15 \times 10^5$
Purely radial	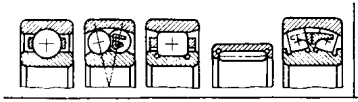		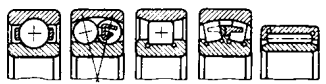	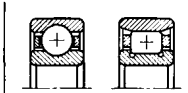	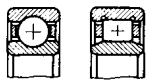
Combined: axial component is small	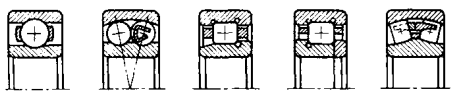			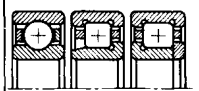	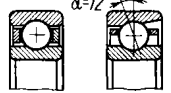
axial component is commensurl able with radia- one	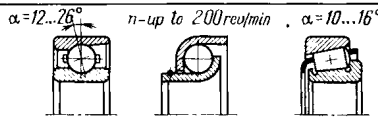			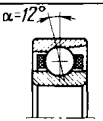	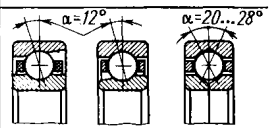
axial component is 2-5 times as large as radial	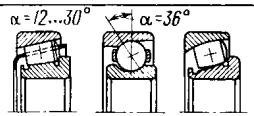	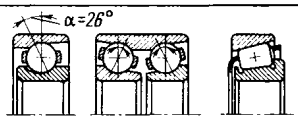		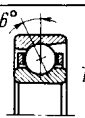	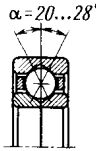
radial compo- nent is very small		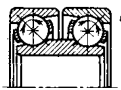			
Purely axial	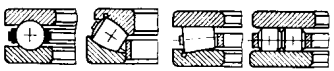	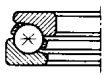		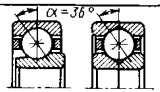	
Oscillatory radial (small-angle oscil- lation)	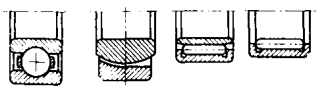		*Designations*: n = rotational frequency, rpm; d_m = mean bearing diameter	*Note*: Before determining the required dyna- mic load capacity and bearing type and size, choose the type most suitable to the specified operating conditions.	

The designer should not specify an excessively long bearing life as this tendency may lead to increased mass of the assembly; moreover, the heavier the bearing, the greater its energy losses and the more limited its maximum rotational frequency.

It is good practice to choose the required bearing in the following sequence:

(1) select the type of bearing tentatively on the basis of the operating conditions, design, and assembly of the bearing unit (use Table 19.5 and a catalogue of rolling bearings);

(2) detail the required type and size of bearing, using the procedure described below;

(3) specify the bearing's accuracy class.

In order to choose the type and size of bearing, the equivalent load needs to be calculated. The bearing life is determined by the contact fatique strength of its working surfaces. Bearing failures except those due to the contact fatigue do not commonly lend themselves to prediction.

With the design relationships given below, the necessary dynamic load capacity C is found, and by this parameter a particular type and size of bearing is selected from a standard rolling bearings catalogue.

Apart from the dynamic load capacity, the catalogue tables list the limiting number of revolutions for the bearings. The values given in the catalogue apply to the 0 class bearings with a stamped cage. For bearings with heavy cages, for precision bearings, and for bearings with forced lubrication and improved heat removal, tbe limiting number of revolutions can be significantly increased.

19.2.2. Equivalent Load

The equivalent load for radial- and angular-contact bearings is taken to mean a constant radial load that provides, when applied to a bearing with the rotating inner race, the same service life as the bearing will have in actual loading and running conditions. For these types of bearings, the equivalent load is determined by the formula

$$P = (XK_vF_r + YF_a)\, K_sK_f$$

where X = radial load factor (Tables 19.6-19.8); Y = axial load factor; F_a = axial load, kgf; K_v = rotational factor (for rotation of the inner race $K_v = 1$, and for rotation of the outer race $K_v = 1.2$); F_r = radial load, kgf; K_s = safety factor, and K_f = temperature factor (see Tables 19.10 and 19.11).

Small axial loads have no adverse effect on the life of radial ball bearings and angular-contact ball and roller bearings; in the latter type such loads are even advisable in order to hold the races against axial displacements and set up a preload necessary for the rigidity of the bearing unit.

In case $\frac{F_a}{K_v F_r} < e$ (here e is the axial loading parameter), the axial load acting on a single-row ball bearing or an angular-contact ball bearing need not be taken into account, that is, $X = 1$ and $Y = 0$.

The values of the parameter e at $\frac{F_a}{K_v F_r} > e$, and also the values of X and Y as a function of $\frac{F_a}{C_0}$ for ball bearings are given in Table 19.6.

Table 19.6

Values of parameters X, Y, and e for calculation of radial and angular-contact ball bearings

Contact angle, degrees	$i\frac{F_a}{C_0}$	Type of bearing						e
		single-row		double-row				
		$F_a/K_v F_r > e$		$F_a/K_v F_r \leq e$		$F_a/K_v F_r > e$		
		X	Y	X	Y	X	Y	
0	0.014	0.56	2.3	1	0	0.56	2.3	0.19
	0.028		1.99				1.99	0.22
	0.056		1.71				1.71	0.26
	0.084		1.55				1.55	0.28
	0.11		1.45				1.45	0.30
	0.17		1.31				1.31	0.34
	0.28		1.15				1.15	0.38
	0.42		1.04				1.04	0.42
	0.56		1.00				1.00	0.44
12	0.014	0.45	1.81	1	2.08	0.74	2.94	0.30
	0.029		1.62		1.84		2.63	0.34
	0.057		1.46		1.60		2.37	0.37
	0.086		1.34		1.52		2.18	0.41
	0.11		1.22		1.39		1.98	0.45
	0.17		1.13		1.30		1.84	0.48
	0.29		1.04		1.20		1.69	0.52
	0.43		1.01		1.16		1.64	0.54
	0.57		1.00		1.16		1.62	0.54
18-20	—	0.43	1.00	1	1.09	0.70	1.63	0.57
24-26	—	0.41	0.87		0.92	0.67	1.44	0.68
30	—	0.39	0.76		0.78	0.63	1.24	0.80
35-36	—	0.37	0.66		0.66	0.60	1.07	0.95
40	—	0.35	0.57		0.55	0.57	0.93	1.14
Self-aligning ball bearings		0.40	0.4 cot α	1	0.42 cot α	0.65	0.65 cot α	1.5 tan α

The values of X, Y, and e for tapered roller bearings and spherical barrel roller bearings are found by the relationship $\frac{F_a}{K_v F_r} \gtrless e$ from Table 19.7, depending on the contact angle α.

Table 19.7

Values of X, K_v, and e parameters for calculation of tapered and spherical roller bearings

Type of bearing	$\frac{F_a}{K_v F_r} \leqslant e$	$\frac{F_a}{K_v F_r} > e$	e
Single-row	$X = 1;\ Y = 0$	$X = 0.4;$ $Y = 0.4 \cot \alpha$	$1.5 \tan \alpha$
Double-row (symmetrically disposed rollers)	$X = 1;$ $Y = 0.45 \cot \alpha$	$X = 0.67;$ $Y = 0.67 \cot \alpha$	$1.5 \tan \alpha$

With single-row spherical roller bearings $\alpha = 0°$, and at $F_a = 0$ the value of X is equal to unity.

For double-row and single-row cylindrical short-roller bearings not capable of carrying axial loads, the equivalent load is determined by the formula

$$P = F_r K_\iota K_s K_t$$

Bearings with flanged rings or with end-face shield washers can take small, preferably intermittent, axial loads owing to sliding contact of rollers ends.

Table 19.8

Values of X, K_v, and e parameters for calculation of angular-contact thrust bearings

Type of bearing	Contact angle, degrees of arc	Type of bearing						e
		single-row		double-row				
		$F_a/F_r > e$		$F_a/F_r \leqslant e$		$F_a/F_r > e$		
		X	Y	X	Y	X	Y	
Angular-contact thrust ball bearing	45	0.66	1	1.18	0.59	0.66	1	1.25
	60	0.92	1	1.90	0.54	0.92	1	2.17
	75	1.66	1	3.89	0.52	1.66	1	4.67
Tapered roller and spherical roller thrust bearing	—	$\tan \alpha$	1	$1.5 \tan \alpha$	0.67	$\tan \alpha$	1	$1.5 \tan \alpha$

Note. At $\alpha = 90°$ (thrust bearing) $F_r = 0$; $X = 0$; $Y = 1$.

In contrast to all the other types of bearings, the equivalent load for thrust ball and roller bearings is axial rather than radial:

$$P_a = F_a K_s K_t$$

For angular-contact thrust bearings, the equivalent load is also axial: $P_a = (XF_r + YF_a) K_s K_t$. The values of X, Y, and e are given in Table 19.8. With large values of the parameter e, these bearings are advisable to use for supporting purely axial loads.

For magneto-type ball bearings with a separable outer ring, $e = 0.20$ at $\frac{F_a}{K_v F_r} > e$, $X = 0.5$, and $Y = 2.5$.

Two angular-contact thrust bearings put back-to-back or face-to-face are regarded as one double-row bearing. When such bearings are mounted in tandem, the values of X and Y are taken just as for single-row bearings, with the radial load divided between them. In double-row angular-contact ball bearings, the axial load is sustained by one of the rows, and at $\frac{F_a}{K_v F_r} > e$, the second row is practically relieved of load.

The axial components S of radial load are determined through the parameter e. For radial and angular-contact bearings $S = eF_r$, and for tapered roller bearings $S = 0.83eF_r$. The radial reaction of a bearing is regarded as applied to the shaft at the point of intersection of the normals, drawn through the centre of the contact area of each ball or roller, with the shaft axis; this point is situated at a distance a from the locating face of the bearing (Fig. 19.1). If load is supported by a single row of rolling elements, the value of a can be found approximately by formulas given in Table 19.9.

Table 19.9

Formulas for calculating the value of a

Type of bearing	Approximate formula
Single-row angular-contact ball bearing	$a = 0.5\left(B + \frac{d+D}{2}\tan\alpha\right)$
Double-row angular-contact ball bearing	$a = 0.5\left(\frac{3}{2}B + \frac{d+D}{2}\tan\alpha\right)$
Single-row tapered roller bearing	$a = \frac{T}{2} + \frac{(d+D)e}{6}$
Double-row tapered roller bearing	$a = \frac{3T}{4} + \frac{(d+D)e}{6}$

The diameters d and D, width B and overall width T for a given type and size of bearing are selected from tables of standard bearing ratings.

Table 19.10

Specifications of safety factor K_s depending on loading conditions

Character of loading	K_s	Type of machine or equipment
Steady, impactless	1.0	Low-power speed reducers and drive mechanisms; rollers in load conveyors; hand-operated cranes, hoists, winches, and pulley blocks; control drives.
Light impacts; momentary overloading up to 125% of rated load	1.0-1.2	Precision gear transmissions; metal-cutting machine tools (except shapers, slotters, and grinders); gyroscopes; lifting gear in cranes; power-operated tackles and winches; low- and medium-power electric motors; light fans and draught blowers.
Moderate impact loads; vibrations; momentary overloading up to 150% of rated load	1.3-1.5	Gear transmissions of 7th and 8th degrees of accuracy; speed reducers of all types; rolling-stock axle bearings; crab-traversing gear, slewing gear, and gib overhang adjusting mechanisms in cranes; spindles in grinding machines, and electric spindles.
The same loading conditions, but higher reliability requirements	1.5-1.8	Centrifuges and separators; axle-bearings and traction motors in electric locomotives; crab wheels and slewing-gear bearings in cranes and excavators; high-power electric machines; power-generation equipment; vehicle wheels.
Significant shocks and vibration; momentary overloading up to 200% of rated load	1.8-2.5	Gears of 9th degree of accuracy; crushers and pile drivers; crank mechanisms; rolls in rolling mills; high-power fans.
Heavy impact loads and momentary overloading up to 300% of rated load	2.5-3.0	Heavy forging machines; log frames; refrigerating equipment; roller conveyors in heavy-section rolling, blooming, and slabbing mills.

Table 19.11

Value of coefficient K_t

ϑ, °C	K_t	ϑ, °C	K_t	ϑ, °C	K_t
125	1.05	175	1.15	225	1.35
150	1.10	200	1.25	250	1.40

The safety factor K_s allows for the effect of external dynamics and other adverse conditions on the operation of the bearing. This factor ranges mostly from 1.0 to 1.5, and more seldom, from 2.0 to 3.0 (Table 19.10).

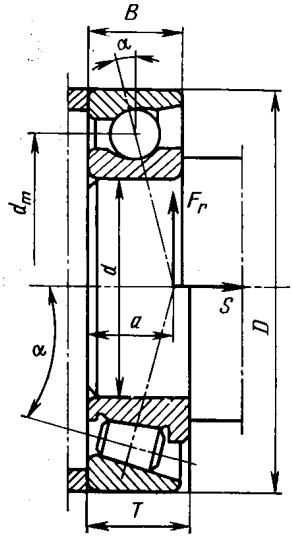

Fig. 19.1. Position of radial reaction on shaft supported by angular-contact bearing

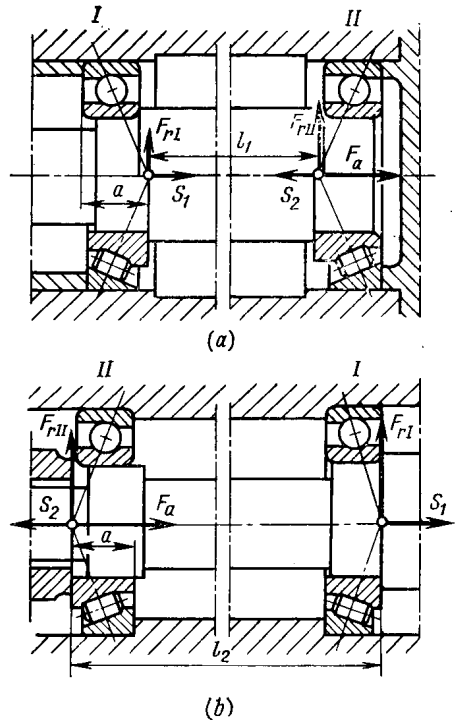

Fig. 19.2. Mounting of angular-contact bearings: with backs directed outwards (*a*) and inwards (*b*)

The temperature factor K_t is equal to 1.0 up to 100°C, and with further rise in temperature, it increases in accordance with the values listed in Table 19.11. At operating temperatures in excess of 200°C, the service life of bearings made from steel IIIX15 sharply decreases. In such conditions, bearings produced from heat-resistant steels are the obvious choice.

19.2.3. Axial Load Ratings for Angular-Contact Bearing Units

The axial force component S dictates the use of identical angular-contact bearings in pairs on one shaft, with the locating faces opposing each other. Two types of mountings are practicable, namely with the wide faces directed outwards or inwards (Fig. 19.2). The axial

load ratings on each of the bearings are determined by the type of mounting and the relation between the external axial load, F_a, and axial components, S_1 and S_2.

19.2.4. Design of Bearing Life

The service life of a bearing is defined as the number of revolutions (or hours of operation at a specified constant rotational frequency) for which the bearing is to function until evidence of contact fatigue emerges in the material of its races or rolling elements.

The rating life is taken to mean the life of a batch of bearings, during which no less than 90 percent of identical bearings are to operate at identical load and rotational frequency without evidence of material fatigue (pitting or flaking) on the working surfaces.

The rating life L (millions of revolutions) or L_h (hours) is computed on the basis of equivalent load P (kgf) and dynamic load rating C (kgf) by the formulas

$$L = \left(\frac{C}{P}\right)^p \quad \text{or} \quad L_h = \frac{10^6 L}{60n}$$

where $p = 3$ for ball bearings, and $p = \frac{10}{3} = 3.33$ for roller bearings; n = frequency of rotation, rpm.

These formulas are suited to any rotational frequency that does not exceed a limiting one indicated in the tables of standard ratings, if $n \geqslant 10$ rpm. At n ranging from 1 to 10 rpm, the calculation is made as for $n = 10$ rpm. At $n < 1$ rpm, the acting load is considered static and is compared with the static load rating C_0 for the given type and size of bearing indicated in standard-rating tables.

The scope of these formulas outside the range of standard rotational frequencies is limited.

The above formulas show that a double increase in the equivalent load leads to a reduction in rating life by a factor of 8 for ball bearings, and by a factor of 10 for roller bearings. For this reason, the acting loads should be determined as accurately as possible so that no arbitrary overload factors are introduced into the design calculation.

19.2.5. Choice of Bearings for Variable Operating Conditions

When load on a bearing varies from $P_{\min}$ to $P_{\max}$ uniformly, as, for instance, in bearings of drums with a single-direction winding, the equivalent load can be found from the formula

$$P = \frac{P_{\min} + 2P_{\max}}{3}$$

If the bearing operation can be broken down into separate stages with a definite duration, then the equivalent load should be deter-

mined by the formula

$$P = \sqrt[3]{\frac{P_1^3 L_1 + P_2^3 L_2 + P_3^3 L_3 + \ldots + P_n^3 L_n}{L}}$$

where P_1, P_2, P_3, . . ., P_n = constant loads acting during L_1, L_2, L_3, . . ., L_n million revolutions; $L = L_1 + L_2 + L_3 + \ldots + L_n$ = the total of millions of revolutions over which all the loads act.

With the known value of P, the rating life for the given bearing is computed by the formula $L = (C/P)^p$, or the required dynamic load rating is found from the formula $C = PL^{1/p}$ for a bearing to be selected.

19.3. HIGH-SPEED BEARINGS. FRICTIONAL LOSSES IN ROLLING BEARINGS

19.3.1. Recommendations on Use of High-Speed Bearings

A modern tendency in the development of machinery and equipment is the increase in speeds and rotational frequencies since fast-operating equipment apart from higher productivity has better weight and size characteristics.

Considerable angular velocities combining with larger sizes of rotational parts, which is due to ever increasing power of such equipment as gas-turbine engines, compressors, and large power-generation machinery, contribute to growth in peripheral speeds along with rotational frequencies.

Bearing failures in such machines are often caused by thermal jamming, catastrophic wear, fracture of cages, and corrosive, or abrasive wear rather than by fatigue pitting. As a rule, such failures are due to incorrect selection of the type and size of bearing, disturbed lubricating conditions, deficient removal of heat from the bearing unit, or inadequate packings. The limiting speed is evaluated approximately with the speed parameter $[d_m n]$, which is the product of multiplying the mean bearing parameter $d_m = \frac{d+D}{2}$ by the maximum operating number of revolutions n for the considered type and size of bearing. Here d is the bore diameter, and D is the outside diameter of the bearing. The recommended maximum values of the speed parameter for standard bearing designs are listed in Table 19.12.

The values of $[d_m n]$ may be taken greater than indicated in the Table with the use of a heavy cage and press-feeding a lubricant of an optimum viscosity.

The factor K_s should be somewhat increased for high-speed bearings (within the range of 1.1 to 1.4) in order to allow for the effect of centrifugal forces acting on the balls.

Table 19.12

Values of parameter $[d_m n]$

Type of bearing	$[d_m n]\ 10^{-5}$ mm rpm		Type of bearing	$[d_m n]\ 10^{-5}$ mm rpm	
	grease lubrication	oil lubrication		grease lubrication	oil lubrication
Ball bearings:			Ball bearings:	1.3	1.8
single-row radial	4.5	5.5	single-row-thrust		
single-row radial shielded	4.5	—	Roller bearings: radial with short cylindrical rollers	4.0	5.0
single-row radial sealed	4.0	—	single-row tapered	2.5	3.5
double-row self-aligning	4.0	5.5	double-row tapered	2.0	3.0
single-row angular-contact with stamped cage	4.0	5.5	four-row tapered	1.8	2.5

Bearings running at high rotational frequencies that exceed the standard rating limits should be calculated with regard to an additional load from centrifugal forces acting on rolling elements; these forces are effective in the contact areas of outer races (F_c):

for a ball

$$F_c = 0.57 \times 10^{-12} D_w^3 n_{ir}^2 d_m \left(1 \mp \frac{D_w}{d_m} \cos \alpha_{or}\right)^2$$

for a roller

$$F'_c = 0.85 \times 10^{-12} D_w^2\, l n_{ir}^2 d_m \times \left(1 \mp \frac{D_w}{d_m} \cos \alpha_{or}\right)^2$$

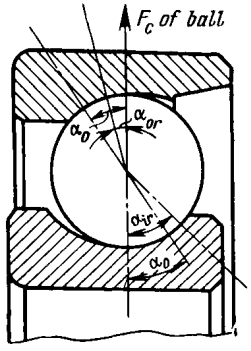

Fig. 19.3. Change in contact angles due to centrifugal action of balls

where D_w = ball or roller diameter, mm; n_{ir} = rotational frequency of the inner race, rpm; $d_m = \frac{d+D}{2}$ = diameter of the rolling-element centres, commonly equal to the mean diameter, mm; l = whole length of the roller, mm; α_{or} = contact angle on the outer race, degrees of arc.

In these formulas the sign "—" within the brackets is taken if the inner race is rotated, and the sign "+", if the outer race is rotated.

The centrifugal forces exerted by balls increase the contact angle on the inner race and reduce it on the outer race ($\alpha_{ir} > \alpha_0 > \alpha_{or}$) (Fig. 19.3); as a result, an accurate determining of contact forces between the balls and the races presents some difficulty.

In engineering calculations, the force on the most heavily loaded ball in its area of contact with the outer race can be found by the

formulas

$$P_{max} = \frac{5F_r}{z} + F_c \quad \text{at} \quad \alpha_0 = 0$$

$$P'_{max} = \frac{F_a}{z \sin \alpha_0} + F_c \cos \alpha_0 \quad \text{at} \quad \alpha_0 > 0 \, (F_r = 0)$$

Beyond a certain rotational speed limit, the contact stresses on outer races become higher than those on the raceways of inner races. Such loading conditions require more elaborate methods of calculating the bearing life, whose description can be found in the special literature on the subject. It is desirable that the contact stresses in ball bearings made from steel ШХ15 and its modifications should not exceed (3-4) $\times$ 10^4 kgf/cm^2 over a normal hardness range of *HRC* 60 to 65.

19.3.2. Design Characteristics of High-Speed Bearings

Related to high-speed bearings are radial and angular-contact ball bearings, including those of the types 276 000, 126 000, and 176 000 with two-, three-, and four-point contact.

High-speed bearings are provided with a heavy cage made of a non-ferrous metal or textolite; they are located mostly from the outer race. The main parameter to govern the choice of a specific bearing series is the contact angle which determines the relation between the axial and the radial load-carrying capacity. Allowance should also be made for a variation in the initial contact angle caused by the centrifugal forces of the balls (the angle decreases on the outer race and increases on the inner race), and for increasing gyroscopic spin of the balls at large contact angles. There is no hard-and-fast rule for the selection of a bearing series, but Table 19.13 may prove helpful.

Table 19.13

Recommended bearing series

$\frac{F_a}{K_v F_r}$	Bearing series	Initial angle of contact	Note
0.3-0.6	36 000	12	The use of light, very light, and extra-light series is advisable
Over 0.6-0.8	46 000 126 000 176 000 276 000	20-26	Light series is to be preferred at very high speeds
Over 0.8	66 000 126 000 176 000	26-36	The 66 000 series is unsuitable at very high speeds

At $\frac{F_a}{K_v F_r} < 0.3$, single-row radial ball bearings should be used.

A special feature of multi-point contact bearings is the capability of carrying heavy two-direction axial loads as well as radial loads. The contact angles in these bearings range from 20 to 30°, and the equivalent load is computed by the formula intended for ball bearings.

Preload is preferable for most angular-contact bearings, and for precision bearing units it is mandatory. The magnitude of the preload is found approximately by the formula

$$A_{pr} \approx 1.7 F_r \tan \alpha$$

19.3.3. Friction Losses in Bearings

With ball and roller bearings, the resistance to rotation is estimated by the amount of static friction torque (start-up torque) or by dynamic torque which is by 30 to 50 percent lower. The amount of both types of torque depends on the type of bearing, its geometry, roughness of the operating surfaces, type of lubricant and method of lubrication, magnitude of the load applied, and rotational frequency or start-up acceleration.

The power expended on overcoming friction in any rolling bearing can be estimated by the mean frictional torque determined by the formula

$$T_f = f_a P \frac{d_m}{2}$$

where P = equivalent load on the bearing determined by the usual dynamic calculation formulas, kgf; f_a = averaged coefficient of dynamic friction related to the diameter d_m of the ball centre circle (Table 19.14).

Table 19.14

Averaged values of coefficient of rolling friction

Type of bearing	$f_a \times 10^3$	Type of bearing	$f_a \times 10^3$
Radial ball bearing, self-aligning type included	1.5-2.0	Radial short-roller bearing	2.0-3.0
Angular-contact thrust ball bearing	2.0-2.5	Tapered and spherical roller bearings	3.5-5.0
Thrust and angular-contact thrust ball bearings	2.5-3.5	Needle roller bearing	5-10
		Thrust roller bearing	5-8

The listed values hold for bearings used with oil and grease lubrication in average service conditions (that is, at standard load and speed ratings).

For practical purposes, the values of f_a given in the Table should be increased 1.5-2 times, since additional friction is bound to emerge in actual bearing units because of the action of sliding-contact packings, manufacturing and assembling inaccuracies, overloading, or contaminated lubricant.

The total resistance to rotation in bearings is a complex parameter combining a large number of components that are hard to analyze. For this reason, determining the friction torque mathematically is very difficult and can be carried out only to a certain approximation.

The value of the rolling friction coefficient largely depends on the bearing's operating conditions: it decreases with increasing load within allowable limits and grows with increasing rotational frequency.

During steady-state running, the moment of resistance to rotation is relatively constant, although it can fluctuate within certain limits, which is especially typical of lightly loaded instrument bearings.

A number of testing apparatus are available for the assessment of the static and dynamic friction torques. The operating principle of apparatus for measuring the static friction torque is based on counterbalancing this torque with a moment of external forces whose magnitude defines the friction torque in the bearing.

The dynamic friction torque is determined by measuring the angle of creeping of the race that is free from the action of the applied external torque but turns together with load under the action of frictional torque.

The power N_f (kW) required to overcome friction in a bearing loaded with a force P (kgf) can be assessed approximately with the formula

$$N_f = \frac{T_f n}{97.4} = f_a P \frac{d_m n}{194{,}800}$$

Accordingly, the generation of heat in the bearing (kcal/h)

$$Q = 860\, N_f$$

19.4. FITS AND LUBRICATION OF ROLLING BEARINGS

19.4.1. Fits

Basic-hole fits are used for mounting bearings on shafts, and basic-shaft fits, for mounting bearings in housings. The USSR State Standards establish the bearing fits and their designations as indicated in (Table 19.15).

The choice of a fit depends on the type and size of bearing, its operating conditions, and on the magnitude, direction, and character of acting loads.

Table 19.15

Bearing fits and their designations

Type of fit	Designations for accuracy classes		Type of fit	Designations for accuracy classes	
	5 and 4	0 and 6		5 and 4	0 and 6
Force fit for thin-walled housings	—	P_7	Locational transition fit	$П_{1п}$	$П_п$
Medium drive fit	$Г_{1п}$	$Г_п$	Close-sliding fit	$С_{1п}$	$С_п$; $С_{зп}$
Light-drive fit	$Т_{1п}$	$Т_п$	Close-running fit	$Д_{1п}$	$Д_п$
Locational interference fit	$Н_{1п}$	$Н_п$	Running fit	—	$Х_п$

Depending on whether or not a given race rotates with respect to the applied radial load, distinction is made between three types of loading: local, circulating, and oscillatory (Fig. 19.4). Each type requires a definite fit between the bearing race and the mating shaft

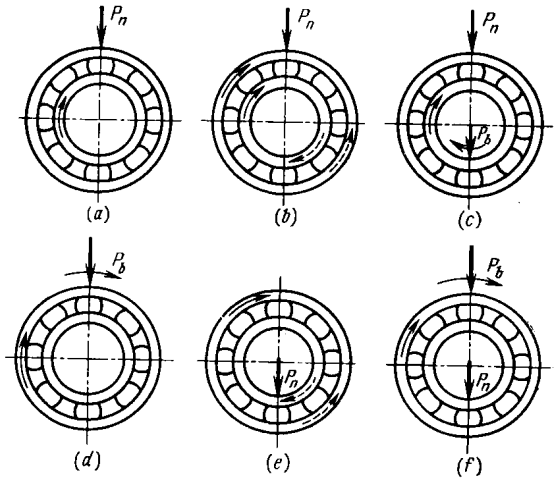

Fig. 19.4. Diagrams of bearing race loading

(*a*) and (*b*) circulating load on inner race and local load on outer race; (*c*) and (*d*) circulating load on both races; (*e*) oscillatory load on outer race and circulating load on inner race; (*f*) oscillatory load on inner race and circulating load on outer race

or housing, namely, a ring carrying a circulating load should be joined to the mating part by a stationary fit; for locally loaded race, a clearance fit or a small-interference fit is typical; and oscillatory loading mostly requires a close sliding fit between the race and its seating.

The correct location of bearings calls for rigid connection of the rotating part of a bearing assembly (shaft or housing) with the race

it carries. The rotating race should be mounted on the shaft or in the housing with a definite amount of interference provided by the $П_п$, $Н_п$, $Т_п$ and $Г_п$ classes of fits. From 60 to 70 percent of the interference is taken up by the raceway of the inner race, and from 30 to 40 percent by the raceway of the outer race. Such a distribution has the effect of reducing the mounting radial clearance in the bearing, which is undesirable in some bearing applications, particularly where small bearings are involved. For this reason, and also for easier fitting and dismantling of bearings, large amounts of interference are not used at light loads. At heavy and impact loads, however, a significant mounting interference is essential to prevent creep of the races with respect to their seatings.

The most frequently used bearing fits are $П_п$ and $Н_п$ for shafts, and $С_п$ for housings.

19.4.2. Lubrication

Rolling bearings are lubricated with fluid lubricants (mineral and synthetic) and greases.

The purpose of lubrication is

(a) to decrease friction between the rolling and sliding surfaces;

(b) to ensure the uniform distribution of heat in all bearing components and the removal of heat generated by friction;

(c) to protect bearing components against corrosion;

(d) to improve the sealing of the housing in order to prevent the ingress of foreign abrasive and contaminating matter.

The main characteristic of lubricating oils is viscosity, which defines the flowability and other properties. The grade of oil for a specific application is, therefore, selected primarily by its viscosity index.

With increasing loads and operating temperatures, oils with a higher viscosity index and flash point are used. Light, thin oils are applicable for small high-speed ball bearings. At temperatures ranging from 200 to 300°C, use can be made of silicone fluids based on methyl silicone.

The amount of oil fed to a bearing depends on its load and rotational frequency, which determine the generation of heat at the contact points. The main oil-feeding systems for bearings include the bath, drip-feed, wick, splash, oil-mist, and circulating types.

Bath lubrication is used for lightly loaded bearing units mounted on horizontal shafts. Oil is poured directly into the bearing housing through suitable holes in the cover so that half the lowest rolling element is immersed. This lubricating system requires highly refined oils because the oil does not circulate in the housing and is changed but periodically.

Lubrication with the aid of drop lubricators is used for lightly loaded bearing assemblies in periodic operation.

Wick oiling is applicable in a wide range of operating conditions. An advantage of such a lubricating method is that the wick ensures removal of foreign matter from the oil supplied to the bearing and feeds the oil by small portions.

Splash lubrication is preferable where bearings are lubricated together with gear transmissions from a common system. The oil splashed produces mist around the bearing.

Circulating systems of lubrication with metering nozzles are very dependable in the operation of bearings at high speeds and loads. Jet lubrication with a group of circularly arranged nozzles is the most effective for bearing applications under severe operating conditions. The use of several nozzles provides for uniform cooling of the bearing around its periphery, which is particularly important for bearings running at high rotational frequencies that cause intense generation of heat.

Oil-mist lubrication through spraying oil by a jet of well-dried compressed air supplied at a pressure of 0.5 to 1.5 kgf/cm^2 is used for lightly loaded high-speed bearings. The air-oil mixture forced through the bearing forms a constant oil film on the working surfaces, ensures good cooling, and protects the bearing against contamination.

Greases are the most suitable lubricants for rolling bearings. A wide application have found calcium, sodium, and calcium-sodium greases. Bearing greases also come in lithium-base grades (ЦИАТИМ-201, ЦИАТИМ-202, ЦИАТИМ-203, ОКБ-122-7, ЛЗ-31, and ЛИТОЛ-24) and aluminium-base grades (АМС-1, АМС-3, and МС-70). Applicable at elevated temperatures are also synthetic lubricants based on silicone fluids (ЦИАТИМ-221, and ЦИАТИМ-221С).

Greases are used for closed-type bearings (that is, having two packings or two shield washers). During assembly of such bearing units, grease is put into them for life.

Grease should take from $^1/_3$ to $^2/_3$ of the free inner space in the bearing housing, and its amount is determined by the operating conditions. One-third of the free space is normally filled in high-speed bearings. The larger amounts of lubricant are allowable in low-speed bearings, where an excess of grease is not harmful.

19.4.3. Self-Lubricating Bearings

Self-lubricating bearings are used in conditions where oils and greases cannot be used.

Such conditions may include high vacuum, intense radioactive radiation, high and extra-low temperatures, and gaseous and aggressive environments.

Self-lubricating bearings employ solid lubricants. There are many substances serving as solid lubricants (see Chapter 9), but the main of them, particularly suited to rolling bearing applications are molyb-

denum disulphide, fluoroplastic, graphite and composites based on these materials.

Some types of self-lubricating bearings, which are being currently under field tests, have the cage made from АСП plastics reinforced with a metal frame.

Soft metals, such as gold, silver, nickel, cobalt, indium, or lead oxide, deposited on the working surfaces in a thin layer, are also used as solid lubricants.

The choice of a particular type of solid lubricant depends on the bearing's operating conditions and manufacturing feasibility.

A selected type of lubricant determines the design of a self-lubricating bearing.

Three main groups of self-lubricating bearings have found applications in engineering practice, and their design features are as follows:

—the races and the cage made from metal are coated with a thin layer of a solid lubricant;
—the races are coated with a solid lubricant, and the cage is made from a non-metal antifriction material reinforced in some designs with a metal frame;
—a cake of a solid lubricant (including АСП plastic) is pressed into a metal cage.

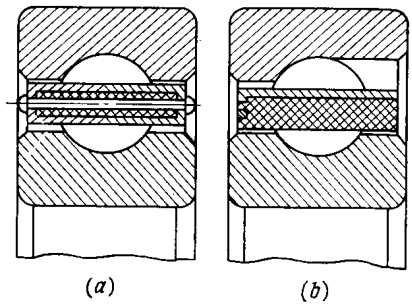

Fig. 19.5. Designs of self-lubricating bearings
(*a*) with metal cage in which antifriction material is embedded; (*b*) with АСП-plastic cage reinforced with metal frame

A bearing in which a cake of an antifriction material containing 50 percent fluoroplastic and 50 percent molybdenum disulphide is embedded in a bronze cage is the most suitable for severe operating conditions (Fig. 19.5).

The balls in such a bearing pick up the antifriction material and spread it over the raceways, so forming a lubricating film between the moving surfaces. This process occurs continuously to result in a long bearing life.

The allowable loads on self-lubricating bearings are lower than those on bearings lubricated with greases; their magnitude must be such as to keep σ_{max} above 15000 kgf/cm^2. At contact pressures exceeding the indicated value, the performance of self-lubricating bearings sharply deteriorates. The cause is that solid lubricants are not capable of removing the heat generated on the surfaces in contact. Moreover, at heavy loads the lubricant film is broken by contact pressure, which leads to increased friction and, as a consequence, to faster wear of the bearing components.

REFERENCES

1. Ковалев М. П., Народецкий М. З. Расчет высокоточных шарикоподшипников. М., «Машиностроение», 1975, 279 с.
2. Опоры осей и валов машин и приборов. Л., Машгиз, 1970, 520 с. Авт.: Н. А. Спицын, М. М. Машнев, Е. Я. Красковский и др.
3. Подшипники качения. Каталог-справочник. М., НИИНАвтопром, 1972, 465 с.
4. Спришевский А. И. Подшипники качения. М., Машгиз, 1969, 632 с.

Chapter 20

SLIDING BEARINGS

20.1. DRY-RUBBING BEARINGS

20.1.1. Calculation of Contact Parameters

Related to contact parameters of sliding (plain) bearings are: (a) the arc of contact between the shaft and the bush, which is defined by the angle of contact $2\varphi_0$; (b) the distribution of contact pressures $p(\varphi)$; and (c) the maximum contact pressure p_m.

The above contact parameters can be calculated by the Hertz formulas [20] for internal contact of two cylinders on condition that [5]

$$\alpha [(1 - \mu_1^2) + (1 - \mu_2^2) \psi] \leqslant 0.092 \qquad (20.1)$$

where

$$\alpha = \frac{P_0}{E_1 \varepsilon}, \quad \psi = \frac{E_1}{E_2}$$

P_0 = load per unit length; $\varepsilon = R_1 - R_2$ = radial clearance in the bearing; indexes 1 and 2 refer to the bearing and shaft materials, respectively.

Since the radii R_1 and R_2 (Fig. 20.1) in sliding bearings differ insignificantly, the formula for the contact angle may be put down as

$$\sin \varphi_0 = \sqrt{\frac{4}{\pi} [(1 - \mu_1^2) + (1 - \mu_2^2) \psi] \alpha} \qquad (20.2)$$

The distribution of contact pressures obeys the equation

$$p(\varphi) = p_m \left[1 - \left(\frac{\varphi}{\varphi_0} \right)^2 \right]^{1/2} \qquad (20.3)$$

The maximum magnitude of pressure at the centre of the contact zone is found by the formula

$$p_m = \frac{2P_0}{\pi R_1 \sin \varphi_0} \qquad (20.4)$$

Where the condition (1) is not met, solutions should be used that impose no limitation on the size of the contact zone. The calculation will be different for two cases.

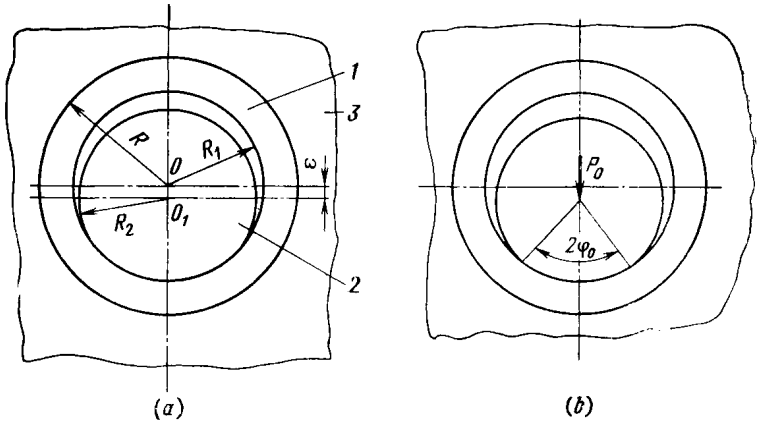

Fig. 20.1. Design diagram for plain bearing
(*a*) before applying load P_0; (*b*) after applying load P_0; *1*—bush; *2*—shaft; and *3*—bearing race

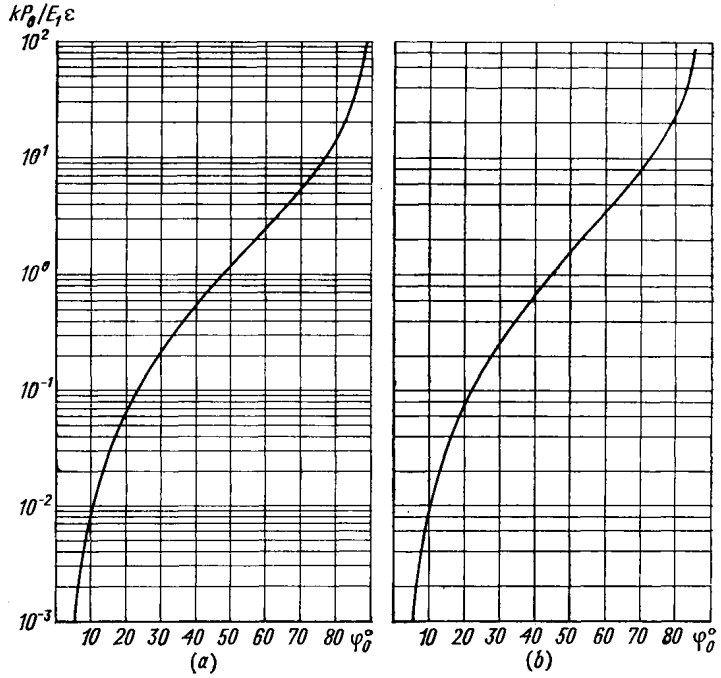

Fig. 20.2. Variation of dimensionless parameter with half contact angle in sliding bearings
(*a*) at $\mu_1 \leqslant 0.5$ and $\mu_1 = 0.5$ for split bush; (*b*) at $\mu_1 = 0.5$ for integral bush

The first case: $\psi < 10^{-2}$. This case is typical of bearings with polymer bushes.

The calculation method for the contact parameters is based on analysis of stress conditions in an elastic annular bush. The design diagram is shown in Fig. 20.1. The solution is obtained on the following assumptions [11, 12, 16]:

1. The bearing is deformed elastically, and its material exhibits the isotropy of the elastic properties.
2. The shaft and the pedestal body are undeformable components.
3. Tangential stresses are absent along the contact arc because the coefficient of friction in sliding bearings is low ($f < 0.3$).
4. The load P is distributed uniformly through the journal length l with a rate $P_0 = \frac{P}{l}$.

It has been established that in the two-dimensional strained state

$$k \frac{P_0}{E_1 \varepsilon} = \varphi(\varphi_0) \tag{20.5}$$

where

$$\varphi(\varphi_0) = \frac{2\varphi_0 - \sin 2\varphi_0}{\cos \varphi_0}$$

The function $\varphi(\varphi_0)$ is graphically represented in Fig. 20.2*a*. The factor k depends on the relative thickness of the bush $\gamma = \frac{R_1}{R}$ and on the Poisson ratio μ_1 for the bush material (Table 20.1).

Table 20.1

Value of k in formula (5)

No.	Reference source	k	Note
1	[11]	$2(1+\mu_1)(1-2\mu_1)\frac{1-\gamma^2}{1-2\mu_1+\gamma^2}$	Bearing bush is deformed as Winkler base, $\gamma > \frac{1}{2}$
2	[16]	$2(1+\mu_1)(1-2\mu_1)\frac{1-\gamma}{1-2\mu_1+\mu_1\gamma}$	—
3	[12]	$2(1+\mu_1)(1-2\mu_1)\frac{(\mu_1 \ln\gamma+\mu_1-1)\ln\gamma}{(1-\mu_1)^2}$	$\lvert \ln\gamma \rvert \ll 1$
4	[19]	$2(1+\mu_1)(1-2\mu_1)\frac{1-\gamma}{\gamma(1-\mu_1)}$	$\gamma > \frac{1}{2}$

With the small bush thicknesses typical of polymer plain bearings the values of k hardly differ from each other (Fig. 20.3).

If $\mu_1 = 0.5$, the length of the contact arc is found by one of the following formulas [17]:

—for a split bearing bush by the formula (20.5), the value of k depending on the relative bush thickness:

$$k = \frac{3}{2}\frac{1-\gamma}{\gamma} \tag{20.6}$$

—for a solid bush

$$k = \frac{P_0}{E_1 \varepsilon} = \varphi_1(\varphi_0) \tag{20.7}$$

where $\varphi_1(\varphi_0) = \frac{2\varphi_0 - \sin 2\varphi_0}{\cos \varphi_0} + \frac{4 \sin \varphi_0}{\pi - \varphi_0}(\tan \varphi_0 - \varphi_0)$, and k is computed by the formula (20.6).

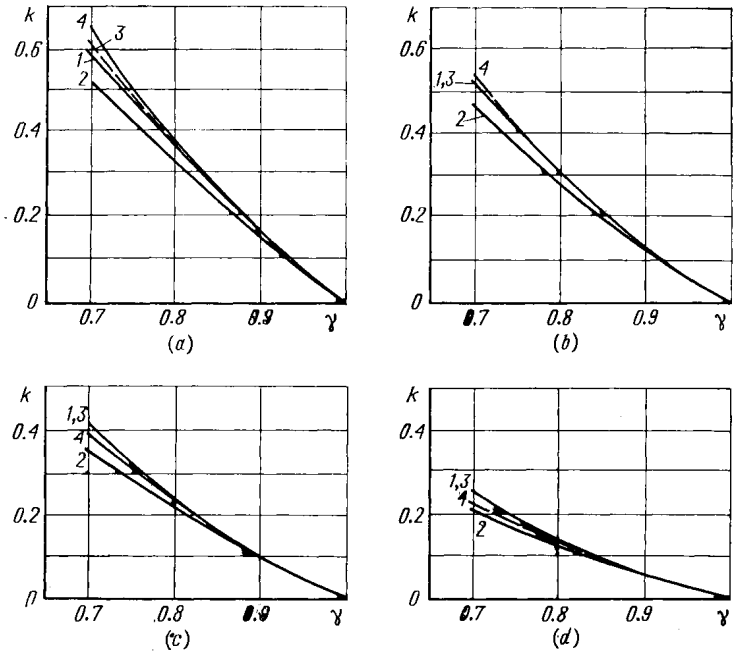

Fig. 20.3. Relationship between coefficient k and parameter γ
(*a*) $\mu_1 = 0.3$; (*b*) $\mu_1 = 0.35$; (*c*) $\mu_1 = 0.40$; and (*d*) $\mu_1 = 0.45$. Reference numerals for curves correspond to ordinal numbers in Table 20.1.

A graph of the function $\varphi_1(\varphi_0)$ is shown in Fig. 20.2*b*. The distribution of pressure along the contact arc length at $\mu_1 \neq 0.5$ obeys the equation

$$p(\varphi)\frac{R_1}{E_1 \varepsilon} = \frac{2}{k}\frac{\cos \varphi - \cos \varphi_0}{\cos \varphi_0} \tag{20.8}$$

that is, at the centre of the contact arc the pressure is a maximum

$$p_m = \frac{2E_1\varepsilon}{kR_1}\frac{1-\cos\varphi_0}{\cos\varphi_0} \tag{20.9}$$

The mean contact pressure $\bar{p} = \frac{P_0}{2R_1\varphi_0}$ is found from the relationship

$$\bar{p}\frac{2kR_1}{E_1\varepsilon} = \varphi_2(\varphi_0), \quad \text{where} \quad \varphi_2(\varphi_0) = \frac{2\varphi_0 - \sin 2\varphi_0}{\varphi_0\cos\varphi_0}$$

With materials having the Poisson ratio $\mu_1 = 0.5$:
for a solid bearing bush

$$p(\varphi)\frac{R_1}{E_1\varepsilon} = \frac{4}{3}\frac{\gamma}{1-\gamma}\left(\frac{\cos\varphi-\cos\varphi_0}{\cos\varphi_0} + \frac{\tan\varphi_0-\varphi_0}{\pi-\varphi_0}\right) \tag{20.10}$$

for a split bush

$$p(\varphi)\frac{R_1}{E_1\varepsilon} = \frac{4}{3}\frac{\gamma}{1-\gamma}\left(\frac{\cos\varphi_0-\cos\varphi_0}{\cos\varphi_0}\right) \tag{20.11}$$

The maximum pressure on the contact arc will be determined from the formulas (20.10) and (20.11), assuming that $\varphi = 0$.

The second case: $\psi > 10^{-2}$. This case applies to bearings with metallic bushes and to those coated with thin antifriction linings (see Vol. 1, Ch. 5 and 9).

The solution of the contact problem stated in this way [13] amounts to an integro-differential equation for the function $p(\varphi)$.

The numerical solution of this equation has shown [7] that the function

$$\varphi_0 = C\left(\frac{\alpha}{1+\alpha}\right)^n \tag{20.12}$$

can be taken as an approximate relationship between half the contact angle and a dimensionless parameter α.

Formulas for computing the exponent n are given in Table 20.2.

Table 20.2

Formulas for calculation of exponent n

$10 \geqslant \psi \geqslant 0.1$	$\psi > 10$	$\psi < 0.1$
$n = m_1\mu_1 + m_2\mu_2 + n_0$* $m_1 = 0.07\,(1 - \lg\psi)$ $m_2 = 0.20\,(1 + \lg\psi)$	$n = 0.41\ \mu_2 + 0.45$	$n = 0.16\ \mu_1 + 0.55$

* Variation of n_0 with ψ is presented in Fig. 20.4.

The coefficient C in the formula (20.12)

$$C = 0.32 \left(\frac{C_0}{0.12} + 1 \right)^n \tag{20.13}$$

where

$$C_0 = \frac{\pi}{4} [(1 - \mu_1^2) + (1 - \mu_2^2)\, \psi] \tag{20.14}$$

With regard to (20.13), the formula (20.12) will take the form

$$\varphi_0 = 0.32 \left[\left(\frac{C_0}{0.12} + 1 \right) \frac{\alpha}{\alpha + 1} \right]^n \tag{20.15}$$

The distribution of the contact pressure is described by the formula (20.3).

The maximum pressure p_m at the centre of the contact arc is computed by the formula

$$p_m = 0.55 \frac{P_0}{R_1} \left(\frac{1}{\varphi_0} + 0.35 \right) \tag{20.16}$$

The initial data for the calculation of contact parameters in sliding bearings are (a) the design characteristics of the bearing unit (l, R_1, ε and γ); (b) the mechanical properties of bearing material (E_1 and μ_1) and shaft material (E_2 and μ_2); and (c) the acting load P.

It should be kept in mind that all the design relationships given in this paragraph apply only to bearings in which $f < 0.3$.

The calculating sequence is as follows:

1. Ascertain whether the contact parameters of a plain bearing can be found from the Hertz theory (see formula (20.1). If the inequality (20.1) is followed, compute the contact angle by formula (20.2), the pressure over the contact area by formula (20.3), and the maximum pressure at the contact area centre by formula (20.4).

2. If the inequality (20.1) is not met, find the parameter ψ. If it turns out to be smaller than 0.01, take the following steps:

(a) With $\mu_1 < 0.5$, find the value of k from the graph in Fig. 20.3 or by calculation with one of the formulas in Table 20.1. At $\mu_1 = 0.5$, determine the value of k by formula (20.6).

(b) With $\mu_1 < 0.5$ and for a split bush at $\mu_1 = 0.5$, solve the left-hand part of equation (20.5). Plotting the obtained values along the ordinate on the graph (see Fig. 20.2*a*), find the contact angle $2\varphi_0$. At $\mu_1 = 0.5$ for a solid bush, solve the left-hand part of equation (20.7) and determine the contact angle by the graph in Fig. 20.2*b*.

(c) With φ_0 known, compute the maximum pressure, p_m, at the contact area. For this purpose use either formula (20.9) (for $\mu_1 < 0.5$) or one of the formulas (20.10), (20.11) (for $\mu_1 = 0.5$), assuming $\varphi = 0$.

The mean contact pressure $\bar{p}$ is found by the formula

$$\bar{p} = \frac{P_0}{2R_1\varphi_0} \tag{20.17}$$

3. If $\psi > 0.01$, the bearing unit is calculated by the formulas corresponding to the second case, and the sequence of calculation is as follows:

(a) Depending on the value of ψ, compute the exponent n by one of the formulas given in Table 20.2 with the use of the graph in Fig. 20.4.

(b) Find the coefficient C_0 by formula (20.14) and the contact angle $2\varphi_0$ by formula (20.15).

(c) Calculate the pressure in the contact zone by formula (20.3), the maximum pressure at the centre of the contact arc by formula (20.16), and the mean pressure by formula (20.17).

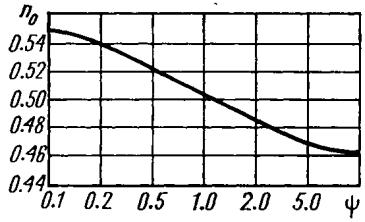

Fig. 20.4. Variation of n_0 with parameter ψ

One more note in conclusion. Special coatings are often applied to the operating surfaces of bearings in order to improve their friction and wear characteristics. If the thickness of the coating, δ, is small compared with the contact arc, that is $\lambda = \frac{\delta}{R_1\varphi_0} \leqslant 0.1$, then the mechanical properties of these coating materials are disregarded in the above calculations. Alternatively, if $\lambda > 10$, the coating is considered thick and it is precisely its mechanical properties that are taken into account, whereas the body to which the coating is applied is assumed undeformable [4].

20.1.2. Analysis of Wear in an Inverse Sliding Pair

The basic premises of analysis [3].

1. The bearing is much more wear-resistant than the mating shaft journal. For this reason the bearing bore diameter is regarded as invariable.

2. The bearing assembly wears at the expense of the journal, which is assumed to retain the shape of a circular cylinder as it wears away. In this instance, for any revolution n of the shaft, the bearing dimensions will obey the relationship

$$R_1 = R_2(n) + \varepsilon(n) = \text{constant}$$

where $R_2(n)$ and $\varepsilon(n)$ = journal radius and radial clearance in the bearing after the nth revolution of the shaft.

3. The Hertz theory is applicable to the calculation of contact parameters with regard to a change of bearing dimensions from revolution to revolution, namely

$$p_m(n) = \sqrt{\frac{\chi(1+y)P_0}{\pi(1+\chi)(1-\chi y)\Theta_\Sigma R_2(0)}} \tag{20.18}$$

$$a(n) = 2\sqrt{\frac{(1+\chi)(1-\chi y)P_0\Theta_\Sigma R_2(0)}{\pi\chi(1+y)}} \tag{20.19}$$

$$p(n;\ x) = p_m(n)\sqrt{1-\left(\frac{x}{a(n)}\right)^2} \tag{20.20}$$

where $\chi = \frac{\varepsilon(0)}{R_2(0)}$; $y = \frac{\varepsilon(n)}{\varepsilon(0)} - 1$; $\Theta_\Sigma = \Theta_1 + \Theta_2$; $\varepsilon(0)$ = initial radial clearance in the bearing; $a(n)$ = half the width of the contact area.

4. The journal's wear rate relates to the contact pressure as

$$I = Kp^m$$

where K and m = parameters which can be either computed by the appropriate formulas (see Vol. 1, Ch. 3) or found experimentally.

The journal's wear $h(n)$ during an nth revolution is determined as

$$h(n) = \int_{-a(n)}^{+a(n)} Kp^m(n;\ x)\,dx = 2a(n)\int_0^1 Kp^m(n;\ t)\,dt$$

where $t = \frac{x}{a(n)}$, which corresponds to the average wear rate on the nth revolution

$$\overline{I}(n) = \frac{h(n)}{2a(n)} = \int_0^1 Kp^m(n;\ t)\,dt \tag{20.21}$$

Making integration of equation (20.21) with regard to (20.20), we find

$$\overline{I}(n) = \frac{\sqrt{\pi}\,\Gamma\left(\frac{m}{2}+1\right)}{2\Gamma\left(\frac{m}{2}+\frac{3}{2}\right)} Kp_m^m(n) \tag{20.22}$$

where $\Gamma(z)$ = gamma function.

Since the numerical value of $h(n)$ is equal to the change in radial clearance on the nth shaft revolution, the wear characteristic of the bearing must conform to the differential equation

$$d\varepsilon = h(n)\,dn$$

whence the number of revolutions at which the clearance ε^* will be reached is

$$n = \int_{\varepsilon(0)}^{\varepsilon^*-\varepsilon(0)} \frac{d\varepsilon}{2\overline{I}(n)\,a(n)} \tag{20.23}$$

If the quantity ε^* is regarded as the maximum allowable clearance in the bearing, formula (20.23) will determine the bearing life as dependent on wear.

With allowance for (20.18), (20.19), and (20.22), expression (20.23) can be given the form

$$n = n_0 F \tag{20.24}$$

where

$$F = \int_0^{y^*} \left(\frac{1-\chi y}{1+y}\right)^{\frac{m-1}{2}} dy; \quad n_0 = \frac{\Theta_\Sigma^m}{K(1+\chi)\chi^{m-1}Q^{\frac{m+1}{2}}} \tag{20.24a}$$

$$y^* = \frac{\varepsilon^*}{\varepsilon(0)} - 1; \quad Q = \frac{P_0\Theta_\Sigma}{\pi(1+\chi)\chi R_2(0)}$$

The values of the integral for different combinations of m and y^* are listed in Table 20.3.

For plain bearings, the effect of χ on the value of F is negligible.

Table 20.3

Numerical values of function F

y^*	m							y^*	m						
	1.0	1.5	2.0	2.5	3.0	3.5	4.0		1.0	1.5	2.0	2.5	3.0	3.5	4.0
0	0.00	0.00	0.00	0.00	0.00	0.00	0.00	5.5	1.75	1.42	1.15	0.95	0.78	0.66	0.56
0.5	0.16	0.16	0.17	0.17	0.17	0.17	0.17	6.0	1.91	1.52	1.22	0.99	0.81	0.68	0.57
1.0	0.32	0.32	0.31	0.30	0.29	0.28	0.27	6.5	2.07	1.63	1.29	1.04	0.84	0.70	0.59
1.5	0.48	0.46	0.44	0.41	0.39	0.36	0.34	7.0	2.23	1.73	1.36	1.08	0.87	0.71	0.60
2.0	0.64	0.59	0.55	0.50	0.46	0.43	0.39	7.5	2.39	1.83	1.42	1.12	0.89	0.73	0.60
2.5	0.80	0.72	0.65	0.59	0.53	0.48	0.43	8.0	2.55	1.93	1.48	1.16	0.92	0.74	0.61
3.0	0.96	0.85	0.75	0.66	0.58	0.52	0.46	8.5	2.71	2.03	1.54	1.19	0.94	0.75	0.62
3.5	1.11	0.97	0.84	0.73	0.63	0.56	0.49	9.0	2.86	2.13	1.60	1.23	0.96	0.77	0.63
4.0	1.27	1.08	0.92	0.79	0.68	0.59	0.51	9.5	3.02	2.22	1.66	1.26	0.98	0.78	0.63
4.5	1.43	1.20	1.00	0.84	0.72	0.61	0.53	10.0	3.18	2.32	1.71	1.29	1.00	0.79	0.64
5.0	1.59	1.31	1.08	0.90	0.75	0.64	0.55								

Example. A dry-rubbing bearing consists of a steel shaft coated with a ФКН-7 polymer-composition layer having a thickness $\delta = 0.25$ mm and a steel bearing bush. The dimensions of the bearing are: $R_2(0) = 25$ mm, $l = 50$ mm; $\varepsilon(0) = 0.05$ mm. The mechanical properties of the materials: for steel $E = 2 \times 10^6$ kgf/cm^2; $\mu = 0.3$, and for ФКН-7 $E = 1.15 \times 10^4$ kgf/cm^2; $\mu = 0.4$. The parameters of the wear law: $K = 4.8 \times 10^{-12}$; $m = 1.4$. The coefficient of friction $f = 0.19$. The load on the bearing $P = 500$ kgf.

Find the bearing life provided that the maximum allowable clearance $\varepsilon^* = 0.2$ mm.

First determine whether the coating may be considered thin. To this end, compute the maximum allowable value of λ_{max}, characteristic of steel-to-steel contact between the shaft and the bush.

1. Compute C_0 by formula (20.14):

$$C_0 = \frac{3.14}{4}[(1-0.3^2)+(1-0.3^2)\,1] = 1.43$$

2. Compute n by the formulas in Table 20.2 at $\psi = 1$, and by the graph given in Fig. 20.4.

$$m_1 = 0.07\ (1 - \lg 1) = 0.07;\ m_2 = 0.20\ (1 + \lg 1) = 0.20$$

$$n_0 = 0.502;\ n = 0.3 \times 0.27 + 0.502 = 0.583$$

3. The dimensionless parameter

$$\alpha = \frac{P_0}{E_1 \varepsilon\,(0)} = \frac{P}{l E_1 \varepsilon\,(0)} = \frac{5 \times 10^2 \times 10^3}{5 \times 2 \times 10^6 \times 5} = 10^{-2}$$

4. Find the angle φ_0 by formula (20.15):

$$\varphi_0 = 0.32 \left[\left(\frac{1.43}{0.12} + 1 \right) \frac{10^{-2}}{10^{-2} + 1} \right]^{0.583} = 0.11$$

5. Compute the parameter λ_{max}

$$\lambda_{max} = \frac{0.25}{0.11 \times 2.5} = 0.09 < 0.1$$

Hence, the coating is thin.

Using the relationship (1), check whether the Hertz theory applies in this instance:

$$[(1 - 0.3^2) + (1 - 0.3^2)\ 1]\ 10^{-2} = 0.0182 < 0.092$$

Thus, the relationships (20.18), (20.19), (20.20) and (20.24) are applicable to the calculation of the contact parameters and the service life of the bearing.

From formulas (20.24*a*) we obtain

$$Q = \frac{10^2 \times 9.1 \times 10^{-7}}{3.14\,(1 + 2 \times 10^{-3})\ 2 \times 10^{-3} \times 2.5} = 5.79 \times 10^{-3}$$

$$n_0 = \frac{(9.1 \times 10^{-7})^{1.4}}{4.8 \times 10^{-12}\,(1 + 2 \times 10^{-3})\ (2 \times 10^{-3})^{0.4}\ (5.79 \times 10^{-3})^{1.2}} = 4.13 \times 10^6$$

For the rated allowable clearance $y^* = \dfrac{\varepsilon^* - \varepsilon\,(0)}{\varepsilon\,(0)} = 3$ and $m = 1.4$, the value of F, found from Table 20.3, will be 0.87. Finally, the bearing life $n = n_0 F = 0.87 \times 4.13 \times 10^6 = 3.6 \times 10^6$ revolutions.

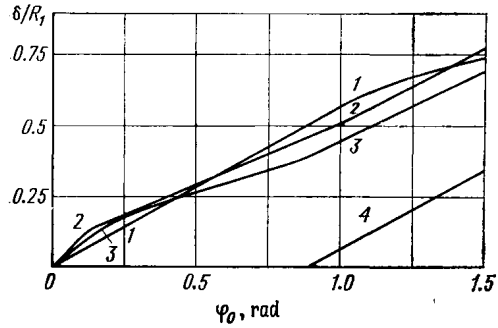

Fig. 20.5. Criteria of bearing-bush wall thickness

1—$\mu_n = 0$; *2*—$\mu_n = 0.17$; *3*—$\mu_n = 0.32$; *4*—$\mu_n = 0.5$

20.1.3. Analysis of Load-Carrying Capacity

The analysis of plain bearings for load-carrying capacity requires the introduction of notions of a thin-walled bush and a thick-walled bush [6]. If the thickness δ of the bush wall exceeds the depth of the plastic flow in it, the bush is called thick-walled. If the bush is deformed throughout the whole depth of the wall, it is considered thin-walled.

In Fig. 20.5, the regions disposed above the appropriate curves relate to thick-walled bushes and the regions lying below the curves

relate to thin-walled bushes. With $\gamma < 0.56$, a bush should be considered thick-walled regardless of $\mu_n = \frac{\tau}{2k}$, where k = plastic constant of the material, and τ = tangential stresses.

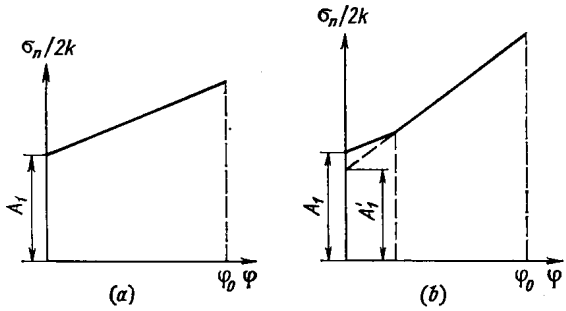

Fig. 20.6. Diagrams for distribution of normal pressures in contact area at $\mu_n = 0$
(*a*) for thick-walled bush; (*b*) for thin-walled bush

Tentative assessment of the plain bearing wall thickness at $f \leqslant 0.1$ and, accordingly $\mu_n \leqslant 0.2$ to 0.3 can be made, ignoring the influence of friction, with the relationship

$$\frac{\delta}{R_1\varphi_0} \geqslant M = \frac{1.8}{\pi}$$

which corresponds to the linear section of the curve (Fig. 20.5) for $\mu_n = 0$.

In a thick-walled bush, the normal contact pressures are distributed in accordance with the relationship [1] (Fig. 20.6*a*):

$$\text{at } \varphi_\lambda \geqslant \varphi \geqslant 0$$

$$p/2k = A_1 + a_1\varphi \tag{20.25}$$

$$\text{at } 2\varphi_0 \geqslant \varphi > \varphi_\lambda$$

$$p/2k = A_2 - a_2(\varphi - 2\varphi_0) \tag{20.26}$$

where

$$A_1 = \frac{\pi}{4} + \frac{1}{2}\arccos 2\mu_n + \frac{1}{2} + \frac{1}{2}\sin\arccos 2\mu_n$$

$$A_2 = \frac{3\pi}{4} - \frac{1}{2}\arccos 2\mu_n + \frac{1}{2} + \frac{1}{2}\sin\arccos 2\mu_n$$

$$a_1 = 1.78(1-\mu_n);\quad a_2 = 1.78;\quad \varphi_\lambda = \frac{A_2 - A_1 + 2a_2\varphi_0}{a_1 + a_2}$$

By integrating equations (20.25) and (20.26) for the contact arc, we will determine the critical load $[P_0]$ in the case of a thick-walled

bush:

$$\frac{[P_0]}{2kR_1} = A_1[\sin\varphi_0 + \sin(\varphi_\lambda - \varphi_0)] + A_2[\sin\varphi_0 - \sin(\varphi_\lambda - \varphi_0)]$$
$$+ (a_1 + a_2)[\cos(\varphi_\lambda - \varphi_0) + \varphi_\lambda \sin(\varphi_\lambda - \varphi_0) - \cos\varphi_0]$$
$$- 2a_2\varphi_0 \sin(\varphi_\lambda - \varphi_0) \quad (20.27)$$

If friction is neglected, expression (20.27) will take the form

$$\frac{[P_0]}{2kR_1} = 2\left(\frac{\pi}{2} + 1\right)\sin\varphi_0 + 3.56(1 - \cos\varphi_0) \quad (20.28)$$

The diagram of distribution of the normal contact pressures in a thin-walled bush at $\mu_n = 0$ is shown in Fig. 20.6*b* [6]. The diagram is symmetrical, so only half of it is given. In the region $\varphi^* \geqslant \varphi \geqslant 0$

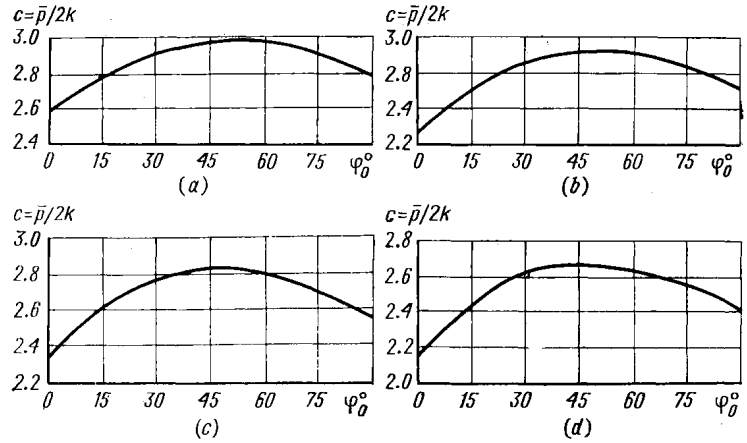

Fig. 20.7. The mean critical pressures *vs* contact angle for thick-walled bearing bush
(*a*) $\mu_n = 0$; (*b*) $\mu_n = 0.1$; (*c*) $\mu_n = 0.2$; (*d*) $\mu_n = 0.3$

adjacent to the contact zone boundary, the stress is distributed linearly according to equation (20.25); here $A_1 = \frac{\pi}{2} + 1$, and $a_1 = 1.78$.

The following relationship holds for the rest of the contact contour:

$$p/2k = A_1' + a_1'\varphi$$

where $A_1' = 2$, and $a_1' = 0.33\ \frac{R_1}{\delta} + 1.78$.

The limiting pressure for a thick-walled bush

$$\frac{[P_0]}{2kR_1} = 2A_1[\sin\varphi_0 - \sin(\varphi_0 - \varphi^*)]$$
$$+ 2a_1[\cos(\varphi_0 - \varphi^*) - \varphi^* \sin(\varphi_0 - \varphi^*) - \cos\varphi_0]$$
$$+ 2A_1' \sin(\varphi_0 - \varphi^*) + 2a_1'[1 + \varphi^* \sin(\varphi_0 - \varphi^*) - \cos(\varphi_0 - \varphi^*)] \quad (20.29)$$

where $\varphi^* = \frac{\pi}{1.8}\frac{\delta}{R_1}$.

Transition from elastic to plastic deformation will come about at the moment that the mean contact stresses calculated by the formula of the theory of elasticity (see Sec. 20.1.1) reach the magnitudes of the mean stresses in the fully plastic conditions (Figs. 20.7 and 20.8).

Equalizing their values, it is possible to find the angle φ_0 and, further, by using relationships (20.27), (20.28) or (20.29), to determine the critical load on the bearing.

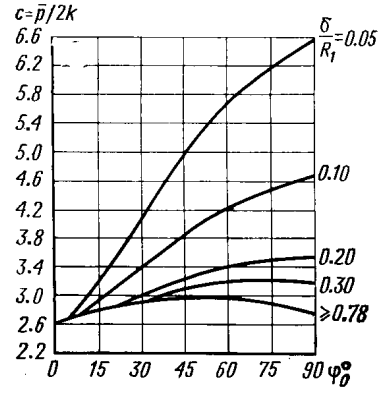

Fig. 20.8. The mean critical pressures *vs* contact angle for thin-walled bearing bush

20.1.4. Analysis of Temperature Conditions

A stationary temperature field in a polymer bush is calculated in [18] on the following assumptions: (1) the work of the frictional forces is completely transformed into heat; (2) the source of heat spread over the contact area causes the distribution of heat flows between the bearing and the shaft, which is characterized by a constant α_t; (3) the thermal conductivity of the bearing housing is much greater than that of the bush and, therefore, the temperature gradient from the housing to the bush is low.

The distribution of temperature in a thin bush has the form

$$\vartheta_1 = c_0(\varphi) + tc_1(\varphi) \tag{20.30}$$

$$c_0(\varphi) = \begin{cases} (1-\gamma_0\rho R_1)^{-1}[\theta(\varphi) - \gamma_0\rho R_1\vartheta_0] & \text{at } |\varphi| > \varphi_0 \\ \theta(\varphi) + \mu_t\rho R_1 p(\varphi) & \text{at } |\varphi| \leqslant \varphi_0 \end{cases} \tag{20.31}$$

$$c_1(\varphi) = \begin{cases} \gamma_0\rho R_1(1-\gamma_0\rho R_1)^{-1}[\vartheta_0 - \theta(\varphi)] & \text{at } |\varphi| > \varphi_0 \\ -\mu_t\rho R_1 p(\varphi) & \text{at } |\varphi| \leqslant \varphi_0 \end{cases} \tag{20.32}$$

where

$$\rho = \ln\frac{R}{R_1}; \quad t = -\frac{\ln r/R_1}{\ln\gamma}; \quad \mu_t = J(1-\alpha_t)\omega f R_1\frac{1}{k_1};$$

ϑ_0 = temperature of air between the shaft and the bearing; $\gamma_0 = H_1/k_1$; H_1 = coefficient of heat exchange between the bearing and the air inside it; J = thermal equivalent of work; k_1 = coefficient of thermal conductivity of the bearing bush; ω = shaft angular velocity; and r = current radius.

From the solution of the problem of thermal conductivity for the bearing shell it follows that

$$\theta(\varphi) = \mu_t(D_0 + D_1\cos\varphi) \tag{20.33}$$

where D_0 and D_1 = constants.

Substituting the second relationships in the equations (20.31) and (20.32) into (20.30), with regard to the expressions (20.33) and (20.8), we shall obtain the race temperature at $|\varphi| \leqslant \varphi_0$ in the form

$$\vartheta_1 = \mu_t \left(D_0 + D_1 \cos\varphi - \frac{2P_0\rho\,(t-1)\,(\cos\varphi_0 - \cos\varphi)}{\sin 2\varphi_0 - 2\varphi_0} \right) \qquad (20.34)$$

Let us express the mean temperature along the contact arc ($t = 0$) as

$$\vartheta_1^* = \frac{1}{\varphi_0} \int_0^{\varphi_0} \vartheta_1\, d\varphi \qquad (20.35)$$

Then, with allowance for (20.34), expression (20.35) will take the form

$$\vartheta_1^* = \mu_t q_* \qquad (20.36)$$

where $q_* = D_0 + D_1 \frac{\sin\varphi_0}{\varphi_0} + \rho R_1 p^*$

$$p^* = \frac{2P_0 \left(\cos\varphi_0 - \frac{\sin\varphi_0}{\varphi_0} \right)}{R_1 (\sin 2\varphi_0 - 2\varphi_0)}$$

The mean linear temperature of the shaft can be represented, according to [2], as

$$\vartheta_2 = \frac{\alpha_t R_2^2 \omega J f p^*}{k_2} \varkappa$$

where $\varkappa$ = dimensionless coefficient;

$$\varkappa = \frac{\varphi_0}{\pi\lambda_2} B; \quad B = 4 + \frac{21.9}{\sqrt{\lambda_2}} \exp\left(-\frac{3.1l}{R_2} \right) \cosh\frac{z}{R_2} - 0.5\lambda_2 \frac{l^2 + 4z^2}{R_2^2};$$

$$\lambda_2 = \frac{R_2 H_2}{k_2}$$

here, H_2 = coefficient of heat transfer from shaft; z = coordinate of a point along the shaft axis $|z| \leqslant \frac{l}{2}$ and k_2 = coefficient of thermal conductivity for shaft.

Averaging the temperature of the shaft along its length by introducing the coefficient $B^* = \frac{2}{l} \int_0^{l/2} B dz$, we obtain the shaft's mean surface temperature in the form

$$\vartheta_2^* = \frac{\alpha_t R_2^2 \omega J f p^*}{k_2} \varkappa^* \qquad (20.37)$$

where

$$\varkappa^* = \frac{\varphi_0}{\pi\lambda_2} B^*; \quad B^* \simeq 4 + \frac{B_1}{\sqrt{\lambda_2}}$$

The coefficient B_1 depends on the ratio of the journal diameter to the bearing length (Fig. 20.9). By equalizing the shaft and bush

mean temperatures in the contact area, ϑ_2^* and ϑ_1^*, we shall find the coefficient of the distribution of heat flows:

$$\alpha_t = \left(1 + \frac{\varkappa^* k_1 p^* R_1}{k_2 q_*}\right)^{-1} \qquad (20.38)$$

The sequence of temperature calculation in the plain bearing is: (1) compute the contact angle φ_0; (2) determine the coefficint of heat-flow distribution α_t from formula (20.38); and (3) compute the maximum and the mean bush temperature by formulas (20.34) and (20.36).

Criterion pv^*. The pv criterion, where $p = \frac{P}{2R_1 l}$ and v = shaft peripheral velocity, is a widely applicable characteristic of operating conditions for plain bearings. The allowable value of this criterion $[pv]$ is determined by the relationship [15]

$$[pv] = \frac{k_{ht}[\vartheta_1]}{2fR_1 l}$$

where k_{ht} = parameter of the bearing's heat transfer; $[\vartheta_1]$ = allowable excess temperature on the working surface of the bearing bush.

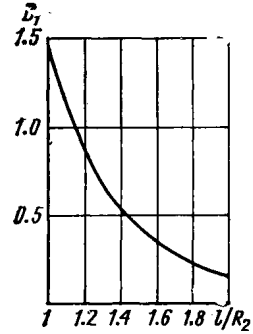

Fig. 20.9. Variation of coefficient B_1 with design dimensions of sliding bearing

Normal operating conditions for a plain bearing should meet the requirement

$$pv < [pv]$$

Typical temperature limits for some polymer materials used in plain-bearing applications are presented in Table 20.4. The heat

Table 20.4

Maximum operating temperatures for polymers used in plain bearings

Polymer	ϑ, °C	Polymer	ϑ, °C	Polymer	ϑ, °C
Polyamides	80-110	Polycarbonates	100-135	Silicone resins	145-200
Polyolefins	70-105	Siloxane elastomers	135-185	Hard fluorine-containing polymers	155-200
Epoxy resins	80-135				

* Increased load on the contacting surface leads to an increase in the number of contact spots rather than to a substantial change in pressure on an individual spot because the loading conditions on a single spot keep invariable. Increased sliding speed can give rise to change in the conditions of formation of the protective film on the contact spots because of the change of their temperature that leads to alterations in the structure of the surface layers. For these reasons, the pv criterion, though frequently applicable, should be used with caution. *Editors.*

transfer parameter depends on the design of the bearing unit. The most frequently used bearing designs are classified [15] into four groups (Fig. 20.10).

The group *I* incorporates bearings mounted in a heavy housing. Bushes held in components that are placed on an axle are referred to groups *II* and *III*; an example is idle gears. The removal of heat from the bearings in groups *I*, *II*, and *III* is effected mainly in a radial direction through the bearing-housing components. Group *IV*

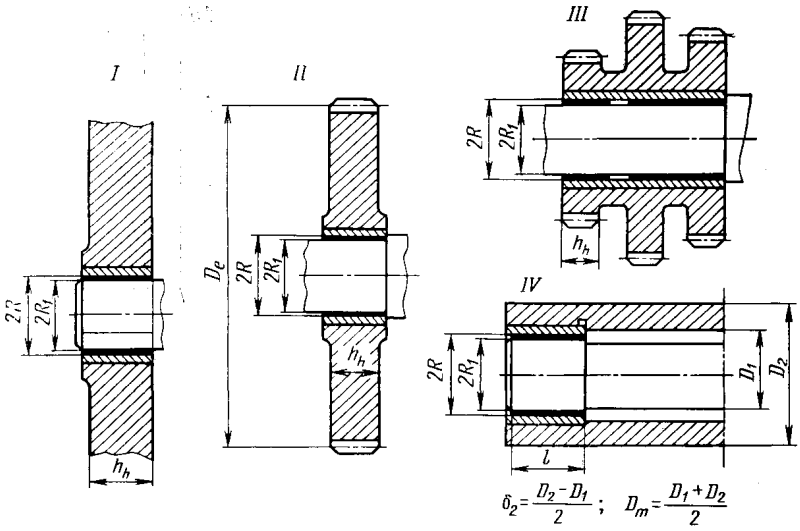

Fig. 20.10. Design classification of sliding bearings

includes bearing housings that have a small radial but a long axial extension. Heat is removed from such a bearing mainly axially.

In the general case, the heat transfer parameter k_{ht} is a sum of the parameters of heat removal through the bearing housing k_h and the shaft k_{sh}.

Depending on the design group, the heat-removal parameter is calculated by the formulas given in Table 20.5. In these formulas

$$A = 2\pi k_p h_h \frac{\gamma}{1-\gamma};$$

$$B_1 = 2\pi R k_{st} h_h m_h \psi; \quad C = H_h F_h \text{ and}$$

$$B_2 = \pi \sqrt{H_h k_{st} \delta_2 D_m (D_m + \delta_2)}$$

The coefficient k_φ allows for a non-symmetrical temperature field around the bearing periphery; at an invariably directed load k_φ = = 0.85 to 0.9 with a rotating bush (groups *I* and *II*) $k_\varphi = 1.0$,

Table 20.5

Formulas for calculation of k_h for plain-bearing design groups

I	*II* and *III*	*IV*
$k_h = \frac{k_\varphi - k_0}{\frac{1}{A} + \frac{1}{B_1}}$	$k_h = \frac{1 - k_0}{\frac{1}{A} + \frac{1}{B_1} + \frac{1}{C}}$	$k_h = \frac{k_\varphi - k_0}{\frac{1}{A} + \frac{1}{B_2}}$

$k_0 = \frac{\vartheta_0}{[\vartheta_1]}$; ϑ_0 = ambient temperature; h_h = wall thickness of the heat-removing housing; k_p and k_{st} = thermal conductivity coefficients for polymer and steel, respectively [W/(m·°C)]; H_h = coefficient of heat exchange between the housing and the environment [W/((m²·°C)]; F_h = heat dissipating area of the bearing housing; D_m and δ_2 = mean diameter and cross-sectional area (group *IV*);

$$m_h = \sqrt{\frac{2H_h}{k_{st}h_h}}$$

$$\psi = \frac{J_1\left(\frac{m_h D_e}{2}\right) K_1(m_h R) - J_1(m_h R) K_1\left(\frac{m_h D_e}{2}\right)}{J_0(m_h R) K_1\left(\frac{m_h D_e}{2}\right) + J_1\left(\frac{m_h D_e}{2}\right) K_0(m_h R)}$$

where $J_0(z)$, $J_1(z)$, $K_0(z)$, and $K_1(z)$ = Bessel's functions of imaginary argument.

The parameter of heat transfer through the shaft is computed by the following formulas. If the shaft may be considered infinitely long

$$k_{sh} = \pi \sqrt{2H_2 k_{st} R_2^3}$$

For the shaft of a limited length L

$$k_{sh} = \pi \sqrt{2H_2 k_{st} R_2^3} \tanh(m_{sh} L)$$

Here H_2 = coefficient of heat exchange between the shaft and the environment, W/(m²·°C); L = shaft length; $m_{sh} = \sqrt{\frac{2H_2}{k_{st} R_2}}$.

20.1.5. Geometric Relationships

The dimensions of metal-fluoroplastic strip are given in Volume 1, and those of bearing bushes made of it, in Table 20.6.

The wall thickness for polyamide bearing bushes is chosen from the following range in mm:

Shaft diameter	10-18	18-30	30-40	40-50	50-65	65-80
Bush wall thickness	0.8-1	1.0-1.5	1.5-2.0	2.5-3.0	3.0-3.5	3.5-4.0

Table 20.6

Bearing bushes from metal-fluoroplastic strip (dimensions, mm)

Inner diameter	Outer diameter	Length	Inner diameter	Outer diameter	Length
10	13	10-12-16	30	33	20-25-32-40-50
12	15	10-12-16-20	32	37	
15	18	10-12-16-20-25			
16	19	10-12-16-20-25	36	41	25-32-40-50
			40	45	32-40-50-60
18	21		55	60	32-40-50-60-65-70
20	23				
22	25	16-20-25-32-40			
25	28				

Note. Tolerances on inner and outer diameter are A_3 and $\Pi_p I_3$, respectively.

The amount of interference for pressing the bush into the housing is chosen according to the relationship Δ_i = (0.03 to 0.05) D_h, where D_h = housing seat diameter, and the radial clearances in the bearing are chosen according to the relationship ε = (0.005 to 0.015) R_2.

The dimensions of graphite bush bearings are presented in Table 20.7.

Table 20.7

Graphite bush bearing (dimensions, mm)

Shaft diameter	Radial clearance	Wall thickness	Shaft diameter	Radial clearance	Wall thickness
Up to 10	0.005-0.015	2	Over 35 to 70	0.04-0.07	6-8
			Over 70 to 100	0.06-0.08	10-12
Over 10 to 20	0.01-0.03	3-5	Over 100 to 150	0.1-0.2	12-18
Over 10 to 35	0.03-0.05		Over 150 to 200	0.2-0.3	18-25

20.2. HYDRODYNAMIC BEARINGS

20.2.1. Classification, Form Errors, and Operating Conditions

Two types of hydrodynamic bearings have found the most extensive use: journal bearings, in which the load is perpendicular to the rotation axis, and thrust bearings, which are loaded along (parallel) to the rotation axis.

Journal bearings are made in the form of a solid bush (sleeve) or a split bush supporting the shaft journal.

Thrust bearings either may form a joint of a plate with the end face of the shaft or the bearing may incorporate many self-aligning pads forming something like a split ring.

By the type of loading, bearings fall into three categories: the first, taking a constant-magnitude load directed invariably with respect to the stationary component of the sliding pair; the second supports a constant load with an orientation invariable relative to the rotational component of the sliding pair (that is, the load rotates together with this component), which occurs in loading by the centrifugal force; and the third category is subjected to a complex-type of loading sometimes referred to as dynamic, in which momentary loads are variable both in magnitude and direction.

The load-carrying capacity of the lubricant film, that is the ability of hydrodynamic bearings to support and carry load through developing a lubricant pad (the hydrodynamic wedge) that separates the mating surfaces, can arise only if the following conditions are met: (1) the rubbing surfaces move relative to each other; (2) there is a viscous liquid or gas between the surfaces; and (3) the shape of the mating surfaces is such as to cause the viscous fluid to enter the narrowing space formed by the rubbing surfaces.

The purpose of the calculation of hydrodynamic bearings is to determine two characteristics: first, the minimum value of thickness of the lubricant film that must separate the mating surfaces in the most severe operating conditions, and the second, the maximum temperature of the load-carrying lubricant film.

The minimum thickness of the carrying lubricant film must be sufficient to exclude the contact of the sliding surfaces during overloading and also to exclude the jamming of the lubricant-contaminating particles whose size exceeds the limits permissible for a given type of joint.

The maximum temperature of the lubricant film must be lower than the temperature limit proper for the combination of the antifriction lining, the mating part material, and the lubricant.

Experience suggests the conclusion that with well-filtrated mineral oils operating at sliding speeds up to 20 m/s, the allowable temperature should not exceed 122°C for babbitt Б83, 160°C for lead bronze, and 200°C for antifriction aluminium alloys.

Synthetic metal-ceramic materials containing fluoroplastic can safely work at temperatures up to 250°C with a heat-resistant lubricant.

Engineering calculations of hydrodynamic bearings are based on the assumption that the mating surfaces of the journal and the bearing bush or the thrust plate and the shaft collar are ideally round or flat.

The effect that form and position inaccuracies have on the design parameters of a sliding pair should be estimated with respect to the operative geometric condition of the parts rather than their preassembled condition. For instance, the cylindrical working surfaces of bearing liners deliberately bored to an oval or elliptical cross-

section may not be considered faulty if the deformations arising in operation cause the oval or ellipse to take a circular shape, whereby surfaces of the liner and the journal mate correctly.

The most harmful geometric form and position inaccuracies for thrust bearings are out-of-flatness of the working surfaces and out-of-squareness of the bearing plate and the collar of the shaft to its rotational axis; for journal bearings such errrors are misalignment of axes in the bearing bush and the shaft journal, radial runout of journals in a multi-journal shaft, and misalignment of bore axes in crankcase bearings.

Any deterioration in the shape and position of the mating surfaces during operation is undesirable and must be prevented.

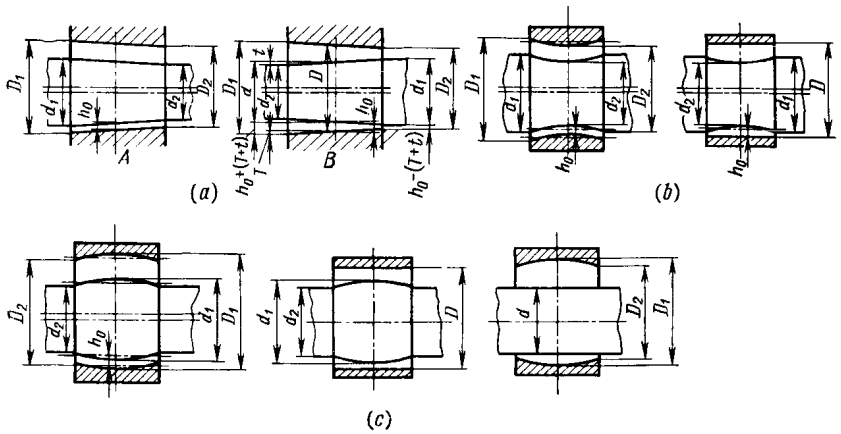

Fig. 20.11. Equivalent surfaces for geometric form errors
(*a*) taper; (*b*) bellmouth; (*c*) barrel

An antifriction lining runs in easily; for this reason, the manufacturing inaccuracies of the surfaces lined with soft antifriction materials do not have such adverse effect as the inaccuracies of hard-material surfaces.

In calculation of hydrodynamic bearings, geometrically true cylinders are substituted for the actual surfaces having form errors (such as taper, barrel, or bellmouth). For instance, instead of a tapered bore and journal, calculation is made for cylindrical surfaces with the diameters D and d for the bearing bore and the journal, respectively (Fig. 20.11).

The dimensions of these equivalent surfaces are then taken as the base for determining the minimum design thickness of the lubricant film.

Corrective factors allowing for the form errors are subsequently introduced.

The value of the coefficient λ which allows for the running-in capacity of the bearing liner surface is 1.0 for steel and bronze, 0.5 for babbitt, and 0.25 for metal-ceramics containing fluoroplastic.

The correction for non-parallelism or misalignment of axes of the bearing and the journal is given by

$$\Delta h_{np} = \lambda s \frac{l}{2B}$$

here, λ = coefficient allowing for running-in capacity of the sliding component; s = mutual departure of axes measured at a distance B (Fig. 20.12).

The correction for the deflection of the shaft section disposed between the support points (Fig. 20.13)

$$\Delta h_{df} = \lambda \frac{f_{df}}{2}$$

where f_{df} = magnitude of deflection of the journal or bore over the bearing length.

The correction allowing for a decrease in the minimum lubricant-film thickness due to misalignment or runout of journals on a multi-

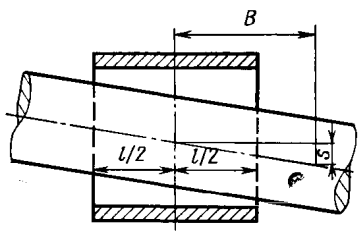

Fig. 20.12. Parallel misalignment of bearing and shaft axes

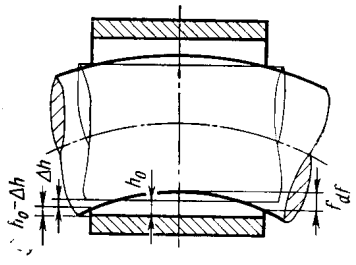

Fig. 20.13. Shaft deflection

support shaft and bearing-bore axes should be determined depending on the stiffness of the mating parts, the direction of journal eccentricities relative to the centrifugal component of load, and the direction of eccentricities of the bearing axes with respect to the stationary component of load.

The measurement and calculation of these quantities during assembly is difficult; for this reason, use is made of an approximate method of determining the correction for the runout between two adjacent journals R_j and bearing-linear axes R_b in the most unfavourable combination

$$\Delta h = \frac{R_j}{2} + \frac{R_b}{2}$$

It should also be kept in mind that in case the sum of the runouts of a journal and the mating bearing is larger than the diametrical clearance Δ, the journal will necessarily deform in rotation; therefore,

$$\Delta > R_j + R_b$$

The sum of the ovalities of a journal and the bearing bore must be, first, smaller than the minimum diametrical clearance, and, second, smaller than half the maximum clearance.

For thrust bearings, the main mating error is the out-of-squareness of the runner and the bearing pads to the shaft axis of rotation:

$$\Delta h_{os} = \lambda_1 os_1 + \lambda_2 os_2$$

where os_1 and os_2 = respective out-of-squareness values for the runner and the bearing pads measured at extreme points.

The surface roughness of a steel bearing component operating on an antifriction lining should be taken such as has developed in service because even a very carefully processed and polished surface develops a surface roughness* proper to the operating conditions of the given sliding pair; this steady-state roughness will be coarser than the initial one with finely machined surfaces, and finer with more coarsely machined surfaces.

For finely ground steel shaft journals of a conventional design operating under average service conditions with a mineral-oil lubrication, the steady-state surface roughness may be assumed to be 0.6 to 1.3 μm R_{max}.

The value of the minimum thickness of the operative film can be expressed as

$$h_{op} = h_0 - (\Delta h_g + R_{max})$$

where h_0 = minimum design value of the lubricant film thickness; Δh_g = correction allowing for geometric form and position errors of the sliding pair, including deflection.

The allowable minimum operative thickness of the lubricant film cannot be constant and identical for all types of machinery. It is established for a specific bearing application, depending on the materials of the sliding pair, dimensions of its components, operating conditions, and quality of manufacture.

Experience in troubleshooting machine bearings has shown that the minimum thickness of the operative lubricant film under the most severe operating conditions should be over 2 μm.

The minimum lubricant film thickness for babbitt-lined thrust bearings of the 2nd accuracy class is determined from empirical rules that establish the value of the sought parameter depending on the diameter (D) of the bearing disc.

With small (20 to 200 mm) outside diameters of the bearing disc, $h_{op} = 3.8 + 0.21D^{3/4}$ μm, and with large diameters (300 to 5000 mm), $h_{op} = 15 + 5 \times 10^{-3}D$ μm; here D is expressed in millimeters.

Polymer-metal-ceramic antifriction materials present no hazard of temporary worsening of bearing operation. Therefore a factor of 0.65 may be introduced into the above formulas.

---

* The choice and prediction of the value of steady-state roughness, that is, roughness that duplicates itself in the process of wear is described in detail in Ch. 2.

20.2.2. Design of Thrust Bearings for Maximum Lubricant-Film Load-Carrying Capacity

In design of a tilting-pad thrust bearing, it is necessary to find an optimum position of the fulcrum point (a spherical or a knife-edge supports) about which the pads will tilt, and an optimum relation between the dimensions of the pads [9].

The optimum can be obtained on condition that the fluid-film friction holds with regard to three parameters: (1) the minimum thick-

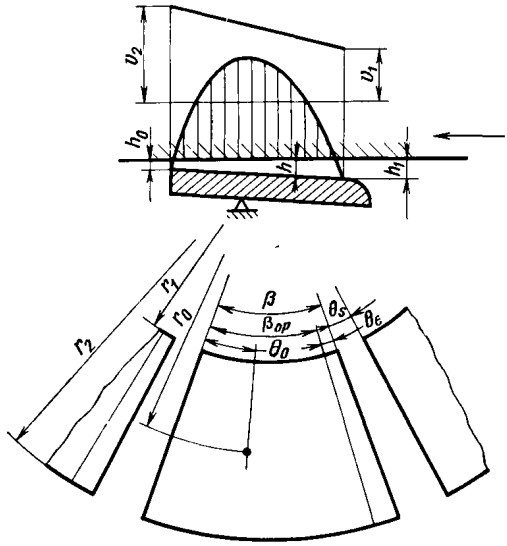

Fig. 20.14. Design diagram for axial (thrust) bearing

ness of the load-carrying lubricant film; (2) the minimum frictional losses; (3) the minimum heating of the load-carrying film.

Described below is a design method that allows the lubricant film of a maximum load-carrying capacity to be obtained, which is vital for compact, heavily loaded machinery.

The basic data for the design calculation are (Fig. 20.14) the total load on the thrust bearing (P), the angular sliding velocity ω, the inner radius (r_1) of the pads, the physico-mechanical properties of the lubricant fluid, the lubricant temperature (ϑ_1) in the space between the pad and the collar near the pad's entry edge; the cooling conditions of the bearing housing and the thrust collar; and the materials of the sliding-pair components.

The degree in which the process is non-isothermic is assessed by the coefficient α. The physico-mechanical properties of lubricant

are characterized by the coefficient α_1 [8]:

$$\alpha_1 = \frac{\ln \frac{\eta}{\eta_m}}{\vartheta_m - \vartheta}$$

$$\alpha = \alpha_1 \Delta\vartheta_{lb}$$

where η = local value of dynamic viscosity of the load-carrying film, kgf·s/m^2; η_m = value of dynamic viscosity related to the mean temperature of the load-carrying film; kgf·s/m^2; $\Delta\vartheta_{lb}$ = heating of lubricant in the load-carrying film, °C; ϑ_m = mean temperature of the load-carrying film;

$$\vartheta_m = \vartheta_1 + \frac{\Delta\vartheta_{lb}}{2}$$

Each pad of the thrust bearing has an entry edge (see Fig. 20.14). The tangential extension of the entry edge

$$\theta_l = p\beta$$

where β = centre angle of the pad with an entry edge; p = proportionality factor (the recommended value of p is 0.10).

The pads are divided with between-pad spaces whose inner peripheral extension is

$$\theta_s = s\beta$$

where s is a factor usually taken to be 0.15 to 0.25.

Assuming a uniform distribution of load among the pads, we shall find the fraction of load alloted to each pad

$$P_i = \frac{P}{i}$$

where i = number of pads.

It is advisable to start the calculation by specifying the value of p_m, the mean pressure on the working surface of the pad. The minimum thickness and maximum temperature of the oil film should then be found from the pressure p_m, and by changing the latter, the appropriate correction should be introduced.

Under these conditions, the outside radius r_2 of the pad will be determined regardless of the number of pads, namely: with the entry edge on one side

$$r_2 = \sqrt{r_1^2 + \frac{P}{\pi p_m} \frac{1+s}{1-p}}$$

and with the entry edges on both sides, made for bi-directional rotation

$$r_2 = \sqrt{r_1^2 + \frac{P}{\pi p_m} \frac{1+s}{1-2p}}$$

The radii of r_2 and r_1 being determined, the bearing ring should be broken into load-carrying sections, that is pads.

An optimum film load-carrying capacity is ensured with the radial-to-mean tangential dimension ratio of the pad as shown in Fig. 20.15

$$D = \frac{2(1-z)}{\beta_{op}(1+z)}$$

Here, $z = r_1/r_2$ = pad's inner-to-outer radius ratio; β_{op} = centre angle of the pad's working portion (without the entry edge).

The temperature conditions of the frictional process are stabilized when the amount of heat Q_f generated from the resistance to sliding caused by the lubricant film is equal to heat Q_{lb} removed by the lubricant escaping through the clearance along the periphery of the pad and heat Q_a dissipating into the ambience, that is

$$Q_f = Q_a + Q_{lb}$$

or, else, when

$$yQ_f = Q_{lb}$$

The value of the coefficient y allowing for the heat resulting from friction and removed by the lubricant through the clearances along the pad's periphery is determined by the bearing' design and operating conditions.

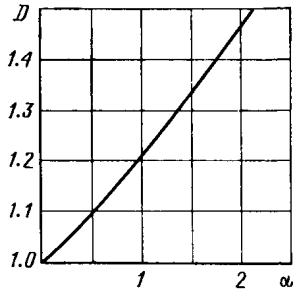

Fig. 20.15. Optimum values of parameter D as dependent on coefficient α allowing for non-isothermal conditions

The sequence of calculation on the basis of the above data should be as follows. First, we assign a likely amount of growth in the temperature $\Delta\vartheta_{lb}$ of the load-carrying film, and also find the value of this growth analytically from the heat balance equation. Then comparing the assigned and the calculated values of $\Delta\vartheta_{lb}$, we make re-calculation to ensure that these values coincide.

From the specified values of $\Delta\vartheta_{lb}$ and ϑ_1 we determine the mean temperature of the load-carrying film, which allows the value of the coefficient α_1, and, whence, the value of coefficient α to be found.

Next we determine the appropriate value of the parameter D for the obtained value of α, using the curve in Fig. 20.15, and, further, find a tentative value of the centre angle for the working portion of the pad, appropriate for the given conditions

$$\beta_{t,\,op} = \frac{2(1-z)}{(1+z)D}$$

The tentative value of the centre angle must suit the number of pads; this should be a whole and, preferably, even number in order to facilitate the balance of the thrust collar.

Now we determine the tentative number of pads, close to an optimum one, from the expression

$$i_t = \frac{2\pi(1-p)}{\beta_{t,\,op}(1+s)}$$

Rounding off the obtained figure to a whole even number, we find the actual number of pads i, and from the latter, the actual tangential extension of the pad's working portion

$$\beta_{op} = \frac{2\pi}{i} \cdot \frac{1-p}{1+s}$$

Allowance should be made for some departure from the specified value of the mean pressure, which has occurred in refining the number of pads:

$$p_m = \frac{p_t}{A_{op}}$$

where A_{op} = working surface area for a single pad.

Now we ascertain whether our selection of the value of $\Delta\vartheta_{lb}$ has been correct.

It has been established [9] that

$$\Delta\vartheta_{lb} = 2.34 \times 10^{-2} y \xi C_{t\alpha} \frac{p_m}{c\gamma} \text{ °C}$$

where ξ = coefficient allowing for disturbances in the current process, which result in higher resistance to rotation and, consequently, higher generation of heat due to friction; c = specific heat of lubricant, kcal/(kg·°C); γ = density of lubricant, kg/dm^3; p_m = pressure, kgf/cm^2.

With the use of mineral oils having an average value of viscosity at an average sliding speed of about 20 m/s in average cooling conditions of the bearing housing, the value of y can be taken to be from 0.85 to 0.90.

The coefficient ξ allows for departure of the bearing conditions in the load-carrying film from ideal ones. The value of this coefficient depends primarily on the extent to which the harmful turbulence arising in the between-pad space and leading to saturation of the lubricant by air is neutralized and to which the between-pad space is cleaned of the used lubricant; it also depends on the bearing design and stiffness; and on the running-in capacity of the sliding components.

The values of the coefficient ξ will vary with the operating conditions, dimensions and quality of manufacture of the thrust bearing, and should therefore be established depending on bearing applications.

Where the area of the pad is near to 400 cm^2 and the mean pressure is about 70 kgf/cm^2, the value of ξ comes up to 1.3. In lighter service conditions, it ranges from 1.1 to 1.2.

The value of the coefficient $C_{t\alpha}$ can be obtained from the curves shown in Figs. 20.16 and 20.17. This provides for the first variant of design for heating $[\Delta\vartheta_{lb}]_d$ of the load-carrying film of lubricant.

As a rule, the result of this variant shows no coincidence with the initially selected value of $[\Delta\vartheta_{lb}]_d$.

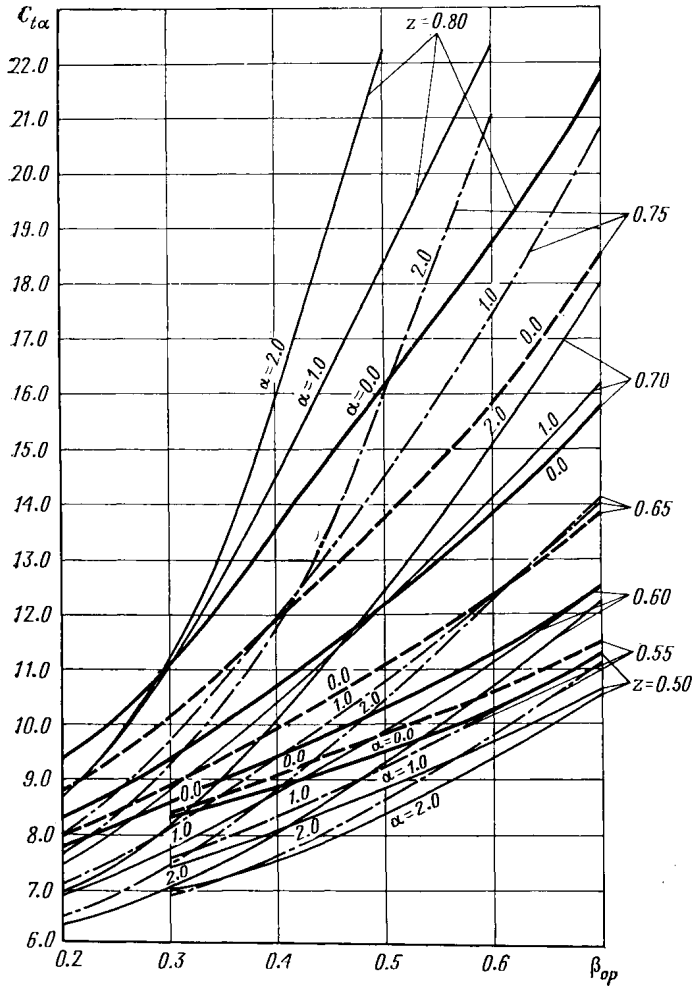

Fig. 20.16. Values of coefficient $C_{t\alpha}$ over the range of $\alpha = 0$-2.0 as a function of tangential length β_{op} of pad's operating portion

By the assumed and the calculated values of $\Delta\vartheta_{lb}$ obtained from the two variants of calculation, a graph can be plotted (Fig. 20.18), in which the assumed value, $[\Delta\vartheta_{lb}]_a$, is plotted along the abscissa and the design value, $[\Delta\vartheta_{lb}]_{ot}$, is plotted along the ordinate. The points thus obtained are connected to give curve *1*. A straight line of the assumed values of $\Delta\vartheta_{lb}$ (curve *2*) is then superimposed on curve *1*. The intersection of the two lines will indicate the condition under which the assumed and the design values coincide.

Having found in this way the bearing temperature conditions, their non-isothermal character, and the optimum number and dimensions of bearing pads, we determine the values of the remaining parameters.

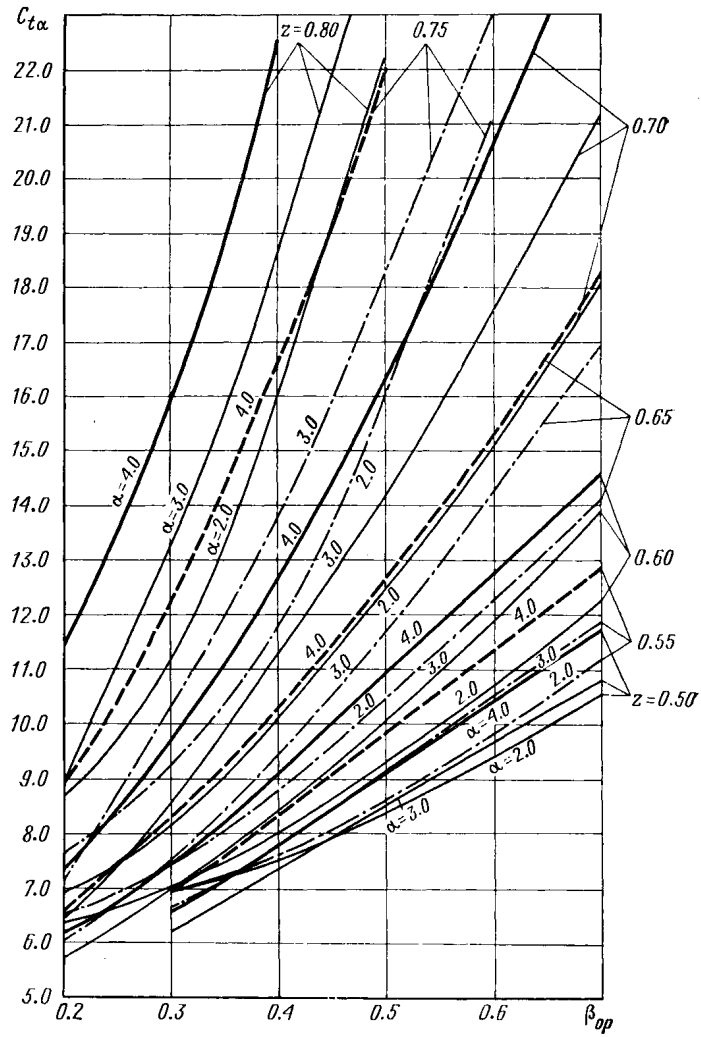

Fig. 20.17. Values of coefficient $C_{t\alpha}$ over the range of $\alpha = 2.0\text{-}4.0$ as a function of tangential length β_{op} of pad's working portion

The minimum thickness (in μm) of the load-carrying film

$$h_0 = \frac{r_2}{C_{h\alpha}} \sqrt{\frac{\eta_m \omega}{P_m}}\, 10^2$$

or

$$h_0 = \frac{e^{-\frac{\alpha}{4}}}{zC_{h\alpha}} r_1 \sqrt{\frac{\eta_{in}\omega}{p_m}}\, 10^2$$

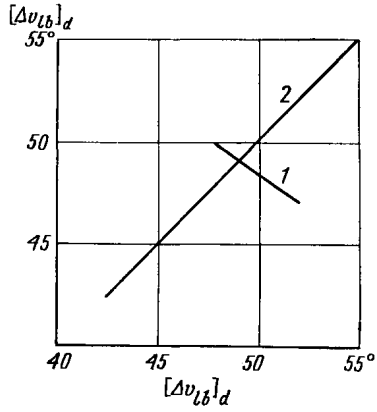

Fig. 20.18. Graphical determination of heating of load-carrying oil film

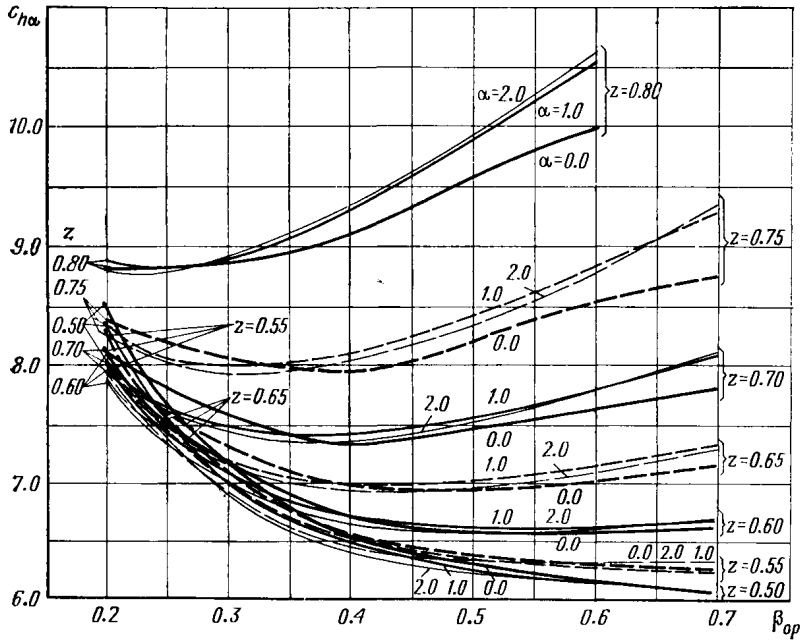

Fig. 20.19. Values of coefficient $C_{h\alpha}$ over the range of $\alpha = 0$-2.0

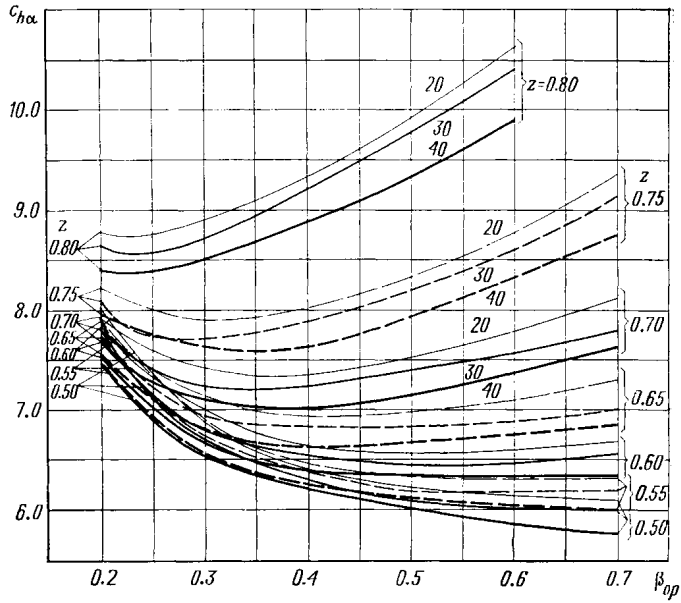

Fig. 20.20. Values of coefficient $C_{h\alpha}$ over the range of $\alpha = 2.0\text{-}4.0$

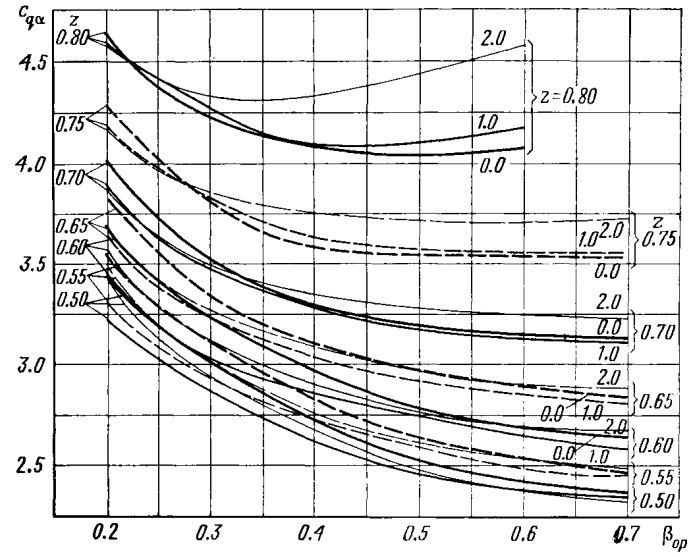

Fig. 20.21. Values of coefficient $C_{q\alpha}$ over the range of $\alpha = 0\text{-}2.0$

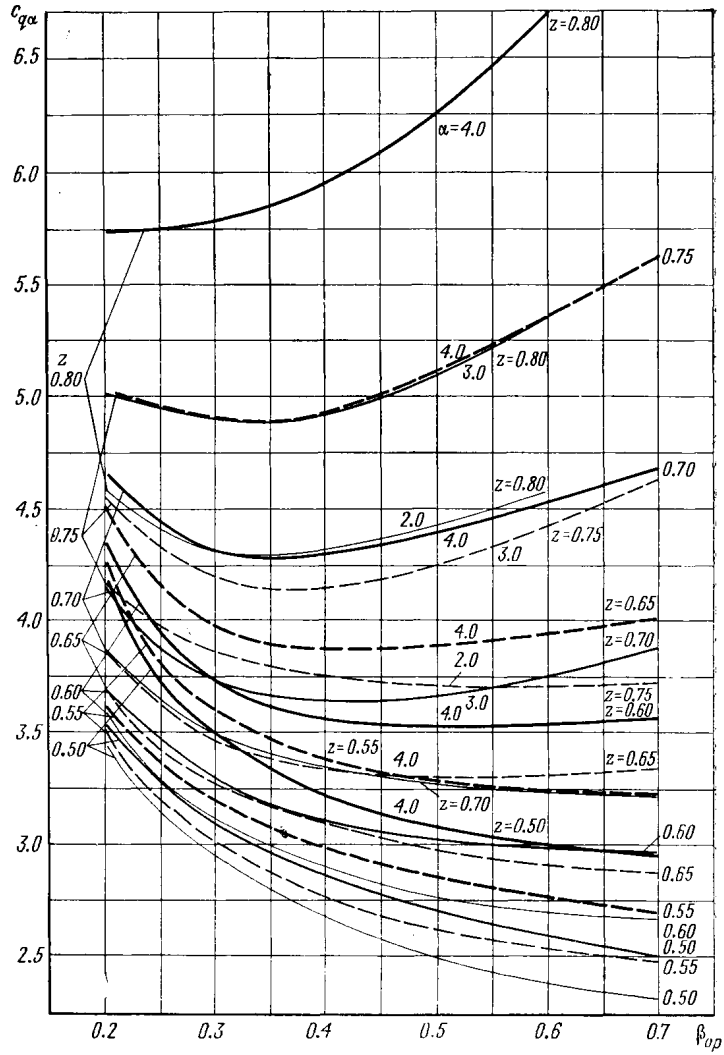

Fig. 20.22. Values of coefficient $C_{q\alpha}$ over the range of $\alpha = 2.0$-**4.0**

where $C_{h\alpha}$ = dimensionless coefficient whose values are given in Figs. 20.19 and 20.20; the dimensions of the other quantities are: r in cm; η_{in} in kgf·s/m²; ω in rad/s; and p_m in kgf/cm².

The heat-generation intensity [kcal/(kgf·s)] of the actual working process in the load-carrying film

$$\xi q_{f\alpha} = 2.34 \times 10^{-7} \xi C_{q\alpha} \omega r_2 \sqrt{\frac{\eta_m \omega}{p_m}}$$

or

$$\xi q_{f\alpha} = 2.34 \times 10^{-7} \xi \frac{C_{q\alpha}}{z} e^{-\frac{\alpha}{4}} \omega r_1 \sqrt{\frac{\eta_{in} \omega}{p_m}}$$

where $C_{q\alpha}$ = dimensionless coefficient, whose values are given for an ideal process (without regard to disturbances induced by the bearing design and operating conditions) in Figs. 20.21 and 20.22.

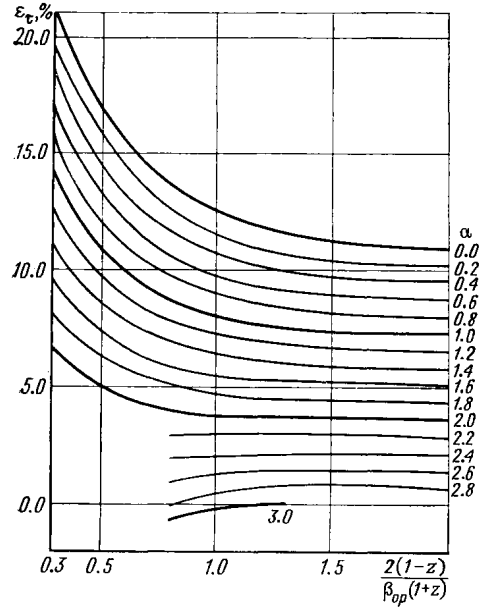

Fig. 20.23. Tangential eccentricity of tilting-pad pivot for maximum load capacity of oil film

The maximum temperature of the load-carrying film

$$\vartheta_2 = \vartheta_1 + \Delta\vartheta_{lb}$$

The values of tangential offset ε_τ of the pivot (or spherical support) for the tilting pad required to achieve the maximum load-carrying capacity of the lubricant film, are given in Fig. 20.23.

$$\varepsilon_\tau = \left[0.5 - \frac{\theta_0}{\beta_{op}}\right] 100\%$$

For ensuring the minimum specific heat evolution and minimum heating of the load-carrying film, the tangential eccentricity values presented in Fig. 20.23 should be increased.

The radial coordinate of the centre of hydrodynamic pressure developing in the load-carrying film (the centre of the spherical support), r_0, or, in relative terms $C_0 = \frac{r_0}{r_1}$ can be determined from the expression $\psi = \frac{z(C_0-1)}{1-z}$ whence $C_0 = \frac{\psi(1-z)}{z} + 1$; the values of the coefficient ψ are given in Fig. 20.24.

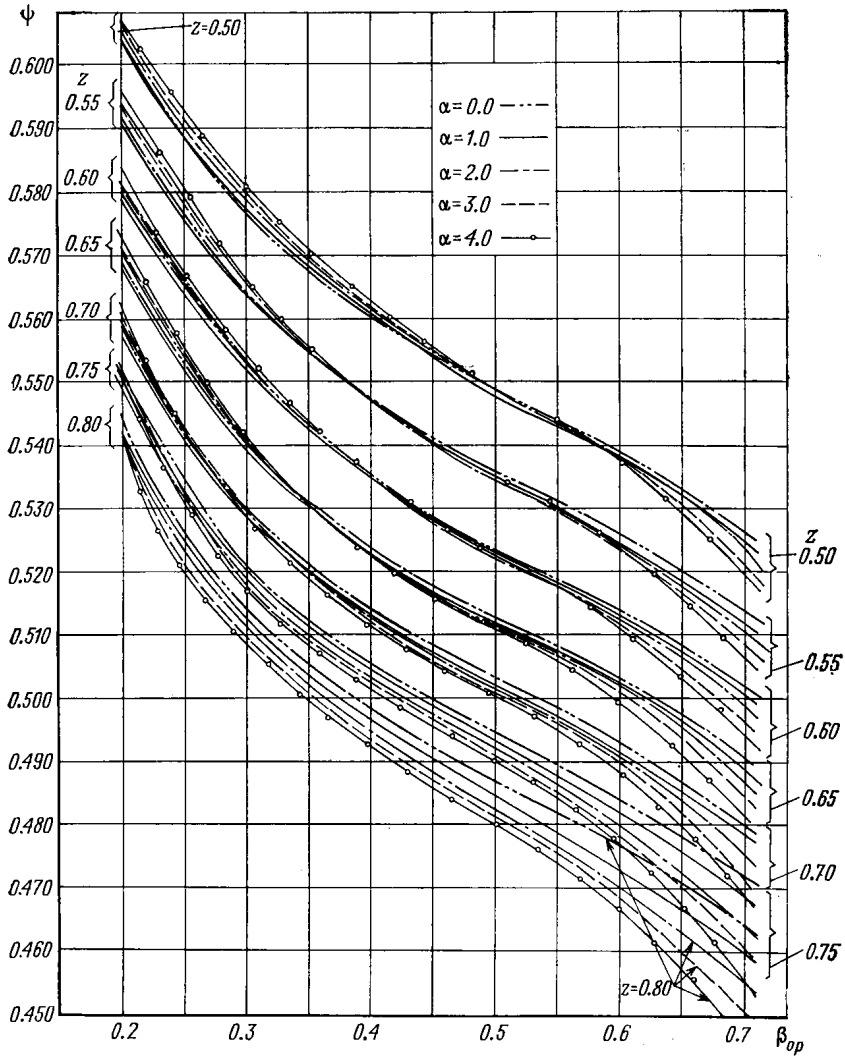

Fig. 20.24. Values of coefficient ψ

The maximum of the temperature field set up near the pad's working surface is disposed at an angle $\theta_{mf} = (0.28 \text{ to } 0.24)\,\beta_{op}$.

Then, the highest temperature near the working surface in steady-state thermal conditions

$$\vartheta_{mf} = \vartheta_1 + \left(1 - \frac{\theta_{mf}}{\beta_{op}}\right) \Delta\vartheta_{lb}$$

20.2.3. Design of Journal Bearings

Let us consider the most frequent case of loading by a force whose magnitude and direction are constant [10].

Two regions arise in the bearing clearance (Fig. 20.25): in the first, the lubricant film is unbroken and in the second, the film is broken up into separate flows. The first region of the lubricant flow is capable of carrying load and is therefore referred to as the loaded one, whereas the second region cannot carry load and is referred to as the unloaded one.

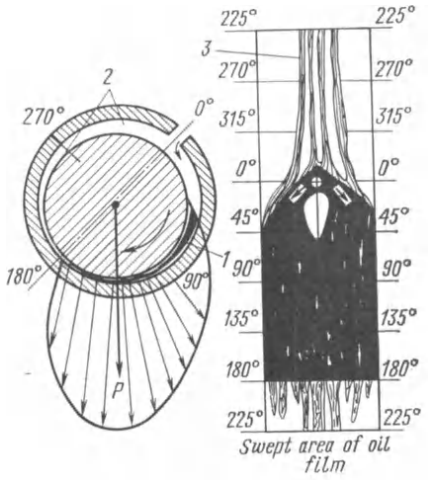

Fig. 20.25. Operating diagram for hydrodynamic journal bearing
1 — oil-film load-carrying region; *2*—unloaded region; *3*—used oil

The initial formation of the loaded region is determined by the location of the oil-feeding means. When fed through a hole (usually disposed in a diametrical section), the oil flow moves radially along it and then, running against the mating-part surface, turns aside by almost 90°. The flow is not only carried by the rotating shaft tangentially, but also spreads toward the end faces squeezing out the exhausted oil that has passed the loaded region of the lubricant film.

As the oil flow moves tangentially, pressure grows inside the film up to a maximum and then goes down to zero at the boundary of the loaded region. Here air penetrates the lubricant which has lost the capacity of filling the clearance growing in a tangential direction. Some underpressure develops in the available space, into which the atmospheric air breaks, dividing the oil flow into separate portions.

The gases given off by heated used oil also contribute to occurrence of breaks in the flow.

There is an optimum location of the feed hole, at which, other conditions being equal, the lowest temperature and highest load-carrying capacity of the oil film can be obtained. This hole must be in the region of the most thick lubricant film.

When oil is force-fed, the angular extension of the load-carrying film depends on the location of the feed hole, the eccentricity of the journal in the bearing clearance, and the feed pressure; it decreases with a greater eccentricity, and increases with a growing oil-feed pressure.

Because of the difficulty of its analytical determining, the film extension can be taken equal to 130° for engineering calculations,

assuming that the journal bearing commonly operates at eccentricity ratios* $\chi = 0.7$ to 0.85, with the location of the oil-feed hole near to the optimum one, and at a feed pressure $p_{lb} = 2$ to 5 kgf/cm^2.

With the axes of the journal and the bearing being parallel, the variation of pressure within the oil film in an axial direction, is

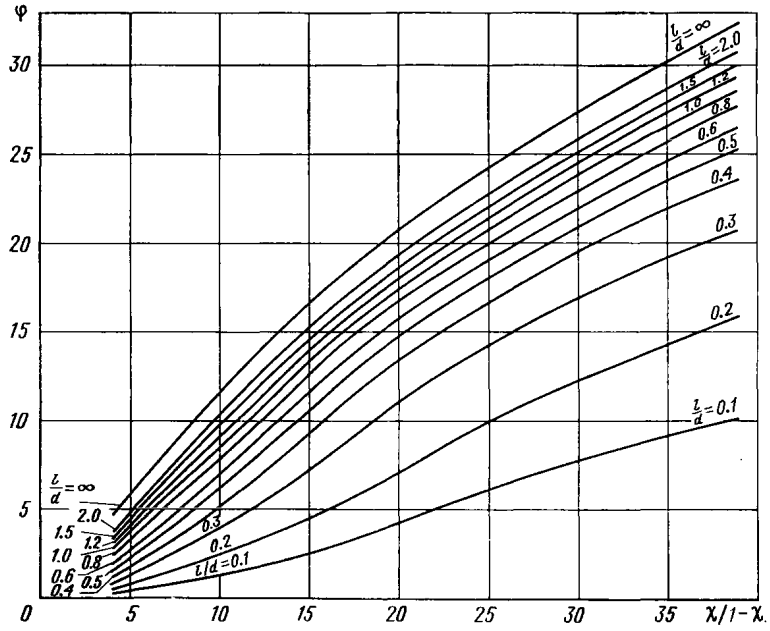

Fig. 20.26. Load coefficient *vs* eccentricity ratio

close to a parabola with an exponent of 2.2 to 2.3. The oil pressure is at a maximum in the central section of the load-carrying region of the bearing.

A mathematical analysis of the process occurring in the lubricant film has revealed a relation between the dimensionless parameter φ, referred to as the loading coefficient, which takes into account the load, design, and operating conditions of the bearing, and χ, which is the eccentricity of the journal in the bearing clearance.

$$\varphi = \frac{P_\alpha}{\omega \eta_m} \left(\frac{\Delta}{d}\right)^2 10^{-4} \qquad (20.39)$$

where Δ = diametrical clearance, μm; d = diameter of the journal, cm.

The value of φ being found, we determine the eccentricity ratio χ with the aid of the graphs given in Fig. 20.26, and, hence, the mini-

* The eccentricity ratio is the displacement of the shaft centre and the bearing-bore centre relative to the bearing clearance.

mum oil film thickness

$$h_0 = \frac{\Delta(1-\chi)}{2}$$

To determine viscosity included in the formula (20.39), it is essential to know the temperature conditions in which the bearing operates.

Friction processes in the loaded and the unloaded region of the oil film are markedly different, therefore the frictional heat evolution in these regions is considered separately.

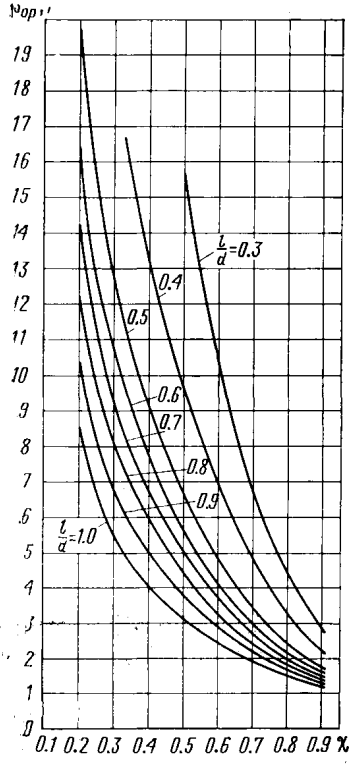

Fig. 20.27. Coefficient $\beta_{op,f}$ *vs* eccentricity ratio

Heat evolution (kcal/s) in the loaded oil-film area

$$Q_{f_{op}} = 1.17 \times 10^{-5}\, p_m d^2\, l\omega f_{op}$$

where f_{op} = operative value of the coefficient of friction effective in the loaded film area;

$$f_{op} = \xi\beta_{op,f}\left(\frac{\Delta}{d}\right)10^{-4}$$

here, ξ = coefficient allowing for departure of the operating process from an ideal one, and specifically for the extent to which the bearing is run in, the stiffness of the construction, and the materials of sliding pair; Δ, μm; l and d, cm, $\beta_{op,f}$ is the design value of the coefficient of friction in the loaded film region (Fig. 20.27).

The values of the coefficient ξ as dependent on the eccentricity are given in Fig. 20.28. They are found experimentally for a well run-in pair of materials (hard steel on lead bronze) used in a bearing construction of a very low stiffness (the conrod bearing in an aircraft twin engine), subjected to loading with a force of a variable magnitude and direction. These values should be looked upon as the deviation limits for the most unfavourable combinations of a non-rigid structure with a pair of mating materials that are most sensitive to departure from an optimum geometric form. With the same materials of the sliding pair, but a rigid bearing construction, the value of this coefficient is close to unity over the whole range of variation of the eccentricity.

Heat evolution in the unloaded area of the oil film depends on the concentration of the local oil flows divided by flows of air, on their

direction, and on the turbulence of their motion; therefore, this kind of heat evolution Q_{fc} (kcal/s) is related to the oil flow through the region considered within the range of $p_{lb} = 1$ to 10 kgf/cm^2;

$$Q_{fc} = \left[\varkappa + \frac{2.7 p_{lb}}{\gamma \Delta}\right] \frac{\eta_m M_2 d^2 \omega}{\Delta^2}$$

where $\varkappa$ = coefficient whose values are given in Fig. 20.29 for two types of structural stiffness: curve *1* for a very non-rigid (limiting) bearing construction and curve *2* for a very stiff construction; the dimensions of the quantities are: M_2, cm^3/s, p_{lb}, kgf/cm^2, η_m, kgf·s/m^2, d, cm, γ, kg/dm^3, Δ, μm, and ω, 1/s.

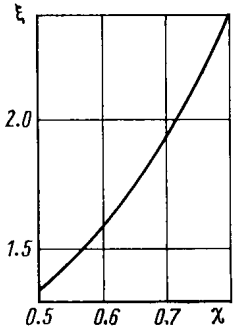

Fig. 20.28. Coefficient ξ *vs* eccentricity ratio

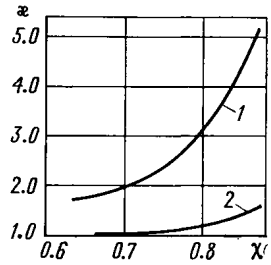

Fig. 20.29. Coefficient $\varkappa$ *vs* eccentricity ratio

The total heat evolution in the bearing due to friction is equal to the aggregate of heat evolutions in the loaded and unloaded regions of the oil film ($Q_f = Q_{f,ol} + Q_{fc}$).

In many applications, the journal bearing serves as a locating part. In such cases, the rotating shaft journal is provided with collars mating with the end faces of the stationary bearing bush to fix the shaft against axial displacements. The size of clearance between the bush ends and the shaft collar has a marked effect on the rate of oil flow through both regions of the film.

The escape of oil through the bearing's clearances is substantially affected by the stiffness of the bearing components because the load-induced deformations cause departure of the local film thickness from the design value.

The oil flow rate (cm^3/s) through the loaded film area is determined by the expression

$$M_1 = \varepsilon_{st} \xi_{ls} \xi_1 d^2 \omega \Delta$$

The values of the coefficient ξ_1 that apply to the ideal shape of the mating surfaces are given in Fig. 20.30.

Experiments with journal bearings having $l/d = 0.68$ at eccentricity values ranging from 0.5 to 0.84 resulted in the following values

of ξ_{st}: for a very rigid bearing $\xi_{st} = 1.0$, and for a bearing of a very low stiffness (the conrol bearing in an aircraft twin engine) $\xi_{st} = 0.4 + 0.11 \frac{\chi}{1-\chi}$.

With a longitudinal clearance equal to 5.7×10^{-3} of the journal diameter and a height of the shoulder of the locating collar equal to 0.1 of the journal diameter, the value of the coefficient $\xi_{ls} = 1.0$, and with a longitudinal clearance of 1.6×10^{-3} of the journal diameter, the same size of the collar shoulder, and the eccentricity ratio ranging from 0.5 to 0.84,

$$\xi_{ls} = 0.5 + 0.039 \frac{\chi}{1-\chi}$$

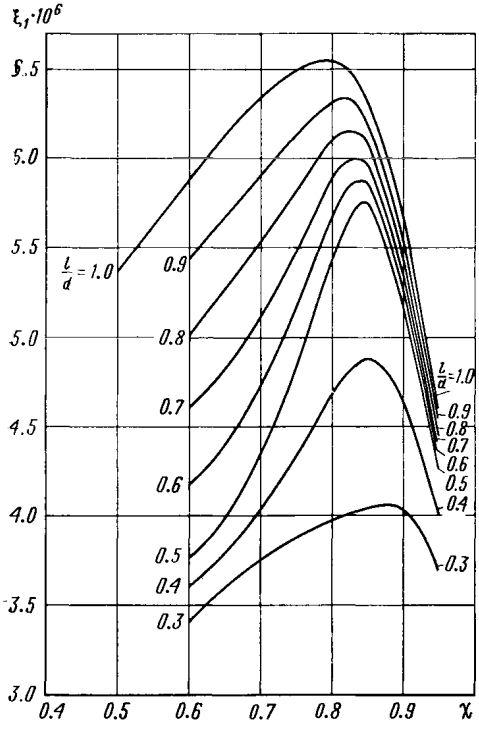

Fig. 20.30. Coefficient ξ_1 *vs* eccentricity ratio

With the oil-feed hole located in the favourable position or near to it (within $\pm 10°$), the hole being provided with a small chamfer (not larger than twice the hole diameter) or a groove at its outlet, the oil flow (cm^3/s) through the unloaded film region can be expressed as

$$M_2 = A \frac{p_{lb}\Delta^3}{\eta_m} \frac{a}{l}$$

here p_{lb} = pressure of the lubricant fed, up to 10 kgf/cm^2; d and l = diameter and length of the operative bearing length, cm.

For a simple type of loading (by a stationary or a centrifugal force), and with the oil-feed hole located close to the favourable position, the coefficient A is determined by the formula

$$A = k_a a_y (0.8v^{4/3} + 0.6)(1 - 0.98k_a\chi) 10^{-9}$$

where k_a = coefficient allowing for the structural stiffness: a_y = = coefficient governed by the amount of the axial clearance; v = = sliding speed up to 12 m/s; and $\chi = 0.5$ to 0.84.

Experiments conducted with a bearing having $l/d = 0.68$ within the eccentricity ratio of 0.5 to 0.93 gave the following values of the above coefficients. For a very stiff bearing construction $k_a = 1$, and

for the construction of a low stiffness (connecting rod in aircraft twin engines), $k_a = 0.9$.

With a longitudinal clearance equal to 5.7×10^{-3} of the journal diameter and a height of the collar shoulder of 0.1 of the journal diameter, the value of the coefficient a_y is 1.0, and for a longitudinal clearance of 1.6×10^{-3} of the journal diameter and the same height of the collar, $a_y = 0.54$.

The efficiency of heat removal by the oil escaping from the loaded and the unloaded region of the film is different.

The loaded region is supplied from the central area of the feed hole with fresh cool oil at a temperature ϑ_1. This oil has no enough time to get hot as it passes through the hole, and it is protected against mixing with the used oil by peripheral flows passing close to the hole walls.

During the passage through the loaded region, the oil gradually heats from the temperature ϑ_1 to the temperature ϑ_2 effective in the area of the minimum thickness of the load-carrying film.

Assuming a linear variation of temperature in the load-carrying film in a tangential direction, and allowing for unequal intensity of flow in different sections of the end faces, the amount of heat (kcal/s) removed by oil from the loaded film region can be expressed as

$$Q_{lb_1} = c\gamma M_1 \frac{\vartheta_2 - \vartheta_1}{2} 10^{-3}$$

where c = specific heat of oil, kcal/(kg·°C); γ = oil density at a temperature equal to the arithmetic mean of the incoming and outcoming oil temperatures, kg/dm^3; ϑ_2 = maximum oil-film temperature, °C; ϑ_1 = temperature of oil entering the feed hole, °C; M_1 = = oil consumption, cm^3/s.

Taking into account incomplete mixing of oil and its excess in the course of feeding, the amount of heat carried away by the oil exhausted from the unloaded bearing region can be given by

$$Q_{lb_2} = 0.8\, c\gamma M_2 (\vartheta_2 - \vartheta_1)$$

The dissipation of heat into the metal surrounding the bearing and the journal depends on the product design. Several heat flows from several sources usually pass over the housing walls, which makes an accurate calculation of the amount sought very difficult.

The total amount of heat (kcal/s) transferred into the metal of the bush and the journal is given by the expression

$$Q_0 = \alpha_0 \Pi d l$$

where α_0 = heat transfer coefficient, kcal/(s·cm^2); d and l = bearing dimensions, cm.

To a first approximation, the value of the heat transfer coefficient is

$$\alpha_0 = 4.7 \times 10^{-7} a (\vartheta_m - \vartheta_0)^{1.3}$$

where a = coefficient dependent on cooling conditions for the bearing housing, namely: $a = 1$ for still air around the housing, $a = 2$ for slightly circulating air; $a = 3$ for a fanned housing; ϑ_m = mean oil-film temperature; ϑ_0 = temperature of the atmosphere surrounding the bearing housing, °C.

The thermal balance equation has the form

$$Q_{f,\,op} + Q_{fc} = Q_{lb1} + Q_{lb2} + Q_0 \qquad (20.40)$$

Solution of the equation (20.40) will allow the value of ϑ_2 to be obtained, that is the value of the maximum temperature effective in the area of the minimum thickness of the load-carrying film.

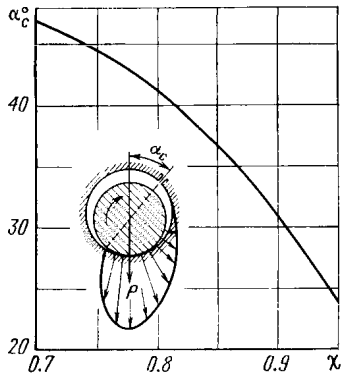

Fig. 20.31. Variation of attitude angle with eccentricity ratio

This equation is most convenient to solve graphically in a way similar to that described above, by specifying a value of $\Delta\vartheta_{lb}$ and seeking the conditions in which the thermal balance holds.

When the value of ϑ_2 is known, it is possible to find the mean temperature of the load-carrying film and the corresponding oil viscosity. The use of the formula (20.39) and the graphs given in Fig. 20.26 will then allow the minimum design value of the load-carrying film thickness to be obtained.

The optimum position for an oil-feeding hole is in the region where the oil film is the thickest, that is on the line connecting the centres of the bearing bush and the journal. Therefore the feed-hole location can be related to the direction of the main load (stationary or centrifugal).

The angle between the centre line (the optimum position of the feed hole) and the load vector is known as the attitude angle α_c. The values of this angle for an elementary type of loading (for instance, by a stationary or a centrifugal force) are given in Fig. 20.31.

20.2.4. Suggestions on Bearing Design

Non-rigid bearing constructions and faults of manufacture and assembly of the components give rise to detrimental dynamic deformations and considerable form and position errors. Hence, the need for larger initial clearances.

The temperature conditions of bearing operation depend to a considerable extent on the amount of clearance, namely, the temperature rises with smaller clearances.

Both theory and experience show that a 0.7 length-to-diameter ratio in a bearing is an optimum to achieve good operating conditions. This ratio can vary within 0.3 to 1.0 for different applications. If it is lower than 0.3, the load-carrying capacity of the oil film falls beyond permissible limits because of an extensive escape of oil through the bearing end faces. If the ratio exceeds 1.0, the mating surfaces are liable to come into local contacts at the ends of the bearing; such contacts disturb the cooling oil flows and thereby raise the operating temperature.

Poor bearing operation due to inadequate journal stiffness can be eliminated by machining the bore of the bush to the shape of a single-sheet hyperboloid.

Securing low temperature conditions is the main goal in designing bearings for severely-loaded modern machinery. This goal is achieved by reducing heat generation and controlling the heat flows arising from friction.

In order to reduce the generation of heat in friction, it is essential primarily to eliminate the local contacts of the operating surfaces, which are due to manufacturing inaccuracies and deformations caused by load, temperature, and inadequate assembly. It is also necessary to use a lubricant of a proper, not excessively high viscosity.

Heat flows are controlled by forming sufficiently intense and well directed flows of oil, which will remove heat primarily from the hot areas.

Increased oil flows can be obtained in three ways: (1) by the appropriate location of oil-feed holes; (2) by raising the oil supply pressure; and (3) by the application of oil of a reasonably low viscosity.

REFERENCES

1. Алексеев Н. М., Добычин М. Н. Определение контактных напряжений при внутреннем соприкосновении цилиндрических тел в условиях идеальной пластичности.— «Машиноведение», 1972, № 6, с. 55-60.
2. Бабешко В. А., Ворович И. И. К расчету контактных температур, возникающих при вращении валка в подшипнике.— «ПМТФ», 1968, № 2, с. 135-137.
3. Блюмен А. В., Харач Г. М., Эфрос Д. Г. Расчетная оценка интенсивности изнашивания и ресурса сопряжения вал — втулка с обратной парой трения.— «Вестник машиностроения», 1976, № 2, с. 29-32.
4. Ворович И. И., Александров В. М., Бабешко В. А. Неклассические смешанные задачи теории упругости. М., «Наука», 1974, 455 с.
5. Гафнер С. Л., Добычин М. Н. К расчету угла контакта при внутреннем соприкосновении цилиндрических тел, радиусы которых почти равны.— «Машиноведение», 1973, № 2, с. 69-73.
6. Добычин М. Н., Алексеев Н. М. Расчет несущей способности подшипников скольжения и вкладышей.— «Машиноведение», 1975, № 1, с. 107-114.
7. Добычин М. Н., Гафнер С. Л. Влияние трения на контактные параметры пары вал — втулка.— В сб.: Проблемы трения и изнашивания. Киев, «Техніка», 1976, с. 30-36.
8. Дьячков А. К. Расчет давлений в масляном слое подушек упорного подшипника при неизотермическом процессе.— «Машиноведение», 1966, № 2, с. 100-111.

9. Дьячков А. К. Оптимальные величины тангенциального эксцентриситета самоустанавливающихся подушек упорного подшипника.— «Машиноведение», 1974, № 2, с. 64-73.

10. Дьячков А. К. Подшипники скольжения жидкостного трения. ВНИТОМАШ. М., Машгиз, 1955, с. 1-151.

11. Ефимов А. Б., Малый В. И. О решении контактных задач металлополимерных подшипников.— Сб.: Исследование в области механических измерений. Труды ВНИИФТРИ. М., 1971, вып. 8 (38), с. 57-64.

12. Контактная задача для кольцевого слоя малой толщины.— «Инженерный журнал МТТ», 1966, № 1, с. 135-139. Авт.: В. М. Александров, В. А. Бабешко, А. В. Белоконь, И. И. Ворович, Ю. А. Устинов.

13. Коровчинский М. В. О некоторых вопросах эластореологии, имеющих приложение в теории трения.— Сб.: Трение и износ в машинах, т. XV. Изд-во АН СССР, 1962, с. 332-374.

14. Коровчинский М. В. Теоретические основы работы подшипников скольжения. М., Машгиз, 1959, с. 1-401.

15. Левин А. Л. Исследование трения и расчет подшипников скольжения из полимерных материалов. Автореферат диссертации. Ростов-на-Дону. РИИЖТ, 1975, 30 с.

16. Необердин Ю. А. Исследование контактных напряжений для прямых и обращенных пластмассовых подшипников скольжения. Автореферат на соискание ученой степени канд. техн. наук. Л. ЛТИ им. Ленсовета, 1973, 24 с.

17. Раевский А. И. Полиамидные подшипники. М., «Машиностроение», 1967, 140 с.

18. Расчет термоупругих контактных давлений в подшипнике с полимерным покрытием.— Сб.: Контактные задачи и их инженерные приложения. М., НИИМАШ, 1969, с. 214-220. Авт.: В. М. Александров, В. А. Бабешко, А. В. Белоконь, В. Е. Ковальчук, В. А. Кучеров, О. М. Пенин, Б. И. Сметанин.

19. Ремизов Д. Д., Власов В. И. Расчет несущей способности металлополимерного подшипника скольжения при невращающемся вале.— Сб.: Исследование и изыскание новых рабочих органов сельскохозяйственных машин. Вып. VIII. М., 1971, с. 38-43.

20. Hertz H. Über die Berühung fester elastischer Korper. Gesam. Werke. Bd. 1. Leipzig, 1895. S. 155.

Chapter 21

TRANSMISSIONS

21.1. GENERAL CONSIDERATIONS

The assessment of the performance of mechanisms is made with regard to their loading conditions, kinematics of contact, operating-temperature conditions, and variation of tribological characteristics. The initial stage of calculation should include the correct determining of the acting forces (with allowance for the process dynamics), rolling and sliding velocities, the actual temperature of the tribological unit (the finding of the mean temperature for the surfaces of the bodies coming into contact is desirable), and the temperature arising in the frictional contact area.

The structure, analysis, and functional characteristics of mechanisms, and the calculation of the acting forces and speeds are discussed in the literature on general engineering mechanics [1]. We shall concentrate, therefore, on the factors critical for the assessment of the frictional contact conditions in the most typical transmission mechanisms.

These factors are the contact pressures, the size of the contact areas and, in some cases, the amount of approach [18].

The main kinematic parameters that have influence on the character of friction, wear, lubrication, and the formation of heat in the load-carrying contact are the rolling and sliding velocities. The rolling, or sweep, velocity in rolling attended by sliding is taken to mean the sum of the velocities at which the contact line moves along the surfaces being in rolling contact. These surface velocities are designated in Fig. 21.1 as v_1 and v_2. The sliding velocity is equal to the vector difference of the surface velocities $\bar{v}_{sl} = \bar{v}_1 - \bar{v}_2$. The sweep velocity is $\bar{v}_{sw} = \bar{v}_1 + \bar{v}_2$; its magnitude determines the flow rate of lubricant in the contact area.

In many mechanisms the contact under load is characterized by a combination of rolling and sliding (toothed gearing, cam and friction drives, rolling bearings, and others). The effect of both sliding and rolling velocities on the friction and wear characteristics of the rubbing surfaces should be taken into account. In cam drives with a roller follower, for instance, the rolling and slidings velocities

are not difficult to determine from the angular velocity and the geometry of the components. With rotating gear wheels, the tooth flanks normally roll and slide, and pure rolling occurs at the pitch point only. Once the pitch point is passed over, the vector of the sliding velocity alters its direction. The rolling velocity of a point on each tooth flank is equal to the projection of the absolute velocity of this point onto the tangent plane. The tooth addendum is the leading surface and dedendum is the retarding surface. The frictional forces arising on the driving tooth are directed away from the pitch point, and those arising on the driven tooth, towards the pitch point.

The average sliding velocity in the contact area of a friction drive or between a ball (or roller) and the ring in a rolling bearing does

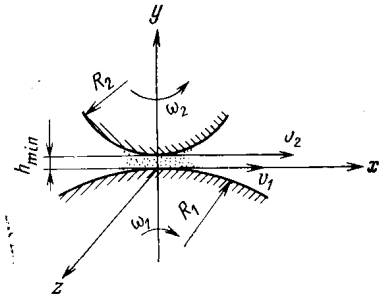

Fig. 21.1. Determining sliding and rolling velocities

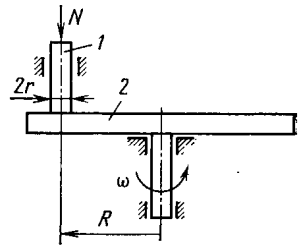

Fig. 21.2. Diagram for calculating sliding distance
1 — cylinder (peg); *2* — disc

not exclusively depend on the contact geometry and the rated speed of motion. It is greatly influenced by the operating conditions, such as the lubricant viscosity and temperature, or the ratio of tangential to normal force in the contact area.

Since the kinematic constraint in the frictional contact is not positive and the interrelation between the contact parameters has a complex nature, the laws of motion found experimentally as functions of the main parameters for a given mechanism are often used for practical engineering calculations. As the growing speeds of motion in machinery induce the exhaustion of the load-carrying capacity of the lubricant film, which leads to intensive wear of the rubbing surfaces, the kinematic calculations become increasingly important, and at the same time, more complex. The correct determining of the sliding distance is also essential.

Let us consider an example (Fig. 21.2). By the sliding distance is meant the distance traversed by the points of the body that take part in the process of friction. Then, for the points of the disc *2* that rub against the cylindrical test specimen *1*, the maximum sliding distance will be $S_2 = 2\,rnt$, and for the points of the specimen *1*, $S_1 = 2\pi\,Rnt$, where t = time, and n = number of revolutions per unit time.

The basic relationships tying up all critical factors are sometimes unavailable. In such cases, the modelling of the process can be carried out with analysis of the dimensions for the physical quantities defining the friction and wear of solids. Such an analysis proves helpful where the complexity of the phenomenon and the lack of knowledge do not allow a sufficiently full mathematical description of the process to be obtained.

The functional relationships characterizing a process and represented as dimensionless criteria of similarity hold true for all the processes whose criteria of similarity are numerically equal to those of the process being studied.

The principle of physical modelling which requires that the model and the object of study should be identical by nature is the most suitable for obtaining the values of the wear rate. The main difficulty when calculating mechanisms for wear is in the correct determining of the wear rate under various conditions. The theory of modelling helps to obtain the necessary characteristics in laboratory conditions identical to field conditions. Another way to this end is to find the wear rate from the basic theoretical relationships and physico-chemical characteristics of the contacting surfaces [14].

21.2. LUBRICANT FILM THICKNESS

The thickness of the lubricant film affects the performance and service life of engineering products. It determines the contact strength, the wear resistance, the load-carrying capacity with respect to scuffing, the frictional forces, and the temperature of contact placed under load. Accordingly, the finding of the film thickness is of vital importance for a proper understanding of the processes that occur in the frictional contact and for the development of calculation methods. The elastohydrodynamic theory of lubrication is applicable to the description of the process of friction and lubrication of solids that roll with sliding. The main problem of the theory consists in finding the contact pressure (Fig. 21.3), the geometry of lubricant film and the temperature by jointly considering the equations that describe the flow of lubricant, the elastic deformations of the solids, and the thermal processes. The flow of lubricant in the clearance is described by the equations characterizing the momentum, the continuity of the flow, and the conservation of energy, and also by the equations of state. The deformation of the bodies is found from the theory of elasticity. The temperature relationships are determined from the energy equation with the use of the appropriate boundary conditions. In the general case, a system of non-linear integro-differential equations for determining pressure, temperature, and the thickness of the oil film are solved numerically with the use of direct and inverse iteration. The analytical relationships, however, are very difficult to obtain. The initial differential equations do not take account of all complex interrelations that take place in the

frictional contact; many physical characteristics of lubricant and other thin surface films on the contacting bodies remain unknown. For this reason, combining theoretical concepts with experimental studies is essential if the relationships suitable to engineering calculations are to be obtained.

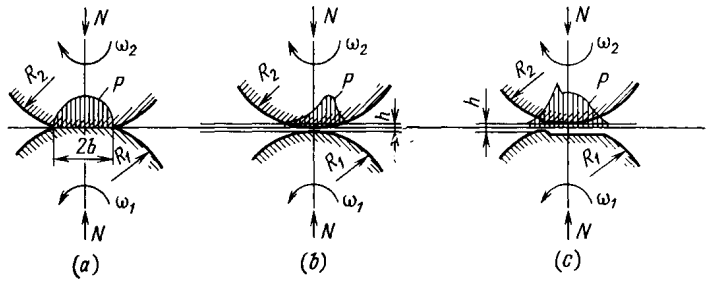

Fig. 21.3. Pressure distribution and shape of clearance in contacting solids (*a*) dry-rubbing elastic solids; (*b*) lubricated rigid solids and (*c*) lubricated elastic solids

The basic equations for an elastohydrodynamic system of solids that execute rolling motion with sliding (the two-dimensional elastohydrodynamic problem of lubrication theory) are*:

$$\frac{\partial p}{\partial x} = 6\eta (v_1 + v_2) \frac{h - h_0}{h^3}$$

at $x = \infty$; $p = 0$; $x = x_0$; $p = \frac{\partial p}{\partial x} = 0$

$$h = h_0 + \frac{x^2 - x_0^2}{2R} - \frac{2}{\pi} \left(\frac{1 - \mu_1^2}{E_1} + \frac{1 - \mu_2^2}{E_2} \right) \int_{-\infty}^{x_0} p(\xi) \ln \left| \frac{\xi - x}{\xi - x_0} \right| d\xi$$

$$\rho c v \frac{\partial \theta}{\partial x} = \lambda \frac{\partial^2 \theta}{\partial y^2} + \eta \left(\frac{\partial v}{\partial y} \right)^2 + \chi v t \frac{\partial p}{\partial x}$$

at $x = -\infty$, $\theta = \theta_0$

$$\theta(x, 0) = \left(\frac{1}{\pi \rho_1 c_1 \lambda_1 v_1} \right)^{1/2} \int_{-\infty}^{x} \lambda \frac{\partial \theta}{\partial y} \Big|_{y=0} \frac{d\varepsilon}{(x - \varepsilon)^{1/2}} + \theta_0$$

$$\theta(x, h) = \left(\frac{1}{\pi \rho_2 c_2 \lambda_2 v_2} \right)^{1/2} \int_{-\infty}^{x} -\lambda \frac{\partial \theta}{\partial y} \Big|_{y=h} \frac{d\varepsilon}{(x - \varepsilon)^{1/2}} + \theta_0$$

$$\eta = \eta_0 e^{\beta p - \alpha \Delta \theta}$$

here v_1 and v_2 = peripheral speeds; h = clearance; h_0 = minimum clearance; R = effective curvature radius $1/R = 1/R_1 + 1/R_2$, where R_1 and R_2 = radii of cylinders; c, λ, c_1, λ_1, C_2, and λ_2 = respective values of specific heat and coefficients of heat conducti-

* For easier analysis, the Reynolds equation is taken in the isothermic form.

vity for the lubricant and the materials of the bodies; β = piezocoefficient of viscosity for the lubricant; α = coefficient relating viscosity to temperature in the Reynolds formula; x and y coordinates along and across the film; ε = additional variable; x_0 = abscissa, where $p = \partial p/\partial x = 0$; χ = coefficient of lubricant's thermal expansion.

Conditions of definitness. Geometrical characteristics: R_1, R_2, length of contact l; surface roughness parameters $Rz\ (a)_1$ and $Rz\ (a)_2$. At the specified loads, effective radii of curvature, contact length, and elastic properties of materials of the contacting bodies, the contact width, $2b$, is determined definitely by the Herz formulas.

Physical properties of lubricant: η_0, ρ_0, c_0, λ_0, β and α. These quantities are taken at a characteristic temperature of the bodies in contact.

The quantities specific to the materials of the contacting bodies: E_1, E_2, μ_1, μ_2, HB, ρ_1, ρ_2, c_1, c_2, λ_1, and λ_2. These are taken at the characteristic temperature.

Also regarded as physical properties are the relationships, obtained in experimental studies, that show the variation of the main physical properties of the lubricant (η, ρ, c, λ, β) and the materials with temperature and pressure.

Boundary conditions are rated for speeds, pressures and temperatures: v_1, v_2, $v_{sl} = v_1 - v_2$; $v_{sw} = v_1 + v_2$; contact load P, load per unit length $P_n = P/l$; $p_{\max}$; and the mean temperature θ_0 of he bodies before their coming into contact: $\theta_0 = \frac{\theta_{01}+\theta_{02}}{2}$, where θ_{01} and θ_{02} = respective temperatures of the bodies brought into contact.

General characteristics. The expressions for general criteria and conditions of similarity are found by using the method of integral prototypes, the basic system of equations, the boundary conditions, and the conditions of definiteness [3]:

$$S_1 = \left(\frac{P_n}{\eta v_{sw}}\right) = \text{idem}$$

$$S_2 = \beta p_{\max} = \text{idem}; \quad S_3 = \frac{\lambda}{\rho_0 c_0 v_{sw} b} = \text{idem}$$

$$S_4 = \frac{\eta_0 v_{sl}^2}{p_0 c_0 v_{sw} b \theta_0} = \text{idem}$$

$$S_5 = \frac{\lambda_0}{\lambda_{01}} \frac{1}{\mathrm{Pe}_{01}^{1/2}} = \text{idem}$$

$$S_6 = \frac{\lambda_0}{\lambda_{02}} \frac{1}{\mathrm{Pe}_{02}^{1/2}} = \text{idem}; \quad S_7 = \alpha\theta_0 = \text{idem}$$

$$S_8 = \frac{P_n (\Theta_1 + \Theta_2)}{R} = \text{idem}; \quad \mathrm{Pe}_{01} = \frac{b v_{01}}{a_{01}}; \quad \mathrm{Pe}_{02} = \frac{b v_{02}}{a_{02}}$$

$$a_{01} = \frac{\lambda_{01}}{c_{01}\rho_{01}}; \quad a_{02} = \frac{\lambda_{02}}{c_{02}\rho_{02}}$$

The physical meaning of the obtained criteria of similarity:

$$S_1 = \left(\frac{P_n}{\eta v_{sw}}\right)$$

is the main elastohydrodynamic criterion that characterizes the load-carrying capacity of the contact, $\frac{P_n}{\eta v_{ws}}$, and its deformability, $S_8 = \frac{P_n(\Theta_1+\Theta_2)}{R}$. An increase in the product ηv_{sw} leads to a growth in the thickness of oil film during rolling, reduction in the coefficient of sliding friction, and a rise in the resistance of the frictional contact to scuffing. This complex is close in structure to the complex $\left(\frac{P_n}{\eta v_{sl}}\right)$ widely applicable to hydrodynamic plain bearings. The radical difference is in a negative influence of sliding velocity (when rolling is attended by sliding) on the oil-film thickness and the contact resistance to scuffing; the latter substantially diminishes with increasing sliding velocities. From the statement of hydrodynamic problem for stiff rolling solids it follows that $\frac{h}{R} = 2.447\frac{\eta v_{sw}}{P_n}$, that is the relative oil-film thickness varies inversely with $S_1 \cdot S_2 = \beta p_{\max}$ and $S_7 = \alpha\theta_0$, these criteria characterizing the physical properties of lubricant as a function of temperature and pressure. $S_3 = \frac{\lambda_0}{\rho_0 c_0 v_{sw} b}$ = ratio of the heat transferred through conductivity to that transferred through convection. $S_4 = \frac{\eta_0 v_{sl}^2}{\rho_0 c_0 v_{sw} b \theta_0}$ = ratio of the heat dissipated inside the oil film to that transferred by convection; $S_5 = \frac{\lambda_0}{\lambda_{01}\mathrm{Pe}_{01}^{1/2}}$ and $S_6 = \frac{\lambda_0}{\lambda_{02}\mathrm{Pe}_{02}^{1/2}}$ = ratios of the heat supplied to lubricant through conductivity to that transferred by the bodies in contact. The Peclet numbers $\mathrm{Pe}_{01} = \frac{bv_{01}}{a_{01}}$ and $\mathrm{Pe}_{02} = \frac{bv_{02}}{a_{02}}$ characterize the ratio of the heat content in the flow in an axial direction to that in a transverse direction. The obtained criteria relationships are general dimensionless characteristics used in composing equations for determining the oil-film thickness, the coefficient of sliding friction, the temparature and the anti-scuffing property of the contact. The structures of the criteria can be used for obtaining both determining criteria (that is, those containing the conditions of definiteness) and criteria to be determined. It should be borne in mind, however, that experimental relationships can be successfully summarized in the obtained characteristics only if the assumed basic mathematical relationships reflect to a full extent the physical interactions inherent in the process being studied. The effect of any factor that has not been taken into consideration will require a refinement of the established general relationships.

The calculation of the film thickness in quasi-isothermal lubricating conditions for steel surfaces can be made by the formula

$$\frac{h}{R} = 1.7 \left(\frac{\eta_0 v_{sw}}{P_n}\right)^{0.7} \left(\frac{P_n \beta}{R}\right)^{0.6} \qquad (21.1)$$

or

$$h = 1.7 \eta_0^{0.7} v_{sw}^{0.7} P_n^{-0.1} R^{0.4} \beta^{0.6*}$$

With allowance for the sliding speed in the contact

$$\frac{h}{R} = 0.3 \left(\frac{\eta_0 v_{sw}}{P_n}\right)^{0.7} \left(\frac{P_n \beta}{R}\right)^{0.6} \left(\frac{\lambda}{\alpha \eta_0 v_{sl}^2}\right)^{0.26} \qquad (21.2)$$

or

$$h = 0.3 \eta_0^{0.44} v_{sw}^{0.7} v_{sl}^{-0.52} P_n^{-0.1} R^{0.4} \lambda^{0.26} \alpha^{-0.26} \beta^{0.6}$$

The dimensions of the quantities: h = cm; η_0 = kgf·s/cm²; P_n = = kgf/cm; R = cm; v_{sw} and v_{sl} = cm/s; β = cm²/kgf; λ = = kgf·cm/(cm·s·°C); α = 1/°C.

Depending on the viscosity of oil and its thermophysical characteristics λ and α, the magnitude of the sliding velocity v_{sl}, at which the effect of sliding becomes perceptible, ranges from 220 to 10 cm/s for the viscosity values ranging from 2 to 1000 cSt (at λ = = 0.012 kgf·cm/(cm·s·°C) and α = 0.02 1/°C.

The oil film thickness values, h, for which the validity of these formulas was checked were from 0.5 to 6 μm.

Table 21.1

Calculation results h, μm

v_{sw}, cm/s	v_{sl}, cm/s						v_{sw}, cm/s	v_{sl}, cm/s					
	10	25	50	80	120	200		10	25	50	80	120	200
	By formula (1)			By formula (2)				By formula (1)			By formula (2)		
50	0.574	—	—	—	—	—	500	2.877	2.8	1.95	1.5	1.24	0.95
100	0.93	0.91	—	—	—	—	2000	7.59	7.4	3.95	3.95	3.27	2.5

Example 1. Determine the oil-film thickness by the formulas (1) and (2) for oil MC-20; ν_{50} = 157 cSt; η = 141.3 × 10^{-8} kgf·s/cm²; P_n = 2000 kgf/cm; R_{eff} = 2.74 cm, λ = 0.012 kgf·cm/(cm·s·°C); α = 0.02 1/°C.

The method of determining the film thickness before the occurrence of scuffing is given in [12].

A study of the frictional force and the oil-film thickness during rolling accompanied with sliding for heavily loaded surfaces led to the relationships presented in [7].

* The oil-film thickness can only increase with sweep velocities up to 10 to 15 m/w.

Figure 21.4 shows the effect of the sweep velocity, viscosity of oil, and contact pressure on the dimensionless value of the oil film thickness and the coefficient of sliding friction, the results being obtained experimentally.

The opposite relation of the above parameters to f and h is noticeable. The dash-line curves show the relationship between the oil-film thickness and the contact parameters, whereas the solid lines

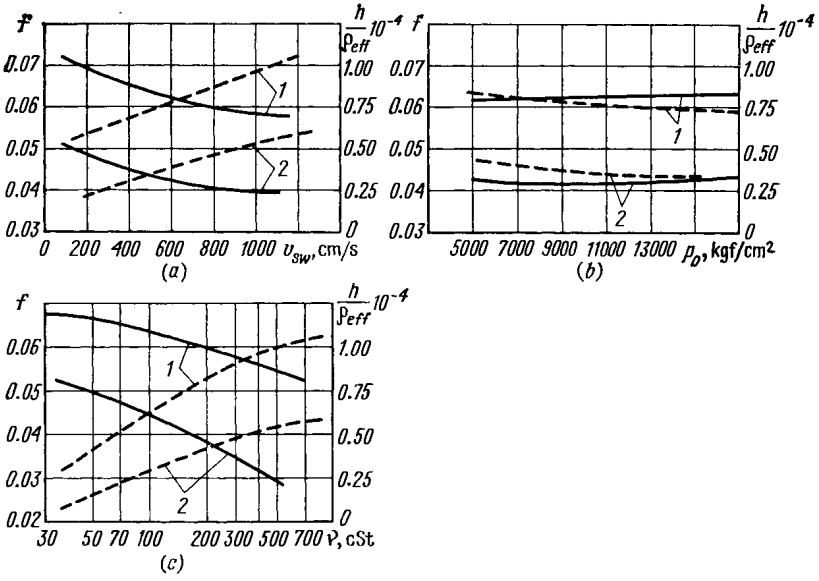

Fig. 21.4. Variation of lubricant film thickness and coefficient of friction at various sliding speeds

(*a*) sweep speed (p_{max} = 12 000 kgf/cm², ν = 110 cSt); (*b*) contact pressure (v_{sw} = = 550 cm/s, ν = 110 cSt); (*c*) oil viscosity (v_{sw} = 550 cm/s, p_{max} = 12 000 kgf/cm²); *1*—at v_{sl} = 20 cm/s; *2*—at v_{sl} = 120 cm/s

refer to the sliding friction coefficient. Increase in sliding velocity leads to simultaneous reduction in both oil-film thickness and coefficient of friction (Fig. 21.5).

21.3. COEFFICIENT OF SLIDING FRICTION

The relationship between the sliding friction coefficient and the sliding velocity during rolling with sliding generally has the form shown in Fig. 21.6. Two peculiar points, A and B, can be indicated on the curve. The point A characterizes the maximum value of the coefficient of sliding friction and defines the region of stable operation for a friction drive. The values of f_{max} are basic for designing the actuators for frictional drives. In a toothed gearing, the lowest

contact strength of the teeth is in the area where the maximum frictional forces arise, whereas the limits of contact-fatigue strength during rolling with sliding vary with maximum coefficients of friction. The point B is indicative of a severe rupture of the oil film and the contacting surfaces; this point, therefore, determines a safe limit of the load-carrying capacity with respect to scuffing. If a mechanism intended to operate in lubricated conditions is designed so that its loading and thermodynamics make for the occurrence of the

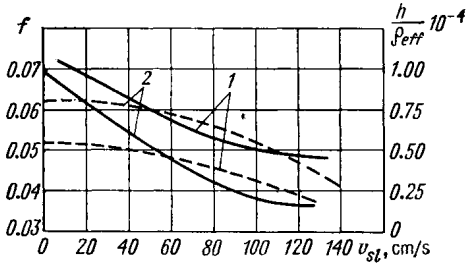

Fig. 21.5. Variation of oil film thickness and coefficient of friction with sliding speeds at different oil viscosities (at v_{sw} = 550 cm/s and p_{max} = 12 000 kgf/cm²)
1—v = 50 cSt; 2—v = 200 cSt

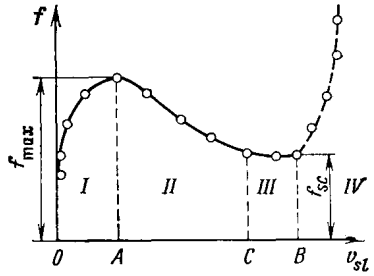

Fig. 21.6. Variation of coefficient of sliding friction with sliding speed (v = const, p = const, and v_{sw} = const)

point B, then scuffing of the surfaces will arise. The curve for the most frequent form of the relationship $f = f(v_{sl})$ in rolling with sliding (v_{sw} = const; p_{max} = const; v = const, Fig. 21.6) can be broken down into four sections: *I*—the section where sliding is low; it characterizes growth in the coefficient of friction with increasing sliding velocity and contains the maximum value of the sliding friction coefficient; *II*—the section where the coefficient of friction decreases with growing sliding velocity; *III*—the section of a small variation of the friction coefficient with sliding velocity and *IV*—that of a rapid growth in the coefficient of friction, where the oil film and the surfaces in contact rupture severely. At high rolling and sliding speeds ($v_{sw} \geqslant 3000$ cm/s), the coefficient of friction shows no rise at the moment of oil-film rupture.

Thus, the mechanisms operating at rolling with sliding in lubricated conditions can function without sudden severe wear and scoring over the range of sliding from the point 0 to the point B, or within the areas *I*, *II* and *III*. The character of the relationship between the coefficient of friction and the sliding velocity is largely determined by the viscosity of oil on the surfaces making contact. Growth in viscosity at increasing speed leads to a sharper rise of f at section *I* and to its fall at section *II*. Increase in the sweep velocity has practically no influence on the character of the relationship $f = f(v_{sl})$. The moment at which scuffing occurs depends significantly

on the sweep velocity at the contact. With small v_{sw}, scuffing arises at insignificant sliding speeds. With increasing viscosity of the oil entering the contact area, severe rupture of the film comes about at higher sliding speeds.

The effect of the sweep velocity in the contact area on the maximum coefficient of friction in operation at different contact pressures is shown in Fig. 21.7. The relationship between the coefficient of friction and the sweep velocity during the initial contact of the bodies at a point or along a line can be characterized in the following way: with increasing sweep velocities the coefficient of friction always diminishes; the degree of influence of the rolling speed of f depends on the contact pressure; the reduction in the coefficient of friction with increasing sweep velocities is more pronounced at their lower magnitudes (up to $v_{sw} \leqslant 150$ to 200 cm/s). The tendency towards smaller dimensions and mass of mechanisms and higher power to be transmitted leads to high contact stresses. The maximum Hertzian pressures in gear transmissions of current machinery reach magnitudes of $p_{max} \geqslant 20 \times 10^3$ kgf/cm^2; some speed reducers operate at $p_{max} \geqslant 40 \times 10^3$ kgf/cm^2. High-pressure friction drives operating in oil with initial contact made at a point are normally designed for contact pressures $p_{max} = (20 \text{ to } 30) \times 10^3$ kgf/cm^2. The relationship between the coefficient of friction, especially its maximum value (f_{max}), and the contact pressure is found to be rather complex. With increasing contact pressure, the coefficient of friction becomes independent of rolling speeds and oil viscosities in low ranges of their magnitude. At high rolling speeds and viscosities an increase in the coefficient of friction is typical at the initial stage of operation. At high p_{max}, the coefficient of friction remains practically unchanged. For some combinations of oil viscosity and rolling speed, no relation between the coefficient of friction and the contact pressure has been established. The factors contributing towards the setup of the contact hydrodynamic lubricating conditions and increase in film thickness lead to an insignificant growth in f with rising contact pressures. Fig. 21.8 shows the region of variation of the maximum coefficient of friction with increasing contact pressures at different oil viscosity values and sweep velocities. The upper boundary for the values of f corresponds to low magnitudes, and the lower boundary, to high magnitudes of ν and v_{sw}.

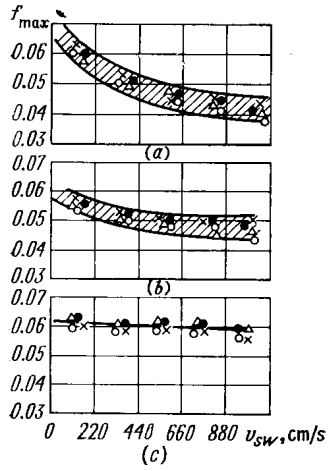

Fig. 21.7. Effect of rolling speed on maximum coefficient of sliding friction at contact pressures (*a*) 12 × 10^3 kgf/cm^2; (*b*) 20 × 10^3 kgf/cm^2; (*c*) 30 × 10^3 kgf/cm^2

Oils used in various applications can substantially differ in viscosity. However, in typical temperature conditions under which transmissions are operated, the values of viscosity range approximately from 2 to 250 cSt. For straight mineral oils, the effect of temperature on the coefficient of friction manifests itself through the viscosity. For oils with additives such a direct relation can be upset and become more complex. The influence of oil viscosity on the

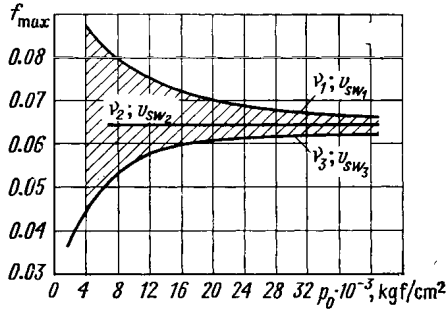

Fig. 21.8. Effect of contact pressure on maximum coefficient of sliding friction ($v_{sw3} > v_{sw2} > v_{sw1}$; $\nu_3 > \nu_2 > \nu_1$)

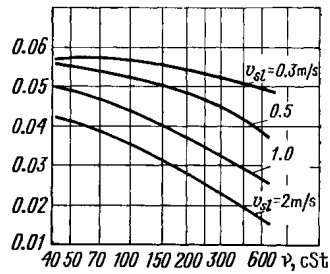

Fig. 21.9. Effect of oil viscosity on coefficient of sliding friction (p_{max} = 8330 kgf/cm², v_{sw} = 1100 cm/s)

coefficient of friction depends on the average temperature of the surfaces coming into contact, the contact pressure, and the sliding speed.

At sliding speeds lower than those corresponding to maximum coefficient of friction, variation of oil viscosity has significant effect on the coefficient of friction; higher values of the latter usually are due to higher values of viscosity. An increase in sliding speed beyond the magnitude corresponding to the maximum coefficient of friction always causes the coefficient of friction to grow and viscosity to diminish. The higher the sliding speed, the greater the extent to which the coefficient of friction varies (Fig. 21.9).

Arise in contact pressure lessens to some extent the influence of viscosity on the coefficient of friction. In the region of the maximum coefficient of friction the effect of oil viscosity is commonly insignificant. On properly run-in surfaces, f decreases with rising oil temperature. An increase in rolling speeds results in somewhat reduced influence of viscosity on the coefficient of friction. In elastohydrodynamic frictional conditions the viscosity and the piezo-coefficient of viscosity are the main parameters of oil to affect the coefficient of friction. The requirements placed on the oils to be used in frictional-transmission applications are conflicting as they call for high coefficients of friction and, at the same time, good wear resistance of the mating parts.

Experiments have shown the identity of the relationships for variation of the coefficients of friction for bodies making contact at a point and along a line. As the shearing stress limit, which depends on the pressure and temperature, is reached in the oil film, a shearing action inside the film occurs. The maximum coefficients of sliding friction arise during rolling with sliding at small absolute magnitudes of sliding speed. The maximum of the coefficient of friction as a function of sliding speed is particularly prominent at high oil viscosities (Fig. 21.6). At low viscosities, the coefficient of friction decreases insignificantly after the peak point as the sliding speed grows. The absolute magnitude of sliding speed at f_{max} depends mainly on the viscosity of oil at the temperature the bodies come into contact and on the contact pressures: the higher the viscosity and the contact pressure, the lower the sliding speed corresponding to the occurrence of f_{max}. As the bodies grow heated, the peak point shifts towards larger sliding speeds. This phenomenon is especially notable in experiments with oils whose viscosity varies considerably with temperature. The processing of the data, obtained from a large number of experiments with mineral oils over a wide range of contact parameters, resulted in empirical formulas appropriate for practical uses. For bodies with a linear initial contact, the maximum coefficient of friction occurs at a speed

$$v_{sl} = \frac{K_1}{p_{max} \lg \left(\frac{\nu_c}{\nu_{oc}} \right)} \tag{21.3}$$

where v_{sl} = sliding speed corresponding to f_{max}, cm/s; $K_1 = 2 \times 10^5$ kgf/(cm·s) = dimensional factor; p_{max} = maximum contact pressure according to Hertz, kgf/cm^2; ν_c = oil viscosity at rubbing-surface temperatures, cSt, ν_{oc} = 1 cSt. The formula is valid for contact pressures of $5{,}000 \leqslant p_{max} \leqslant 30\,000$ kgf·cm^2 and viscosities of $2 \leqslant \nu_c \leqslant 1000$ cSt. If the viscosity ν_c on the contacting surfaces is lower than 5 cSt, the latter value should be substituted into the formula.

For the initial contact made at a point, the formula for determining the sliding speeds that correspond to maximum coefficient of friction has the same structure as that for the linear contact:

$$v_{sl} = \frac{K_2}{p_{max} \lg \left(\frac{\nu_c}{\nu_{oc}} \right)} \tag{21.4}$$

where $K_2 = 10^6$ kgf/(cm·s) = dimensional factor.

The formula holds true if the entering quantities vary over the following ranges: $10\,000 \leqslant p_{max} \leqslant 45\,000$ kgf/cm^2; $10 \leqslant \nu_c \leqslant 1000$ cSt.

At viscosities lower than 10 cSt, the latter value should be substituted. Variation in the sliding speed corresponding to the maximum coefficient of friction at different oil viscosity and contact press-

ure is shown in Fig. 21.10. The condition of occurrence of the maximum coefficient of friction (or the maximum tangential stress in the oil film) can be expressed in the form

$$\lg\left(\frac{\nu_c}{\nu_{oc}}\right)^{\frac{P_{max}v_{sl}}{K}} = 1$$

where $K = K_1 = 2 \times 10^5$ kgf/(cm·s) for the initial contact along a line, and $K = K_2 = 10^6$ kgf/(cm·s) for the initial contact at a point. Dynamic viscosity can be readily introduced instead of kinematic viscosity into the above relationships. Knowing the absolute value of sliding speeds for definite contact conditions the specific sliding (in percent) can be found at the occurrence of the maximum coefficient of friction:

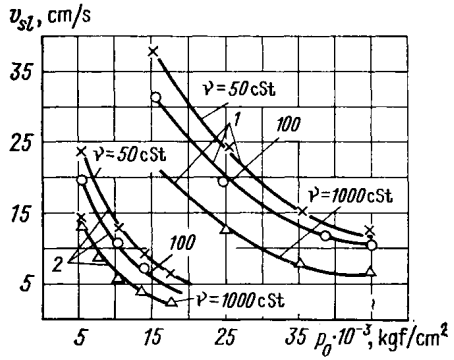

Fig. 21.10. Variation of sliding speed, at f_{max}, with contact pressure (v_{sw} = = 800 cm/s) for initial contact
1 — at a point contact; and *2*—along a linear contact

$$\eta_1 = \frac{v_{sl}}{v_{sf}} \cdot 100\%$$

where v_{sf} = surface velocity for one of the test specimens (v_1 or v_2) or the sweep velocity (v_{sw}).

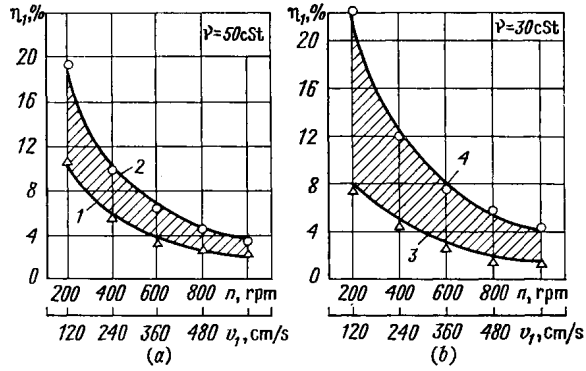

Fig. 21.11. Variation of specific sliding with surface speed of the leading body at initial contact
(a) at a point contact and (b) along a linear contact; *1* — $p_{max} = 45 \cdot 10^3$ kgf/cm², — $p_{max} = 25 \cdot 10^3$ kgf/cm², *3* — $p_{max} = 15 \cdot 10^3$ kgf/cm², *4* — $p_{max} = 5 \cdot 10^3$ kgf/cm²

Figure 21.11 shows the region of variation of the experimental values of $\eta_1 = \frac{v_{sl}}{v_1} 100$ (v_1 = surface speed of the leading specimen)

at different contact pressures and at a definite viscosity taken as a function of surface velocity (v_1) and rotational frequency (n).

The occurrence of an extremum point on the curve $f = f(v_{sl})$ can be explained in various ways depending on the assumed premises: for instance, whether the oil in the contact area is regarded as viscous-plastic body or whether shear in the oil film at the point A (see Fig. 21.6) is accounted for by the thermal effect due to dissipation of mechanical energy inside the oil film.

The formula for calculation of the coefficient of friction in the region of its maximum value has the form

$$f_{max} = \frac{c(p)}{\nu_c^{a(p)} v_{sw}^{b(p)}}$$

where ν_c = oil viscosity at the temperature the mating surfaces come into contact, cSt; $c(p)$, $a(p)$, $b(p)$ = quantities depending on

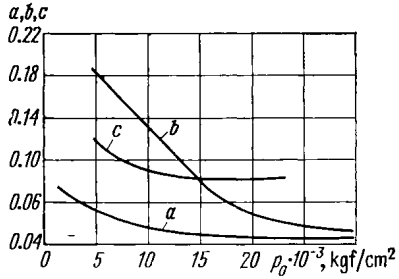

Fig. 21.12. Variation of parameters a, b and c with contact pressure

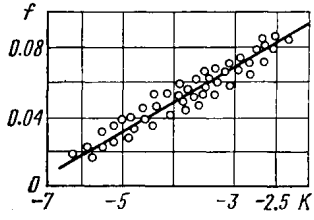

Fig. 21.13. Comparison between design and experimental data on coefficient of sliding friction at

$$K = \lg \frac{pHB}{\nu_c v_{sl} R_{eff} E_{eff}}$$

the contact pressure (Fig. 21.12). The region of the experimental testing of the formula: ν_c = (2 to 300) cSt; v_{sw} = (100 to 5000) cm/s; p_{max} = (5000 to 45 000) kgf/cm².

The formula for calculation of the coefficient of friction is presented most generally in the following form [11]

$$f = \frac{AP_n^{0.1}\left[10 + \lg\left(\frac{HBRa}{E_{eff}R_{eff}}\right)\right]}{\nu_c^{0.07}(v_1+v_2)^{0.1}(v_1-v_2)^{0.35}R_{eff}^{0.25}} \qquad (21.5)$$

where $A = 0.09$ is a dimensional factor; P_n = load per unit length, kgf/cm; HB = hardness of the softer contacting body, kgf/cm², Ra, cm. The formula is applicable at $\nu > 1$ cSt; $P_n \geqslant 300$ kgf/cm; $p_0 \geqslant 4000$ kgf/cm²; $v_{sw} \geqslant 100$ cm/s; $v_{sl} > 20$ cm/s; $R > 0.5$ cm; $Ra > 10^{-5}$ cm; $HB > 5000$ kgf/cm².

The coefficient of sliding friction for run-in lubricated bodies that roll with sliding varies, on the average, from 0.008 to 0.1 over a speed range of 100 to 10 000 cm/s.

The analytical relationship for determining the coefficient of sliding friction, which applies to sliding bodies, makes allowance for variation of load, sliding speed, oil viscosity, hardness of the softer material, effective curvature radius, and the materials' elastic moduli

$$f = 0.02 \lg \frac{PHB}{\nu_c v_{sl} R_{eff} E_{cff}} + 0.14$$

The formula ensures an accuracy of 10 to 15 percent for metal bodies with contact characteristics of $30 \leqslant HRC \leqslant 62$; $5 \leqslant \nu_c \leqslant 600$ cSt; $50 \leqslant v_{sl} \leqslant 450$ cm/s; and $1.0 \leqslant P \leqslant 50$ kgf, which corresponded to the initial stresses of $p_{max} = 3500$ to 15 000 kgf/cm^2 calculated for experiments by the Herz formulas; after the experiments, the compressive stresses decreased to $p_{max} = 50$ to 3000 kgf/cm^2 because of wear of the contact sphere.

The coefficient of friction as a function of the dimensionless complex is graphically represented in Fig. 21.13; the main relationships are given in [8].

21.4. LOAD-CARRYING CAPACITY OF SOLID LUBRICANT COATINGS

The rupture of the solid lubricating film in a heavily loaded contact leads to a higher coefficient of friction, to intensive wear, and, in vacuum, to welding. So, the need arises for study of conditions that result in the loss of load-carrying capacity of the lubricant film and for determining the factors that affect the breaking load. The minimum load leading to severe rupture of solid lubricating film and to direct contact of the rubbing surfaces is taken as the indicator of the load-carrying capacity of the contact operating with a solid lubricant.

The load capacity of a thin plastic film pressed between rigid plates, that is, the load that results in squeezing the film out, rapidly grows with reducing the film thickness and increasing the extension of the contact and can exceed substantially the yield limit of hardened steels.

The application of shearing force markedly reduces the film load capacity by diminishing the normal load which squeezes out the lubricant. The plastic flow of the film is attended with elastic and, in some cases, plastic deformation of the surfaces pressed together; the magnitude of the deformation grows, with increasing load capacity of the oil film and decreasing stiffness of the bodies in contact.

The critical load destroying the lubricant film is largely determined by the mechanical properties of the coating and the substrate material, by the film thickness, the geometric characteristics of the

contacting surfaces, their temperature, and speed of relative motion. It is known that the material structure factors, the temperature and speed conditions of deformation, and the stress diagram affect the behaviour of the material in deformation significantly. The character of destruction of one and the same material can vary from brittle to plastic depending on the conditions of deformation. In a loaded direct contact under an indenter the lubricant film retains integrity, decreasing in thickness with growing load and penetration, which is determined from the value of electrical resistance at the contact, whereas the lubricant film outside the loaded contact area comes off in the form of brittle flakes. Thus, the solid lubricant film is capable of being deformed plastically together with the underlying metal.

At the initial stage of deformation, the softer coating is deformed first because its strength characteristics differ from those of the backing. However, the film flow pressure grows rapidly as the film thickness decreases and the contact area expands. Further increase in load causes growth in the deformation of the underlying material. At a certain thickness of the film, called the critical thickness, simultaneous plastic flow of the surface layer and the underlying material occurs. This deformation stage is of particular interest because, as experiments show, it is precisely the plastic deformation of the backing that finally squeezes the lubricant out of the contact.

The load causing the plastic flow of the material significantly depends on the character of pressure distribution. During the plastic flow of the softer surface film the normal pressure on the backing material shows a markedly non-uniform distribution. The highest pressure acts at the centre, and the lowest on the periphery of the contact area. Under such conditions local plastic flow can occur, the load that causes this flow proving lower than the load that leads to the flow of the material under a rigid plunger. The zone of plastic flow if focused at the centre of the contact area, where the condition of equality between the pressure in the lubricant and the yield limit of the backing materials applies. A photograph of a cross-section of a coated specimen (Fig. 21.14) shows the character of combined deformation of dissimilar materials impressed with a spherical indenter. A combined flow of the solid lubricant and the backing material is identifiable.

The mechanics of film rupture during compression with shear is revealed most clearly by the process of the initial tangential motion of an indenter located in an impression made in a coated surface. It is assumed that the operative surface of the indenter is fully loaded. Initially, the central area of the contact spot is subject to plastic deformation. The hard zones at the inlet and the outlet are retained until the appropriate change in the geometry of the boundary causes the yield-limit condition to emerge. Thereby, the soft layer is extruded partially or completely from the inlet or the outlet zone.

During the experiment, the spherical indenter was slowly passed along the metal surface coated with a solid-lubricant film, and the load was increased gradually. With the growing load the resistance at the contact dropped down to the value of contact resistance of metal bodies and the coefficient of friction rose owing to the absence of lubricant in the contact area. The load corresponding to this contact condition was taken as the *ultimate load P* [9].

The relationship between the ultimate load P and the hardness of the backing, obtained in the experiment with an indenter having

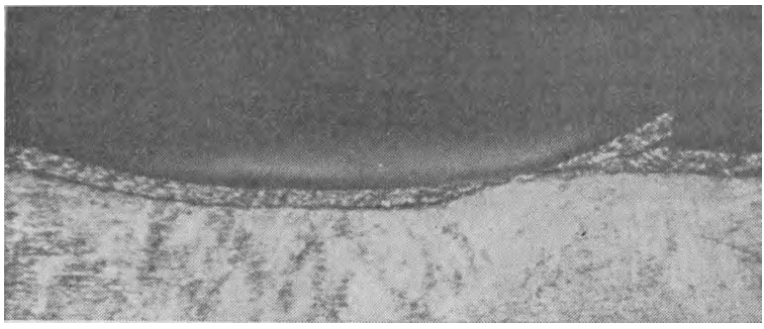

Fig. 21.14. Cross-section of coated specimen with indentation and shear of material

a radius $R = 200$ μm, is shown in Fig. 21.15. The relationship between the same load P and the lubricant film thickness (the indenter radius $R = 1.15$ to 2.37 mm) is shown in Fig. 21.16. The backing material was copper. The load rises with the film thickness reaching the limit at some thickness value dependent on the radius of the indenter. Analysis of theoretical assumptions and experimental results has made it possible to set out the factors having the major effect on the design load limit P_d. Among these are: σ_y = = yield limit of the backing in undirectional compression; τ_{sh} = = yield limit of the coating in shear; E = elastic modulus of the backing; R = indenter radius; and Δ = coating film thickness.

Combinations of the dimensionless parameters that affect the process under investigation can be obtained with the theories of similarity and dimensional analysis. It proved to be possible to find the value of the coefficient and the exponents for the dimensionless parameters:

$$\frac{P_d}{\sigma_y R^2} \approx 145 \left(\frac{\Delta}{R}\right)^{0.3} \left(\frac{\sigma_y}{E}\right)^{0.45} \left(\frac{\tau_{sh}}{\sigma_y}\right)^{0.3} \qquad (21.6)$$

or, in a form more suitable for calculation;

$$P_d \approx 145 \sigma_y^{1.15} R^{1.7} \Delta^{0.3} \tau_{sh}^{0.3} E^{-0.45}$$

The obtained expression makes it possible to assess the effect of each of the geometric and strength factors on the load carrying capacity of solid-lubricant coating. Experiments at low and elevated

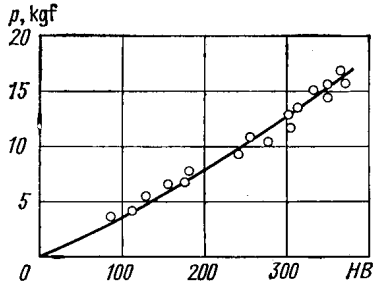

Fig. 21.15. Variation of load limit with hardness of backing material (lubricant ВНИИ НП-230; $E=2.2\cdot10^4$ kgf/mm²)

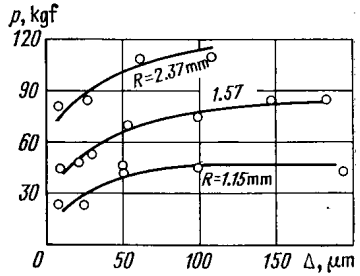

Fig. 21.16. Variation of load limit with coating film thickness (lubricant ВНИИ НП-212; $E = 1\cdot10^4$ kgf/mm²; HB50)

temperatures revealed a marked decrease in the load capacity of solid lubricant films with rising temperature.

A comparison of the load limits calculated by formula (21.6) with experimental data is presented in Table 21.2.

Table 21.2

Results of calculation and experimental finding of load limits

Material		σ_y	τ_{sh}	R	Δ	$E\cdot10^{-4}$, kgf/mm² backing	P_{exp}	P_d/P_{exp}
backing	coating	kgf/mm²		mm				
Steel 20X13	ВНИИ НП-212	60	0.8	1.575 1.18	0.03		126 85	1.01 0.91
Steel 3	ВНИИ НП-230	39	1.2	1.18	0.05	2.1	80	0.84
Steel 08X18H9T	ВНИИ НП-212	65	0.8	1.25	0.03		140	0.8
Steel 45*		180	1.2	0.2	0.01		20	1.1
Alloy AMr-6	ВНИИ НП-212	30	1.2	1.18	0.025	0.7	60	1.02
Titanium		86	0.8	1.18	0.03	1.2	145	1.08

* Heat-treated.

21.5. GENERAL PRINCIPLES OF WEAR CALCULATION

In order to extend the service life of engineering equipment under abrasive-wear conditions* it is necessary to provide protection against the ingress of dust, to remove abrasive particles from lubricant, to improve the hardness of the bodies in contact, and to increase the lubricant film thickness in the sliding-contact areas [22, 23].

The measures towards the desired results may include increasing the viscosity of oil, improving the physico-mechanical properties of the contacting materials, strengthening the contacting surfaces and changing the surface geometry, using the appropriate filtration of lubricant and optimum lubricating systems, sealing the rubbing surfaces and, if required, reducing the acting load.

Because of plastic deformation during compression and shear, protective surface films can be ruptured in the real contact areas of rubbing surfaces. For decreasing the rate of adhesive wear, it is essential to provide protective covering of friction surfaces, and to ensure the formation of physical and chemical protective adsorption layers as well as lubricant films and coatings. Tool marks on the machined surface and the structure of the material should make for rupture of welded junctions, that is, for secure contact at separate points. The surface lay should not be parallel to the vector of motion for the sliding bodies. Adhesive wear is most typical for dry-rubbing joints or those with solid lubricant coatings, especially during operation in vacuum or inert-gas environments. Good performance under such conditions can provide composite materials with a complex surface structure including binding components and reinforced polymers; special lubricating methods can also be helpful.

The experience of operation of lubricated tribological joints indicates the feasibility of controllable chemical interaction of the surfaces with the ambience: oxygen, chemically active oil additives, surfactants, or acid oil compounds. As a result of these processes, a weak surface layer emerges on the rubbing surfaces, which is destroyed by friction and periodically recovers. This layer reduces the friction force and increases the temperature resistance of the frictional contact, but is subject to intense wear.

In order to control the process of wear, the conditions need to be established that favour the occurrence of the desired chemical reactions with the view of adjusting the temperature, concentrations, and interaction times; the optimum choice of the rubbing materials and the lubricant is also essential.

During chemical and mechanical wear the rubbing surfaces remain relatively smooth and destruction of the materials is "soft". This type of wear is complex by nature and is associated with many chemical, physical, and mechanical factors that characterize the

* The mechanism of wear in abrasive interaction is described in Chapter 12.

materials, lubricant, operating conditions, environment, temperature conditions and interaction time.

The method of calculation of wear life by contact strength (absence of pitting) has found a wide recognition. For some mechanisms, anti-scoring resistance (absence of seizure) is estimated. However, no reliable calculating method for "soft" wear, (wear-away) can be found in literature at present because the attending physico-chemical processes are complicated, and the factors that influence the wear of surfaces are diverse. Taking as an example gear wheels, we shall illustrate below the principle of calculation of various mechanisms for wear life. The structure of this calculation method little depends on the nature of wear process because the intensity of physico-chemical processes in the frictional contact is allowed for by a special component found experimentally.

The calculating method to be disclosed makes it possible to find the service life of a transmission by the specified wear rate, or, conversely, the average wear rate by the specified service life for different types of gear transmissions. The accuracy of the calculation by the obtained formulas depends primarily on the correct assessment of the wear rate, which even in stationary external conditions is often variable.

The calculation for wear and service life is advisable to make for a characteristic (the most critical) point on the tooth flank, for which the wear rate under the given operating conditions must be known. If it is established that during operation of the tooth the wear rate is variable, this fact can be allowed for by calculating the life span at different wear rates and subsequently adding together the obtained values.

Comparison of wear rates obtained on various testing machines and on actual gear transmissions (by calculation with the formulas given below) allows optimum laboratory test techniques to be chosen for gear materials.

The linear wear rate is convenient to use for the analysis. A large body of experimental data examined in the process of deriving the main equation has given reasons for the assumption that slip in the contact area is largely responsible for destruction of the tooth flank surface. This conclusion is also confirmed by the field practice for gear transmissions made from a wide variety of materials. It is known that the linear wear rate* is characterized by the ratio $I_h =$

---

* This formula applies essentially to the sliding distance traversed by a rectangular contact spot over the tooth flank on the assumption that wear per unit contour area is uniform; the value of I in this formula can only be valid for particular conditions because the amount of wear is dependent on surface roughness, load and the coefficient of friction.

At present, a broader approach to the calculation is possible, in which the effect of surface roughness, mechanical properties, and contact fatigue characteristics can be regarded. This approach is discussed in Chapter 3, where calculation formulas for the assessment of wear rate are given. *Editors.*

$= \frac{dh}{dS} \approx \frac{h}{S}$, where h = depth of the worn layer, and S = sliding distance. The use of the parameter I is advisable for many reasons. The main of them are: (1) the relationship for I as a function of rolling and sliding velocities, load, temperature and other variables, established for some models in laboratory conditions or for a particular gear transmission, can be extended to other operating condit-

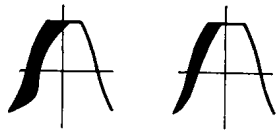

Fig. 21.17. Types of gear **tooth** wear

ions; (2) the wear rate can be used for the assessment and specification of materials from the standpoint of their suitability for the given rubbing conditions.

Severe wear in a large number of gears in average unlubricated conditions has been found to be of two main types (Fig. 21.17). The most typical type of wear for heavily loaded gears, illustrated in Fig. 21.17*a*, is characteristic of both slow- and high-speed transmissions. Its peculiarity is in that the volume of the worn material grows from the pitch point to the tip, that is towards the area where sliding is more intense. The other type of wear (Fig. 21.17*b*) is characterized essentially by uniform wear of the tooth flank and applies to lightly loaded gears used in instrument applications and to transmissions with solid lubricant coatings. In high-speed transmissions small indentations can develop on the tooth flanks where the teeth come into engagement.

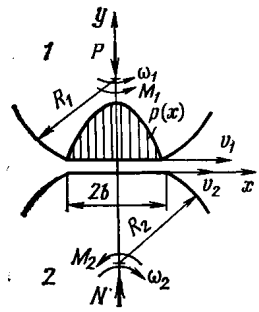

Fig. 21.18. Distribution of pressure in contact area of gear teeth

The thickness of the layer worn from the tooth flank is $h \approx IS$. The sliding distance S for one mesh cycle over a contact spot calculated according to Hertz, will be found from the following considerations: the contacting time for the solid *1* (Fig. 21.18) is $t = 2b/v_1$, for the solid *2*, $t = 2b/v_2$. The distance traversed by a point of the solid *1* during the time in which the contact with the solid *2* is made over the area $2b$ is $S_1 = 2bv_1/v_2$. Hence, the sliding distance over the time a single contact is made will be $S = 2b\,(v_1 - v_2)/v_2$. The relationship between the sliding distance and the position of a point in contact will be expressed by the equation $S = (x + b)\,(v_1 - v_2)/v_2$.

After simple transformations we have the formula for calculation of the worn-layer thickness for the retarding flank

$$h_2 = 2.25 I_2 \sqrt{P_n (\Theta_1 + \Theta_2) R_{eff}} \frac{v_{sl}}{v_2} n_2 z_2 t_2$$

and for the leading flank

$$h_1 = 2.25 I_1 \sqrt{P_n (\Theta_1 + \Theta_2) R_{eff}} \frac{v_{sl}}{v_1} n_1 z_1 t_1$$

where P_n = load per unit length of contact line, kgf/cm; v_{sl} = = sliding velocity, cm/s; $v_{2,1}$ = surface velocities for the retarding and the leading tooth flank, cm/s; $n_{1,2}$ = rotational frequency of the gears, rpm; $z_{1,2}$ = number of gears in mesh with the given gear (for instance, for a pair of gears $z = 1$, and in a planetary gearing, usually, $z = 3$ for sun and crown gears, and $z = 2$ for a satellite); and t = operating time, min.

Minor transformations will give the wear life of a pair of gears

$$t_2 = \frac{|h|_2}{2.25 I_2 [P_n R_{eff} (\Theta_1 + \Theta_2)]^{1/2} \left(i_{1,2} \frac{R_1}{R_2} - 1 \right) n_2 z_2}$$

where $|h|$ = permissible amount of wear for gear teeth, cm; R_{eff} = effective curvature radius of tooth flanks, cm.

For identical materials, with $\mu_1 = \mu_2 = 0.3$, the expression will take the form

$$t_2 = \frac{|h|_2 E_{eff}^{1/2}}{3 I_2 (P_n R_{eff})^{1/2} \left(i_{1,2} \frac{R_1}{R_2} - 1 \right) n_2 z_2}$$

The permissible amount of wear $|h|$ is generally a specified parameter except for a critical case in which the solid lubricant coating is worn away or the tooth bending strength is determined by wear. Experiments show that as gear teeth wear, the transmission efficiency drops and, because of growing dynamic loads, noise in the gearing increases. For this reason, the life of a gear pair is determined by assigning the permissible amount of wear $|h|$. The following suggestions concerning the use of the above formulas seem appropriate. If the initial values of the transmission parameters are substituted into the formulas, the obtained wear life will be a minimum. The reason is that the effective curvature radius in the dedendum increases as the tooth wears away, with the result of higher rolling velocities and lower contact pressures. It should be borne in mind, however, that in the process of wear the dynamic load changes. For this reason, the calculation method should be refined so as to take into account the kinetics of wear of the teeth and its influence on the actual contact geometry, speed and force characteristics of the transmission. Of vital importance is experimental and theoretical determining of wear over a wide range of contact parameters and environments. Unfortunately, differences in data process-

ing methods lead in many cases to losses of valuable information. For mechanisms working without lubrication, particularly in vacuum, adhesive wear of the operating surfaces is typical. Here, wear is due to contact of compressed surfaces and diffusion of wear debris, which occurs, for instance, in pure rolling of bodies with solid-

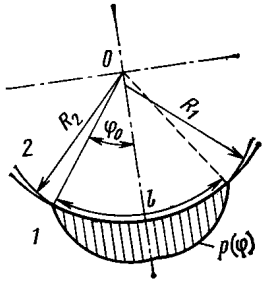

Fig. 21.19. Distribution of pressure in sliding bearing

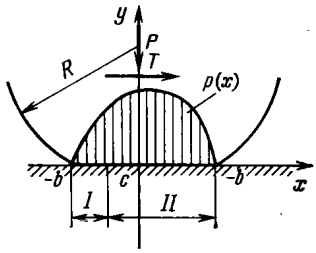

Fig. 21.20. Distribution of pressure during pure rolling
I—sliding zone; *II*—engagement zone

lubricant coatings. In this case, the wear rate is found by the formula

$$h = 2.25I\sqrt{P_n(\Theta_1+\Theta_2)R_{eff}}nzt$$

The average wear rate for the teeth of each of the gears are calculated by the formula obtained after transformation of the above expressions:

$$I = \frac{hv_{1,2}}{2.25\sqrt{P_n(\Theta_1+\Theta_2)R_{eff}v_{sl}}nzt}$$

where h = amount of wear obtained experimentally, cm; $v_{1,2}$ = =surface velocity, for instance, of the retarding tooth flank portion (dedendum); $v_{sp} = \omega_p R_{dp}$, $v_{swh} = \omega_{wh} R_{dwh}$. Here v_{sp} and v_{swh} = = surface velocities of tooth dedendum for the pinion and the wheel, cm/s; ω_p and ω_{wh} = angular velocities of the pinion and the wheel, 1/s; and R_{dp} and R_{dwh} = dedendum curvature radii for the pinion and the wheel, cm.

Let us quote some average wear rates for gear wheels operating without lubrication in high vacuum ($p = 10^{-8}$ mm Hg). The module is 0.5 to 2 mm, maximum Hertzian contact pressures up to 10 000 kgf/cm^2, teeth sliding speed in contact up to 200 cm/s, rolling speed up to 500 cm/s, and temperature up to 200°C. The wear rate I of solid lubricant coatings ВНИИ НП-212, ВНИИ НП-213, and ВНИИ НП-229 is from 10^{-5} to 10^{-6}. In such conditions special composite materials normally have a wear rate of 10^{-5} to 10^{-8}; this rate depends on many factors, the degree of vacuum included.

A sliding bearing, a hinge joint, and other shaft-sleeve-type joints are preferable to calculate, in our opinion, in the following sequence. Referring to Fig. 21.19, we determine the sliding distance from the

contact arc length obtained experimentally or theoretically by the solution of the contact problem for elastic solids outlined by cylindrical surfaces with slightly differing radii. Over one revolution, the sliding distance for the points located on the rotating component is equal to the contact length. For the points of the stationary component, the sliding distance is equal to the perimeter of the contact surface on the moving component, that is $2\pi R_2$ for a sliding bearing. Over an operating time t, the sliding distance is $S_1 = 2\pi R_2 nt$; $S_2 = \ln t$. The initial contact zone depends on the elastic properties of materials of the contacting bodies, the geometric characteristics, and the load, and can be determined from the solution of the contact problem in the theory of elasticity.

By the value of angle φ_0, we find the contact arc and the amount of wear for the mating components 1 and 2:

$$h_1 = \int_0^{S_1} I_1 \, dS; \quad h_2 = \int_0^{S_2} I_2 \, dS$$

where S_1 and S_2 = sliding distances for the components 1 and 2. If the wear rate does not change over the sliding distance, these equations can be readily transformed into the form $h_1 = I_1 S_1$ and $h_2 = I_2 S_2$. The allowed amount of wear $|h|$ being known, we find the service life (t):

$$|h| = (R_1 + h_1) - (R_2 - h_2); \quad t = \frac{|h| - (R_1 - R_2)}{(I_1 2\pi R_2 - I_2 l) n}$$

Experimental studies of plain bearings conducted in air and in vacuum ($p = 10^{-8}$ mm Hg) showed that with decreasing the sliding speed down to 50 cm/s, specific load to 200 kgf/cm^2 and temperature to 100°C, the wear rate I for various types of solid lubricant films usually varied in the range of 10^{-7} to 10^{-8}.

Experiments with oscillatory-motion joints in vacuum ($p = 10^{-8}$ mm Hg) at specific loads up to 150 kgf/cm^2, temperatures up to 100°C, low sliding speeds, and calculation of these joints by the disclosed method gave wear rates I of 10^{-6} to 10^{-7}. The experiments revealed a substantial growth in wear rate with load; this relationship, however, was not always linear. It should be noted that the existence of two different sliding paths in the shaft-sleeve joint leads to an important conclusion, namely, that for higher wear life the solid lubricant coating should be applied to the component having the shorter sliding path. Experiments have confirmed this conclusion.

Rolling with a tangential force acting in the contact plane is encountered in cams, friction drives, road rollers and other mechanisms. The contact area generally consists of an engagement section and a sliding section (Fig. 21.20). The coordinate of the point that separates these sections can be determined from the equation $c =$

$= b\left(1 - 2\sqrt{1 - \frac{k}{f}}\right)$, where b = half the width of the contact area, calculated according to Hertz; f = coefficient of sliding friction; and k = coefficient of engagement, equal to the tangential-to-normal-load ratio. The wear of solids during the passage of the contact length $2b$ can be expressed as

$$h = \int_{-b}^{c} I_{eng}\, dy + \int_{c}^{b} I_{sl}\, dy$$

where I_{eng} and I_{sl} = wear rates over the engagement and sliding sections. Difference in wear rates over these sections is difficult to assess experimentally, because it is the total resulting wear only (change in mass or dimension) that is commonly followed in experiments rather than the whole picture of wear kinetics and the place of formation of each wear particle. For this reason, in the case of pure rolling (without sliding) it is convenient to use an experimental, summarized rate of wear. Here, it should be noted that sliding velocity is not always the main factor to affect the wear rate; for instance, with the use of some types of solid-lubricant coatings, wear due to rolling has turned out to be worse than due to sliding.

The foregoing method of calculation for wear is helpful in many instances and for a wide variety of mechanisms; it allows experimental data to be assessed and the service life to be predicted. Emphasis should be placed on the need to regard the actual contact conditions, which tend to change as the mating parts wear away.

Example 2. An unlubricated gear transmission is made from a special grade of metal-ceramics ($E_{1,2} = 1.6 \times 10^5$ kgf/cm^2). It has the following dimensions and operating conditions: $m = 1$, $z_p = 22$; $z_w = 74$, $A = 48$ mm, $\alpha = 20°$ of arc, $b = 3$ mm, $d_p = 22$ mm, $d_w = 74$ mm, $M_t = 3.5$ kgf·cm, and $n_p = 4000$ rpm.

According to the results of tests, the amount of wear for the pinion and the wheel was $h_p = 0.31$ mm, and $h_w = 0.2$ mm, respectively; the number of loading cycles was $N_p = 4.15 \times 10^7$ and $N_w = 1.24 \times 10^7$.

Let us find the wear rate for the teeth. The character of the wear corresponded to Fig. 21.1*a*. The formula for determining the wear rate, derived from the above equations, has the form

$$I = \frac{hv_{1,2}}{2.25\sqrt{P_n(\Theta_1 + \Theta_2) R_{eff} v_{sl} nzt}}$$

The values of the quantities entering into the formula are found in the following way: h, from the results of the experiment; v_s = surface velocity, for instance, of the retarding portion (dedendum) of the tooth flank

$$v_{sp} = \omega_p R_{dp}; \quad v_{sw} = \omega_w R_{dw}$$

where v_{sp} and v_{sw} = surface velocities of the dedendum in the pinion and the wheel, respectively; ω_p and ω_w = angular velocities of the pinion and the wheel, 1/s; R_{dp} and R_{dw} = dedendum curvature radii in the pinion and wheel teeth, respectively, cm; here $R_{dp} = R_p - l_w$; $R_{dw} = R_w - l_p$; R_p and R_w — curva-

ture radii of the pinion and the wheel at the pitch point, cm

$$R_p = \frac{A \sin \alpha}{i+1}; \quad R_w = iR_p$$

A = centre distance, cm; i = transmission ratio; α = pressure angle; l_p and l_{wh} = distances along the path of contact, traversed by the teeth contact point over a period of engagement of the pinion and wheel in the addendum, cm;

$$l_p = \frac{h'_p}{2}\left[\sqrt{\left(\frac{d_p}{h'_p}\sin\alpha\right)^2 + 4\left(\frac{dp}{h'_p}+1\right)} - \frac{d_p}{h'_p}\sin\alpha\right]$$

$$l_w = \frac{h'_w}{2}\left[\sqrt{\left(\frac{d_w}{h'_w}\sin\alpha\right)^2 + 4\left(\frac{d_w}{h'_w}+1\right)} - \frac{d_w}{h'_w}\sin\alpha\right]$$

h'_p and h'_w = pinion and wheel tooth addendum, respectively; d_p and d_w = pitch circle diameters for the pinion and the wheel, cm; P_n is determined by the formula

$$P_n = \frac{2M_t k}{bd_p \cos\alpha}$$

here M_t = torsional moment on the wheel shaft, kgf·cm; k=coefficient allowing for dynamic loads; b = face width, cm; R_{eff} is given by

$$R_{eff} = \frac{R_p R_w}{R_p + R_w}$$

The sliding speed v_{sl} for the pinion and the wheel is found by the formulas

$$v_{slp} = (\omega_p + \omega_w) l_w$$

$$v_{slw} = (\omega_p + \omega_w) l_p$$

here v_{slp} and v_{slw} = sliding velocities in the dedendum of the pinion and wheel teeth, cm/s.

The number of meshing cycles

$$N = nzt$$

Using the given formulas, we have

Parameters	ω, s^{-1}	R, cm	l, cm	R_d, cm	v_s, cm/s	P_n, kgf/cm	R_{eff}, cm	v_{sl}, cm/s
Pinion	418.67	0.38	0.23	0.11	46.06	19.75	0.29	146.65
Wheel	124.47	1.27	0.27	1.04	129.45			124.9

The wear rate of the pinion teeth $I_p = 4.1 \cdot 10^{-8}$, and that of the wheel teeth $I_w = 29.5 \cdot 10^{-8}$.

21.6. FATIGUE PITTING OF SURFACES IN CONTACT

This type of surface destruction arises as a result of repeatedly deforming micro-volumes of the material, which has the effect of producing cracks and tearing away material particles. Pitting occurs in well lubricated mechanisms under the action of contact stresses

during pure rolling and rolling with sliding (for instance, in gear transmissions, rolling bearings, friction drives, cam drives, and compactors).

The fatigue strength of a thin surface layer 15 to 25 μm thick depends on its stress and deformation conditions, physico-mechanical properties of the material, physico-chemical properties of the lubricant, thickness of the lubricant layer, and kinematics of the contact. Among the factors to affect fatigue resistance are the condition of the surface layer (chemical and mechanical properties and residual stresses, which depend on the part's manufacturing technology), surface quality (microgeometry), stress concentration and degree of running-in, service conditions (loading frequency, temperature, chemical environment), and scale factor.

Rise in the coefficient of friction favours the emergence of pitting; therefore, all other things being equal, the area of the minimum contact strength corresponds to the area where maximum contact forces arise. For example, pitting in gear transmissions commonly begins near the pitch point at sliding speeds of 2 to 50 cm/s which bring about maximum coefficients of friction. It should be noted that the use of a sliding velocity producing the maximum coefficient of friction is essential for experimentally determining the fatigue curves on roller-type testing machines.

Pitting due to fatigue leads to the formation of cavities with diameters of hundredths of a millimetre which grow in size with time. The usual results are noise and vibration, decrease in bearing area, growth in load concentration, contact stresses and plastic deformation; the rate of wear increases and scoring is poss ble. Pitting can be limited in extent. It occurs during the initial period of service and depends on the concentration of load on small areas or separate irregularities. Here, the cause is usually the inaccuracies of manufacturing and assembly. As running-in is in progress, the action of the load extends to a larger area, and pitting ceases. The intensity of pitting and the time it originates are determined primarily by the magnitude of contact pressures, the number of loading cycles, the material hardness, the surface geometry and the thickness of the lubricant film. The concept of pitting as a fatigue process is supported by its kinetics, which can be described by an equation of the $\sigma^m N = \text{const}$ type, where σ = maximum magnitude of the contact compressive stress; N = number of loading cycles; and m = = exponent.

Studies of the resistance of materials to loading during sliding contact give a fatigue curve, which is plotted in the $\sigma - N$, $\sigma - \lg N$, or $\lg \sigma - \lg N$ coordinate systems (Fig. 21.21*a* and *b*). The equations of the fatigue curves have the form [19]

$$\sigma_0 + k \lg N = \sigma + k \lg N_0; \quad \sigma^m N = \sigma_0^m N_0$$

where σ_0 = fatigue limit, which is the maximum compressive stress that a test specimen can sustain without rupture at a specified

basic number of cycles N_b (normally $N_b = 10^7$); N_0 = number of cycles corresponding to the break point on the fatigue curve; k and m = fatigue curve parameters; σ = acting stress amplitude; N = = number of cycles up to the specimen rupture.

Design values of contact compressive or shear stresses arising at an angle of 45° to the direction of normal pressure at a depth of $0.786b$ and equal to $0.3\sigma_{com}$ should not exceed the allowable value found experimentally. If the equivalent number of loading cycles (N_e) equals or exceeds the basic cycle number, then the fatigue limit is taken as the basis for determining the allowable stress; if the

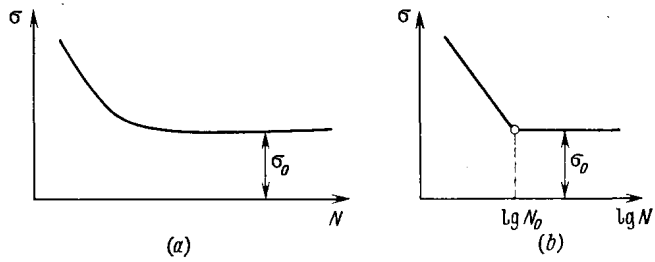

Fig. 21.21. Fatigue curve
(*a*) in conventional coordinates; (*b*) in semilogarithmic coordinates

equivalent number of cycles is smaller than the basic number, the allowable stress is found from the fatigue strength $[\sigma] = \sigma_0 \sqrt[m]{\frac{N_b}{N_e}}$. The magnitude of the fatigue limit is essentially a function of the material hardness, that is $\sigma_0 = kHB$.

The method of determining the allowable contact stresses in the design for pitting resistance and the methods for improving the fatigue resistance of surfaces are discussed in detail in [16, 21, and 24].

The conditions of lubrication and thickness of the lubricant film have a marked effect on the development of pitting. The film-thickness influence manifests itself both through the tangential stresses arising in the contact area (specific friction forces) and through changes in the character and number of interactions of surface asperities on the contacting bodies. Increasing thickness of the lubricant film reduces the number of the interacting asperities, the time taken by their deformation, the adhesion interactions, the dynamic contact loads, and the arising friction forces. The influence of the film thickness on the life of the rubbing pair is convenient to express as the relationship of the loading cycle number or the allowable stress and the dimensionless (effective) film thickness $\frac{h}{\sqrt{Ra_1^2 + Ra_2^2}}$ where Ra_1 and Ra_2 = respective values of the arithmetic mean deviation

of the profile for the contacting surfaces. Experimental results indicate that the value of the above ratio must be at least 3 or 4 if fluid friction in the contact area is to be ensured.

21.7. TEMPERATURE CRITERION OF SCUFFING

Increase in force and temperature loading of mechanisms gives rise to dangerous rupture of contacting surface known as scuffing, or scoring. The indications of scuffing are deep scratches, torn-away material, dents, bulges, or melted spots formed on the contacting surface. Scuffing is often characterised by severe wear of the mating parts and can bring about the failure of the mechanism. In solids sliding at low and medium speeds, scuffing causes normally a sharp rise in the coefficient of sliding friction, and rise in temperature of the mating surfaces; moreover, dynamic processes arise that result in mechanical oscillations and noise. In high-speed mechanisms, the growth in the coefficient of friction is not imminent. Scuffing is encountered in heavily loaded gear transmissions, cams, hinge joints, bearings, piston-and-cylinder joints, valves, machine-tool guideways and other tribological components.

The development of scuffing is greatly affected by load, sliding and rolling velocities, roughness of the mating surfaces and their material, physico-mechanical properties of the lubricant, quantity and quality of additives to the base oil, lubrication method, and other factors.

In lubricated mechanisms, scuffing starts to develop with the desruption of the thin oil film that separates the solids in contact. Such disruption can be caused by plastic deformation, wear of individual asperities of the contacting surfaces in a cold state or loss of the lubricating properties of oil at high contact temperatures. These processes are usually referred to as *cold* and *hot* scuffing. The factors of primary importance for cold scuffing are the degree of contact density, the wear resistance of separate irregularities, their plasticity and the tendency to form adhesive bonds. Among the vital external parameters are the load at which scuffing is likely to emerge, the rolling and sliding velocities, and the temperature.

Cold scuffing is typical of low-speed and stationary contact mechanisms. The occurrence of hot scuffing is greatly affected by all the factors that lead to increase in actual temperatures and to reduction in the oil-film thickness.

The necessary conditions for the emergence of scuffing are the removal of the adsorbed and oxide surface films, and the plastic deformation that brings the clean ("juvenile") surfaces into direct contact. The main factors to influence scuffing are the temperature of the solids, deformation, stress conditions, and physical properties of the materials and environment. At low contact temperatures and work-hardening of the material, the welded junctions originating

because of plastic deformation may have higher strength than the bulk material. In this case, the surface ruptures in the weaker-material region, giving rise to scores and faster wear.

Oxide films and impurities on the surface impede the formation of welded junctions. With rising surface temperature, the metal becomes softer, the surface films are partially removed, the real area of contact grows, and, as a result, the tendency of the surfaces to scuff sharply increases. Scuffing or, rather, scuff resistance is determined by mechanical, thermal, and chemical processes. The welded junctions generally arise at separate points of real contact. The intensity and kinetics of this process depend not only on external factors, such as load, temperature, and physico-chemical properties of environment, but also on the physical, chemical, and structural properties of the contacting materials and the rate of formation and destruction of the protective layers, which is governed by the kinematics of sliding contact as well as by the properties of the surface layers and environment. The temperature criterion of scuffing suggested by Blok is based on the hypothesis that there is a critical temperature of oil-film disruption for each material-lubricant combination. The critical scuffing temperature for straight oils is assumed to be constant and independent of speeds, load, and bulk temperature. The contact temperature is represented as the sum of the bulk, or rather, surface temperature, θ_0, before the solids come into contact, and the momentary temperature rise ϑ. The temperature θ_0 is found experimentally or calculated from the joint's thermal balance. The temperature rise for cylindrical bodies that execute the rolling motion with sliding is determined by the Blok formula

$$\vartheta = 0.83 \frac{fP_n (v_1 - v_2)}{(\sqrt{\lambda_1 \gamma_1 c_1 v_1} + \sqrt{\lambda_2 \gamma_2 c_2 v_2}) \sqrt{b}}$$

where v_1 and v_2 = surface velocities of the solids, cm/s; λ_1 and λ_2 = coefficients of thermal conductivity for the materials of the surfaces, kgf·cm/(cm·s·°C); γ_1 and γ_2 = density of the materials, kgf/cm^3; c_1 and c_2 = specific heat values for the materials, kgf·cm/(kg·°C); b = half the width of the contact strip, cm.

The scuffing absence condition is expressed as the inequality

$$\theta_0 + \frac{0.83 f P_n (v_1 - v_2)}{(\sqrt{\lambda_1 \gamma_1 c_1 v_1} + \sqrt{\lambda_2 \gamma_2 c_2 v_2}) \sqrt{b}} < \theta_{\Sigma cr}$$

$\theta_{\Sigma cr}$ = total critical temperature at which scuffing arises. The use of this criterion requires the knowledge of the absolute values of $\theta_{\Sigma cr}$ and of whether the temperature remains invariable as the main frictional factors change [2, 4, 5]. Analysis of a large number of experiments conducted by various investigators shows that the critical temperature is not constant; its range for straight oils is $\theta_{\Sigma cr}$ = 120 to 250°C.

Oscillograms of torsional moments, surface temperatures, and oil-film thickness, taken simultaneously from test specimens, have made

it possible to follow the moment of the emergence and the subsequent development of scuffing [4]. If the contacting components operate under safe conditions which involve no hazard of oil film disruption, then the frictional force relationships are essentially similar to those given by the elasto-hydrodynamic theory of lubrication. The generalized frictional force applied to one of the rubbing components will in this case be expressed as $F = \int\int_S \tau_{lb}\, dS$, where τ_{lb} = tangential shear stress in the oil film; and S = shearing area. More intensive sliding and increased load or coefficient of friction (which can occur because of rising temperature or reduced rolling velocity), that is, change in contact parameters towards increased contact temperature will produce reduction in the oil-film thickness. All other things being equal, the protective film breaks and local scuffing of the surfaces in contact takes place where heat generation is at a maximum or stress concentration occurs (for instance at an individual asperity). Owing to disruption of the oil film at one or several points, the friction force at this moment increases; it can be represented by two components

$$T = \sum_{i=1}^{n} \tau_{ilb}\Delta S_{ilb} + \sum_{k=1}^{l} \tau_{kdr}\Delta S_k$$

where τ_{kdr} = tangential stress on the dry surface.

If the area of the oil film rupture is insignificant, then the total frictional force (or the coefficient of friction) changes little despite the fact that the tangential stresses in the two considered instances are unequal ($/\tau /_{lb} < /\tau /_{dr}$). At the moment of film disruption, the local coefficient of friction between metal surfaces sharply rises; calculations and experiments show, however, that intense heat evolution (a momentary temperature rise) leads to local softening of the metal, and, subsequently, to reduction in the local coefficient of friction. Metal fusion in micro-contact spots will originate hydrodynamic friction, and in the welded junctions the tangential shearing stress τ_{wj} will sharply increase. In the general case, the friction force at the contact under scuffing conditions may be represented as consisting of the following components (Fig. 21.22):

$$T = \sum_{i=1}^{n} \tau_{ilb}\Delta S_{ilb} + \sum_{k=1}^{l} \tau_{kdr}\Delta S_{kdr} + \sum_{d=1}^{m} \tau_{d\,fus}\Delta S_{d\,fus}$$

$$+ \sum_{v=1}^{p} \tau_{vwj}\Delta S_{vwj} = T_{lb} + T_{dr} + T_{fus} + T_{wj}$$

where T_{lb}, T_{dr}, T_{fus}, and T_{wj} = tangential forces arising in the lubricant, on the dry surface, in the fused metal, and in the welded junctions, respectively. The initial destruction of the surface usually occurs at a single or several contact points. In roller specimens, for instance, the specific features of scuffing development are

as follows: the depth of the surface damage when scuffing initially emerges depends primarily on load and rolling velocity, the rupture being more severe with heavier loads and lower speeds; the rate of expansion of the damage out of a single junction is determined by the degree in which the surface is prepared to scuffing. For instance, during the running-in period, welded junctions originate at individual asperities; the initial light scuffing does not worsen, however, because the whole contact area is not thermally prepared for the process to occur.

The grade of oil is a major factor to hold back the development of scuffing. The main characteristics determining the load capacity of the oil film are the viscosity of oil at the temperature the surfaces come into contact, the physico-chemical properties, and the content of anti-scuff additives. The oil-film thickness in the contact depends on the viscosity of oil and on the value of the piezo-coefficient of viscosity. The higher the viscosity, the lower the coefficient of sliding friction and the larger the oil-film thickness. As a result, the growth in oil viscosity reduces the contact heat evolution due to sliding friction, and the separation of the contacting surfaces by the oil film becomes more reliable, which, on the whole, contributes to increase in the load-carrying capacity of the contact with respect to scuff resistance. The anti-scuffing properties of oils are improved by phosphorous, chlorous, and sulphurous additives.

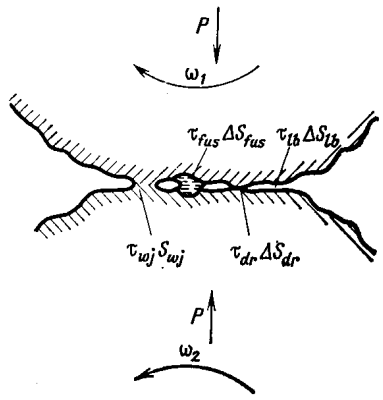

Fig. 21.22. Diagram of multi-component friction

At elevated contact temperatures and pressures, phosphorus, chlorine, and sulphur react on the surface layer and form protective compounds that prevent metal surfaces from welding together. As a certain temperature level is reached, the destruction and re-formation of the protective layers proceeds continuously. The influence of the bulk temperature on the oils containing S, Cl, and P, in contrast to straight mineral oils, can be favourable because it intensifies the chemical reactions of the additives with the metal surfaces. It has been established experimentally that in these conditions the allowable scuffing load grows, and the design critical temperatures can be very high ($\Theta_{cr} \approx 250$ to 350°C).

The general expression for the scuffing criterion, obtained by the author, is

$$K = \frac{0.78 f \sqrt[4]{P_n}\,(v_1 - v_2)}{(\sqrt{\lambda_1 \gamma_1 c_1 v_1} + \sqrt{\lambda_2 \gamma_2 c_2 v_2})} \sqrt[4]{\frac{1}{R_{eff}\,(\Theta_1 + \Theta_2)}} \qquad (21.7)$$

The condition of absence of the scuffing risk has the form of $K < K_{cr}$. The critical value of the scuffing criterion, found experimentally for a variety of materials and lubricants combinations [5,6], is normally close to 2.

The structure of the equation (21.7) confirms the basic mechanism of scuffing for solids that roll with sliding, which involves the thermal destruction of the lubricant in micro-contact areas [6].

Substituting the expression for the coefficient of friction into the equation (21.7), one can derive the relationship between the limiting

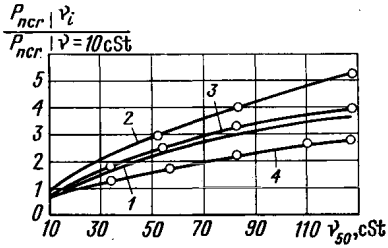

Fig. 21.23. Effect of oil viscosity on scuffing load

1—curve calculated by formula (21.7); *2*, *3*, and *4*—approximation of experimental data according to [25],[26], and [27], respectively

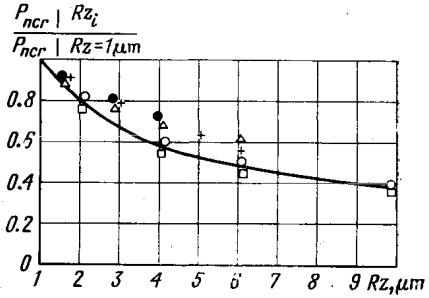

Fig. 21.24. Effect of surface geometry on scuffing load (design curve); the points correspond to data from [27] at peripheral speeds ● —8.6 m/s, △ —17.2 m/s, + — 34.4 m/s and to data from [25] at rotational speeds ○ —3300 rpm and □ — 10 000 rpm

load or sliding velocity and the oil viscosity, surface geometry, rolling velocity, and other parameters.

The effect of oil viscosity on scuffing load, determined by calculation and experimentally, is illustrated in Fig. 21.23, and the effect of surface roughness, in Fig. 21.24.

In toothed gearing, the effect of gear parameters on the load-carrying capacity (with regard to scuffing) has been found to be like this. With increasing module the absolute and the relative sliding velocity grows, with the result of rising contact temperature. As is seen from the obtained equations, the ultimate load capacity of the contact in respect of scuffing is bound to diminish with the increasing module; this conclusion is confirmed by experiments conducted on product-gear transmissions. For the stated reasons, the load capacity of toothed gearing must increase with the reduced addendum of the tooth. A larger pressure angle causes a higher rolling velocity, which reduces the coefficient of sliding friction and enlarges the effective contact curvature radius. The experimental studies conducted so far give but rough estimation of the influence the effective curvature radius has on the scuff-load capacity. The ultimate load per unit tooth length varies inversely with the gear

facewidth despite the increase in the total load. This effect is explained in [4].

Increase in facewidth-to-diameter ratio can be conducive to load concentration on the extremes of the tooth. Surface geometry has a marked effect on the scuffing load limit. A coarser roughness increases the coefficient of friction, local temperatures, and plastic contact deformations, that is, increases the tendency to oil film disruption and formation of welded junctions. The manufacture of parts with a better surface finish and a preliminary running-in operation can improve the load carrying capacity of teeth with respect to scuffing. Surface lay is also important, namely, the contact must be intermittent.

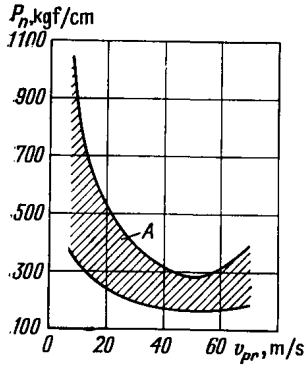

Fig. 21.25. Variation of scuffing load with rotational frequency (or peripheral speed v_{pr})
A – scuffing region

The rolling and sliding velocities rise with the gear rotational frequency. A higher sliding velocity increases the oil-film thickness and reduces the coefficient of friction and the contact temperature of the solids in spite of some temperature rise in the oil film. Increase in sliding velocity reduces the coefficient of friction; however, the total heat generation and contact temperature go up, and the oil film thickness decreases. Thus, the general influence of the rolling and the sliding velocity is opposite, that is an increase in rolling velocity raises the scuffing load, and increase in sliding velocity leads to its reduction.

The initial thermal action brings the scuffing load down as the rotational frequency grows. The form of the curve $P_n = f(n)$, with its steep fall, is typical (Fig. 21.25). Some rise in scuffing load in the region of high rotational frequencies is explained, in our view, by the formation of tribochemical protective films (frictional polymers) on the surfaces at elevated temperatures and by decrease in the intensity of action of the heat source; specifically, the thickness of the boundary heat layer diminishes and so does the wear rate in scuffing conditions at high speeds, which is found experimentally in gear transmissions. This effect is made clear by the thermal analysis of scuffing [6].

Some investigations have revealed a relationship between the amount of residual austenite in the metal and the scuffing load. With increased amount of residual austenite, the contact load capacity diminished. No perceptible effect on material hardness on scuffing load has been detected experimentally; however, with a lower hardness, gear teeth become more prone to pitting and plastic deformation. On the whole, hard steels are more preferable as far as the wear resistance, contact strength, and anti-scuffing proper-

ties are concerned. The contact load capacity with regard to scuff-resistance can be increased by nitriding and phosphatizing the tooth-flank surfaces. The theoretical concepts of scuffing lead to the conclusion that the materials with high thermophysical parameters and hardness as well as those which lend themselves to thermochemical strengthening, carbonitriding, and other surface-strengthening processes hold a potential for heavily loaded transmissions.

The contact load-carrying capacity is not so much affected by the temperature of the lubricant being fed (or oil bath) as by the bulk temperature of the gears in mesh, which governs the "inlet" viscosity of the thin oil film directly on the teeth surfaces. This temperature influence on oils of different chemical compositions and on those with anti-scuff additives is variable.

It has been shown experimentally that the running-in process has effect on the formation of the boundary lubricant film, increasing its thickness and stability [17]. Thin lubricant films have been found to increase their thickness at low rolling velocities as compared with the design values. The formation of the oil film is also affected by the environment, the chemical activity of the metal, and the time during which rubbing occurs. Adsorption processes, high contact pressures, and the stress and deforming conditions of metal surfaces contribute to the formation of structurally-organized layers [17].

21.8. MAGNETIC-POWDER LUBRICATION

Intense wear of parts is in many cases the chief cause that prevents the development of high-performance machinery and equipment for operation in vacuum, inert and aggressive ambiences, and under radiation. The traditional lubricating methods and materials are ineffective at temperatures over 250 to 300°C and at temperatures under —100°C. Extended service life of tribological components can be achieved by developing new structural and lubricating materials and lubrication methods operative in extreme conditions.

Promising are solid lubricants, which are capable of reducing friction forces and sustaining high contact loads, are stable in vacuum and inert environments, and show good resistance to radioactivity. Their engineering applications, however, are restricted to tribological units having short service life. The cause of this limitation is that no methods have been so far available for long-term supply of lubricant to the frictional surface by circulation. Solid lubricants are commonly used as coatings; they are incorporated into self-lubricating composite materials or fed to the rubbing surfaces by the transfer method.

The useful volume of lubricant coatings is limited by the thickness of the film, which, for a number of reasons, cannot exceed 20 to 30 μm. With self-lubricating composites, lubrication is effected through their wear. Solid lubricants are, as a rule, diamagnetic: they

are, virtually, insensitive to magnetic field. However, if some amount of special ferromagnetic substances is added to them, they acquire ferromagnetic properties without any appreciable loss of lubricating capability. For instance, mixing molybdenum disulphide and nickel powders together in volume contents of 80 percent MoS_2 and 20 percent Ni imparts magnetic properties to the lubricant, and the mixture is attracted to the mating parts at magnetic inductions from 300 G and higher [10, 15]. Other additives may also be introduced. Solution to the problem of placing the lubricant proves to be fairly simple. In gearing applications, the gears are located in a closed casing at the bottom of which the lubricant is placed and activated by a magnetic field. It is exactly this mode of placing a magnetically active lubricant—beyond the contact area, but near the rubbing surface—that allows the use of a considerable amount of lubricant.

The potential of the magnetic method of lubricant supply is primarily determined by the following advantages: (a) service life of a mechanism can be extended by increasing the volume of lubricant circulating in the tribological unit as it operates; (b) the lubricant holds better on the rubbing surface under the action of magnetic field; and (c) the same lubricant particles can be repeatedly fed to the rubbing surface after they have been thrown away from it. A rational forming of the magnetic field in the area of location of the operating components offers the possibility of supplying the lubricant to the components continuously. In these conditions, every ferromagnetic particle, tied with the lubricant particles by molecular forces, is acted upon by a magnetized part with the attraction force $\Phi = \chi_0 VH \frac{\partial H}{\partial x}$, where χ_0 = magnetic sensitivity of a ferromagnetic particle; V = volume of the particle; H and $\frac{\partial H}{\partial x}$ = intensity and the gradient of intensity of the magnetic field within the location of the particles.

Modern mechanisms generally operate in variable load and kinematic conditions, which require adjustment of lubricant supply. The magnetic method offers a solution to this complicated problem. Increase or decrease in magnetization of the mating components depending on the operating conditions causes changes in the amount of lubricant fed to these components. The lubricant should be used in a powdered aggregate state so that its separate particles are loosely connected with the whole mass of the mixture and are located along the magnetic lines. To introduce the lubricant into the contact area, its particles must be at least 1/2-1/3 of the permissible size dictated by the jamming-free condition for the between-parts clearance.

The magnetic activity of the mixture is affected by the shape of ferromagnetic particles. An elongated shape improves the ability of the lubricant to adhere to the rubbing components and increases the lubricants' content in one and the same volume of the mixture. As a rule, the mixture is obtained by mechanically mixing the start-

ing components. This operation is not always sufficient, and the obtained mixture should be processed additionally, in the presence of magnetic field, for instance by squeezing between rollers that rotate with sliding. This operation will strengthen the adhesion between the particles of the lubricant and the ferromagnetic substance.

The presence of the magnetic field provides for simultaneous orientation of ferromagnetic particles. After the operation, individual particles of the original components combine to form larger flake-shaped particles with a size depending on the pressure of the rollers and the intensity of the magnetic field. The magnetic lubrication method can be used in many tribological applications, for

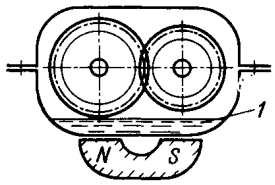

Fig. 21.26. Magnetic-powder lubrication of toothed gearing
1—magnetically active lubricant

instance, in gear transmissions, plain bearings, or cam mechanisms. The ways of application may also vary. Thus, for example, gears can be magnetized by an external magnet placed outside the lubricant housing or by magnets located on the rotating gears. In both instances, the gears should be mounted in a closed housing of a nonmagnetic material, which should also contain a magnetically active lubricant.

The essence of the adjustable lubricant supply is in the correspondence between the intensity of magnetization of the rubbing components and the amount of the lubricant supply. The magnetization intensity can be adjusted by varying the current in the solenoid of an electric magnet or by displacing a permanent magnet relative to the components. An electric supply source is required in the former case, and a device to move the magnet in the latter. The choice of the particular design solution is dependent on the general layout of the mechanism. A speed reducer employing the magnetic lubrication method is diagrammatically shown in Fig. 21.26. The performance of magnetically lubricated tribological units was tested on roller specimens and on a three-step four-shaft speed reducer. The lubricant used in all the tests was a mixture with a volume content of 80 percent MoS_2 and 20 percent Ni. In the starting conditions, the level of the lubricant was close to the rubbing surfaces, without touching them. The service-life tests were conducted without replacement of the lubricant. The roller specimens were made from steel 20X13 (*HRC* 45) with a diameter of 44 mm, a width of the operating strip of 5 mm, and a surface roughness of 1.25 to 2.5 μm *Ra*. The operating conditions were: the load 8 to 75 kgf, the Hertzian maximum contact stresses up to 7100 kgf/cm^2, the roller peripheral speeds 10 to 300 cm/s;

the sliding speeds in the contact were varied within the range of 0 to 290 cm/s. The gear wheels were made from steel 30ХГСА, with a hardness of *HRC* 35 and a surface roughness of 1.25 to 2.5 μm *Ra*. The number of teeth in gear pairs was: $z_1 = 104$; $z_2 = 64$; $z_3 = 104$; $z_4 = 64$; $z_5 = 84$; $z_6 = 84$; the module was 0.5 mm, and the width of the operating strip was 5 mm. The testing conditions were: the rotational frequency of the input shaft 200 rpm, and that of the output shaft 530 rpm; the torque M_t on the input shaft 36 kgf·cm. With these parameters, the Hertzian maximum contact stresses at the first step were 7450 kgf/cm², and the sliding speed was 7.3 cm/s.

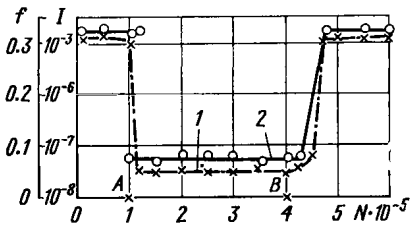

Fig. 21.27. Variation of coefficient of friction and wear rate with number of loading cycles

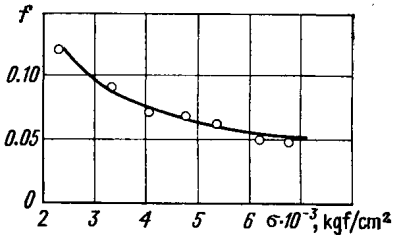

Fig. 21.28. Variation of coefficient of friction with compressive stress in magnetic-powder lubrication

The amount of the magnetic induction measured in the middle of the clearance between the magnet and the rubbing-part surface was from 200 to 500 G.

The experiments produced the following results. Bringing the magnet closer to the rubbing parts intensified the lubricant supply and reduced the coefficient of friction f, the wear rate I, and noise. As the magnet was moved away and lubricant films became disrupted, these characteristics returned to the initial values. Fig. 21.27 illustrates the variation of the coefficient of friction (curve *1*) and the wear rate (curve *2*) with the number N of loading cycles for roller specimens at a contact stress $p_{max} = 4100$ kgf/cm² and a sliding speed of 125 cm/s. The points A and B mark the moments of time the magnet was brought closer to and moved away from the housing. The following average values were established for the roller specimens run in unlubricated conditions: $f \approx 0.3$; $I = 2 \times 10^{-5}$; and with lubrication $f \approx 0.05$ to 0.065; $I \approx 6 \times 10^{-8}$. Thus, the application of the magnetic lubrication method has given in this instance a reduction in wear by a factor of 3 and in the coefficient of friction, by a factor of 4 to 5.

Increased hardness of the specimens produced still better results. Fig. 21.28 shows the coefficient of friction as dependent on the contact stress when lubricating with a mixture of molybdenum disulphide and nickel, the data being obtained experimentally. By the character and the absolute values, the curve $f = \varphi(p_{max})$ is similar

to that effective for lubrication with pure molybdenum disulphide. The service-life tests were conducted to investigate the feasibility of the magnetic lubrication method with transmissions consisting of several gear pairs. A speed reducer was tested under the above conditions for 115 h with 1.38×10^6 cycles of the driving gear. After the test run, the reducer was taken apart and inspected. The gears were found to be in a good order; insignificant evidence of wear was detected on the addendum of the teeth only. The reducer was quite suitable for further operation [10]. The magnetic-powder lubrication method has the potential for use in gaseous environments and in vacuum.

21.9. TRANSFER LUBRICATION

This is one of the methods of supplying a solid lubricant to the friction area by small portions. Transfer of the lubricant is feasible even with very light loads. The allowable wear of lubricating elements may, without any harm, greatly exceed that of the principal rubbing parts that sustain and transmit load [20].

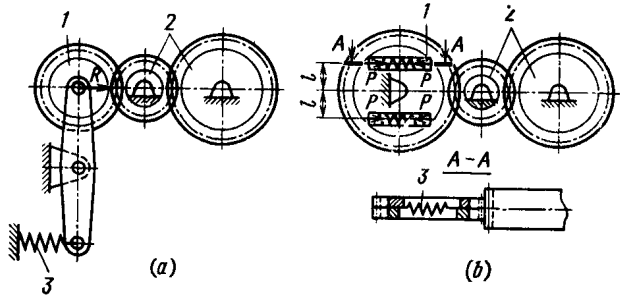

Fig. 21.29. Design of lubricating gear for transfer lubrication
1—lubricating gear; *2*—work gears; *3*—springs

As a result, the useful life is substantially increased. In gear transmissions, the lubricating element is made in the form of a special gear which meshes with a work gear. The lubricating gear carries no work load and, as it wears away, transfers the solid lubricant to the rubbing surfaces of the gears under load. The lubricating gear can be held against its mating work gear by two methods: radially (Fig. 21.29*a*), with the lubricating gear secured on a lever and spring-pressed to the work gear, and tangentially (Fig. 21.29*b*), with the lubricating gear consisting of two halves and having its teeth spring-pressed against the work gear teeth.

An experimental transfer-lubricated reducer was operated in a 10^{-7} to 10^{-9} mm Hg vacuum at temperatures from 20 to 250°C [13].

The characteristics of the lubricating gears were: the number of teeth 110 and the diameter of the reference circle 66 mm.

During the experiments, the rotational frequency at the input of the reducer was varied over a range of 1500 to 4500 rpm and torque M_t, from 0.5 to 5.0 kgf·cm; the pressure P of the lubricating gear against the work gear was from 0.05 to 3 kgf. The peripheral speed of the working and the lubricating gears reached 330 cm/s, and the sliding speed of teeth at the contact, 110 cm/s; the contact stresses in work gears reached the magnitudes $P_{max} = 10\,000$ kgf/cm^2. The materials used for the lubricating gears were BAMK-1, BAMK-21, and BAMK-22. The work gears were made from steel 20X13, with a hardness of *HRC* 48 to 51; the module was 0.6 mm, and the pressure angle $\alpha = 20°$. Trial tests and calculations showed that the power required to rotate the lubricating gears was very low, namely from 1 to 2 percent of the power being transmitted. The efficiency of lubrication at pressures of the lubricating gears ranging from 0.05 to 3 kgf showed no significant change because the reducer's efficiency remained constant. With increase in the transmitted torque and power, the efficiency of the reducer rose on the average from 45 to 90 percent. The amount of wear of the lubricating gear was proportional to the number of loading cycles and increased with radial load. Experiments with the transfer lubrication method have indicated that a slight pressure on the lubricating gear was sufficient to keep it in mesh with the work gear. Gears produced from nitrided titanium BT-14 were tested for performance without transfer lubrication. The experiment was conducted in a vacuum of 8×10^{-6} mm Hg at a temperature of 110°C. The rotational frequency of the reducer was 4000 rpm, with an input torque of 3.0 kgf·cm. The reducer was run for 3 h and 5 min and was stopped because of severe scuffing of the gears. Inspection revealed traces of scuffing on the driving and driven tooth flanks over the whole working depth. Welded particles of metal from the mating gear were detected in tooth spaces. Scuffing in the form of scores, cavities, traces of plastically deformed or torn-away material was the most dangerous and typical surface damage in the experiments. For the chosen materials, the intensity of scuffing increased with growth in contact pressure, speed, and temperature. The life of the reducer in the experiments was limited mainly by the life of the lubricating gear and accidental ingress of foreign particles—fragments of the lubricant and wear debris—into the rolling bearings. It was demonstrated experimentally that under the above conditions an irrecoverable failure of the reducer due to severe scuffing of unlubricated gears made from steel 20X13 hardened to *HRC* 50, occurred in 2 to 3 h. At the same time a reducer with transfer lubrication was capable of operating for 100 h. Depending on the operating conditions and gear materials, the efficiency of the reducer could vary from 50 to 90 percent. The optimum radial pressure of the lubricating gear made from BAMK-22 was maintained at about 100 gf. It should be noted that at least one lubricating gear is necessary for each pair of work gears.

21.10. CALCULATION OF TRANSMISSION EFFICIENCY

An experimental and theoretical analysis of the power balance in a dry-running reducer has shown that the sliding friction losses in gears, idle-running losses, and losses in rolling bearings account for the main fraction of the energy lost. The power transmitted by a mechanism consisting of a pair of gears and rolling bearings is

$$N_{in} = N_{out} + N_{g,sl} + N_{g,rl} + N_b$$

where N_{in} and N_{out} = input and output power of the gearing, respectively; $N_{g,sl}$ and $N_{g,rl}$ = power expended on sliding and rolling friction in the gearing; N_b = power expended on friction in the bearings.

The accuracy of calculation of the efficiency is determined primarily by the correct choice of the coefficient of sliding friction, which depends on pressure, temperature, type of lubricant, sliding and rolling velocity, and other conditions.

The analytic expression for the efficiency of the reducer will take the form

$$\eta_{red} = \frac{1}{1 + \frac{N_{ir}}{N_{up}} + \frac{N_{pl}}{N_{up}}}$$

where N_{ir} = power spent on idle rotation; N_{up} = useful power; N_{pl} = power losses in transmitting the work load. From this expression it follows that with increase in useful power (torque), the relative fraction of the idle-running losses (N_{ir}/N_{up}) will diminish, and the total efficiency will grow accordingly. Experiments indicated that the idle-running power increases approximately in a direct proportion to rotational frequency; for this reason, the N_{ir}/N_{up} ratio can be replaced by the M_{ir}/M_{up} function. The friction torque in rolling bearings varies directly with load, and, hence, with the mass of the gears and shafts at idle running; the useful power is proportional to the peripheral force on the gear. For the convenience of further assessment of idle-run losses, let us introduce a criterion $K_{iri} = \frac{G_i}{P_i}$, where G_i = mass of the components supported by bearings (shafts, gears, and the like); and P_i = peripheral force. For a single gear, after substitution of the expressions for determining mass (G) and peripheral force (P) arising in the first meshing pair, we shall have

$$K_{iri} = \frac{\pi \gamma_{gi} d_{gi}^3 \left(l_{gi} + l_{shi} \frac{\gamma_{shi}}{\gamma_{gi}} \frac{d_{shi}^2}{d_{gi}^2} \right)}{8 M_{ti}}$$

where γ_{gi}, and γ_{shi} = density of the gear and shaft materials, respectively, kg/cm^3; d_{gi} = gear reference circle diameter, cm; d_{shi} =

= mean diameter of the shaft, cm; M_{ti} = torque transmitted by the gear, kgf·cm; l_{gi} and l_{shi} = effective lengths of the gear and the shaft, respectively, cm. The idle-run criterion for the whole reducer (that is, for all the gears) will be

$$K_{\Sigma ir} = \sum_{i=1}^{n} K_{iri}$$

where n = number of gears. The given method of energy calculation for reducers running dry, for instance in space, leads to the conclusion that the efficiency will rise with the diminishing value of $K_{\Sigma ir}$, that is with the reduced mass of parts supported by bearings. All other things being equal, the reducer's efficiency with a change in the gravity force will be variable because of varying $K_{\Sigma ir}$

$$K_{\Sigma ir} = \frac{g_i}{g_e} \sum_{i=1}^{n} \frac{\gamma_{gi} \pi d_{gi}^3 \left(l_{gi} + l_{shi} \frac{\gamma_{shi}}{\gamma_{gi}} \frac{d_{shi}^2}{d_{gi}^2} \right)}{8 M_{ti}}$$

where g_e = gravity force in earth conditions; g_i = gravity force in particular space conditions. For instance, on the moon surface, the value of $K_{\Sigma ir}$ should be one-sixth that on the surface of the earth; hence, with other conditions being identical, the gear-transmission efficiency must be higher. It should be kept in mind that, with low powers transmitted, the energy lost in idle running of a reducer made from conventional materials will be relatively high. The above analysis points to some ways of increasing the total efficiency of a speed reducer and enables the designer to allow for its changes depending on the bearing friction losses, to which no proper consideration has been given so far.

REFERENCES

1. Артоболевский И. И. Теория механизмов. М., «Наука», 1965, 776 с.
2. Генкин М. Д., Кузьмин Н. Ф., Мишарин Ю. А. Вопросы заедания зубчатых колес. М., Изд-во АН СССР, 1959, 147 с.
3. Дроздов Ю. Н. Обобщенные характеристики в анализе трения и смазки тяжело нагруженных тел.— «Машиноведение», 1974, № 6, с. 70-74.
4. Дроздов Ю. Н. Новый метод исследования и расчета противозадирной стойкости контакта.— Труды научно-технического совещания по методам оценки противоизносных и противозадирных свойств смазочных материалов. М., «Наука», 1969, с. 153-168.
5. Дроздов Ю. Н. Уточненный метод расчета на задир пар трения в тяжело нагруженных механизмах.— «Вестник машиностроения», 1971, № 4, с. 25-29.
6. Дроздов Ю. Н. Тепловой аспект проблемы заедания катящихся со скольжением тел.— «Машиноведение», 1972, № 2, с. 71-79.
7. Дроздов Ю. Н., Рещиков В. Ф. О коэффициенте трения и толщине масляной пленки в тяжело нагруженном контакте.— «Вестник машиностроения», 1968, № 2, с. 9-12.
8. Дроздов Ю. Н., Арчегов В. Г. Расчет коэффициента трения в тяжело нагруженном контакте при скольжении.— «Машиноведение», 1975, № 6, с. 81-83.

9. Дроздов Ю. Н., Пучков В. Н. Методика оценки несущей способности твердых смазок при высоких давлениях и повышенных температурах. Трение и изнашивание при высоких температурах. М., «Наука», 1973, с. 11-14.
10. Дроздов Ю. Н., Павлов В. Г., Ромашкин О. Г. Теплостойкий редуктор с магнитным способом подачи твердой смазки.— «Вестник машиностроения», 1976, № 8, с. 18-22.
11. Дроздов Ю. Н., Смирнов В. И. Исследование коэффициента трения скольжения при высоких параметрах контакта.— «Вестник машиностроения», 1977, № 6, с. 19-23.
12. Дроздов Ю. Н., Туманишвили Г. И. Толщина смазочного слоя перед заеданием трущихся тел.— «Вестник машиностроения», 1978, № 2, с. 8-10.
13. Дроздов Ю. Н., Овсеенко Г. Р., Павлов В. Г. Ротапринтный способ смазки в сухих зубчатых редукторах.— «Вестник машиностроения», 1973, № 7, с. 26-29.
14. Крагельский И. В. Трение и износ. Изд. 2-е. М., «Машиностроение», 1968, 480 с.
15. Павлов В. Г., Дроздов Ю. Н. Повышение долговечности узлов сухого трения.— «Вестник машиностроения», 1975, № 11, с. 34-37.
16. Петрусевич А. И. Зубчатые передачи. Детали машин. Справочник, т. 3. Изд. 3-е. Под ред. А. Н. Ачеркана. М., «Машиностроение», 1969, с. 15-216.
17. Райко М. В. Смазка зубчатых передач. Киев, «Техніка», 1970, 194 с.
18. Расчеты на прочность в машиностроении, т. II, М., Машгиз, 1958, 974 с.
19. Серенсен С. В., Когаев В. П., Шнейдерович Р. М., Несущая способность и расчеты деталей машин на прочность. М., «Машиностроение», 1975, 488 с.
20. Трояновская Г. И. Применение самосмазывающихся материалов при ротапринтной смазке.— «Вестник машиностроения», 1974, № 4, с. 51-54.
21. Устиненко В. Л. О влиянии окружной скорости на контактную прочность зубчатых колес. Детали машин. № 22. Киев. «Техніка», 1970, с. 26-27.
22. Хрущов М. М. Закономерности абразивного изнашивания. Износостойкость. М., «Наука», 1975, с. 5-28.
23. Хрущов М. М., Бабичев М. А. Абразивное изнашивание. М., «Наука», 1970, 252 с.
24. Часовников Л. Д. Передачи зацепления. Изд. 2-е. М., «Машиностроение», 1969, 487 с.
25. Borsoff V. N. Predicting the scoring of gears to establish the limits of load. Machine Design, 1965, No. 1, p. 132-136.
26. Huges I. R., Waight F. H. The Lubrication of Spur Gears International conference on Gearing. Inst. Mech. Eng. London 1958, pp. 135-143.
27. Niemann G., Lechner G. Die Freß — Grenzlast bei Stirnrädern aus Stahl. Erdöl und Kohle, 1967, No. 2, S. 96-106.